

**Novel microemulsions with an
anionic/non-ionic surfactant mixture**

Dissertation

zur Erlangung des akademischen Grades eines
Doktors der Naturwissenschaften (Dr. rer. nat.)
der Fakultät für Biologie, Chemie und Geowissenschaften
an der Universität Bayreuth

vorgelegt von
Dipl.-Biochem. Univ.
Lukas Wolf

Bayreuth,
Dezember 2011

Die vorliegende Arbeit wurde in den Jahren 2009 – 2011 in Bayreuth unter der Betreuung von Herrn Prof. em. Dr. Heinz Hoffmann in den Laboren der Firma *BayColl* im „Zentrum für Neue Materialien Bayreuth“, Wolfsbach, durchgeführt.

Vollständiger Abdruck der von der Fakultät für Biologie, Chemie und Geowissenschaften der Universität Bayreuth genehmigten Dissertation zur Erlangung des akademischen Grades eines Doktors der Naturwissenschaften (Dr. rer. nat.).

Promotionsgesuch eingereicht am:	7. Dezember 2011
Zulassung durch die Prüfungskommission:	14. Dezember 2011
Tag des wissenschaftlichen Kolloquiums:	17. April 2012

Amtierender Dekan:
Prof. Dr. Beate Lohnert

Prüfungsausschuss:

Prof. Dr. em. Heinz Hoffmann	(Erster Gutachter)
Prof. Dr. Yeshayahu Talmon	(Zweiter Gutachter)
Prof. Dr. Karlheinz Seifert	(Vorsitzender)
Prof. Dr. Stephan Förster	

„Grundlagenforschung betreibe ich dann, wenn ich nicht weiß, was ich tue.“

W. von Braun

Table of Contents

0. TABLE OF CONTENTS	7
1. SUMMARY	8
1.1. English Version	8
1.2. German Version.....	9
2. INTRODUCTION.....	10
2.1. Microemulsions and their applications	10
2.2. Phase behaviour of surfactants	12
2.3. Microemulsions with non-ionic surfactants.....	15
2.4. Microemulsions with ionic surfactants	17
2.5. Objectives of this thesis	19
3. SYNOPSIS	21
3.1. The surfactant system $\text{Ca}(\text{DS})_2/\text{Mg}(\text{DS})_2 - \text{IT } 3$	21
3.2. Solubilization of oil into the surfactant mixture	22
3.3. Cryo-TEM imaging of the microemulsion system $\text{Ca}(\text{DS})_2/\text{IT } 3 - \text{H}_2\text{O}/\text{M}_2$	24
3.4. Dynamic properties of microemulsions in the single phase channels.....	28
3.4.1. <i>Introduction of the microemulsion system $\text{Mg}(\text{DS})_2/\text{IT } 3 - \text{H}_2\text{O}/\text{decane}$</i>	28
3.4.2. <i>Electric birefringence and rheology measurements</i>	30
3.5. Cryo-TEM of microemulsions with a High Internal Phase Microemulsion (HIPME) structure	35
3.6. PFG-NMR self diffusion measurements.....	38
3.6.1. <i>PFG-NMR self diffusion measurements in the single phase channels</i>	38
3.6.2. <i>Influence of excess salt to the microemulsion system</i>	40
3.7. Outlook.....	42
4. REFERENCES.....	44
4.1. Literature	44
4.2. List of figures.....	46
5. PUBLICATIONS	47
5.1. Overview of publications and individual contribution.....	47
5.1.1. <i>Microemulsions from silicone oil with an anionic/nonionic surfactant mixture</i>	49
5.1.2. <i>Cryo-TEM imaging of a novel microemulsion system of silicone oil with an anionic/nonionic surfactant mixture</i>	60
5.1.3. <i>Dynamic Properties of Microemulsions in the Single-Phase channels</i>	69
5.1.4. <i>Microemulsions with a HIPME (High Internal Phase Microemulsion) structure</i>	90
5.1.5. <i>PFG-NMR in the Single Phase Channels of Microemulsions with an anionic/non-ionic surfactant mixture</i>	98
6. ABBREVIATIONS AND SYMBOLS.....	109
7. PRESENTATIONS AT INTERNATIONAL MEETINGS.....	110
8. ACKNOWLEDGEMENT.....	111
9. ERKLÄRUNG	112

1. Summary

1.1. English Version

Microemulsions consist of water, oil and surfactant. In contrast to ordinary emulsions, microemulsions are transparent and thermodynamically stable phases. They appear to be macroscopic single-phase systems but are, however, based on highly complex nanostructures. From the scientific point of view, the so far most studied and best understood microemulsion systems consist of water, oil and either a single non-ionic surfactant or an electrically charged ionic surfactant. Both systems are significantly different, for example in their phase behaviour, thermal stability or their nanostructures. Systems with ionic/non-ionic surfactant mixtures, however, have not yet been investigated intensely.

In this work, the phase behaviour of an anionic/non-ionic surfactant mixture with different oils was investigated. The phase diagrams exhibit two optically isotropic microemulsion regions with increasing oil content at constant temperature and surfactant concentration, the so called single phase channels. The two isotropic single phase channels are separated by an optically anisotropic phase region. The microemulsion channel below the anisotropic region extends from the aqueous phase, starting with increasing oil concentration and increasing mass fraction of the non-ionic co-surfactant in the surfactant mixture to the middle of the phase diagram and ends there. The upper single phase channel runs through a steep minimum, with respect to the surfactant/co-surfactant ratio, continuously from the aqueous to the oil-rich side of the phase diagram. In contrast to microemulsions with single non-ionic surfactants, the microemulsion channels are isothermal. The different single-phase regions were examined with various physico-chemical methods. The nanostructures could be identified by measuring electric conductivity, SANS, PFG-NMR and by electron microscopy. While the lower single phase channel consists of small oil droplets in a continuous aqueous phase, which swell with increasing oil content, the nanostructure in the upper channel undergoes a complex structural transition. The oil-free sample, which has a bicontinuous sponge structure, is transformed to a water-in-oil polyhedral foam structure by solubilizing only a few percent of oil. For this so far unknown microemulsion structure, we introduced the term high internal phase microemulsion (HIPME) due to structural similarities to the known high internal phase emulsions (HIPE). This complex structural transition could be observed by transient electric birefringence. The determined structural relaxation times, which also determine the viscosity of the fluids, run through a sharp maximum at the transition point from the bicontinuous to the w/o-foam structures. The observed HIPME structures are probably caused by the presence of the electric charge of the anionic surfactant. The electric charge on the surfactant monolayer leads to a comparably high interfacial tension between the diluted aqueous surfactant phase and the oil. Consequences of this high interfacial tension are oil continuous polyhedral foam structures instead of bicontinuous structures, which are obtained in similar microemulsion systems with single non-ionic surfactants. By shielding the electric charges by the addition of salt, the oil continuous HIPME structures are disturbed what can be concluded from an increased conductivity and mobility of the water fraction, followed by NMR.

1.2. German Version

Mikroemulsionen bestehen im einfachsten Fall aus Wasser, Öl und Tensid(en). Es handelt sich dabei im Gegensatz zu normalen Emulsionen um transparente, thermodynamisch stabile Phasen. Diesen makroskopisch einphasig erscheinenden Systemen liegen jedoch hoch komplexe Nanostrukturen zu Grunde. Die in wissenschaftlicher Hinsicht bislang am besten untersuchten und verstandenen Mikroemulsionssysteme bestehen entweder aus Wasser, Öl und einem einzigen elektrisch ungeladenen nicht-ionischen Tensid oder einem elektrisch geladenen ionischen Tensid. Beide Systeme unterscheiden sich grundlegend, unter anderem in ihrem Phasenverhalten, ihrer Temperaturstabilität oder ihren Nanostrukturen. Systeme mit Mischungen aus ionischen und nichtionischen Tensiden dagegen wurden bisher kaum untersucht.

Im Rahmen dieser Arbeit wurde das Phasenverhalten einer anionischen/nichtionischen Tensidmischung mit verschiedenen Ölen bei konstanter Temperatur und konstantem Tensidgehalt untersucht. Die Phasendiagramme weisen jeweils zwei optisch isotrope Phasengebiete, so genannte Einphasenkanäle, mit steigendem Öl-Gehalt auf. Die beiden Mikroemulsions-Einphasenkanäle sind voneinander durch ein optisch anisotropes Phasengebiet getrennt. Der Mikroemulsionskanal unterhalb des anisotropen Bereichs erstreckt sich von der wässrigen Phase ausgehend mit wachsendem Öl- und nichtionischen Co-Tensid-Anteil bis in die Mitte des Phasendiagramms und endet dort. Der obere Einphasenkanal verläuft durch ein steiles Minimum, in Bezug auf das Tensid/Co-Tensidverhältnis, durchgehend von der wässrigen zur ölreichen Seite des Phasendiagramms. Im Gegensatz zu Mikroemulsionen mit nichtionischen Tensiden handelt es sich um isotherme Einphasenkanäle. Die einphasigen Gebiete wurden mit diversen physikalisch-chemischen Methoden untersucht. Mittels Leitfähigkeits-, SANS-, PFG-NMR-Messungen und elektronenmikroskopischen cryo-TEM Aufnahmen konnten die Nanostrukturen identifiziert werden. Während im unteren Einphasenkanal die Strukturen aus kleinen Öl-Tröpfchen in einer kontinuierlichen Wasserphase bestehen, welche mit zunehmendem Öl-Gehalt anschwellen, kommt es im oberen Einphasenkanal zu einer komplexen Strukturänderung. Während der ölfreien Probe eine bikontinuierliche Schwammstruktur zu Grunde liegt, wandelt sich diese mit bereits wenigen Prozent an Öl zu einer polyedrischen Wasser-in-Öl Schaumstruktur. Für diese, in Mikroemulsionen bislang unbekannt, Struktur wurde der Begriff High Internal Phase Microemulsion (HIPME) eingeführt, aufgrund ihrer strukturellen Parallelen zu bereits bekannten High Internal Phase Emulsionen (HIPE). Mittels transientscher Elektrodoppelbrechung konnte dieser komplexe strukturelle Übergang nachvollzogen werden. Die ermittelten strukturellen Relaxationszeiten, welche zudem die Viskosität der Mikroemulsionen bestimmen, weisen ein deutliches Maximum am Übergangspunkt von der bikontinuierlichen zur HIPME-Struktur auf. Grund für die beobachtete HIPME-Struktur ist vermutlich der Anteil der elektrischen Ladung des anionischen Tensids. Diese sorgt für eine vergleichbar hohe Grenzflächenspannung zwischen der wässrigen verdünnten Tensid-Phase und des Öls. Konsequenz dieser hohen Grenzflächenspannung sind ölkontinuierliche Schaumstrukturen anstatt bikontinuierlicher Strukturen, welche man in vergleichbaren Mikroemulsionen mit rein nichtionischen Tensiden erhält. Durch Abschirmen der elektrischen Ladungen mit Salz werden die HIPME-Strukturen gestört, was sich in einem Ansteigen der Leitfähigkeit und einer erhöhten Mobilität der Wasserphase äußert, welche mit NMR beobachtet wurde.

2. Introduction

2.1. Microemulsions and their applications

Since their discovery by Hoar and Schulman, microemulsions were much in the focus of interest by scientists in the field of colloid and polymer science. In 1943, they described in *Nature* “Transparent Water-in-Oil Dispersions” as they observed transparent oil-continuous systems at high soap/water ratios at the presence of an alcohol, fatty acid, amine or other non-ionic amphipatic substances.¹ They believed that the dispersed water is present in sub-microscopic micelles, consisting of a water-core which is surrounded by a surface monolayer of surfactant-ion-pairs which are interspersed with non-ionic amphiphilic molecules. The hydrocarbon portions of the surfactants are oriented outwards of the micelle towards the continuous oil phase (Fig. 2.1). In addition, they estimated the size of the “oleopathic hydro-micelle” by simple geometric considerations (core-shell model) to a few nanometers, explaining the optical properties of the dispersion. They later introduced the term “microemulsion” as optically isotropic transparent phases, consisting of oil, water and surfactants.²

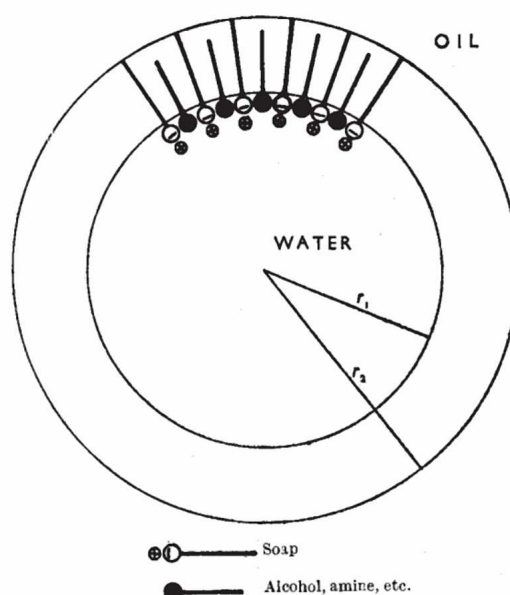


Fig. 2.1 Model of the “oleopathic hydro-micelle” by Schulman and Hoar, consisting of ionic soap and a non-ionic co-surfactant, forming an transparent water-in-oil microemulsion.

In contrast to ordinary emulsions, microemulsions are thermodynamically stable.³ Three different main types of nanostructures can be distinguished in microemulsions, namely oil droplets in a continuous water phase (o/w), water droplets in a continuous oil phase (w/o) and bicontinuous structures.⁴

¹ T. P. Hoar, J. H. Schulman, *Nature* **1943**, 152, 102-103.

² J. H. Schulman, W. Stoeckenius, L. M. Price, *J. Phys. Chem* **1959**, 63, 1677-1680.

³ M. Gradzielski, H. Hoffmann, *J. Phys. Chem* **1994**, 98, 2613-2623.

⁴ F. Lichterfeld, T. Schmeling, R. Strey, *J. Phys. Chem.* **1986**, 90, 5762-5766.

However, microemulsions were already prepared coincidentally before their discovery and used for example since 1928 in domestic cleansing products. A microemulsion prepared from carnauba wax, water, oleic acid, sodium borate and potassium hydroxide for example was sold under the name “AeroWax” and was used as floor polish solution.⁵

An extensive research on microemulsions was finally caused by the two oil crises in 1973 and 1979. Water-surfactant mixtures were pumped into oil-wells that were running dry (tertiary oil recovery). By doing this, oil, which is left in the pores of the rock, can be easily removed as a microemulsion with an ultra-low interfacial tension. Of course, this form of enhanced oil recovery needs a lot of understanding of the phase behaviour of surfactants, the behaviour of the interfacial tension at the water/oil interface and the formation of microemulsions.⁶

Today, microemulsions can be found in various fields of applications. E.g., microemulsions are used in pharmaceutical science as drug delivery systems.⁷ The small size of the microemulsion droplets allows the drugs to penetrate into the blood circuit before being digested in the stomach and therefore arriving faster their targets.

In textile industry, microemulsions can be used as carrier for water insoluble functionalized silicone oils that are used as fabric softeners for improving the feel of textiles.⁸ The dispersion of the oil in microemulsions allows any dilution by water and an optimal spreadability on the treated textile surface. Products are also available that contain modified silicone oils in microemulsion solutions that are applied on textiles to make the surface hydrophobic and dirt repellent.

Another possible application of microemulsions is the use as additive for fuels to reduce the emission of soot.⁹ The water, solubilized in the fuel in form of a thermodynamically stable microemulsion, accelerates the decomposition of the hydrocarbon chains during the combustion of fuel due to radical formation of water. Therefore, the exhaustion of soot can be reduced by 70-80%. In addition, the enthalpy of the evaporating water decreases the combustion temperature. This decreases the formation of toxic nitrogen oxides (NO_x).

A further large field of applications for microemulsions is, of course, the cosmetic industry. Microemulsion formulations that are used as skin care products allow faster uptake of additives that help to retain moisture, reduce impurities, remove everyday dirt, etc. Also many products with “ultrafine emulsions” are established that are prepared on the base of microemulsions.¹⁰ Other examples for applications can be found in food industry, agrochemical industry, environmental detoxification, biotechnology and even more.¹¹

⁵ H. Mollet, A. Grubenmann, in: *Formulierungstechnik – Emulsionen, Suspensionen, Feste Formen*; Wiley-VCH, Weinheim-Germany, **2000**.

⁶ C. Stubenrauch, in: *Microemulsions: Background, New Concepts, Applications, Perspectives*, Wiley-VCH, **2009**.

⁷ M. J. Lawrence, G. D. Rees, *Advanced Drug Delivery Reviews* **2000**, 45, 89-121.

⁸ D. Gräbner, L. Xin, H. Hoffmann, M. Drechsler, O. Schneider, *J. Colloid Interf. Sci.* **2010**, 350, 516-522.

⁹ L. Bemert, S. Engelskirchen, C. Simon, R. Strey, *Am. Chem. Soc., Div. Fuel Chem.* **2009**, 54, 290-291.

¹⁰ R. Miyahara, K. Watanabe, T. Ohmori, Y. Nakama, *J. Oleo Sci.* **2006**, 55, 403-411.

¹¹ B. K. Paul, S. P. Moulik, *Current Science* **2001**, 80, 990-1001.

2.2. Phase behaviour of surfactants

The existence of kinetically stable emulsions or thermodynamically microemulsions would not be possible without surfactants. If energy is added to a water/oil system by stirring or shaking the mixed components, a very unstable dispersion of water in oil or oil in water is the result. This state relaxes quickly to the native state. By adding a surfactant to this mixture, the interfacial tension between water and oil is reduced what allows to establish more stable dispersions of the components.¹² Depending on the mixing ratios of the components and the type of the used surfactant, the results are either water-in-oil (w/o) or oil-in-water (o/w) emulsions.

All this is possible because surfactants have amphiphilic properties. This means in general, they are composed of a hydrophilic and a lipophilic part (Fig. 2.2).

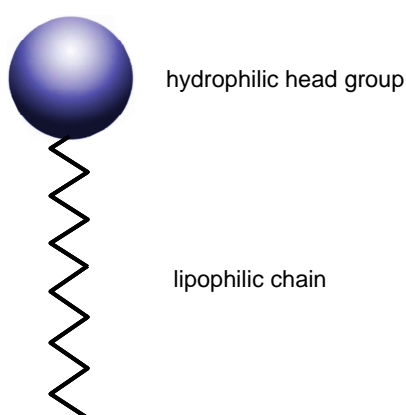


Fig. 2.2 Simplified illustration of a surfactant with a hydrophilic head group and a lipophilic chain.

There is an enormous variety of different surfactants on the market. There are for example non-ionic surfactants, anionic-/cationic surfactants, zwitterionic surfactant¹³, double-chain surfactants¹⁴ or even polymerizable surfactants¹⁵.

In dependence of the used surfactant type, surfactant concentration, temperature or surfactant mixtures, various nanostructures can form in aqueous solutions.¹⁶

Very often, micellar structures are found in diluted surfactant solutions. The aggregation of surfactant molecules to micelles is steered basically on hydrophobic interactions. In aqueous solutions, the lipophilic alkyl-chains of the surfactants form the inner core of the micelle and are separated from the aqueous phase by the hydrophobic head groups. The structure of the aggregates is determined by the packing parameter P ¹⁷:

¹² L.M. Prince, Ed., in *Microemulsions: Theory and Practice*, Academic Press, New York, **1977**.

¹³ A. Gonenne, R. Ernst, *Analytical Biochemistry* **1987**, 87, 28-38.

¹⁴ F. M. Menger, J. S. Keiper, *Angewandte Chemie* **2000**, 39, 1906-1920.

¹⁵ M. Summers, J. Eastoe, *Advances in Colloid and Interface Science* **2003**, 100-102, 137-152.

¹⁶ H. Hoffmann, *Ber. Bunsenges. Phys. Chem.* **1994**, 98, 1433.

¹⁷ J. N. Israelachvili, D. J. Mitchell, B. W. Ninham, *J. Chem. Soc. Farady Trans. II* **1976**, 72, 1525.

$$P = \frac{V_t}{a_0 \cdot l_0}$$

with V_t = volume of the lipophilic chain, l_0 = length of the lipophilic chain and a_0 = required space for the head group. Depending on the packing parameter, the micelles can be spherical micelles, rod-like micelles, disc-like micelles, worm-like micelles or inverse micelles. The micellar phase is described in literature as L_1 phase, the inverse micellar phase as L_2 phase.

When the surfactant concentration is sufficiently high, the molecules can also form double layers. In the classic lamellar phase, the lipophilic surfactant chains are arranged in the inner area of the lamella and the hydrophilic heads in the outside, facing the water phase. The lamellar phase is described as L_α phase in literature. Characteristic for the lamellar phase is the occurring birefringence between crossed polarizer foils (Figure 2.3). The birefringence is caused by the anisotropic properties of the phase, as the lamellas are highly ordered structures. For this reason they are also called liquid crystalline phases.¹⁸ The dilution of the lamellar phase leads to an increasing distance between the surfactant bilayers. This sometimes results in the appearance of fascinating iridescent colours, as the interlamellar distance is matching with the wave length of visible light, leading to interference effects.¹⁹

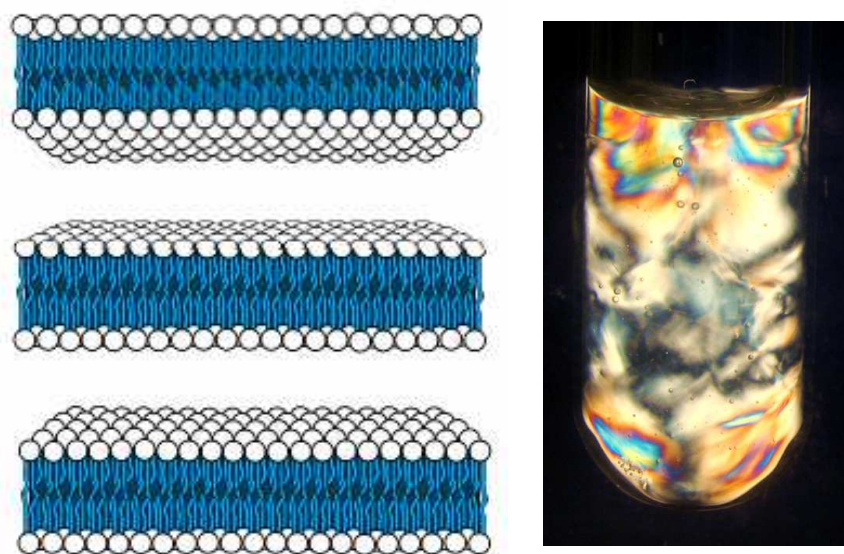


Fig. 2.3 Illustration of a classical lamellar phase and photo of a lamellar phase between crossed polarizer foils.

The viscosity of lamellar phases is quite low, as the membrane double layers can easily slide against each other under shear. This changes when the surfactant double layers arrange to multilamellar vesicles that are formed and arranged like the skin of an onion. The highly viscous multilamellar

¹⁸ K. Fontell, *J. Colloid Interf. Sci.* **1973**, 44, 318-329.

¹⁹ G. Platz, C. Thunig, H. Hoffmann, *Progr. Colloid Polym. Sci.* **1990**, 83, 167-175.

vesicles also show birefringence between crossed polarizers, but show a different texture compared to the classical planar lamellar phase.²⁰

A phase that is closely related to the classical lamellar L_α phase is the bicontinuous L_3 phase. Because of its unusual nanostructure, the highly dynamic L_3 phase is often described as sponge phase.²¹ The L_3 phase shows low viscosity and no birefringence between crossed polarizers. Without detailed investigations, it can easily be mistaken for an L_1 phase.²² L_3 phases are encountered when L_α phases are made more lipophilic by changing a physicochemical parameter of the surfactant system. This is most easily done by increasing the co-surfactant/surfactant ratio in non-ionic surfactant systems²³, by increasing the temperature in alkylpolyglycol systems²⁴ or by increasing the salt-concentration in mixed surfactant systems in which one compound is an ionic surfactant²⁵.

At the beginning of the discovery of the L_3 phase, there has been a big controversy about its structure. For example, a model suggested that the L_3 phase can be formed from the neighboring lamellar phase by breaking up its bilayers into discrete disk-like micelles that are randomly orientated and have the same diameter as the interlamellar distance of the bilayers of the L_α phase.²⁶ This model allowed simple calculations concerning like the scattering behaviour or rotational diffusion coefficients and explained the macroscopic viscosity. However, this model turned out to be wrong, as freeze fracture electron microscopy micrographs showed that the L_3 phase consists of multiconnected but self-avoiding folded bilayers. It also was shown that the bicontinuous sponge phase is formed, when the lamellar phase becomes perforated by passages and therefore transformed from a classical L_α phase to an L_3 phase (Fig. 2.4).²⁷

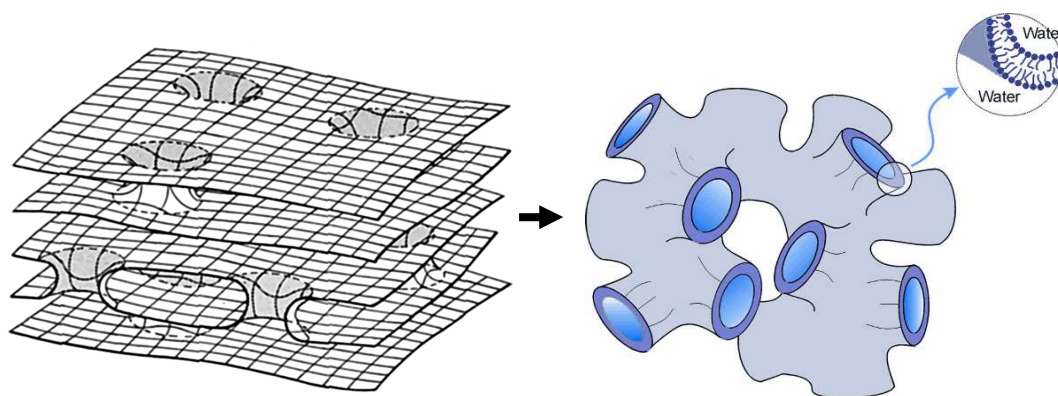


Fig. 2.4 Transformation from L_α phase to bicontinuous L_3 phase by forming passages through the surfactant bilayers of the lamellar phase.

²⁰ S. Haas, H. Hoffmann, C. Thunig und E. Hoinkis, *Colloid Polym. Sci* **1999**, 277, 856-867.

²¹ B. Schwarz, G. Mönch, G. Ilgenfritz, R. Strey, *Langmuir* **2002**, 16, 8643-8652.

²² R. Beck, Y. Abe, T. Terabayashi, H. Hoffmann, *J. Phys. Chem. B* **2002**, 106, 3335-3338.

²³ M. Jonströmer, R. Strey, *J. Phys. Chem.* **1992**, 96, 5993-6000.

²⁴ D. J. Mitchell, G. J. T. Tiddy, L. Waring, T. Bostock, M. P. McDonald, *J. Chem. Soc., Faraday Trans 1* **1983**, 79, 975.

²⁵ K. Fontell in: *Colloidal Dispersions and Micellar Behavior*; ACS Symposium Series No. 9; American Chemical Society: Washington, DC, **1975**; p 270.

²⁶ C. A. Miller, M. Gradzielski, H. Hoffmann, U. Krämer, C. Thunig, *Colloid Polym. Sci.* **1990**, 268, 1066-1072.

²⁷ R. Strey, W. Jahn, G. Porte, P. Bassereau, *Langmuir* **1990**, 6, 1635-1639.

2.3. Microemulsions with non-ionic surfactants

Since the 80s of the 20th century, there has been an increasing focus on the research of the fascinating nanostructures of microemulsions by various methods as self-diffusion NMR²⁸, small angle X-ray²⁹ and neutron scattering³⁰ or transmission electron microscopy³¹. All these measurements helped to establish the knowledge we have today about microemulsions.

Probably most investigated and mostly understood microemulsion systems are those with a single non-ionic surfactant of the type C_iE_j , where i = length of the lipophilic alkyl-chain and j = number of the hydrophilic ethylene oxide groups. When mixed with oil and water, these non-ionic systems show an interesting feature in the phase behaviour, namely the existence of so called “single phase microemulsion channels”. In such channels it is possible to pass from the aqueous phase to the oil phase without crossing phase boundaries at constant surfactant concentrations (Figure 2.5). The nanostructure in these channels changes continuously with increasing mass fraction of oil from oil swollen micelles (o/w microemulsion) to bicontinuous structures at equal amounts of water and oil to inverse micellar structures with oil forming the continuous phase (w/o microemulsion).³²

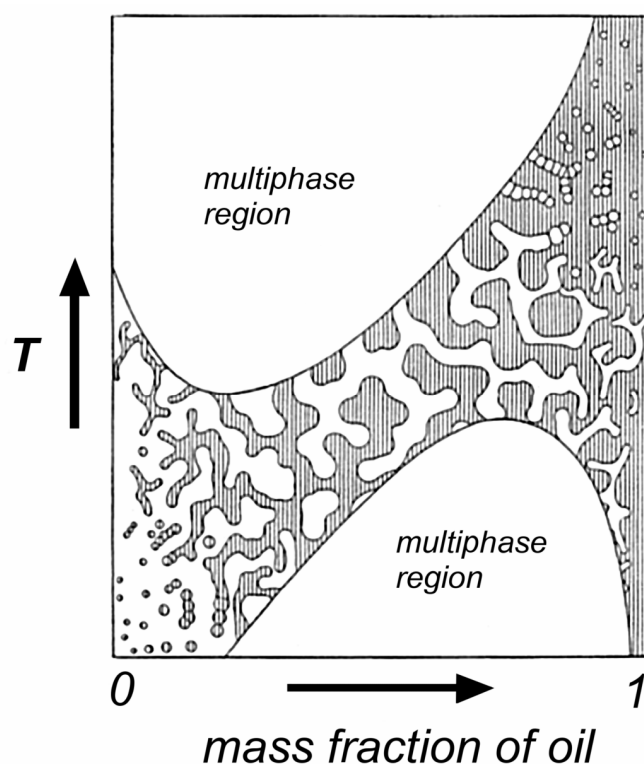


Fig. 2.5 Illustration of the single phase channel in a typical microemulsion system with a single non-ionic surfactant of the type C_iE_j . Schematic overview of the nanostructure indicated in the channel, where the white region indicates the water-rich and the grey shaded areas indicate the oil-rich domains.

²⁸ U. Olsson, P. Schurtenberger, *Langmuir* **1993**, 9, 3389-3394.

²⁹ T. N. Zemb, S. T. Hyde, P.-J. Derian, I. S. Barnes, B. W. Ninham, *J. Phys. Chem.* **1987**, 91, 3814-3820.

³⁰ T. Sottmann, R. Strey, S.-H. Chen, *J. Chem. Phys.* **1997**, 106, 6483-6491.

³¹ R. Strey, *Colloid Polym. Sci.* **1994**, 272, 1005-1019.

³² F. Lichterfeld, T. Schmeling, R. Strey, *J. Phys. Chem* **1986**, 90, 5762-5766.

The changing nanostructures can be easily followed by a steady decrease of the electric conductivity within the channel with increasing mass fraction of oil, when little salt is added to the system.³³

The occurrence of the single-phase channel has to do with the change of the amphiphilic properties of the non-ionic surfactant as non-ionic surfactants of the type C_iE_j become more lipophilic with increasing temperature.³⁴ With increasing temperature, the curvature of the amphiphilic monolayer changes from convex to flat and finally to concave (Fig. 2.6). The reason for this lies in the shrinking of the hydrophilic head-groups (EO-groups). At low temperatures, the size of the surfactant head group is larger than that of the hydrophobic chain, leading to an amphiphilic film curved around the oil. By increasing the temperature, the size of the EO-head group is shrinking, whereas the size of hydrophobic chain increases due to the increasing number of chain conformations and the increasing penetration of oil molecules. These trends lead to a gradual change of the interfacial curvature.³⁵ As a consequence the microemulsion structures change, from the water side, from small oil droplets in water, to bicontinuous structures in the middle of the phase diagram, to w/o droplets on the oil side.

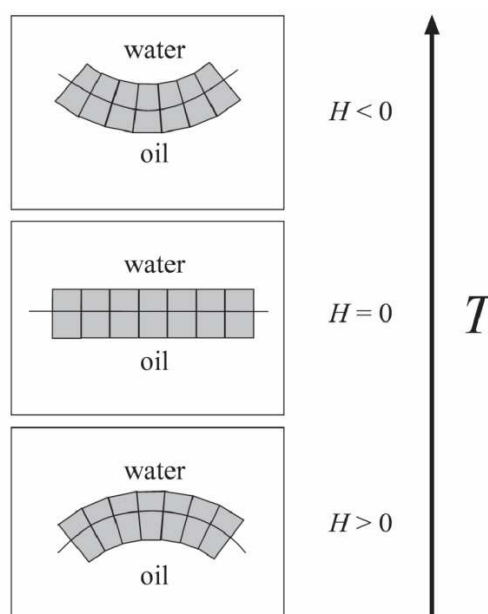


Fig. 2.6 Mean curvature H of a non-ionic surfactant film at the oil/water interface with increasing temperature. The size of the hydrophilic EO-head group is shrinking whereas the size of the lipophilic chain is increasing by raising temperature.

The interfacial tension between the oil and the water is a sensitive parameter for the change of the interfacial curvature. Optimum solubilisation of oil in a system with non-ionic surfactants is obtained

³³ M. Kahlweit, et. al, *J. Colloid Interf. Sci* **1987**, 118, 450.

³⁴ K.. Shinoda, *Proceedings of the 5th International Congress of Surface Activity, Barcelona, Spain, Vol. 2, 1969*, 275-283.

³⁵ J. Lyklema, in: *Fundamentals of interface and colloid science, Volume V: Soft Colloids*, Academic Press Inc, **2005**.

at the minimum of the interfacial tension of the diluted aqueous surfactant solution against the oil.³⁶ For non-ionic surfactants, ultra-low interfacial tensions against the oil-phase are observed that can be as low as 10^{-3} mN/m. A typical curve for the change of the interfacial tension is shown in Fig. 2.7.

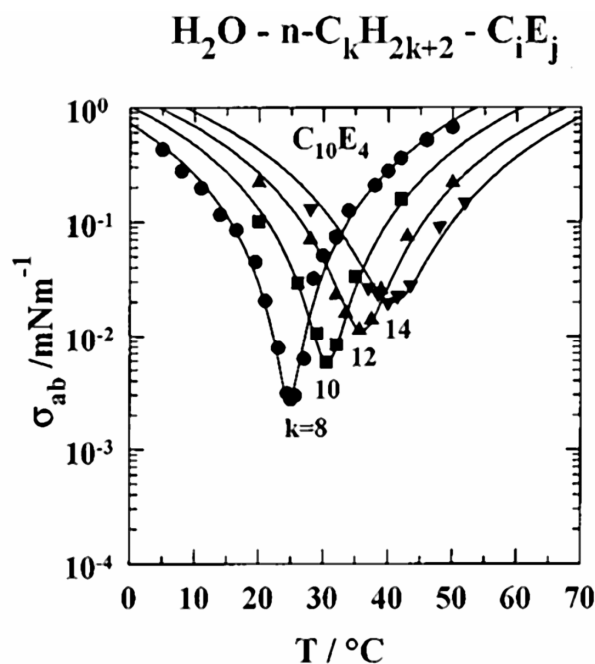


Fig. 2.7 Ultra low interfacial tension of the diluted non-ionic surfactant C_{10}E_4 against alkane oils with the chain length k between 8 and 14.

Bicontinuous microemulsions are obtained in the region of the minimum of the interfacial tension, as low interfacial tensions allow non-spherical structures due to the equilibrium in the interfacial curvature.

2.4. Microemulsions with ionic surfactants

The situation in microemulsion systems with ionic surfactant is very different compared to microemulsions with non-ionic surfactants. The probably most investigated systems are those with AOT (sodium di-2-ethylhexylsulfosuccinate), decane, H_2O and DDAB (didodecyldimethylammonium bromide), dodecane, H_2O .^{37,38} The single phase regions in such systems are usually plotted in triangular phase diagrams (Gibbs phase diagrams). An example for such a phase diagram of the system DDAB, dodecane, H_2O is shown in figure 2.8. The isotropic phase regions (microemulsions) in these triangle presentations are very different for those of non-ionic surfactants.³⁹ Systems with ionic

³⁶ T. Sottmann and R. Strey, *J. Chem. Phys.* **1997**, 106, 8606–8615

³⁷ M. Kotlarchyk, S.-H. Chen, J. S. Huang, M. W. Kim, *Phys. Rev. Lett.* **1984**, 53, 941-944.

³⁸ K. Fontell, A. Ceglie, B. Lindman, B. Ninham, *Acta Chemica Scandinavica A40* **1986**, 247-256.

³⁹ M. Kahlweit, R. Strey, *Angew. Chem. Int. Ed. Engl.* **1988**, 24, 654-668.

surfactants, which have been studied usually, contain large isotropic regions in the middle of the triangle while phase diagrams with non-ionic surfactants are very different and contain narrow isotropic channels. However, microemulsion systems with single ionic surfactants channels do not have single phase channels that pass from the aqueous side without crossing a phase boundary continuously to the oil side of the phase diagram.

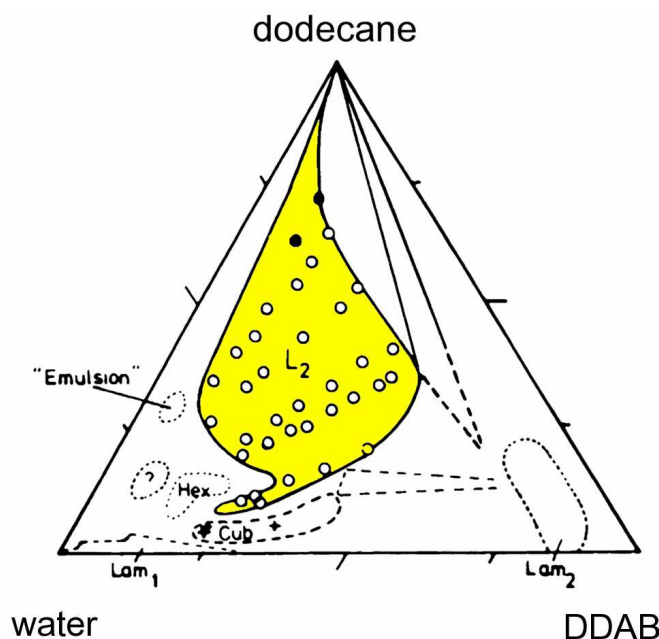


Fig. 2.8 Ternary phase diagram of the system DDAB, water and dodecane. The single phase microemulsion area L_2 is indicated as yellow.

The nanostructures of microemulsions with ionic surfactants have been investigated in detail by SANS, SAXS, electrical conductivity and finally imaged by freeze fracture electron microscopy.⁴⁰ The results showed that the morphology of the microemulsions for equal amounts of water and oil is completely different to those of non-ionic surfactants. Instead of a bicontinuous microemulsion phase, there was found a water-in-oil droplet structure. In Figure 2.9, two FF-TEM micrographs show the droplet structure of the systems AOT-decane- H_2O and DDAB-dodecane- H_2O . It is possible to dilute these phases with oil without the droplets would change in size or structure. The droplet structure is caused by the electric charges of the ionic surfactant that result in higher interfacial tensions compared to microemulsion systems with non-ionic surfactants. However, it was shown by conductivity experiments that the oil-continuous w/o-droplet structures at equal amounts of water and oil can be transformed to samples that have similar bicontinuous features as microemulsions with non-ionic surfactants by shielding the charge on the surfactant layers by excess salt.⁴¹

⁴⁰ W. Jahn, R. Strey, *J. Phys. Chem.* **1988**, 92, 2294-2301.

⁴¹ W. Sager, W. Sun, H.-F. Eicke, *Progr. Colloid Polym. Sci.* **1992**, 89, 284-287.

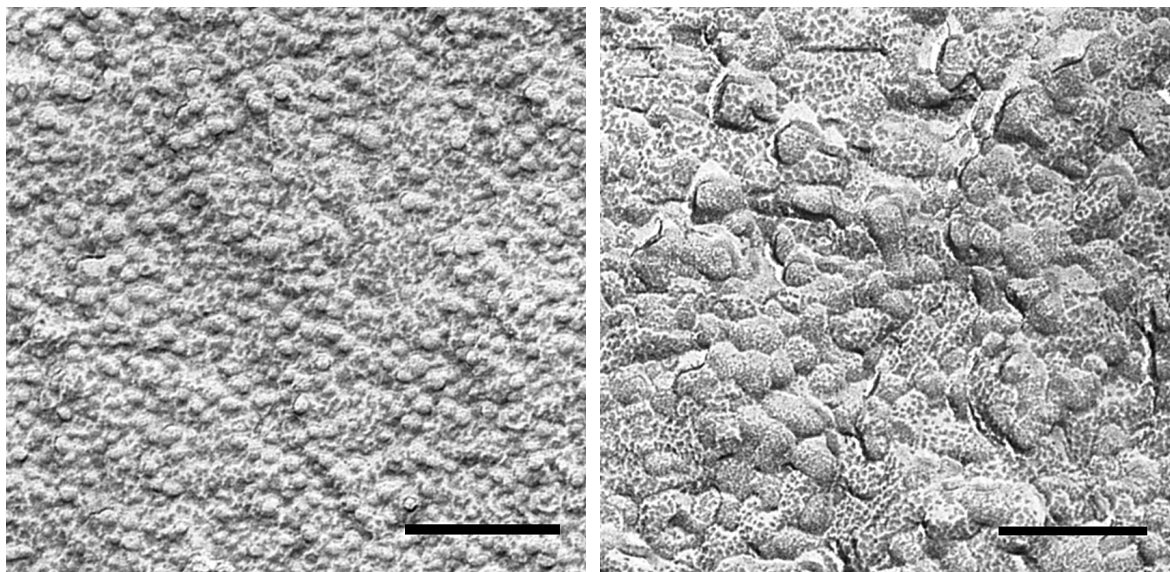


Fig. 2.9 FF-TEM micrographs of w/o-microemulsions with ionic surfactants at equal amounts of water and oil. Left micrograph: droplet structure of the system AOT (20 wt %), decane and water, right picture: aggregated structure of deformed droplets of the system DDAB (13.9 wt %), dodecane and water. Scale bar = 200 nm.

In addition, microemulsions from ionic surfactants are less sensitive to temperature changes and stable over a wider temperature range than microemulsions with non-ionic surfactants, which quickly can drop out of phase when the temperature is not adjusted accurately by a few degrees.

2.5. Objectives of this thesis

Microemulsion systems with single non-ionic surfactants and single ionic surfactants are investigated in detail and well understood. However, there are only few studies of properties of microemulsions with mixed surfactants. The behaviour of mixtures with different surfactants is not easy to predict, as the temperature effect on the solubility and the phase behaviour of non-ionic and ionic surfactants are very different.⁴² It should be noted that some results on the influence of ionic surfactants on phase diagrams of non-ionic microemulsions have already been published.⁴³ It was observed that the isotropic channels were widened by the influence of ionic surfactants and that the surfactant efficiency was increased.⁴⁴ Nevertheless, there is no information on the structures of the isotropic channel, and no detailed phase diagrams of a four-component system were established.

⁴² H. Kunieda, K. Hanno, S. Yamaguchi, K. Shinoda, *J. Colloid Interf. Sci.* **1985**, 107, 129-137.

⁴³ M. Kahlweit, B. Faulhaber, G. Busse, *Langmuir* **1994**, 10, 2528-2532.

⁴⁴ J. A. Silas, E. W. Kaler, *Langmuir* **2001**, 17, 4534-4539.

As shown in 2.3, the evolution of the different microemulsion structures in the single phase channel of non-ionic surfactants is based on the change of the interfacial curvature with temperature. It is known that the interfacial curvature can also be controlled by the interfacial composition, when a hydrophilic surfactant is mixed with a lipophilic co-surfactant.⁴⁵ Such a situation is shown in Figure 2.10.

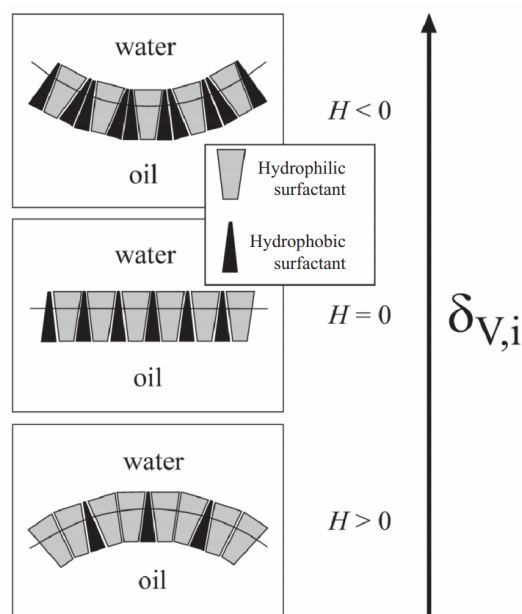


Fig. 2.10 Change of the mean curvature H by mixing a hydrophilic with a hydrophobic surfactant. The decrease of H with increasing amount of the hydrophobic surfactant in the composition of the interface $\delta_{V,i}$ is caused by the smaller head group of the hydrophobic co-surfactant compared to the hydrophilic surfactant.

The aim of this work was to establish a microemulsion system with a surfactant mixture based on an anionic hydrophilic and a lipophilic co-surfactant and to prepare a phase diagram of a four-component system at constant temperature. As it is well known that the increase of temperature makes ionic surfactants more hydrophilic while non-ionic surfactants become more lipophilic⁴⁶, it was hoped that these both effects would compensate in such a microemulsion system and therefore result in a system that is mostly independent to temperature variations. This is of great interest for possible applications, for example in the field of cosmetic industry or other areas like enhanced oil recovery.

In addition, the similarities and the differences of such mixed systems compared to the basic non-ionic or ionic microemulsion systems should be investigated by different physicochemical methods, as conductivity, rheology, PFG-NMR and electron microscopy.

⁴⁵ J. Reimer, O. Södermann, T. Sottmann, K. Kluge, R. Strey, *Langmuir* **2003**, 19, 10692-10702.

⁴⁶ S. Ajith, A. K. Rakshit, *J. Phys. Chem* **1995**, 99, 14778-14783.

3. Synopsis

3.1. The surfactant system $\text{Ca}(\text{DS})_2/\text{Mg}(\text{DS})_2 - \text{IT 3}$

In the publication „Microemulsions from silicone oil with an anionic/non-ionic surfactant mixture“, we first introduced a new surfactant combination, that turned out to be an interesting choice for the preparation of microemulsions. The main idea was to establish a microemulsion phase diagram in the style of non-ionic microemulsion systems, in which isotropic microemulsion single phase channels exist that run from the aqueous side of the phase diagram to the oil-side without passing a phase boundary. Instead of varying the temperature to influence the interfacial curvature of the surfactant film, we wanted to establish such single phase channels in an isothermal microemulsion system by adjusting the mixing ratio of two different surfactants, namely a hydrophilic and a lipophilic one. Although the idea to use surfactant mixtures for the preparation of microemulsions is not new, no detailed phase diagrams with such a system have been investigated yet. As hydrophilic surfactant, we chose calciumdodecylsulfate, as it was already known that Ca^{2+} -salt of SDS can form lamellar phases and even sponge-like phases, when it is mixed with short chain alcohols as co-surfactants. This is not possible for normal SDS. As lipophilic co-surfactant we chose an industrial non-ionic surfactant that is based on a highly branched isotridecanol which is etherified with an average number of three ethylene-oxide groups (isotridecyltriethyleneglycolether, abbreviated as IT 3). By mixing both surfactants, we received a huge variety of different phases, starting by a micellar L_1 phase with the pure $\text{Ca}(\text{DS})_2$, going over to a large birefringent lamellar area with increasing mass fraction of the lipophilic co-surfactant and finally ending with a two-phase situation in that the IT 3 is forming inverse micelles which are separating from the lower aqueous phase (Fig. 3.1). Rheological results indicated that the lamellar structures change from multilamellar vesicles to planar lamellas with increasing mass fraction of the lipophilic co-surfactant.

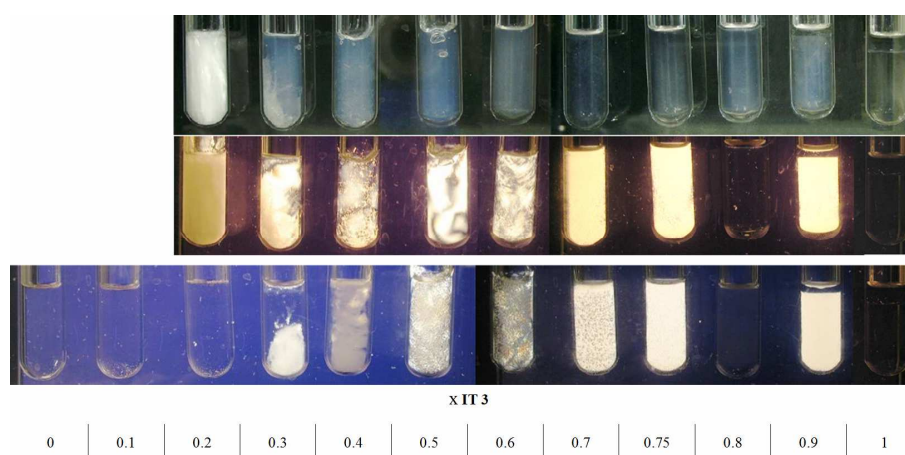


Fig. 3.1 Surfactant mixtures of $\text{Ca}(\text{DS})_2$ (two upper rows) or $\text{Mg}(\text{DS})_2$ (lower row) with increasing mass fraction x of IT 3. First row shows surfactant mixtures with $\text{Ca}(\text{DS})_2$ in direct light. Second and third rows show samples with $\text{Ca}(\text{DS})_2$ and $\text{Mg}(\text{DS})_2$ between crossed polarizers. Samples prepared with a total surfactant concentration of 15% (w/w), phases observed at $T = 40^\circ\text{C}$.

All samples were prepared with a constant surfactant concentration of 15% (w/w) and the phase behaviour was investigated at 40 °C. Most important results are the presence of two isotropic microemulsion single phase channels, which are separated by a birefringent anisotropic area. The upper microemulsion channel extends from the aqueous side of the phase diagram continuously to the oil-side, while the lower single phase channel ends in the middle of the phase diagram at equal amounts of water and oil.

As already mentioned, such microemulsion channels also exist in phase diagrams with single non-ionic surfactants, where the hydrophilic-lipophilic balance is adjusted by raising temperature. An example of such a phase diagram with $C_{12}E_5$ as surfactant and tetradecane as oil is shown in figure 3.3.⁴⁷

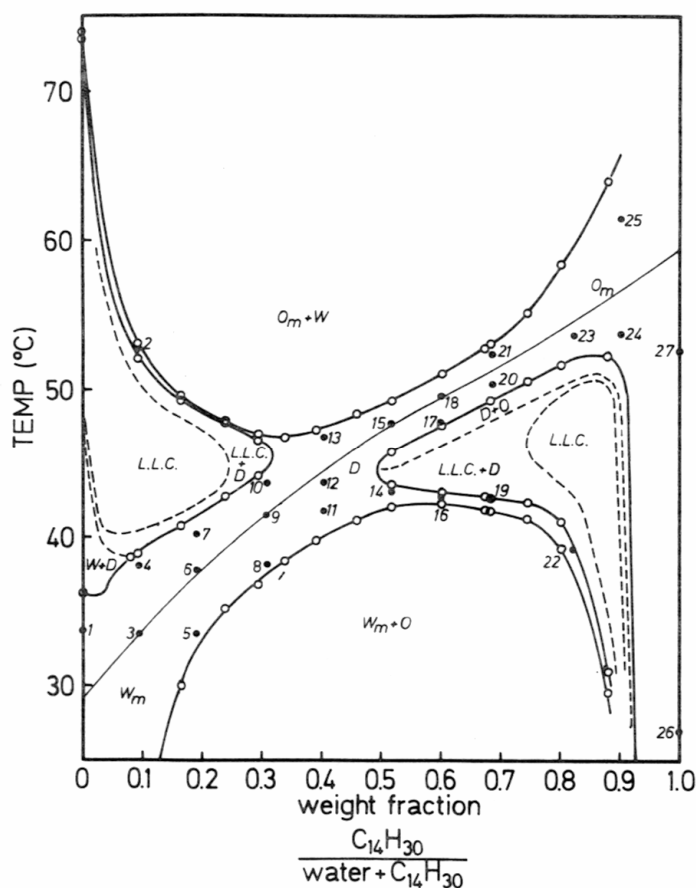


Fig. 3.3 Phase diagram of the system $C_{12}E_5 - H_2O/Tetradecane$ with constant 16.6 wt % surfactant. W_M = water continuous microemulsion, O_M = oil continuous microemulsion, D = bicontinuous microemulsion, $L.L.C$ = lyotropic liquid crystalline.

In such systems the nanostructure on the microemulsion changes with increasing temperature and with increasing oil content from oil-droplets in a continuous water phase to bicontinuous microemulsions at equal amounts of water and oil and finally to water-droplets in a continuous oil-phase at the oil-rich

⁴⁷ U. Olsson, K. Shinoda, B. Lindman, *Journal of Physical Chemistry*, **1986**, 90, 4083.

side of the phase diagram. The upper channel that starts at the isotropic L_3 sponge phase at higher temperature joins the lower channel in the first half of the phase diagram.

An important difference between both shown phase diagrams is the fact, that the microemulsion channels are not connected with each other in the mixed anionic-non-ionic surfactant system.

Although microemulsions from both channels are transparent and optical isotropic, samples in the upper single phase channel are somewhat bluish and show some shear induced birefringence with up to 40% of oil in the solvent mixture. This is a first indication, that the nanostructures in both channels must be very different. Conductivity experiments finally gave evidence, that this is indeed the case. While the conductivity values in the lower single phase channel stayed about the same, there was found an abrupt decrease of the electrical conductivity in the beginning of the upper single phase channel with only about 5% of oil in the solvent mixture. At equal amounts of oil and water, no conductivity could be detected any longer. We concluded from the results, that the nanostructure in the upper channel might switch from a bicontinuous morphology to a water-in-oil system, while the oil-in-water structures in the lower channel remain the same with increasing oil-concentration.

3.3. Cryo-TEM imaging of the microemulsion system $\text{Ca}(\text{DS})_2/\text{IT 3} - \text{H}_2\text{O}/\text{M}_2$

To verify the different nanostructures which were concluded from the experimental results that were presented in the first publication about the new microemulsion system, we tried to image them directly by cryogenic transmission electron microscopy (cryo-TEM) and discussed the results in a second publication. In the cryo-TEM technique, a small droplet of the sample is pipetted on a perforated carbon film that is supported by a TEM copper grid. With the help of a piece of filter paper, excess liquid is blotted away until a thin liquid film with a desired average thickness of about 200 nm is left in the holes of the perforated carbon. After blotting, the specimen is plunged into a suited cryogen for vitrification. After vitrification, the specimen is transferred under liquid nitrogen into the electron microscope. The specimen preparation can be performed in a so called controlled environment vitrification system (CEVS), in which both the atmosphere as well as the temperature can be controlled.⁴⁸ This point is very important for the specimen-preparation of temperature sensitive samples and/or samples that contain volatile compounds.

For the preparation of the water-continuous samples, we used liquid ethane as cryogen as it provides cooling-rates that are fast enough to vitrify H_2O and no ice-crystals should disturb the image. The imaging of the binary surfactant system could be performed without major problems and the results supported the rheological results. The cryo-TEM micrographs show a transition from multilamellar vesicles to planar lamellas with increasing mass fraction of IT 3 in the surfactant mixture. We finally observed the transition from a lamellar structure to a bicontinuous network-structure of the neighbouring L_3 phase (Figure 3.4). As the cryo-TEM method only shows a two-dimensional

⁴⁸ Y. Talmon, in: "Seeing Giant Micelles by Cryogenic-Temperature Transmission Electron Microscopy (Cryo-TEM)", in "Giant Micelles", chapter 5, R. Zana, E. A. Kaler, Eds., CRC Press, New York, 2007, 163-178.

projection of the various domains, the sponge-like character of the phase is not as well visible as with other methods as freeze fracture electron microscopy, that can reproduce better the three-dimensional morphology.⁴⁹ That is why the structure seen on the cryo-TEM micrograph could also be taken for a network of thread-like micelles instead of a bicontinuous sponge phase.

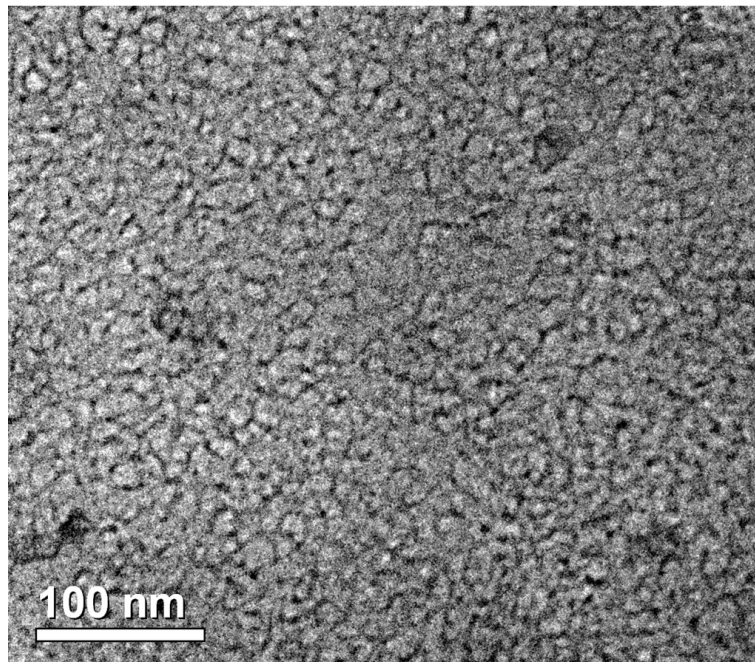


Fig. 3.4 Cryo-TEM micrograph of sample with 15% (w/w) surfactant $\text{Ca}(\text{DS})_2/\text{IT } 3$, $x \text{ IT } 3 = 0.77$, prepared at 40 °C. Micrograph shows bi-continuous network-structure of the L_3 phase.

The imaging of the microemulsion phases with the silicon oil was more challenging. Although we tried to saturate the atmosphere in the CEVS, it was for example not possible to image clearly the structure of the microemulsions in the lower single phase channel. Instead of tiny microemulsion droplets, small unilamellar vesicles and also multilamellar vesicles were mostly imaged. The problems with the sample preparation were obviously caused by the high volatility of the short chain silicone oil, as relaxation experiments indicated. Hexamethyldisiloxane has evaporation rates which are comparable to acetone. In such relaxation experiments, a certain amount of time is stopped after the blotting-procedure during cryo-TEM specimen preparation, before the sample is plunged into the cryogen. Thereby it can be investigated if the nanostructure changes due to small changes in the sample composition. In figure 3.5, two cryo-TEM micrographs of the same sample from the lower single phase channel with 15% of oil in the solvent mixture are shown. While the micrograph of the quickly prepared specimen shows structures that remind to oil-swollen micelles and some multilamellar vesicles, the micrograph of the specimen that has been prepared with a delay of 30 seconds before the plunging shows collapsed structures and large (multilamellar) vesicles. The

⁴⁹ H. Hoffmann, C. Thunig, U. Munkert, H. W. Meyer, W. Richter, *Langmuir* **1992**, 8, 2629-2638.

conclusion is that the composition of the original microemulsion must have changed to the neighbouring lamellar phase by losing some oil.

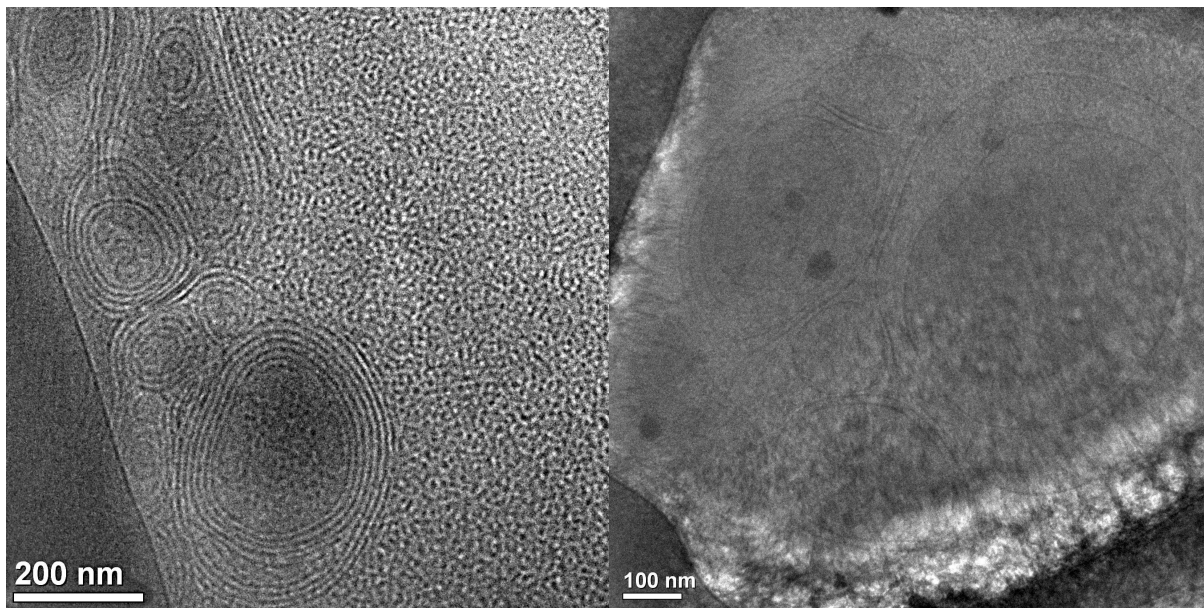


Fig. 3.5 Cryo-TEM micrographs of sample with 15% (w/w) surfactant $Ca(DS)_2/IT\ 3$, $x\ IT\ 3 = 0.4$, $x\ M_2 = 0.15$, prepared at 40 °C. Left picture: quick specimen-preparation, tiny droplets with size of ~ 12 nm and multilamellar vesicles; right picture: micrograph of same sample, but prepared with 30 seconds relaxation time, collapsed irradiated structures and some huge vesicles.

For the oil-continuous microemulsions from the upper channel, we had to change the cryogen from liquid ethane to liquid nitrogen for the cryo-TEM specimen preparation, as the ethane would have dissolved the oil.⁵⁰ Nevertheless, the cooling rate of liquid nitrogen is sufficient to vitrify the oil. In Figure 3.6, two cryo-TEM micrographs from the upper single phase channel are shown. The micrograph of the sample with 5% oil in the solvent mixture shows a fascinating bicontinuous structure, in which the water-domains are encircled by twisting surfactant layers. Undeniably, the bicontinuous structure with 5% oil looks very different in comparison to the fishing-net-like structure of the oil-free L_3 phase that is shown in figure 3.4. Obviously, there is a major structural transition, when some oil is solubilized between the surfactant bilayers of the L_3 phase. This also explains the drastic decay of the conductivity in this region, as the constraints for the transport of the ions must be much larger than in the L_3 phase. The cryo-TEM micrograph of the microemulsion sample with equal amounts of water and oil doesn't show a bicontinuous structure anymore. Instead, there can be seen densely packed water droplets in a continuous oil phase. Some droplets seem to have black cores on the micrograph. All these particles are crystalline ice which is formed during the rapid cooling process. As liquid nitrogen had to be used as cryogen, the cooling rate was not sufficient to vitrify the water. Thus, the small water domains freeze into crystalline hexagonal ice. These nano-crystals are randomly oriented with respect to the electron beam, so that only a few satisfy Bragg's law for electron

⁵⁰ L. Belkoura, C. Stubenrauch and R. Strey, *Langmuir* **2004**, 20, 4391–4399.

diffraction, and those appear dark. The ice crystals that do not diffract the electrons appear light grey. The successfully imaged water-in-oil microemulsion droplets confirmed the conclusions that were drawn from the conductivity results. The sizes of the microemulsion droplets are consistent with simple geometric considerations. Obviously, the structural changes within the microemulsion channels are different in our anionic/non-ionic surfactant mixture compared to microemulsion systems with a single non-ionic surfactant where bicontinuous microemulsions dominate the area in the phase diagram with equal amounts of water and oil. The observed water-in-oil-structure in the new microemulsion system with the mixed surfactant system is probably caused by the electric charges of the anionic surfactant $\text{Ca}(\text{DS})_2$. One has to mention that water-in-oil structures at a water:oil ratio of 1:1 were already found in microemulsions with the anionic surfactant AOT, water and decane.⁵¹ Nevertheless, no continuous microemulsion single-phase channel region exists in such a system that reaches from the aqueous to the oil-rich side of a phase diagram at constant surfactant concentration. In this respect, the situation in the new mixed anionic/non-ionic surfactant system is somewhere between, as it combines the features of a continuous single phase channel that can be found in non-ionic systems with the presence of water-in-oil-microemulsions at equal amounts of water and oil that are found in microemulsions with the anionic AOT.

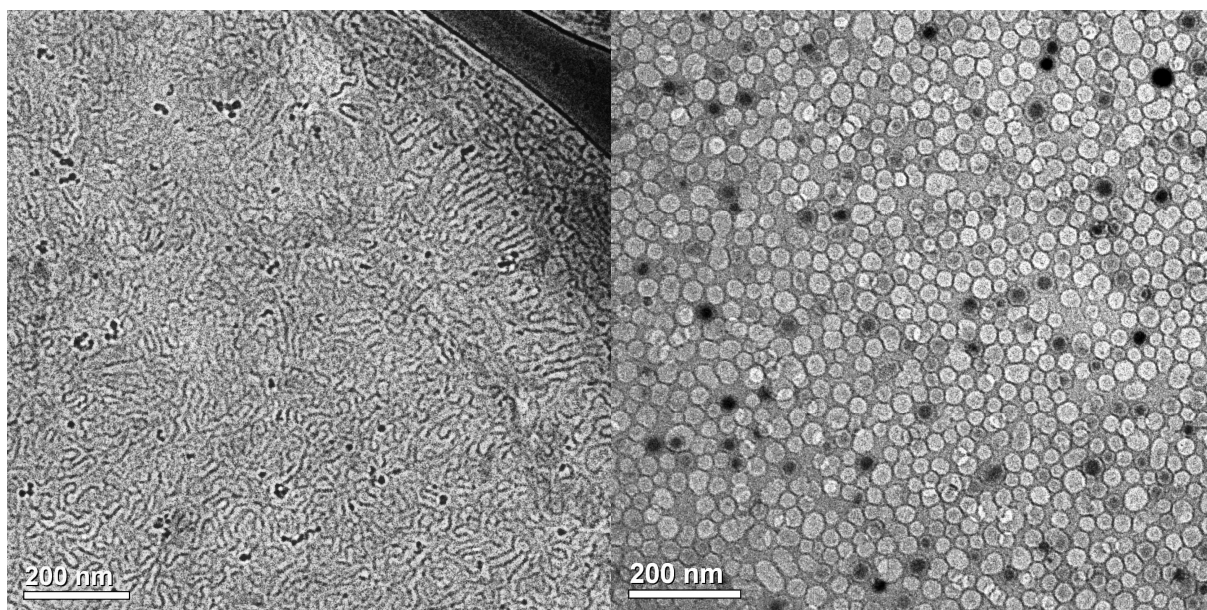


Fig. 3.6 Cryo-TEM micrographs of samples in the upper single phase channel with 15% (w/w) surfactant, left picture: $\text{Ca}(\text{DS})_2/\text{IT 3}$, $x \text{ IT 3} = 0.65$, $x \text{ M}_2 = 0.05$, sponge-like structure; right picture: $x \text{ IT 3} = 0.9$, $x \text{ M}_2 = 0.5$, densely packed water droplets in continuous oil-phase.

⁵¹ W. Jahn and R. Strey, *J. Phys. Chem.* **1988**, 92, 2294–2301.

3.4. Dynamic properties of microemulsions in the single phase channels

3.4.1. Introduction of the microemulsion system $\text{Mg}(\text{DS})_2/\text{IT 3} - \text{H}_2\text{O}/\text{decane}$

Although the initially investigated microemulsion system showed some new interesting properties, we had to modify the system for more detailed investigations. First problems in experiments with the initially investigated system occurred because of the high Krafft-temperature of the $\text{Ca}(\text{DS})_2$ around 60 °C. Microemulsions with higher mass fractions of $\text{Ca}(\text{DS})_2$ in the lower single phase channel suffered from precipitation of the surfactant at room temperature. We therefore investigated the phase diagram at 40 °C to compensate this problem. In addition, the high volatility of the silicone oil made other experimental investigations of the microemulsions more complicated, as the cryo-TEM micrographs already indicated. The high temperature of 40 °C even increased the problem of volatility. This made rheological or electric birefringence experiments impossible, as small amounts of the silicone oil evaporated during the measurements. For the modified system, we first replaced the $\text{Ca}(\text{DS})_2$ by $\text{Mg}(\text{DS})_2$, as it has a lower Krafft-temperature of 25 °C. The silicone oil was replaced by the less volatile hydrocarbon oil n-decane, as we knew from initial solubilisation experiments that n-decane behaves similar like M_2 . To prevent freezing artefacts in planned freeze-fracture electron micrographs, we prepared all samples with 20% of glycerol in the aqueous fraction. All these modifications made it possible to establish a phase diagram at room-temperature that didn't suffer from evaporation of oil. This modified microemulsion system was introduced in the third publication "Dynamic Properties of Microemulsions in the Single Phase Channels".

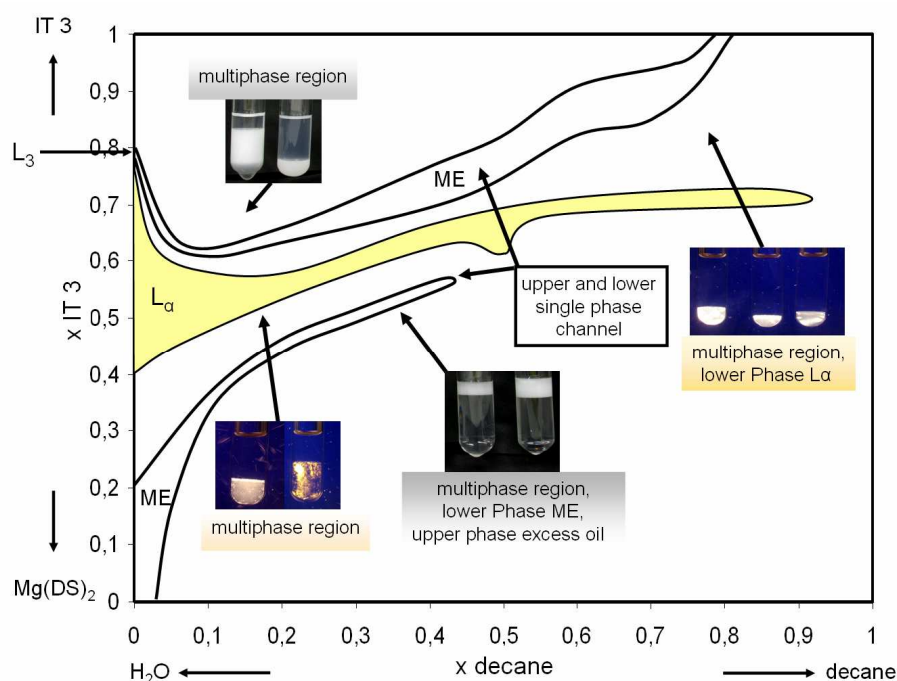


Fig. 3.7 Phase diagram of system $\text{Mg}(\text{DS})_2/\text{IT 3} - \text{H}_2\text{O}/\text{decane}$ at 15% (w/w) surfactant and 25 °C, 20% glycerin in H_2O , $x \text{ IT 3}$ = mass fraction of IT 3 in the surfactant mixture, $x \text{ decane}$ = mass fraction of decane in the solvent mixture. "ME" indicates isotropic microemulsion area, and L_α indicates area of anisotropic lamellar channel.

The phase diagram of the new microemulsion system (Figure 3.7) shows more or less the same features as the phase diagram with the silicone oil. Nevertheless, there are some minor differences that are worth emphasising. In contrast to the microemulsion system with the silicone oil that was investigated at 40 °C, the upper single phase channel of the new system doesn't run completely to the oil-side of the phase diagram. The microemulsion channel only extends to about 80% of oil in the solvent mixture. Obviously, the co-surfactant IT 3 is not lipophilic enough to solubilize more than 80% of oil at room temperature. This can be changed by rising the temperature from 25 °C to again 40 °C. Another difference is related to the single phase lamellar region that separates both microemulsion channels. In the new system, this anisotropic region is notably larger and extends from 0% to 90% oil. Such large anisotropic single phase regions do not exist in the phase diagrams of non-ionic microemulsions. Moreover, all phases within this anisotropic region are temperature stable from 10 °C to at least 40 °C.

To check, if the nanostructures in the single phase channels are the same as in the previously investigated microemulsion system, the conductivity values were measured again to distinguish between water- and oil continuous microemulsions. While the conductivity values in the lower channel remained on high values and only changed slightly with the surfactant composition, the decay of the conductivity within the upper single channel was even more drastically compared to the previously investigated system. With only about 10% of oil, the conductivity decreases three orders of magnitude (Figure 3.8).

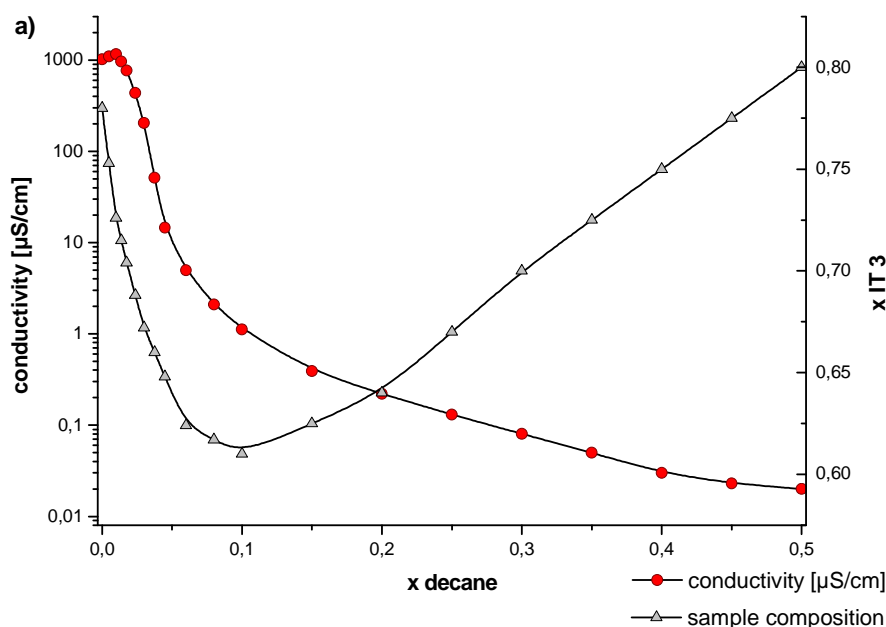


Fig. 3.8 Plot of conductivity in the upper single phase microemulsion channel; conductivity values (red dots) and IT 3 content (grey triangles) against mass fraction of decane in the solvent mixture.

Again, the nanostructure must go through a drastic transition from a bicontinuous to an oil-continuous system. Small angle neutron scattering experiments showed, that the interlamellar distance is

increasing from about 20 nm in the L_3 phase to about 40 nm in the microemulsion with 10% decane. By raising the oil-concentration to 30% decane, the interlamellar distance doesn't change much. This indicates that the main structural transition must be between 0% and 10% of oil. Freeze fracture electron micrographs confirmed again, that the structure in the upper channel changes from a bicontinuous sponge phase to globular particles, while the micrographs for the lower channel showed this time well-defined tiny oil droplets in a continuous water phase.

3.4.2. Electric birefringence and rheology measurements

To study the dynamic behaviour of the microemulsions, the samples were investigated by the electric birefringence method. This method is based on the fact that an electric field can cause an orientation of colloidal particles in solution if the particles have a permanent dipole moment or an anisotropy of the electric polarisability. As a result of this orientation, the solution becomes optically anisotropic or birefringent.⁵² The intensity of the birefringence is detected by a photomultiplier and the signal recorded in dependence of time. The basic process of such an orientation and the resulting signal of a simple system are illustrated in Figure 3.9.

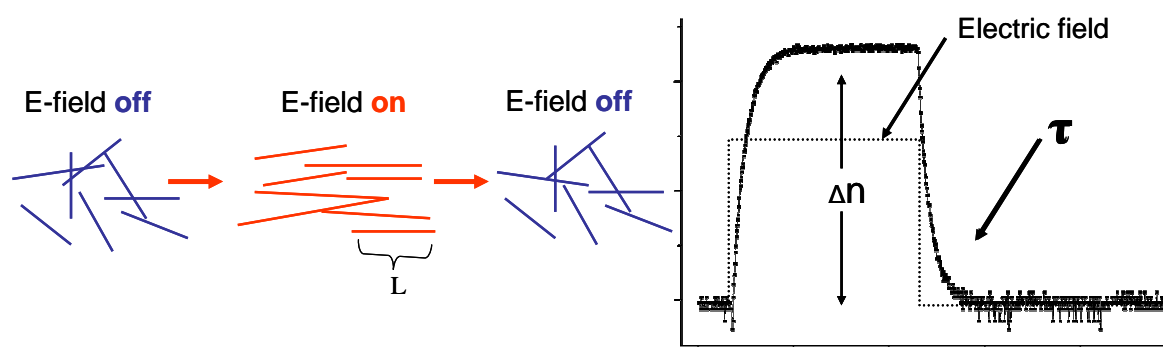


Fig. 3.9 Particles with the length L get orientated in the electric field. The anisotropic orientation causes an increase in the signal intensity. The maximum amplitude Δn indicates an equilibrium state of the oriented particles. By turning off the electric field, the signal decays with the relaxation time τ .

When the electric field is turned off, the particles with the length L randomize by losing their anisotropic orientation. This causes an exponential decay of the birefringence signal which can be fitted with a single time constant τ . The time constant τ is called relaxation time and is proportional to the third power of the particle length ($\tau \sim L^3$). This means that the electric birefringence is a very sensitive method to detect very small changes in the size of particles.

In Figure 3.10, the design of the electric birefringence device is drafted. The light beam of a 3.5 mW HeNe laser is polarized linearly by a Glan prism polarizer and traverses the sample cell (Kerr cell). Having passed the cell, the light beam enters a second polarizer which is set in crossed position to the

⁵² H. Hoffmann, W. Schorr, *J. Phys. Chem.* **1981**, *85*, 3160–3167.

first polarizer. The light that emerges from the second polarizer is detected by a fast photomultiplier. The output voltage of the photomultiplier is recorded by a fast transient recorder (Voltcraft DSO-2090) and directly imaged with a computer. The transient recorder is connected to a high voltage pulse generator. After a trigger impulse, an electric field is produced in the Kerr cell by applying rectangular voltage pulses of short rise and fall times (~ 25 ns) to the electrodes. The pulse length can be adjusted from 50 ns to 10 ms, the maximum voltage is 2.5 kV.

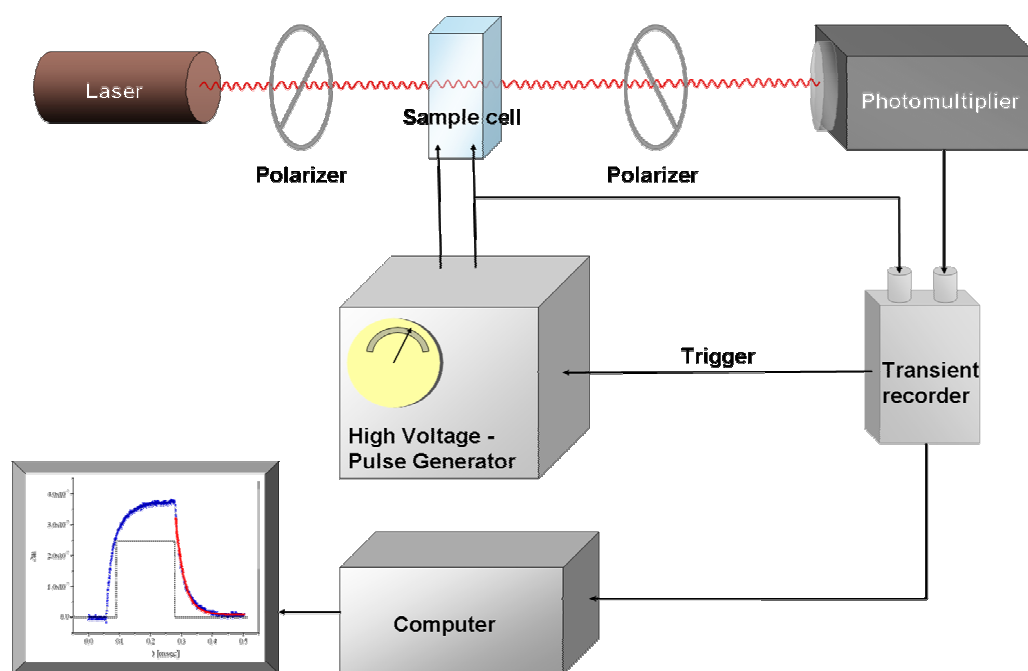


Fig. 3.10 Design of the electric birefringence device.

Electric birefringence measurements are usually carried out on colloidal systems to determine the dimension of particles and their optical anisotropy.⁵³ Good results were also obtained by measuring the signals of L_3 phases.⁵⁴ The signals are caused by the deformation of the bicontinuous structures in the electric field. The structural relaxation time controls the macroscopic dynamic properties of the phase. Electric birefringence measurements were made all along the microemulsion single phase channel to determine these structural relaxation times. While the signal for the L_3 phase is a simple signal where both the build-up as well as the decay of the birefringence can be fitted with a single time constant, the signal becomes very complicated, when more than 0,5% of oil are solubilized in the L_3 phase. An example for the signal of a sample of the upper microemulsion channel that contains 6% of decane is shown in figure 3.11. When the electric field is turned on, there is a superposition of three separate processes with three different relaxation times. When the field is turned off, all processes are visible

⁵³ W. Schorr, H. Hoffmann, *Physics of Amphiphiles: Micelles, Vesicles and Microemulsions: Proceedings of the International School of Physics*; V. Degiorgio, M. Corti, Eds.; North-Holland: Amsterdam, **1985**; pp 160-180.

⁵⁴ C. A. Miller, M. Gradzielski, H. Hoffmann, U. Krämer, C. Thunig, *Progr. Colloid Polym. Sci.* **1991**, 84, 243.

again. The final process is the longest with a relaxation time of 14 ms. Similar complicated signals have been observed for electric birefringence measurements on dispersion of clay particles. The complicated signals in these systems are due to the fact that a fraction of the particles align parallel to the electric fields, whereas another fraction aligns perpendicular to the field.⁵⁵

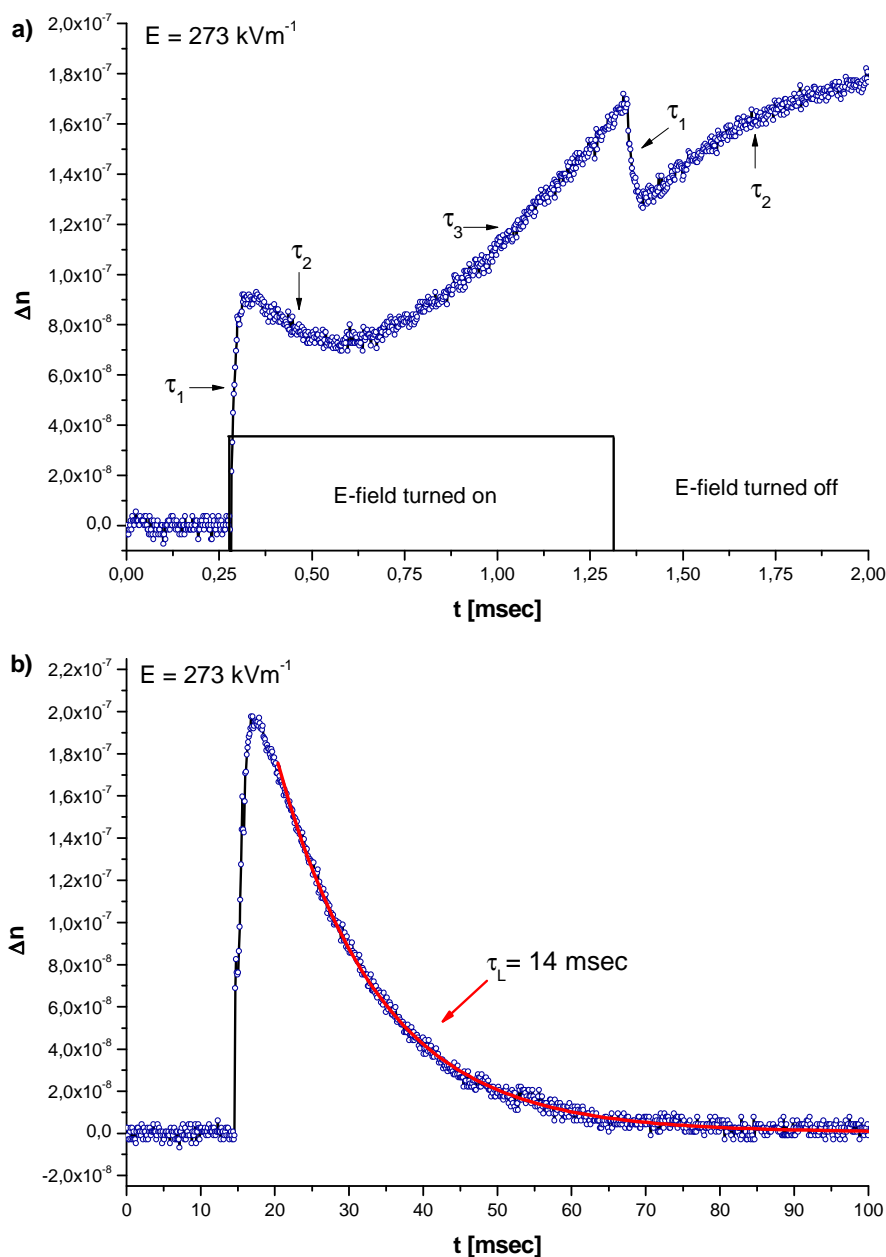


Fig. 3.11 EB-signal for a microemulsion of the upper single phase channel with 6% decane in the solvent mixture. a) signal shown with time sweep of 2 msec, b) signal with time sweep of 100 msec, longest relaxation $\tau_L = 14$ msec. The signals identify three different relaxation processes. Duration of electric pulse = 1 msec.

⁵⁵ Y. Yamaguchi, H. Hoffmann, *Colloids Surf. A* **1997**, *121*, 67-80.

As the longest relaxation times of the final decay of the signal dominate over the shorter times, they were called main structural relaxation times. Signals were recorded all along the upper channel and the main relaxation times determined by analyzing the exponential decay of the final process. In addition, there was measured the zero-shear viscosity of the microemulsions. An overview of the main structural relaxation times and the zero shear viscosities in the upper single phase channel can be found in figure 3.12.

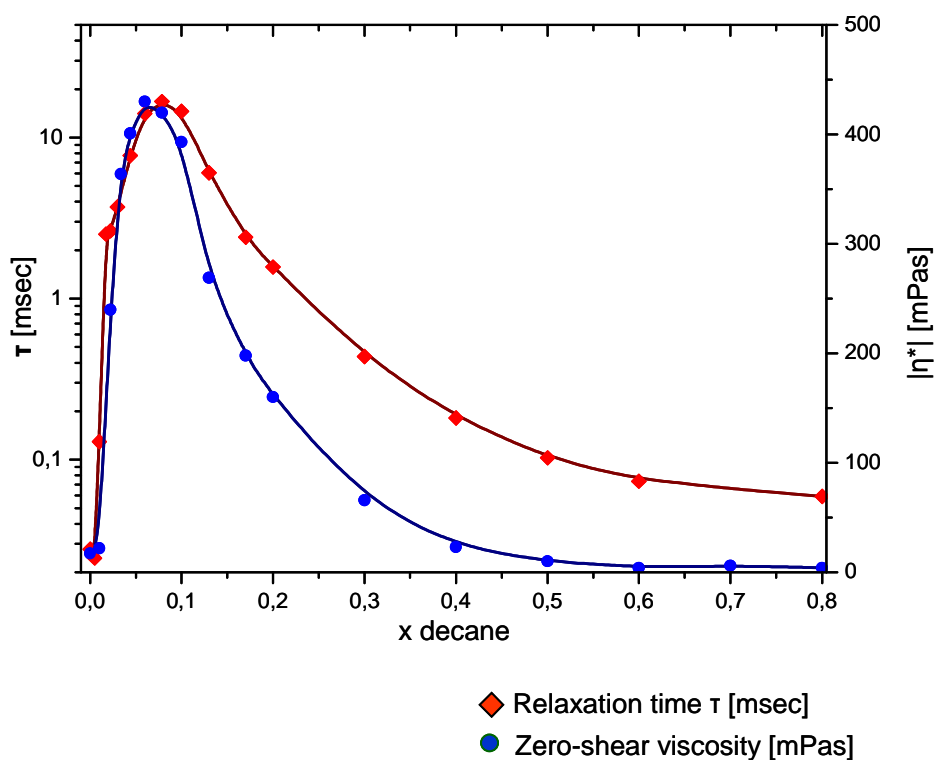


Fig. 3.12 Plot of the longest relaxation time τ and the zero shear viscosity of microemulsions in the upper single-phase channel against the mass fraction of decane in the solvent mixture.

The relaxation time increases three orders of magnitude and shows a maximum around 6-10% decane. At the same time, the zero shear viscosity increases two orders of magnitude. With further increasing mass fraction of decane, the relaxation time and the viscosity decrease again. The structural relaxation times around the maximum that were determined by electric birefringence also could be determined by rheology.

As conductivity data already implied, there must be a complex transition mechanism from the bicontinuous L_3 phase to a water-in-oil structure with only around 6-10% oil. The complicated signals for microemulsions with low oil content are obviously related with this transition mechanism and show that several microstructures exist in the fluid which are in equilibrium with each other. For higher oil content above 10% oil, EB-Signals become less complicated again. This indicates that the structural transition is complete. The structural relaxation time then is decreasing again due to the

decreasing droplet size of the w/o droplets with increasing oil content. The viscosity maximum is also the result of a switch in the nanostructure from a low viscous flexible L_3 phase to a densely packed w/o-HIPE structure. Obviously, the structural relaxation time controls the viscosity of the fluid.

In the lower single phase channel, simple electric birefringence signals were found that are caused by the deformation of droplets in the electric field. This indicates that the nanostructure doesn't change much in this channel. With increasing mass fraction of oil, the main structural relaxation time increases with the viscosity, as the droplet size increases (Figure 3.13). The initial decay of the viscosity is due to the transformation of worm-like micelles in binary surfactant mixture to spherical micelles by solubilizing oil.

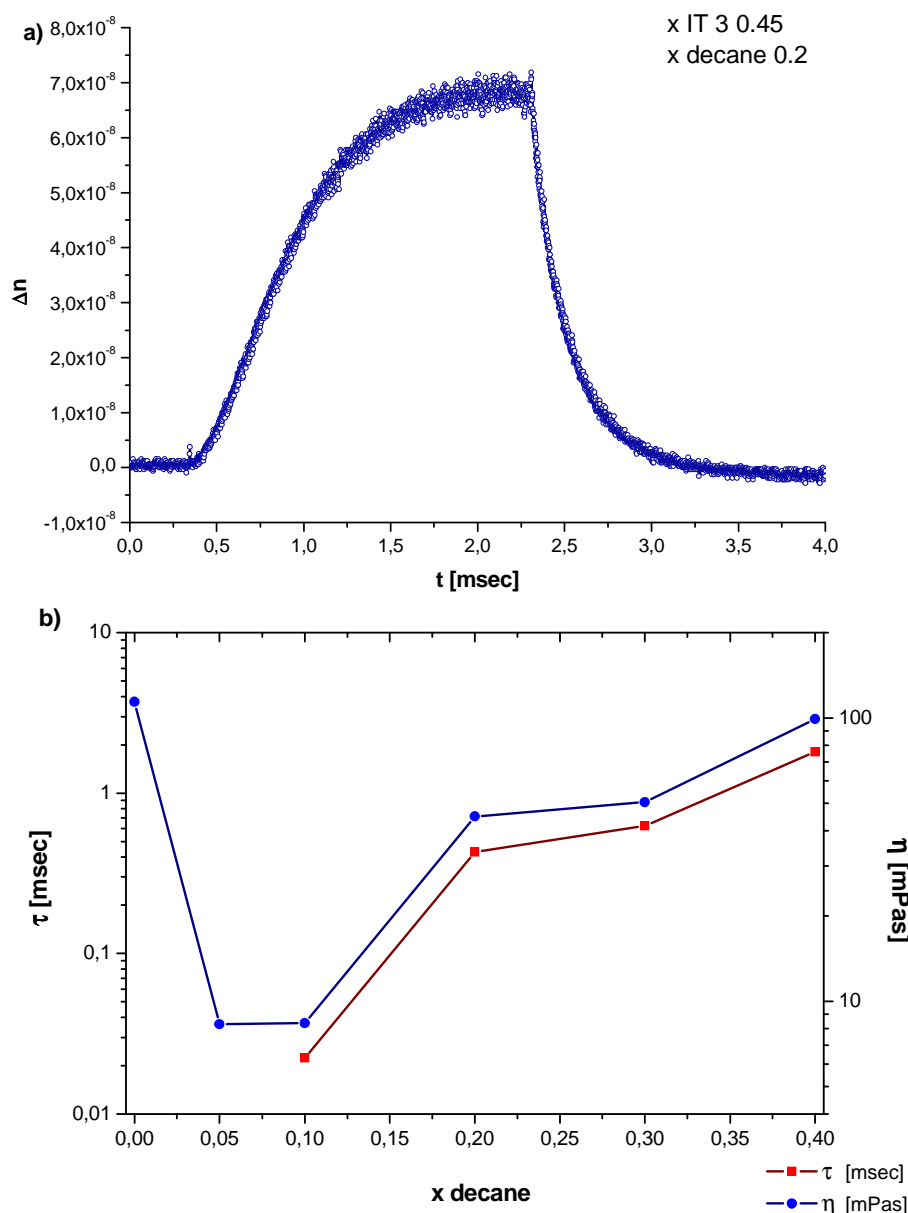


Fig. 3.13 Results of electric birefringence in the lower single phase channel. a) EB-signal of a microemulsion from the lower single phase channel with 20% decane in the solvent mixture. b) Overview of main structural relaxation time and zero shear viscosity with increasing oil content in the lower single phase channel.

3.5. Cryo-TEM of microemulsions with a High Internal Phase Microemulsion (HIPME) structure

As the conductivity and electric birefringence results showed the presence of an oil-continuous high internal phase droplet structure with less than 10% of oil, cryo-TEM experiments were performed to image these new microemulsion structures directly. The results were published in a fourth manuscript. Unfortunately, oil continuous phases with linear hydrocarbons like n-decane cannot be investigated by cryo-TEM. Linear hydrocarbons tend to crystallize when they are quenched into the liquid cryogen during the specimen preparation. Branched hydrocarbons, however, can be vitrified and do not crystallize. Therefore, we tried to add some iso-octane to the decane in order to stay as close as possible to the decane system and hoped that this would help to prevent the crystallization process. Good results cryo-TEM results of phases with linear oils that were mixed with branched compounds serving as cryoprotectants are already reported.⁵⁶

Cryo-TEM experiments with pure decane/iso-octane mixtures failed, it was not possible to gain pictures of clean vitrified oil-films. Instead, only dark crystal structures of the oil could be imaged, that were sensitive to the electron beam and suffered from irradiation damage. As a consequence, we gave up the idea to use a mixed oil. A cryo-TEM micrograph of such structures is shown in figure 3.14. The ratio of n-decane/iso-octane was 7/3.

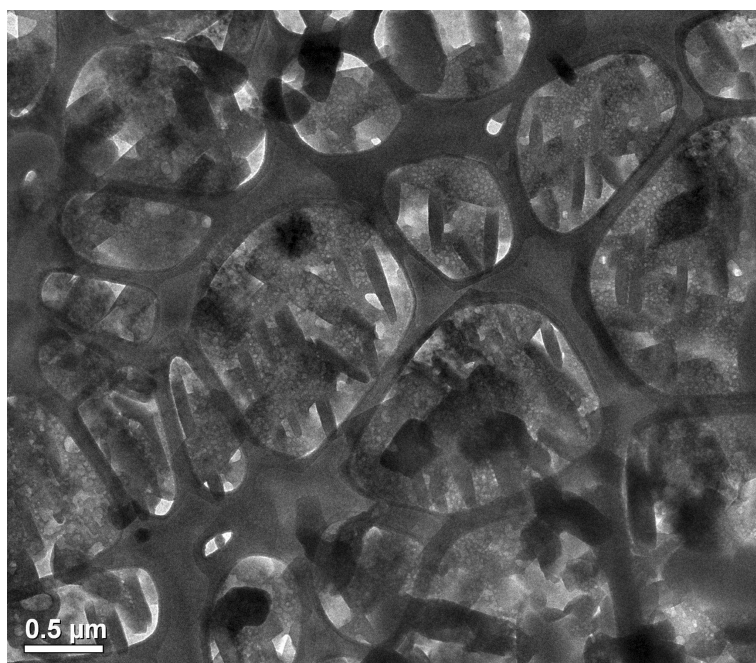


Fig. 3.14 Cryo-TEM micrograph of n-decane/i-octane, ratio 7/3 (w/w), prepared at RT, cryogen: liquid nitrogen.

In another study, the sponge structure of a bicontinuous microemulsion with a single non-ionic surfactant was already successfully imaged by cryo-TEM. The sample was prepared with the

⁵⁶ D. Danino, R. Gupta, F. Satayavolu, Y. Talmon, *J. Colloid Interf. Sci.* **2002**, 249, 180-168.

surfactant $C_{12}E_5$, iso-octane, H_2O and had a water/oil ratio (w/w) of 7/3. The micrographs clearly show a sponge structure with typical dimensions of water and oil domains around $0.2\ \mu\text{m}$.

Microemulsions of the new mixed surfactant system therefore were prepared with pure iso-octane for cryo-TEM investigations instead of decane. Fortunately, the microemulsion samples from the upper channel showed the same properties as samples with decane. The same abrupt decrease of the conductivity as well as the maximum of the viscosity around 6-10% of oil was found. Moreover, it was not necessary to adjust the surfactant/co-surfactant ratio to obtain single phase microemulsions, the phase composition was about the same.

While the cryo-TEM pictures of the L_3 phase without oil showed the well-known bicontinuous network-structures, the situation changes drastically when only 6% of iso-octane are solubilized into the phase. In Figure 3.15, micrographs of the microemulsion from the upper channel with 6% of iso-octane in the solvent mixture are shown.

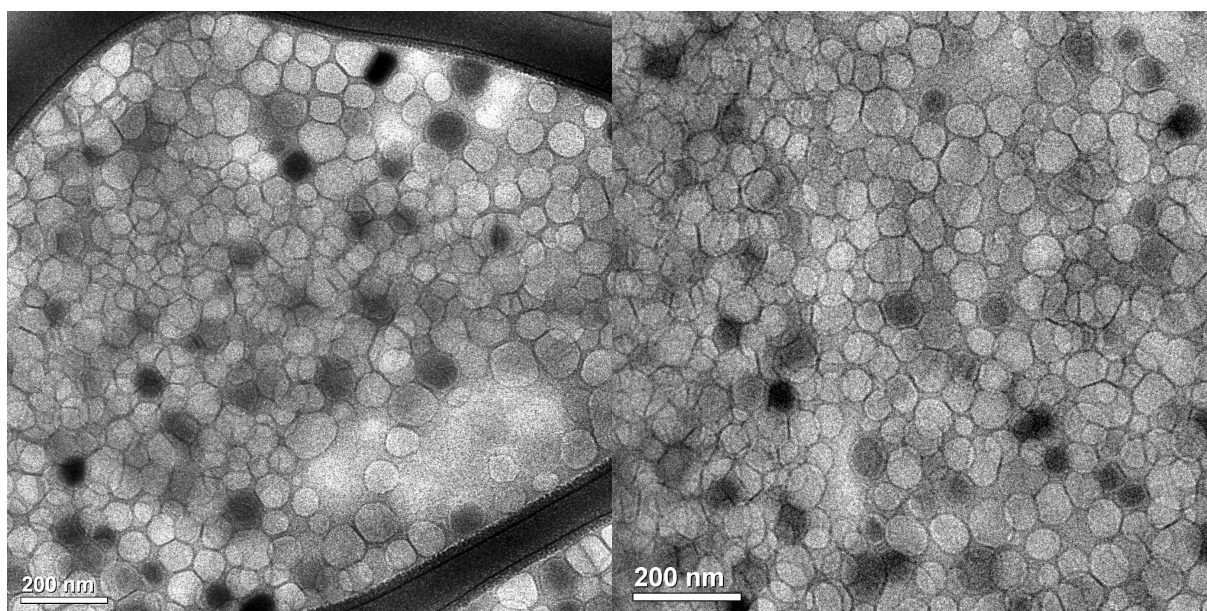


Fig. 3.15 Cryo-TEM micrographs of a microemulsion from the upper single phase channel with 15% surfactant $Mg(DS)_2/IT\ 3$, $x\ IT\ 3\ 0.62$, $x\ iso-octane\ 0.06$, quenched from $25\ ^\circ\text{C}$.

They clearly show a densely packed w/o-droplet structure, which look like a “polyhedral foam” that has thin films with a thickness of about 3 nm. The diameter of the water domains is about 50 nm. The thin film was obviously made of the surfactants with the hydrocarbon in between the two monolayers, and the water inside the polyhedra. The structures look very much like the structures found in high internal phase emulsions (HIPE). HIPEs are concentrated systems with a large volume of the dispersed phase. Those high volume fractions result in the deformation of droplets into polyhedra, which are separated by thin films of the continuous phase. In such situations the size of the structures are usually in the range of several μm and can easily be seen by light microscopy. Both o/w and w/o-systems of

HIPEs are known.⁵⁷ Based on that, we call the newly found microemulsion structure HIPME (High Internal Phase Micro-Emulsion). Such structures have so far only been observed in real emulsions that are, like any other emulsions, thermodynamically unstable.⁵⁸ In the microemulsion sample with the HIPME structure, the water domains are not connected with each other. This can be concluded from the fact that the ice-crystals in dark have the same size as the ice crystals in grey. In spite of their small oil content, the HIMPE phases have a conductivity that is about 3 - 4 orders of magnitude lower than the conductivity of the L₃ phase. The thin surfactant films are practically impenetrable for the transport of ions, explaining the low conductivity of the sample. Microemulsions with a HIPME structure were imaged successfully all along the upper single phase channel (Fig. 3.16).

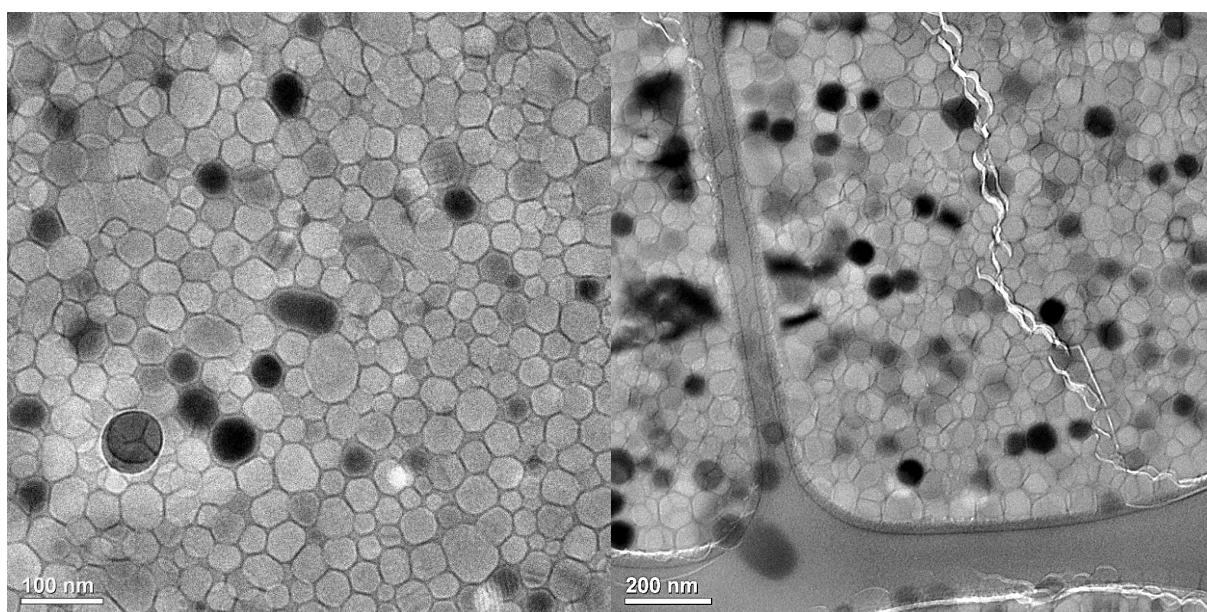


Fig. 3.16 Cryo-TEM micrographs of a microemulsion with a HIPME structure. Left: sample containing 30% of iso-octane, right: sample containing 50% of iso-octane in the solvent mixture.

The HIPME structures are obviously the result of the electric charges in the surfactant layers, contributed by the anionic Mg(DS)₂. They cause high interfacial tensions, leading to spherical structures instead of a bicontinuous morphology. It is likely, that transitions to bicontinuous structures can be provoked by shielding the electric double-layers in ionically charged systems by excess salt.

⁵⁷ N. R. Cameron, D. S. Sherrington, *Adv. Polym. Sci.* **1996**, 126, 163-214.

⁵⁸ H. Hoffmann, G. Ebert, *Angewandte Chemie* **1988**, 27, 902-912.

3.6. PFG-NMR self diffusion measurements

To underline and to verify the previously obtained results, the microemulsion channels were investigated by pulsed-field gradient nuclear magnetic resonance spectroscopy (PFG-NMR). This method is a special technique, based on nuclear magnetic resonance spectroscopy (NMR). In contrast to normal NMR measurements, inhomogeneous magnetic fields are used. With the help of additional magnetising coils, linear field-gradients are generated and thus locally changing magnetic fields. This allows performing spatially resolving NMR experiments, in which local information can be obtained like the position or the movement of particles, which are visible for NMR. Therefore, PFG-NMR can give detailed information about the structure, fluidity and emulsion type but also indications about the interaction between surfactant and co-surfactant at the interface. More details about the PFG-NMR method can be found in literature.⁵⁹ In a fifth publication, the results of PFG-NMR experiment in the microemulsion single phase channels are reported. In addition, the influence of excess salt to the system was investigated by interfacial tension, conductivity and NMR-measurements, as we tried to transform a high internal phase microemulsion to a bicontinuous microemulsion by shielding the electric charges of the anionic surfactant.

3.6.1. PFG-NMR self diffusion measurements in the single phase channels

The PFG-NMR analysis is focussed on those spectral regions which can either be clearly assigned to single system constituents (water and decane) or to the mixture of the surfactants (Mg(DS)₂/IT 3). The integrals of these three spectral regions strongly depend on the strength of the gradient pulse, hereby indicating the average displacement of the corresponding system constituents during the period between the pulses which was set to 50 ms. In a plot of the logarithmic signal intensity vs. the parameter $\gamma^2 G^2 \delta^2 (\Delta - \delta/3)$ (with γ being the gyromagnetic ratio of protons, G the strength of the gradient field, δ and Δ the duration of and the spacing between the two gradient pulses), the slope is equal to the negative apparent self diffusion coefficient of the given component in the heterogeneous system (Stejskal-Tanner plot). If the component is located in two different environments leading to clearly different self diffusion properties, the plot will show two sections with clearly different slopes. If the component is encapsulated in very small droplets, the motion within the droplets becomes undetectable. In this case, the observed slope reflects the velocity of the Brownian motion of the droplets.

In Figure 3.17, a Stejskal-Tanner plot for water and the surfactant in the L₃ phase is shown. The water signal follows a steep decay, corresponding to a self diffusion constant that is just slightly lower than the value for free bulk water. This indicates that water forms a continuous phase that is only slightly affected by phase boundaries of the surfactant layers. In contrast, the signal for MDS/IT3 follows a relatively flat decay. This means there is only a restricted mobility of the Mg(DS)₂ and IT3 molecules.

⁵⁹ P. Heitjans, J. Kärger, eds., in: *Diffusion in condensed matter: methods, materials, models*, Springer Germany, 2005, 421.

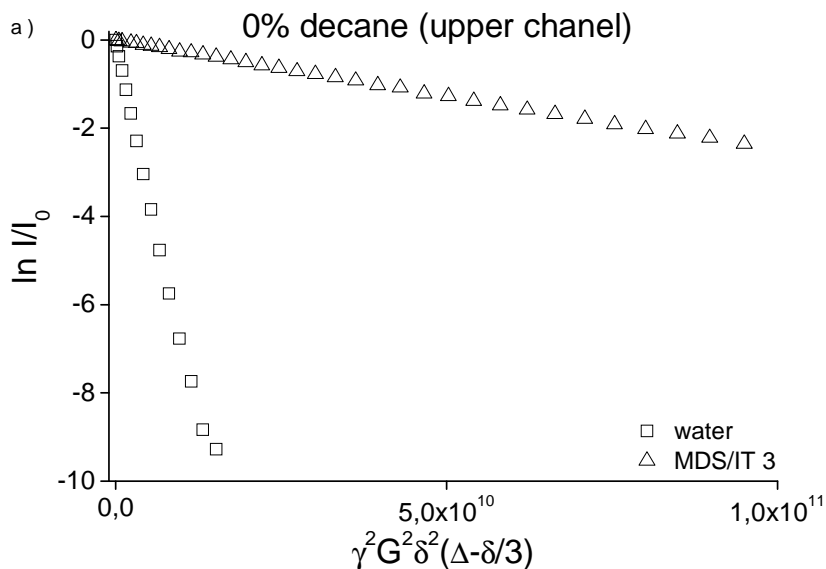


Fig. 3.17 Stejskal-Tanner plot for water and the surfactants in the L_3 phase.

The situation changes significantly when decane is added to the system. The mobility of water is much reduced. In contrast, the diffusion rates for decane exhibit values which come close to the bulk diffusion rate of decane. In this situation, the self diffusion constant for the water fraction is too small to be assigned to bulk water in a continuous phase. This shows that the observed water molecules are encapsulated in small droplets which undergo Brownian motion in the continuous decane phase.

In Figure 3.18, the diffusion constants of H_2O in the upper single phase channel are summarized with increasing decane content.

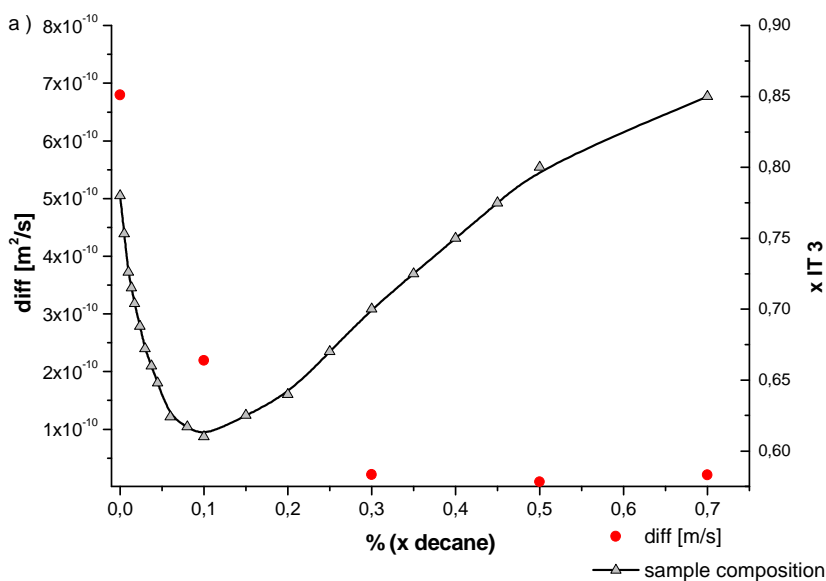


Fig. 3.18 Self diffusion constants of H_2O in the upper microemulsion channel as a function of the decane content.

The data for the self diffusion coefficients of water show a clear correlation with the corresponding conductivity plot that was shown in Fig. 3.8.

In contrast to the results for the upper channel, the variations between the PFG-NMR results of different positions in the lower channel do not indicate dramatic structural changes. The data resemble those of the upper channel in absence of decane. All in all, the data are clearly in accordance with o/w microemulsions.

3.6.2. Influence of excess salt to the microemulsion system

As already mentioned in 3.1, our mixed anionic/non-ionic surfactant system has a very high interfacial tension against the oil phase. In case of the microemulsion system with decane, the minimum interfacial tension of 2.5 mN/m is reached at a surfactant/co-surfactant ratio of 1:1. In non-ionic microemulsion systems, ultra low values as $1 \cdot 10^{-3}$ mN/m are reached. We assumed that by shielding the charge of the anionic surfactant by adding excess salt would lower the interfacial tension. Similar effects were already reported for the anionic surfactant diethylhexyl sodium sulphosuccinate (AOT), where ultra-low interfacial tensions against oil were reached with additional NaCl.⁶⁰

Nevertheless, the interfacial tension couldn't be lowered significantly in our system, no ultra-low interfacial tensions were detected when excess NaCl was added to the surfactant mixtures. However, the upper and lower borders of the single phase regions are shifted to lower $x_{IT\ 3}$ values by $x_{IT\ 3} \sim 0.07$ when NaCl is added to the $Mg(DS)_2$ in a molar ratio of 1:1. The shift to lower $x_{IT\ 3}$ values means that the system in total becomes more lipophilic, as less amount of the lipophilic co-surfactant IT 3 in the surfactant mixture is needed to solubilize the oil. By measuring the electric conductivity of a microemulsion with 30% of decane with increasing salt concentration, it was checked if the shift of the phase boundaries might also be accompanied by a change in the internal nanostructure of the microemulsion sample. A plot of the conductivity in the single phase region with increasing NaCl concentration is shown in figure 3.19. The conductivity from the NaCl-free to the microemulsion with a molar ratio of $Mg(DS)_2:NaCl = 1:1$ increases about three orders of magnitude from a low value of 3 $\mu S/cm$ to $\sim 1000 \mu S/cm$. The conductivity increases in a sigmoid curve with an inflection point around 50% NaCl and not linearly with increasing NaCl concentration. At first look it seems like the nanostructure changes from a w/o-HIPME system to a bicontinuous-like nanostructure.

⁶⁰ R. Aveyard, B. P. Binks, S. Clark, J. Mead, *J. Chem. Soc. Faraday Trans. 1* **1986**, 82, 125-142.

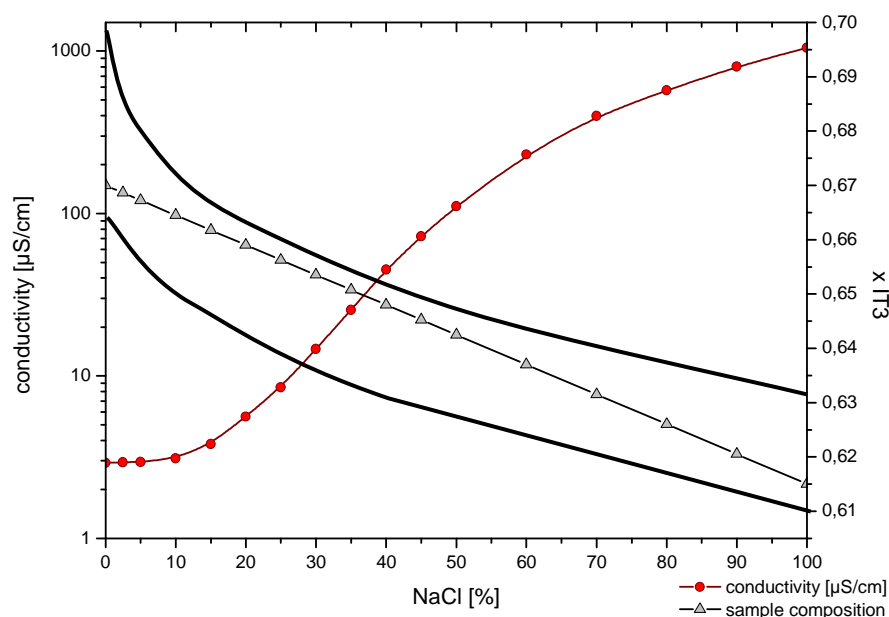


Fig. 3.19 Plot of conductivity in the single phase region of a microemulsion with x decane 0.3 and increasing NaCl concentration at 25 °C. 100% NaCl corresponds to a molar ratio of $Mg(DS)_2:NaCl = 1:1$.

To proof this, we compared two microemulsions with different salt concentrations by PFG-NMR. The first sample without NaCl had the composition of x IT 3 0.7 and x decane 0.3. The second sample had the composition of x IT 3 0.615, x decane 0.3, and the molar ratio of $Mg(DS)_2:NaCl = 1:1$ (Fig. 3.20).

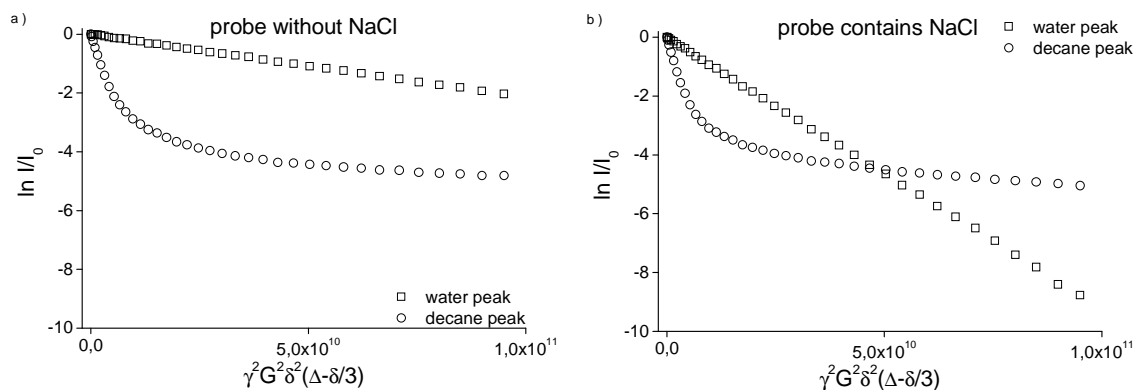


Fig. 3.20 Stejskal-Tanner plots for decane and water of a microemulsion from the upper single phase channel with 30% decane in the solvent mixture. a) plot for microemulsion without excess NaCl, b) plot with excess NaCl.

The mobility of water is much reduced in the sample without NaCl. When NaCl is added to the system, the mobility of water is increasing. Nevertheless, the diffusion rate is much slower compared to the bicontinuous L_3 phase (Fig. 3.17) where it is close to bulk water. The diffusion behaviour of decane doesn't change with NaCl. Therefore we conclude, that the main structure still is present as HIPME-phase.

Although the conductivity would indicate a transition from a HIPME structure to a bicontinuous structure by adding salt to the microemulsion, one has to reconsider precisely the conductivity value of the transformed microemulsion with NaCl that is about factor 10 lower than it would be for the same NaCl concentration in pure H₂O. Considering the conductivity values and the NMR-results, we assume that the morphology is not a true bicontinuous sponge-like structure as it is the case for microemulsions with a single non-ionic surfactant. It is conceivable that the charge on the surfactant monolayer with the anionic surfactant is shielded by the addition of NaCl and thus the repulsion forces are decreased. Consequently the system becomes highly dynamic. This might allow the water-domains to fuse together and form passages, in which the ions can be transported in the aqueous phase and therefore increase the conductivity of the system. Therefore we assume the nanostructure with NaCl to be a HIPME-structure with some defects. It is worth mentioning that these phases are very temperature stable (at least from 5 °C to 80 °C).

All in all the NMR results are in good agreement with conductivity data and the cryo-TEM pictures that are shown in 3.5. The question, if the nanostructure with NaCl is present as a pseudo-bicontinuous HIPME structure with defects, can surely be answered by cryo-TEM or FF-TEM. The discrepancy between the comparably high conductivity values and the slow mobility of water is, however, still unclear.

3.7. Outlook

This work has shown that microemulsions with an anionic/non-ionic surfactant mixture have indeed different properties compared to microemulsion systems with either a single non-ionic or a single ionic surfactant. The situation in such a system is somewhere in between both situations. The discovery of the HIPME phases with very low oil content might be of important interest for industry, like cosmetics. Applications of transparent sun lotion are thinkable, in which a few percent of UV-absorber are co-solubilized in the oil-phase, for example.

Nevertheless, some questions are still open and should be further investigated. We think that the results we found are of general importance. This should, however, be verified with other surfactant combinations. Mixtures of surfactants like AOT, DDAB or alkyl ether sulfates in combination with non-ionic surfactants are conceivable. It should however be noted that preliminary results with another surfactant combination were already very promising and are now further examined in *Shiseido* company. The phase behaviour of the surfactant combination was identical to the combination that was used in this study and the HIPME structures are also present in this system.

In addition, the influence of the used oil should be further analysed. First experiments showed, that even iso-hexadecane can be easily solubilized in the investigated microemulsion system without any problems. For this case, the lower single phase channel even reaches to 60-70% of oil in the solvent, while the conductivity still stays at high levels. It is likely that this phase can be described as oil-in-water HIPME. Also the temperature dependency in the single phase channels should be checked in detail.

Another point that should be further investigated is the temperature stable anisotropic lamellar channel, that reaches from 0 – 90% of oil in the decane-system. It should be tried to identify the nanostructures in this channel, either directly by cryo-TEM or by FF-TEM. PFG-NMR measurements are also possible. This channel also might be of interest for various applications, as the phases are more or less transparent and have a yield stress. This means, small particles could be dispersed in these phases that stay in solution without sedimentation. It would also be interesting to know, if other oils can be solubilized inside this liquid crystalline channel.

In addition, it should be possible to thicken or gelify the microemulsion by introducing polymers into the continuous water or oil phase. Even the direct use of polymerizable surfactants might be effective, which could be directly used for the formation of a microemulsion.

All in all, this work has shown that there are still a lot of fascinating properties of microemulsions that have not been known before and there are surely more interesting results in the field of microemulsion and surfactant science, which will be revealed in future.

4. References

4.1. Literature

- [1] T. P. Hoar, J. H. Schulman, *Nature* **1943**, 152, 102-103.
- [2] J. H. Schulman, W. Stoeckenius, L. M. Price, *J. Phys. Chem* **1959**, 63, 1677-1680.
- [3] M. Gradzielski, H. Hoffmann, *J. Phys. Chem* **1994**, 98, 2613-2623.
- [4] F. Lichterfeld, T. Schmeling, R. Strey, *J. Phys. Chem.* **1986**, 90, 5762-5766.
- [5] H. Mollet, A. Grubenmann, in: *Formulierungstechnik – Emulsionen, Suspensionen, Feste Formen*; Wiley-VCH, Weinheim-Germany, **2000**.
- [6] C. Stubenrauch, in: *Microemulsions: Background, New Concepts, Applications, Perspectives*, Wiley-VCH, **2009**.
- [7] M. J. Lawrence, G. D. Rees, *Advanced Drug Delivery Reviews* **2000**, 45, 89-121.
- [8] D. Gräbner, L. Xin, H. Hoffmann, M. Drechsler, O. Schneider, *J. Colloid Interf. Sci.* **2010**, 350, 516-522.
- [9] L. Bemert, S. Engelskirchen, C. Simon, R. Strey, *Am. Chem. Soc., Div. Fuel Chem.* **2009**, 54, 290-291.
- [10] R. Miyahara, K. Watanabe, T. Ohmori, Y. Nakama, *J. Oleo Sci.* **2006**, 55, 403-411.
- [11] B. K. Paul, S. P. Moulik, *Current Science* **2001**, 80, 990-1001.
- [12] L.M. Prince, Ed., in *Microemulsions: Theory and Practice*, Academic Press, New York, **1977**.
- [13] A. Gonenne, R. Ernst, *Analytical Biochemistry* **1987**, 87, 28-38.
- [14] F. M. Menger, J. S. Keiper, *Angewandte Chemie* **2000**, 39, 1906-1920.
- [15] M. Summers, J. Eastoe, *Advances in Colloid and Interface Science* **2003**, 100-102, 137-152.
- [16] H. Hoffmann, *Ber. Bunsenges. Phys. Chem.* **1994**, 98, 1433.
- [17] J. N. Israelachvili, D. J. Mitchell, B. W. Ninham, *J. Chem. Soc. Faraday Trans. II* **1976**, 72, 1525.
- [18] K. Fontell, *J. Colloid Interf. Sci.* **1973**, 44, 318-329.
- [19] G. Platz, C. Thunig, H. Hoffmann, *Progr. Colloid Polym. Sci.* **1990**, 83, 167-175.
- [20] S. Haas, H. Hoffmann, C. Thunig und E. Hoinkis, *Colloid Polym. Sci* **1999**, 277, 856-867.
- [21] B. Schwarz, G. Mönch, G. Ilgenfritz, R. Strey, *Langmuir* **2002**, 16, 8643-8652.
- [22] R. Beck, Y. Abe, T. Terabayashi, H. Hoffmann, *J. Phys. Chem. B* **2002**, 106, 3335-3338.
- [23] M. Jonströmer, R. Strey, *J. Phys. Chem.* **1992**, 96, 5993-6000.
- [24] D. J. Mitchell, G. J. T. Tiddy, L. Waring, T. Bostock, M. P. McDonald, *J. Chem. Soc., Faraday Trans I* **1983**, 79, 975.
- [25] K. Fontell in: *Colloidal Dispersions and Micellar Behavior*; ACS Symposium Series No. 9; American Chemical Society: Washington, DC, **1975**; p 270.
- [26] C. A. Miller, M. Gradzielski, H. Hoffmann, U. Krämer, C. Thunig, *Colloid Polym. Sci.* **1990**, 268, 1066-1072.

- [27] R. Strey, W. Jahn, G. Porte, P. Bassereau, *Langmuir* **1990**, 6, 1635-1639.
- [28] U. Olsson, P. Schurtenberger, *Langmuir* **1993**, 9, 3389-3394.
- [29] T. N. Zemb, S. T. Hyde, P.-J. Derian, I. S. Barnes, B. W. Ninham, *J. Phys. Chem.* **1987**, 91, 3814-3820.
- [30] T. Sottmann, R. Strey, S.-H. Chen, *J. Chem. Phys* **1997**, 106, 6483-6491.
- [31] R. Strey, *Colloid Polym. Sci.* **1994**, 272, 1005-1019.
- [32] F. Lichterfeld, T. Schmeling, R. Strey, *J. Phys. Chem* **1986**, 90, 5762-5766.
- [33] M. Kahlweit, et. al, *J. Colloid Interf. Sci* **1987**, 118, 450.
- [34] K. Shinoda, *Proceedings of the 5th International Congress of Surface Activity, Barcelona, Spain, Vol. 2, 1969*, 275-283.
- [35] J. Lyklema, in: *Fundamentals of interface and colloid science, Volume V: Soft Colloids*, Academic Press Inc, **2005**.
- [36] T. Sottmann and R. Strey, *J. Chem. Phys.* **1997**, 106, 8606–8615.
- [37] M. Kotlarchyk, S.-H. Chen, J. S. Huang, M. W. Kim, *Phys. Rev. Lett.* **1984**, 53, 941-944.
- [38] K. Fontell, A. Ceglie, B. Lindman, B. Ninham, *Acta Chemica Scandinavica A40* **1986**, 247-256.
- [39] M. Kahlweit, R. Strey, *Angew. Chern. Int. Ed. Engl.* **1988**, 24, 654-668.
- [40] W. Jahn, R. Strey, *J. Phys. Chem.* **1988**, 92, 2294-2301.
- [41] W. Sager, W. Sun, H.-F. Eicke, *Progr. Colloid Polym. Sci.* **1992**, 89, 284-287.
- [42] H. Kunieda, K. Hanno, S. Yamaguchi, K. Shinoda, *J. Colloid Interf. Sci.* **1985**, 107, 129-137.
- [43] M. Kahlweit, B. Faulhaber, G. Busse, *Langmuir* **1994**, 10, 2528-2532.
- [44] J. A. Silas, E. W. Kaler, *Langmuir* **2001**, 17, 4534-4539.
- [45] J. Reimer, O. Södermann, T. Sottmann, K. Kluge, R. Strey, *Langmuir* **2003**, 19, 10692-10702.
- [46] S. Ajith, A. K. Rakshit, *J. Phys. Chem* **1995**, 99, 14778-14783.
- [47] U. Olsson, K. Shinoda, B. Lindman, *Journal of Physical Chemistry*, **1986**, 90, 4083
- [48] Y. Talmon, in: *Seeing Giant Micelles by Cryogenic-Temperature Transmission Electron Microscopy (Cryo-TEM)*, in “*Giant Micelles*”, chapter 5, R. Zana, E. A. Kaler, Eds., CRC Press, New York, **2007**, 163-178.
- [49] H. Hoffmann, C. Thunig, U. Munkert, H. W. Meyer, W. Richter, *Langmuir* **1992**, 8, 2629-2638.
- [50] L. Belkoura, C. Stubenrauch and R. Strey, *Langmuir* **2004**, 20, 4391–4399.
- [51] W. Jahn and R. Strey, *J. Phys. Chem.* **1988**, 92, 2294–2301.
- [52] H. Hoffmann, W. Schorr, *J. Phys. Chem.* **1981**, 85, 3160–3167.
- [53] W. Schorr, H. Hoffmann, *Physics of Amphiphiles: Micelles, Vesicles and Microemulsions: Proceedings of the International School of Physics ; V. Degiorgio, M. Corti, Eds.; North-Holland: Amsterdam, 1985*; pp 160-180.
- [54] C. A. Miller, M. Gradzielski, H. Hoffmann, U. Krämer, C. Thunig, *Progr. Colloid Polym. Sci.* **1991**, 84, 243.
- [55] Y. Yamaguchi, H. Hoffmann, *Colloids Surf. A* **1997**, 121, 67-80.
- [56] D. Danino, R. Gupta, F. Satayavolu, Y. Talmon, *J. Colloid Interf. Sci.* **2002**, 249, 180-168.
- [57] N. R. Cameron, D. C. Sherrington, *Adv. Polym. Sci.* **1996**, 126, 163-214.

- [58] H. Hoffmann, G. Ebert, *Angewandte Chemie* **1988**, 27, 902-912.
- [59] P. Heitjans, J. Kärger, eds., in: *Diffusion in condensed matter: methods, materials, models*, Springer Germany, **2005**, 421.
- [60] R. Aveyard, B. P. Binks, S. Clark, J. Mead, *J. Chem. Soc. Faraday Trans. 1* **1986**, 82, 125-142.

4.2. List of figures

- Fig. 2.1 taken without modification from: T. P. Hoar, J. H. Schulman, *Nature* **1943**, 152, 102-103.
- Fig. 2.2 created in Microsoft PowerPoint 2003.
- Fig. 2.3 illustration prepared in Micrografx PicturePublisher 9, photo of sample taken by myself.
- Fig. 2.4 illustrations taken from: R. Strey, W. Jahn, G. Porte, P. Bassereau, *Langmuir* **1990**, 6, 1635-1639. modified with imaging software PicturePublisher 9.
- Fig. 2.5 illustrations taken from: C. Stubenrauch, in: *Microemulsions: Background, New Concepts, Applications, Perspectives*, **2009**. Modified with imaging software PicturePublisher 9.
- Fig. 2.6 illustrations taken from: J. Lyklema, in: *Fundamentals of interface and colloid science, Volume V: Soft Colloids*, Academic Press Inc, **2005**. Modified with imaging software PicturePublisher 9.
- Fig. 2.7 taken from: T. Sottmann and R. Strey, *J. Chem. Phys.* **1997**, 106, 8606–8615.
- Fig. 2.8 taken from: K. Fontell, A. Ceglie, B. Lindman, B. Ninham, *Acta Chemica Scandinavica A40* **1986**, 247-256. Modified with imaging software PicturePublisher 9.
- Fig. 2.9 taken from: W. Jahn, R. Strey, *J. Phys. Chem.* **1988**, 92, 2294-2301. Modified with imaging software PicturePublisher 9.
- Fig. 2.10 illustrations taken from: C. Stubenrauch, in: *Microemulsions: Background, New Concepts, Applications, Perspectives*, **2009**.
- Fig. 3.1-3.2 taken from first publication, L. Wolf, H. Hoffmann, K. Watanabe, T. Okamoto, *Phys. Chem. Chem. Phys.*, **2011**, 13, 3248-3256.
- Fig. 3.3 taken from: U. Olsson, K. Shinoda, B. Lindman, *Journal of Physical Chemistry* **1986**, 90, 4083.
- Fig. 3.4-3.6 micrographs from electron microscopy, taken during stay at Technion, Haifa, Israel in January 2009.
- Fig. 3.7-3.8, 3.11-3.13 taken from third publication, L. Wolf, H. Hoffmann, W. Richter, T. Teshigawara, T. Okamoto, *J. Phys. Chem. B* **2011**, 115, 11081–11091.
- Fig. 3.9-3.10 prepared in Microsoft PowerPoint 2003.
- Fig. 3.14-3.16 micrographs from electron microscopy, taken during stay at Technion, Haifa, Israel in January-February 2010.
- Fig. 3.17-3.20 taken from draft of fifth manuscript, L. Wolf, H. Hoffmann, J. Linders, C. Mayer, submitted to *Soft Matter* December 2011.

5. Publications

5.1. Overview of publications and individual contribution

I wrote all manuscripts together with my supervisor Heinz Hoffmann. Kei Watanabe, Tohru Okamoto and Takashi Teshigawara from the Shiseido Company, Japan, were responsible for financial support. The cryo-TEM imaging was done in cooperation with the group of Yeshayahu Talmon during two stays at the Technion, Haifa (Israel). The cryo-TEM micrographs were discussed together with Yeshayahu Talmon. FF-TEM micrographs were obtained by Walter Richter at the Centre for Electron Microscopy in Jena, Germany. He helped to discuss the FF-TEM images. SANS-data were obtained from the ILL in Grenoble, France. I thank Thomas Hellweg for the opportunity to measure our samples there. The electric birefringence experiments were performed in our laboratories. Dieter Gräßner helped me to operate the electric birefringence device. The data were processed and evaluated by myself.

The manuscript containing PFG-NMR results was written in cooperation with Jürgen Linders and Christian Mayer from the University of Duisburg-Essen, Germany. PFG-NMR self diffusion experiments were performed by Jürgen Linders and discussed together with Christian Mayer. Jürgen Linders and Christian Mayer contributed the NMR-part of this publication.

- Microemulsions from silicone oil with an anionic/non-ionic surfactant mixture

Published in *Physical Chemistry Chemical Physics* **2011**, *13*, 3248-3256 by Lukas Wolf*, Heinz Hoffmann*, Kei Watanabe and Tohru Okamoto. DOI: 10.1039/C0CP00062K.

*corresponding author

- Cryo-TEM imaging of a novel microemulsion system of silicone oil with an anionic/non-ionic surfactant mixture

Published in *Soft Matter* **2010**, *6*, 5367-5374 by Lukas Wolf, Heinz Hoffmann*, Yeshayahu Talmon, Takashi Teshigawara and Kei Watanabe. DOI: 10.1039/C0SM00049C.

*corresponding author

- Dynamic Properties of Microemulsions in the Single-Phase Channels

Published in *Journal of Physical Chemistry B*, **2011**, *115*(38), 11081-11091 by Lukas Wolf*, Heinz Hoffmann, Walter Richter, Takashi Teshigawara and Tohru Okamoto. DOI: 10.1021/jp2036789.

*corresponding author

- Microemulsions with a HIPME (High Internal Phase Microemulsion) structure

Published in *Journal of Physical Chemistry B*, **2011** by Lukas Wolf*, Heinz Hoffmann, Takashi Teshigawara, Tohru Okamoto, Yeshayahu Talmon. DOI:

*corresponding author

- PFG-NMR Self Diffusion Measurements in the Single Phase Channels of a Microemulsion System with an anionic/non-ionic Surfactant Mixture

Submitted to *Soft Matter* in December **2011** by Lukas Wolf*, Heinz Hoffmann, Jürgen Linders and Christian Mayer.

* corresponding author

current status: under revision

5.1.1. Microemulsions from silicone oil with an anionic/non-ionic surfactant mixture

Lukas Wolf*, Heinz Hoffmann*, Kei Watanabe and Tohru Okamoto

*corresponding author

Published in *Physical Chemistry Chemical Physics* **2011**, *13*, 3248-3256.

DOI: 10.1039/C0CP00062K.

Microemulsions from silicone oil with an anionic/nonionic surfactant mixture†

Lukas Wolf,^{*a} Heinz Hoffmann,^{*a} Kei Watanabe^b and Tohru Okamoto^b

Received 30th March 2010, Accepted 2nd December 2010

DOI: 10.1039/c0cp00062k

Microemulsion phases have been prepared for the first time from the silicone oil “M₂” (hexamethyldisiloxane) and a surfactant mixture of a nonionic surfactant “IT 3” (isotridecyltriethyleneglycoether) and an ionic surfactant Ca(DS)₂ (calciumdodecylsulfate). For such a surfactant mixture the hydrophilicity of the system can be tuned by the mixing ratio of the two components. With increasing IT 3 content, the surfactant mixtures show a L₁-phase, a wide L_α-region and a narrow L₃ sponge phase. For constant temperature, two single phase channels exist in the microemulsion system. The lower channel (low IT 3 content) ends in the middle of the phase diagram with equal amounts of water and oil, the upper channel begins with the L₃-phase and passes all the way to the oil phase. Conductivity data show that the upper channel has a bi-continuous morphology up to 40% oil while the lower channel consists of oil droplets in water. In contrast to previous studies on nonionic systems, the two single phase channels are not connected and microemulsions with equal amount of oil and water do not have a bicontinuous structure.

Introduction

Microemulsions (ME) are thermodynamically stable fluids that consist of oil, water and a few percent of surfactant.¹ They usually are low viscous, more or less transparent and optically isotropic liquids. Microemulsions are used in many applications because of their fascinating properties. One of the reasons for their usefulness is that both polar and apolar compounds can be dissolved in microemulsions. They are therefore used for agrochemical, cosmetic, pharmaceutical and other industrial formulations where it is necessary to bring two components in a fluid together which normally are not miscible. Detailed investigations on microemulsions over the last 40 years have shown that the components of the fluids are not dispersed with each other on a molecular level like in miscible solvent mixtures but the fluids are highly structured on a scale of 1–100 nm. Domains of oil and water, with well defined interfaces from surfactants, alternate with each other. These domains are in equilibrium with each other and are very dynamic in behaviour. They constantly change their shape and size on a time scale of micro- to milliseconds. Today, the basic behaviour of nonionic microemulsions is well understood on

the basis of theoretical models in which the mean curvature of interfaces,¹ the bending constants of surfactant monolayers² and the interfacial tension between oil and water³ play a central role. Depending on the composition of the fluids the structures in the fluids can be oil swollen micelles (o/w-microemulsions), bicontinuous structures or water swollen inverse micelles (w/o-microemulsions).

Microemulsions can be prepared either from nonionic or from ionic surfactants.^{2–6}

The single phase regions in systems that consist of oil, water and surfactants are usually plotted in triangular phase diagrams.

The isotropic phase regions (microemulsions) in these triangle presentations are very different for ionic surfactants and for nonionic surfactants.^{7,8} Systems with ionic surfactants, which have been studied usually, contain large isotropic regions in the middle of the triangle while phase diagrams with nonionic surfactants are very different and contain narrow isotropic channels.⁹ For constant surfactant concentration, these channels usually pass from the aqueous side without crossing a phase boundary continuously to the oil side of the phase diagram.

Detailed phase diagrams with many different systems in which the oil and the surfactants were varied have shown that two channels exist in microemulsions with nonionic surfactants and with variable temperature.¹⁰ The two channels are connected with each other in the middle of the phase diagram and the phase region in between the channels contains an L_α-phase. Small angle neutron scattering measurements have

^a University of Bayreuth, BZKG/BayColl, Gottlieb-Keim-Str. 60, 95448 Bayreuth, Germany. E-mail: heinz.hoffmann@uni-bayreuth.de, lukas.wolf@frenet.de

^b Shiseido Research Center, 2-2-1 Hayabuchi, Tsuzuki-ku, Yokohama, Japan 224-8558. E-mail: kei.watanabe@to.shiseido.co.jp

† Electronic supplementary information (ESI) available: Test tube pictures for the established phase diagram. See DOI: 10.1039/c0cp00062k

shown that the micellar structures in the low temperature channel evolve from globular o/w structures, transform to bicontinuous structures in the cross-over region and change continuously to globular w/o structures in the high temperature channel.¹¹ The structures in the upper channel are of a bicontinuous nature right from the aqueous side.¹²

The goal of this investigation was to prepare microemulsions from the highly volatile silicone oil hexamethyldisiloxane (M_2), water and a nonionic/anionic surfactant mixture.

Microemulsions from several silicone oils and nonionic surfactants have already been published.¹³ But as far as we know, a phase diagram with the silicone oil M_2 had not yet been prepared and investigated in detail. It was known however that M_2 behaves similarly in solubilisation experiments as decane.¹⁴ Viscoelastic solutions with wormlike micelles are transformed to low viscous micellar solutions with the same molar amount of decane or of M_2 . The saturation concentration for both oils is also about the same. It could therefore be expected that microemulsions from M_2 can be formed and the phase diagram with M_2 should look similar for decane for the same surfactant system. To achieve our goal, a mixed nonionic/anionic surfactant system was used. This system had to be optimized for the temperature region at which the microemulsion was to be prepared.

Surfactants for the formation of microemulsions can be optimized by interfacial tension measurements.¹⁵ Maximum solubilisation occurs when the interfacial tension of a dilute surfactant solution has its lowest interfacial tension against the oil phase.¹⁶ Furthermore it is known that low interfacial tensions are observed for surfactant systems which form liquid crystalline L_α -phases or L_3 -phases at low surfactant concentrations of a few percent.¹⁷ Ideal surfactant systems for the formation of microemulsions can therefore be recognised based on their phase behaviour.¹⁸

Ionic surfactants like sodiumdodecylsulfate are very hydrophilic and do not give L_α -phases when mixed with water soluble nonionic surfactants. The situation is improved when Na^+ -ions are replaced by bivalent Ca^{2+} -ions. Previous investigations had shown that in mixtures of SDS and tetradecyldimethylaminoxide the L_1 -phase could be transformed to a L_α -phase simply by substituting the Na^+ -ions by Ca^{2+} -ions.¹⁹ Solutions of $Ca(DS)_2$ on their own are still L_1 -phases in which wormlike micelles are present.²⁰ If such solutions are mixed with nonionic compounds that are generally used as co-surfactants one obtains L_α -phases in a wide composition region. As a co-surfactant the nonionic surfactant IT 3 (isotridecyltriethyleneglycolether) was used. It is commercially produced and is worldwide available under the name "Marlipal O13/30" as other well-known nonionic surfactants like "Triton X 100".²¹ The compound is a highly branched isotridecanol, etherified with average 3 EO-groups. Despite its polydispersity, it acts mostly like a pure surfactant for the observed phases.

In a general sense the optimum condition for microemulsions for a particular temperature can be adjusted by mixing a hydrophilic surfactant that forms a L_1 -phase and a lipophilic surfactant that is not soluble in the aqueous phase but forms its own L_2 -phase.²² The used surfactant mixture in our study thus consists of an ionic surfactant that is just a bit

too hydrophilic to form a L_α -phase and a co-surfactant that is a bit too lipophilic to form a L_α -phase on its own. The combination of the two surfactants forms a L_α -phase over a wide surfactant composition. For the aim of this project, we used this surfactant-system which could form L_α -phases and hopefully would form microemulsions of silicone oils.

It should be noted that some results on the influence of ionic surfactants on phase diagrams of nonionic microemulsions have already been published.²³

It was observed that the isotropic channels were widened by the influence of ionic surfactants. There was however no information on the structures of the isotropic channel. As far as we know, our investigations on the described microemulsion results are really the first with a detailed phase diagram that had been established with a nonionic/ionic surfactant mixture. Some of the results turned out to be surprising and could not have been expected on the basis of previous results. The main novel features are: an L_3 -phase with an anionic/nonionic surfactant mixture, a microemulsion with equal amounts of oil and water that cannot have a bicontinuous structure and two isotropic channels that are not connected.

Results and discussion

The surfactant mixtures

In Fig. 1, samples of mixtures of two surfactants are shown that fulfil the criteria described in the Introduction. The surfactants are Ca- or Mg-dodecyl sulfate ($Ca(DS)_2$, or $Mg(DS)_2$) and isotridecyltriethyleneglycolether IT 3. The Ca- or Mg-salts can be easily prepared from sodiumdodecylsulfate, and IT 3 is commercially available. $Ca(DS)_2$ has a high Krafft-temperature of $K_T = 50$ °C and can therefore only be used at higher temperatures or at room temperature, when the Krafft-temperature has been reduced by the second component to room temperature.²⁴ $Mg(DS)_2$ has a lower Krafft-temperature of $K_T = 25$ °C. Fig. 1 shows three rows of samples of the surfactant mixtures.

The first two rows contain samples of $Ca(DS)_2$ with increasing mass fraction of IT 3. The total concentration is constant at 15% (w/w) and temperature is at 40 °C. The lower row of the two shows the same samples between crossed polarizers and a third row shows samples with $Mg(DS)_2$ and IT 3 again with polarizers.

The $Ca(DS)_2$ /IT 3 mixtures contain crystalline precipitates up to a mass fraction of x IT 3 = 0.4. The samples from x IT 3 = 0.5 to 0.75 are birefringent and contain a highly swollen L_α -phase. The sample with x IT 3 = 0.8 is optically isotropic and has a low viscosity. It is a L_3 -phase. The L_3 -phase can be recognised based on its microstructure from cryo-TEM measurements.²⁵ Surprisingly, the samples with an even higher mass ratio of IT 3 contain two phases with a L_α -phase as the larger volume fraction. For normal behaviour of hydrophilic and lipophilic mixtures one would have expected to find multiphase regions without an L_α -phase.²⁶ It is conceivable that the two components are no longer miscible in bilayers and phases are formed with different mixing ratios. It is noteworthy to mention that in the combination of $Ca(DS)_2$ and IT 3 a sample with a two phase L_α / L_3 -situation could not

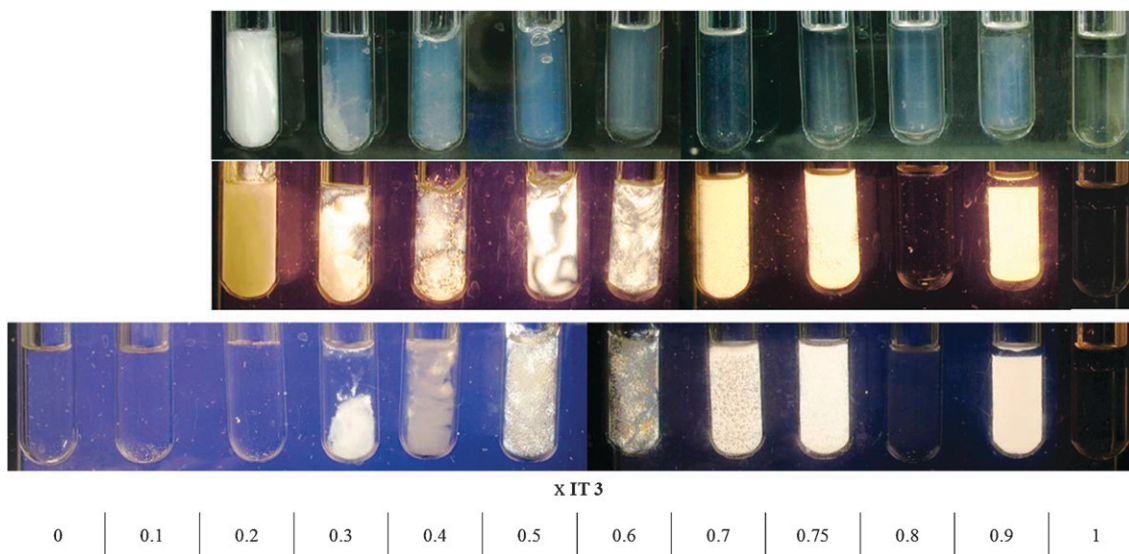


Fig. 1 Surfactant mixtures of $\text{Ca}(\text{DS})_2$ (two upper rows) or $\text{Mg}(\text{DS})_2$ (lower row) with increasing mass fraction x of IT 3. First row shows surfactant mixtures with $\text{Ca}(\text{DS})_2$ in direct light. Second and third rows show samples with $\text{Ca}(\text{DS})_2$ and $\text{Mg}(\text{DS})_2$ between crossed polarizers. Samples prepared with a total surfactant concentration of 15% (w/w), phases observed at $T = 40^\circ\text{C}$.

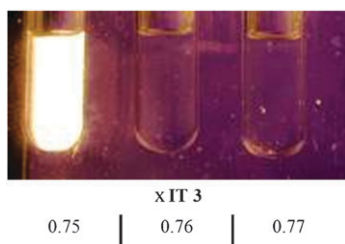


Fig. 2 Surfactant mixture $\text{Ca}(\text{DS})_2/\text{IT 3}$ with $x \text{ IT 3}$ 0.75–0.77, 15% surfactant (w/w), shown at 40°C between crossed polarizers.

be observed when the composition of the samples was varied in small steps. This is shown in Fig. 2. Even for the condition when the composition was varied stepwise one percent by one percent the samples were within the single L_α -phase region or in the single L_3 -phase region. The samples with the $\text{Mg}(\text{DS})_2/\text{IT 3}$ mixtures form more or less the same phases as the $\text{Ca}(\text{DS})_2$ mixtures.

The mixtures with $x \text{ IT 3} = 0.1$ and 0.2 are viscous single phase regions of an optically isotropic L_1 -phase and the sample with $x \text{ IT 3} = 0.3$ is a L_1/L_α two phase sample. The samples with $x \text{ IT 3} = 0.8$ show again a L_3 -phase, and the sample with $x \text{ IT 3} = 0.9$ contains a two phase region with one phase being a L_α -phase. It is remarkable that the mixtures with ionic surfactants form a L_3 -phase.²⁷ Many investigations have shown that neutral L_3 -phases are transformed to L_α -phases when small fractions of the surfactants are replaced by ionic surfactants.²⁸ The existence of the L_3 -phase in the investigated system is probably linked to the fact that the bi-valent metal-ions bind strongly to the dodecylsulfate and the surfactants show only weak dissociation. These surfactants behave therefore very similar like nonionic surfactants.

While the existence of the L_3 -phase in the used system at $x \text{ IT 3} = 0.76$ is unexpected, it is noteworthy that such a phase had also been observed in the phase diagram of $\text{Ca}(\text{DS})_2$

with octanol or lower chain length alcohols.²⁴ In this investigation it was furthermore shown that the L_3 -phase disappeared when 10% of the $\text{Ca}(\text{DS})_2$ was replaced by SDS. What was even more surprising was the appearance of a L_α -phase for co-surfactant ratios well above the existence region of the L_3 -phase. These observations show that the observed sequence of phases for the present system cannot be due to the fact that the used co-surfactant IT 3 is not a pure and single component but must be caused by the bivalent counter-ions. The experimental behaviour furthermore points out that the theoretical understanding of multicomponent systems leaves much to be desired. More experimental results in combination with theoretical models are necessary to come to a better understanding of such complex systems.

Surface and interfacial tension measurements

The samples with the highest solubilisation capacity should be samples with the lowest surface or interfacial tension values. These parameters were therefore measured for a 0.5% surfactant solution as a function of the mixing parameter. Plots of the surface tension measurements are shown in Fig. 3A for the $\text{Ca}(\text{DS})_2/\text{IT 3}$ system, and in Fig. 3B for the interfacial tension values for the $\text{Mg}(\text{DS})_2/\text{IT 3}$ system against the silicone-oil hexamethyldisiloxane.

The lowest surface tension ($\sigma \approx 26.4 \text{ mN m}^{-1}$) is obtained at $x \text{ IT 3} = 0.55$ while the lowest interfacial tension is obtained at $x \text{ IT 3} = 0.4$ with $\gamma \approx 4 \text{ mN m}^{-1}$. These measurements confirm that the samples, that have a composition in the range of a L_α -phase, have indeed low σ and γ values. It should be noted however that the interfacial tension between the oil and water phases in the presence of nonionic surfactants, that results in the formation of microemulsions, is usually in the range of $1 \times 10^{-3} \text{ mN m}^{-1}$.²⁹ That is three orders of magnitude lower. It is conceivable that this difference comes from the fact that the used surfactant mixture contains an

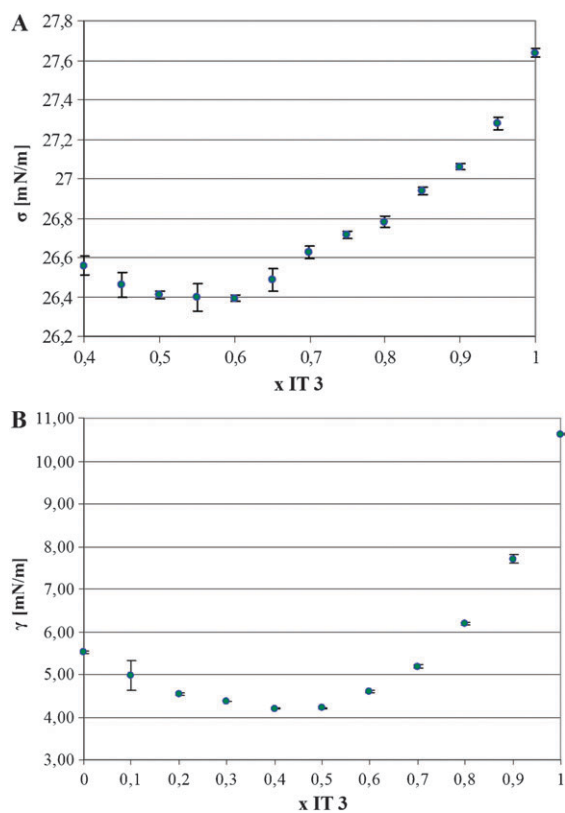


Fig. 3 Surface tension of the surfactant system $\text{Ca}(\text{DS})_2/\text{IT } 3$ (A) and interfacial tension of the surfactant system $\text{Mg}(\text{DS})_2/\text{IT } 3$ against silicone oil hexamethyldisiloxane (B), measured at 25 °C, surfactant concentration 0.5% (w/w).

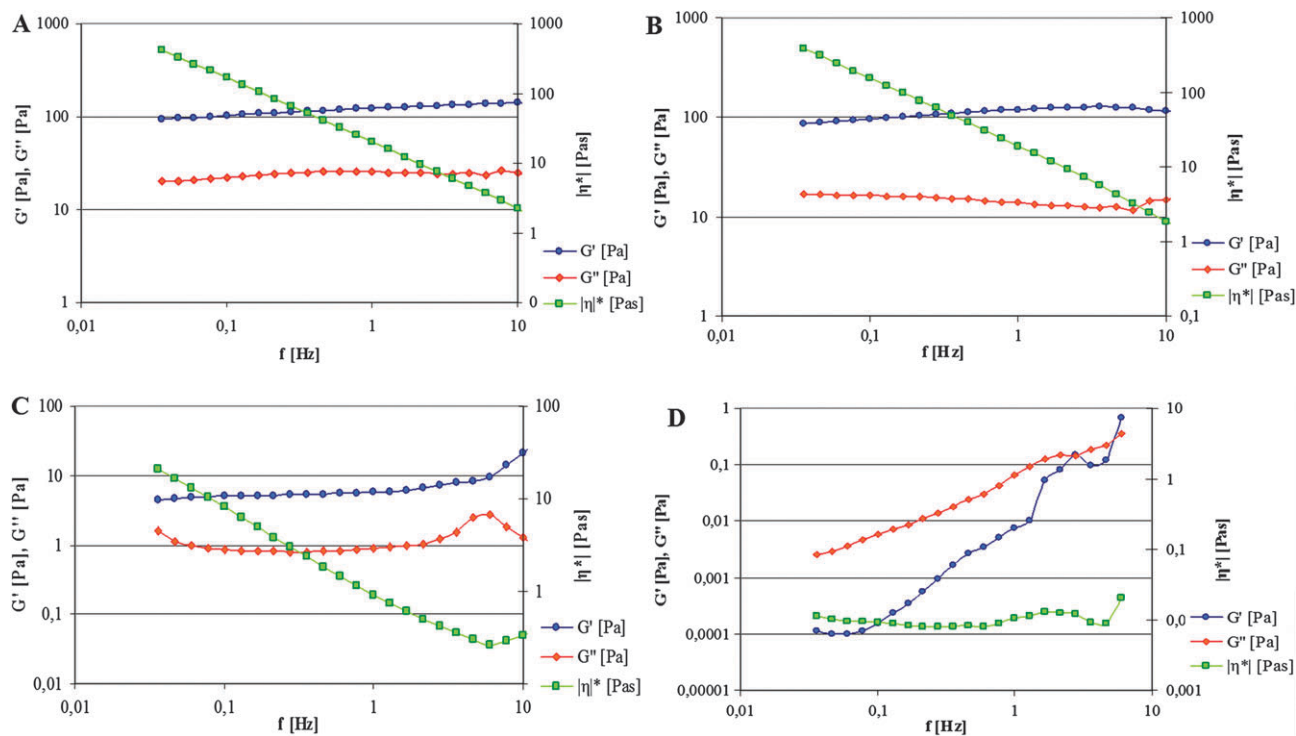


Fig. 4 Rheograms of samples in the L_α -region, surfactant system $\text{Ca}(\text{DS})_2/\text{IT } 3$, surfactant concentration 15% (w/w), measured at 40 °C. (A) x IT 3 = 0.5, measured at $\tau = 5$ Pa. (B) x IT 3 = 0.6, measured at $\tau = 5$ Pa. (C) x IT 3 = 0.7, measured at $\tau = 0.1$ Pa. (D) x IT 3 = 0.75, measured at $\tau = 0.2$ Pa.

ionic surfactant and the charges were not shielded by excess salt. Surfactant phases with an ionic surfactant and excess salt can have extremely low interfacial tension against the oil phase as observed by C. A. Miller *et al.*³⁰ The interfacial tension of double chain surfactants, which have been used for the preparation of microemulsions, against oil is also in the range of 0.1–1 mN m⁻¹.³¹ It is conceivable that the higher interfacial tensions of the charged surfactant systems are the reason for the different behaviour of the investigated system from microemulsions with nonionic surfactants.

Rheological results

The phases with different mixing ratios of the two components have different rheological properties. The pure $\text{Mg}(\text{DS})_2$ -solution is already a viscous “shear thinning solution”. The L_α -phases are viscoelastic phases with a yield stress value. They have already a weak gel-character. The L_3 -phase finally is a low viscous Newtonian solution. Rheograms of samples in the L_α -region at 40 °C were measured and are shown in Fig. 4.

At a mass fraction of 0.5 (Fig. 4A), the storage modulus G' runs above the loss modulus G'' at a level of 100 Pa and is independent of the frequency f at a shear stress of $\tau = 5$ Pa. With increasing mass fraction of IT 3, the level of G' first keeps constant at 100 Pa at x IT 3 = 0.6, and then drops to ~ 8 Pa at x IT 3 = 0.7 at $\tau \approx 0.1$ Pa, but is still independent of f (Fig. 4C). The decay of the storage modulus G' with increasing mass fraction of IT 3 and the fact that G' breaks in at lower shear stress τ show that the L_α -phase loses its gel-like character with increasing x IT 3. At x IT 3 = 0.75, measured at $\tau \approx 0.2$ Pa (Fig. 4D), G' increases in the double

log plot with a slope of 2 while G'' increases with a slope of one, indicating that the L_α -phase lost most of its gel-like character. By reason of the rheological results, we assume a structural change in the L_α -phase from multilamellar vesicles to planar lamellas with increasing x IT 3.

The change of the rheological properties from the L_α to the L_3 -phase by a very small change of the binary surfactant mixture is one of the most startling effects in surfactant science. In the present situation, the difference of the properties of the two phases is especially large because one of the components is ionically charged. But even for systems with nonionic surfactants and co-surfactants the differences between the two phases are remarkable.¹⁸ It should be mentioned that both phases consist of bilayer structures. The origin of the huge change in the rheological and other properties lies in the formation of passages between adjacent bilayers when the L_3 -phase is approached.³²

Solubilisation of hexamethyldisiloxane (M_2) in the different surfactant mixtures

The surfactant mixtures with 15% (w/w) of surfactant and at different mixing ratios were used to solubilise increasing amounts of oil. Photos of test tubes of samples between crossed polarizers can be seen in the ESI.† The phase behaviour of the samples was plotted in a phase diagram (Fig. 5). The special features of the diagram are two isotropic phase channels, a lower channel that begins at the water side at x IT 3 = 0.1 and a higher channel that begins around

x IT 3 = 0.8, the mass fraction of the L_3 -phase. The upper channel first decreases with increasing oil content and then increases slowly with further increase in oil content to the oil corner. The lower channel increases smoothly and seems to end in the middle phase region. In between the two channels are single phase L_α -regions or multiphase regions with one phase being a L_α -phase. The phase diagram shows that it is possible in surfactant mixtures to observe single phase channels for a constant temperature to reach from the water side to the oil side. Such channels have not yet been observed for one component surfactant systems. Under such conditions the temperature has to be changed to observe the single phase channel. While the co-surfactant content in the lower phase channel is increasing with increasing oil content, it is the other way around for the upper phase channel. In this case the co-surfactant content passes through a minimum.

An interesting consequence of this behaviour is that the single L_3 -phase, where the channel begins, is transformed over a multiphase region with increasing oil solubilisation into the upper phase microemulsion with 30% of oil. It is noteworthy that preliminary results with decane as oil have shown a similar behaviour. The shape of the channel for isothermal conditions is thus a consequence of the used surfactant mixture and not of the oil. Of general interest on the phase diagram is also the fact that with increasing solubilisation of the oil into the L_α -phase, the widest extension of the L_α -phase is in the middle of its existence region. At this composition the L_α -phase can solubilise more than its own weight of oil, before it

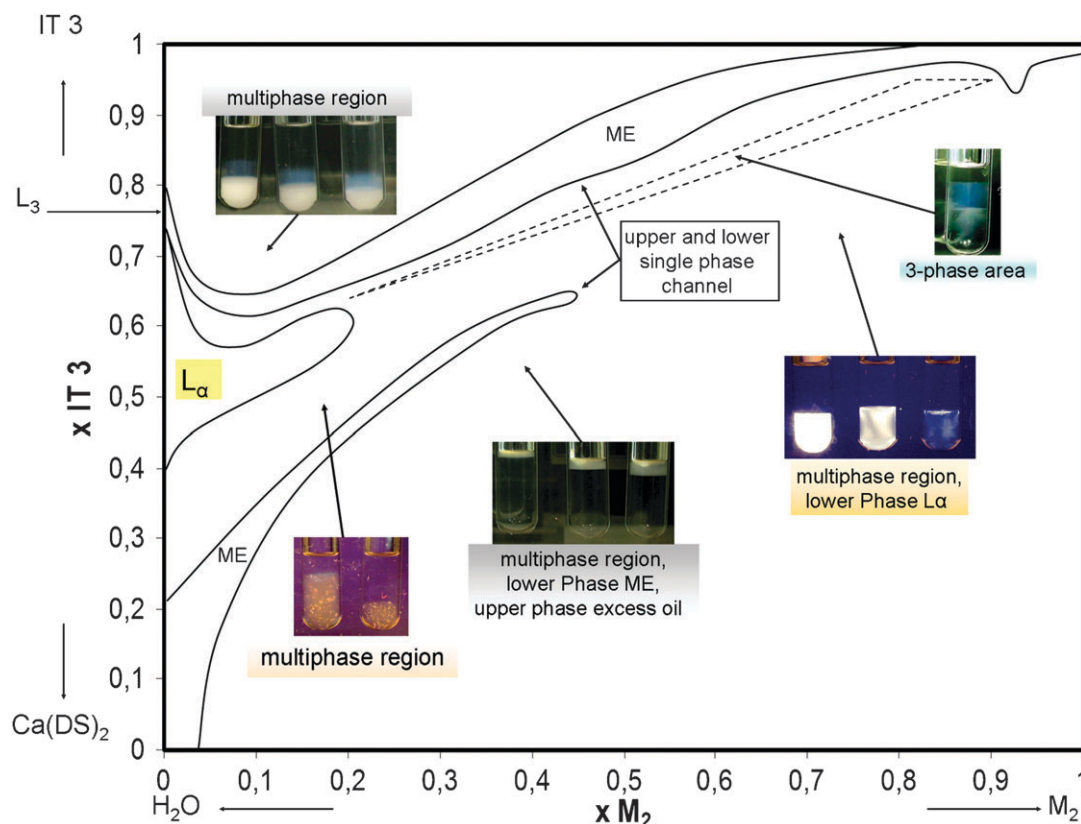


Fig. 5 Phase diagram of the system $\text{Ca}(\text{DS})_2/\text{IT } 3\text{-H}_2\text{O}/M_2$ with 15% (w/w) surfactant and 85% (w/w) solvent. Phases observed at 40 °C. Abbreviation “ME” stands for “microemulsion” and indicates area of isotropic microemulsion channels.

breaks down. The high content of oil in a L_{α} -phase is however not a special feature of the used oil or the surfactant mixture. Other microemulsion phase diagrams have been reported with L_{α} -phases that contain more oil than surfactant and where the surfactant is a nonionic surfactant.³³ It is however interesting to note that such L_{α} -phases exist that consist of two monolayers of surfactant that encloses the oil in between the monolayers and the whole package is like a sandwich.

The multiphase region between the two channels

The multiphase region between the two isotropic channels is very large and dominates the phase diagram. It extends to 45% of oil on the oil axis. Other phase diagrams for microemulsions with nonionic surfactants do not have such a large multiphase region. In the surfactant composition region between x IT 3 = 0.2 and 0.55 the two phase regions are the L_{α}/L_1 -region. The L_{α} -phases on the water side are transformed with increasing amount of oil into two phase regions and finally into the single phase channel. The amount of oil that is necessary to destroy the L_{α} -phase increases with the mass fraction of IT 3 in the surfactant mixture. It is interesting to note that the surfactant phase with x IT 3 = 0.55 can accommodate more than its own weight of oil before some of the L_{α} -phase is transformed to a microemulsion phase.

Close to the upper channel, the situation is more complicated.

Most interesting are the sequence of phases in the surfactant composition between x IT 3 = 0.6 and 0.7. With x IT 3 = 0.6, the L_{α} -phase is transformed with 5% of oil into the two phase L_{α}/ME region and with 20% of oil the system re-enters the single L_{α} -phase. For higher oil ratios the system approaches the lower single phase channel in a two phase L_{α}/ME region. With x IT 3 = 0.65, the phase diagram becomes even more complicated. With 5% oil, the L_{α} -phase is transformed into the upper isotropic channel. In the oil region between 20% and 40%, a two phase region with the L_{α} -phase and an isotropic phase exists, in which the L_{α} -phase first increases with the oil content and then decreases again (see tube pictures of samples in ESI[†]). It is likely that the isotropic phase in the two phase region first is a ME from the upper phase channel while it is a ME from the lower phase channel in the second region.

An even different situation is observed with x IT 3 = 0.7. The pure L_{α} -phase is again transformed with little oil into the

bi-continuous channel. With more oil, multiphase regions are observed that have no L_{α} -region.

The search for a connection of both single phase channels

We were surprised not to find a connection between the lower and the upper single phase channel as would have been expected from known phase diagrams with nonionic surfactants. The reason for this could have been that the composition of the investigated samples was not close enough to detect the connection. To search for a possible connection between both single phase channels, more samples between both channels were investigated. Fig. 6 shows a row of samples that have been prepared by mixing directly a sample from the end of the lower single phase channel with a sample from the upper single phase channel.

The first mixed sample with a composition of x IT 3 = 0.675 and x M_2 = 0.46 is already a two phase sample with a lower L_{α} -phase and an upper isotropic phase. While we did not analyse the upper phase, it looked like it consists of pure M_2 .

This result is a strong indication of existing tie lines between the L_{α} -phase and pure M_2 . It would mean that an isotropic channel cannot exist in between the lower and the upper single phase channel.

In the following samples, the volume of the L_{α} -phase decreases and the volume of the upper phase increases, a sign that the distance of the composition of the sample is increasing from the L_{α} -phase and decreasing from the upper phase. With the sixth sample with the composition x IT 3 = 0.775 and x M_2 = 0.5, the situation changes completely. The sample clearly consists now of three phases, a lower L_{α} -phase, a middle bluish microemulsion phase and an upper oil phase. This three-phase area is followed by a two phase area with a decreasing lower L_{α} -phase and an upper bluish microemulsion phase. With x IT 3 = 0.85 and x M_2 = 0.53, the sample reached the upper isotropic single phase channel. More samples with this three phase situation were found and drafted as a triangle in the phase diagram (Fig. 5). This three phase area indicates that there cannot be a connection of both single phase channels.

The properties of the samples in the single phase channels

It is evident from visual inspection of the samples that the structure of two samples with the same amount of oil but at different surfactant ratios is not the same. An overview of

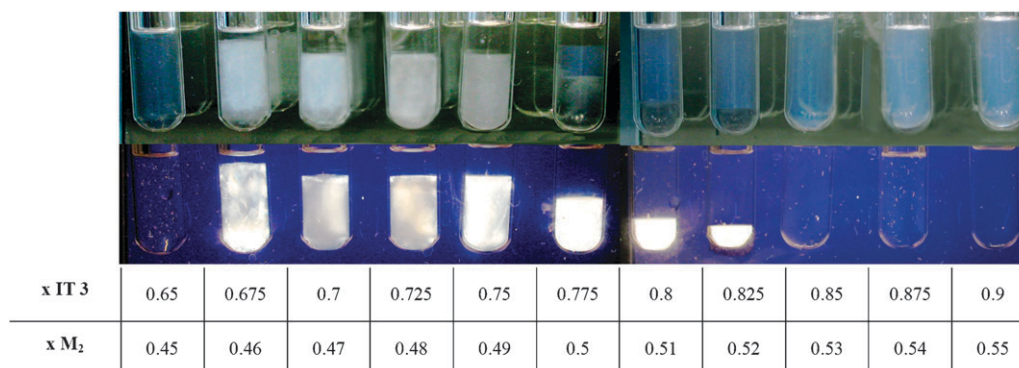


Fig. 6 Mixtures of a sample from the lower and upper single phase channels of the system $\text{Ca}(\text{DS})_2/\text{IT 3}-\text{H}_2\text{O}/\text{M}_2$ with x M_2 = 0.45 and x M_2 = 0.55. Upper row shows samples without crossed polarizers, lower row shows samples in between crossed polarizers at 40 °C.

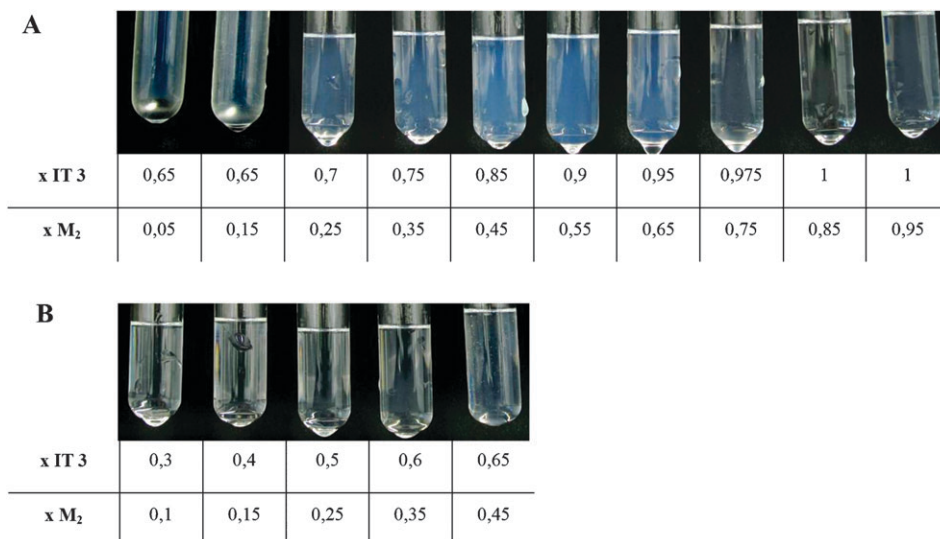


Fig. 7 Overview of selected samples in the upper (A) and lower (B) single phase channel of the system $\text{Ca}(\text{DS})_2/\text{IT 3}-\text{H}_2\text{O}/\text{M}_2$ at 40°C .

samples in the upper and lower single phase channels with increasing amount of oil is shown in Fig. 7.

Samples from the upper phase channel (Fig. 7A) are somewhat bluish and the scattering intensity of the samples increases from the water corner to samples with 65% of oil. Samples with larger oil content scatter less. All samples from the lower phase channel scatter much less (Fig. 7B). Samples from the upper channel show flow birefringence up to 40% oil, while the samples from the lower channel do not show flow birefringence. These features are a first indication that the upper channel has a bi-continuous structure while the lower channel consists of oil droplets in a continuous water phase. The structures of the microemulsions in the channels are now already reported³⁶ and the physicochemical properties like their rheology and their structural relaxation

times will be given in another manuscript. It also will be shown that the obtained phase diagram changes only little if M_2 is replaced by decane. The obtained results are thus typical for microemulsion phase diagrams with mixed nonionic/ionic surfactant mixtures. The temperature stability of the samples in both channels hasn't been investigated in detail, but it was observed that the samples in the lower single phase channel were less sensitive to temperature changes than the samples in the upper single phase channel, especially close to the L_3 -phase. This can be explained by the higher mass fraction of a temperature sensitive nonionic surfactant in the upper channel. Nevertheless, all samples are stable in a wider temperature range than samples with nonionic surfactant mixtures that are only stable within around $\pm 1^\circ\text{C}$.

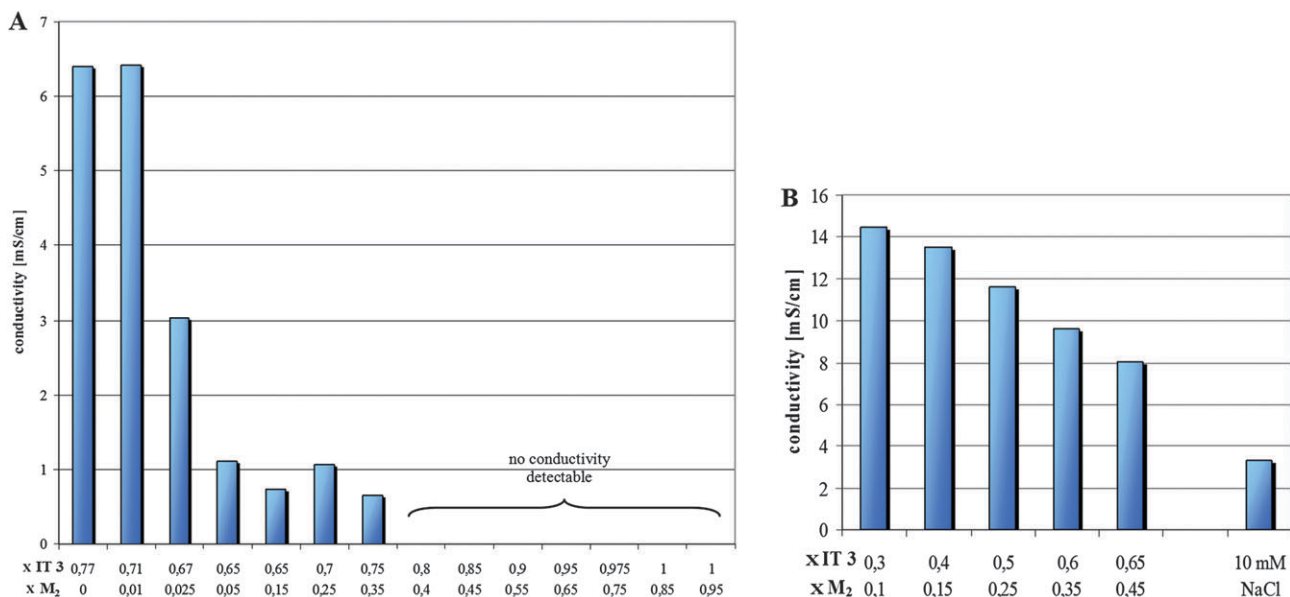


Fig. 8 Conductivity measurements in the upper (A) and lower (B) single phase channel of the system $\text{Ca}(\text{DS})_2/\text{IT 3}-\text{H}_2\text{O}/\text{M}_2$ at 40°C .

Conductivity measurements

For conductivity measurements, all samples have been prepared with 10 mM NaCl. A plot of the conductivity in the two channels against the weight fraction of oil is given in Fig. 8. Note that the conductivities in the lower channel (Fig. 8B) are much higher at the water corner than those in the upper channel (Fig. 8A). The reason for this is that the $\text{Ca}(\text{DS})_2$ concentration is much higher in the lower channel. If the conductivities are normalized to the same $\text{Ca}(\text{DS})_2$ concentration they are about the same. The conductivities decrease linearly with the oil content to the middle of the phase diagram, which is where the channel ends. The reason for the decrease is mainly the decreasing mass fraction of $\text{Ca}(\text{DS})_2$. The conductivities therefore indicate that the microstructure in the lower channel does not change and that the channel consists of a continuous water phase in which oil droplets are dispersed.

The situation is different in the upper channel. In this channel the conductivity drops for a few percent of oil (5%) to only about 18% of its value in the L_3 -phase even though the fraction of $\text{Ca}(\text{DS})_2$ is increasing from 23% to 35%. For higher mass fraction of oil the conductivities remain about constant and drop to zero for $x M_2 = 0.4$. The conductivities thus indicate a dramatic change in the microstructure of the bi-continuous channel with solubilisation of small amounts of oil into the L_3 -phase. Obviously the constraints in the microemulsion for the transport of the ions must be much larger than those in the L_3 -phase. This means that the water channels in the ME-phase must be much smaller than those in the L_3 -phase where the conductivity is only about 2/3 of the value of the normal aqueous phase without a surfactant. The complete break-down of the conductivity for oil fractions larger than 0.4 means that the system changes from a bi-continuous structure to a w/o-structure. Conductivities in the isotropic channels of microemulsions from nonionic surfactants have been reported in the literature.³⁴ In the upper channel the reported conductivities decrease continuously with increasing oil content. These measurements have helped to establish the view which we have today from the structures in the upper channel. With increasing oil content the bicontinuous L_3 -phase swells with the solubilised oil between the bilayers and is finally transformed at high oil content to a w/o system. With equal amount of oil and water both SAXS-data and conductivities show that this phase is still a bicontinuous phase.³⁵ Our conductivity measurements unambiguously show that the structures in the upper channel of the investigated system are different from the structures of known systems with nonionic surfactants. We find a rather abrupt transition from the L_3 -structure to another bicontinuous structure with swollen aqueous channels at around 10% of oil and another abrupt transition at 40% of oil to a w/o structure.

The microemulsion with equal amount of oil and water does not have a bicontinuous structure. In the meantime, this has been confirmed by cryo-TEM images, which show clearly a w/o-structure.³⁶

Finally, at the end of the discussion we would like to draw attention to several experimental observations which have been made during this investigation and which to our knowledge are not theoretically understood and need further scouting. To mention here are the existence of the L_3 -phase in

the anionic nonionic surfactant mixture, the occurrence of a second L_α -region after the existence of the L_3 -phase and a structural transition in the bi-continuous upper phase channel.

Conclusion

The ternary phase diagram of the silicone oil hexamethyl-disiloxane M_2 , water and a surfactant mixture of the ionic surfactant $\text{Ca}(\text{DS})_2$ and the nonionic surfactant isotridecyl-triethyleneglycolether IT 3 has been established as a function of the mass fraction of IT 3.

Two isotropic single phase channels occur in the system with increasing oil content $x M_2$. The lower channel, that is the one with the lower x IT 3 value, begins at the phase boundary of the L_1 -phase toward the L_α -phase. This channel increases with increasing $x M_2$ and ends in the middle of the phase diagram at x IT 3 = 0.65. This channel contains oil droplets in a continuous water phase (o/w-system). The upper channel begins at the L_3 -phase and passes with increasing oil content through a shallow minimum to the oil side. It has, like the L_3 -phase, a bi-continuous structure until 40% oil, and then switches to a w/o structure to the oil side. The microemulsion with equal amount of water and oil does not have a bicontinuous structure. Phases of bicontinuous structure show a strong flow birefringence. Samples from the o/w and the w/o channel are transparent and show no flow birefringence.

In contrast to phase diagrams with one component, surfactant mixtures with surfactants can form channels that pass from the water to the oil side at constant temperature. The amphiphilic properties for the channels can be adjusted by changing the composition of the surfactant mixture instead of the temperature.

The upper channel and the lower channel are not connected with each other. It is likely that the non-connectivity is due to the influence of the ionic surfactant and the high interfacial tension of the surfactant system against oil, which promotes the formation of globular structures instead of a bicontinuous topology.

In total, the investigation has shown that microemulsion phase diagrams, that are established with mixtures of an anionic and a nonionic surfactants, differ from the phase diagram that can be produced with ionic or with nonionic surfactants. We propose that the situation in our system is somewhere between and of general importance.

Experimental

Materials

Sodiumdodecylsulfate (SDS, cryst. research grade) was purchased from the Serva Co., Heidelberg. The nonionic surfactant isotridecyltriethyleneglycolether, in the following text abbreviated as IT 3, was obtained from the Sasol Co., Hamburg (product name Marlipal O13/30). $\text{MgCl}_2 \cdot 6\text{H}_2\text{O}$ and $\text{CaCl}_2 \cdot 2\text{H}_2\text{O}$ were purchased from the Grüssing Co., Filsum.

The silicone oil hexamethyldisiloxane, abbreviated as M_2 , was obtained as a gift from the Wacker Co., München.

Preparation of $\text{Ca}(\text{DS})_2$ and $\text{Mg}(\text{DS})_2$

For the preparation of $\text{Ca}(\text{DS})_2$ and $\text{Mg}(\text{DS})_2$, 400 mM SDS-solutions were mixed with either 200 mM CaCl_2 or MgCl_2

solution under stirring. The bi-valent counter ions Ca^{2+} and Mg^{2+} bind strongly to the dodecylsulfate than the sodium-ion, leading to a precipitation of $\text{Ca}(\text{DS})_2$ in solution below its Krafft-temperature of 50 °C and $\text{Mg}(\text{DS})_2$ below its Krafft-temperature of 25 °C. The solutions were heated up to 60 °C for the solution with CaCl_2 or warmed up above 25 °C for the solution with MgCl_2 to get a clear solution and then cooled down to 20 °C. After precipitation, $\text{Ca}(\text{DS})_2$ and $\text{Mg}(\text{DS})_2$ were washed several times with de-ionised water to remove excess salt. The purity was checked then by measuring the conductivity of the flow through. The washed $\text{Ca}(\text{DS})_2$ and $\text{Mg}(\text{DS})_2$ were dried several days in a cabinet dryer at 50 °C and used without further purification.

Preparation of samples

All samples were prepared by weighing in directly the components in test tubes, first surfactant and co-surfactant, H_2O , and as the last component M_2 due to its high volatility. The test tubes have been sealed with a teflon tape, tempered at 40 °C in a water bath and vortexed several times thoroughly. This temperature was necessary to prevent the crystallization of $\text{Ca}(\text{DS})_2$ in microemulsions with a mass fraction of $x_{\text{IT } 3} < 0.5$. All samples have been incubated at least 3 days at 40 °C before being investigated for their phase behaviour. For the phase diagram, the samples below the mass fraction of $x_{\text{IT } 3} = 0.3$ had to be prepared with $\text{Mg}(\text{DS})_2$ instead of $\text{Ca}(\text{DS})_2$ to avoid problems with precipitation of $\text{Ca}(\text{DS})_2$. The surfactant concentration of 15% (w/w) was necessary to find the single phase channels. In general, the phase diagram has been scanned with a resolution of 5% in the composition of the mass fraction of IT 3 and M_2 . More detailed steps have been investigated in the beginning of the upper single phase channel and in between the two single phase channels to find a possible connection of both channels. The multiphase samples were viewed without and in between crossed polarizers.

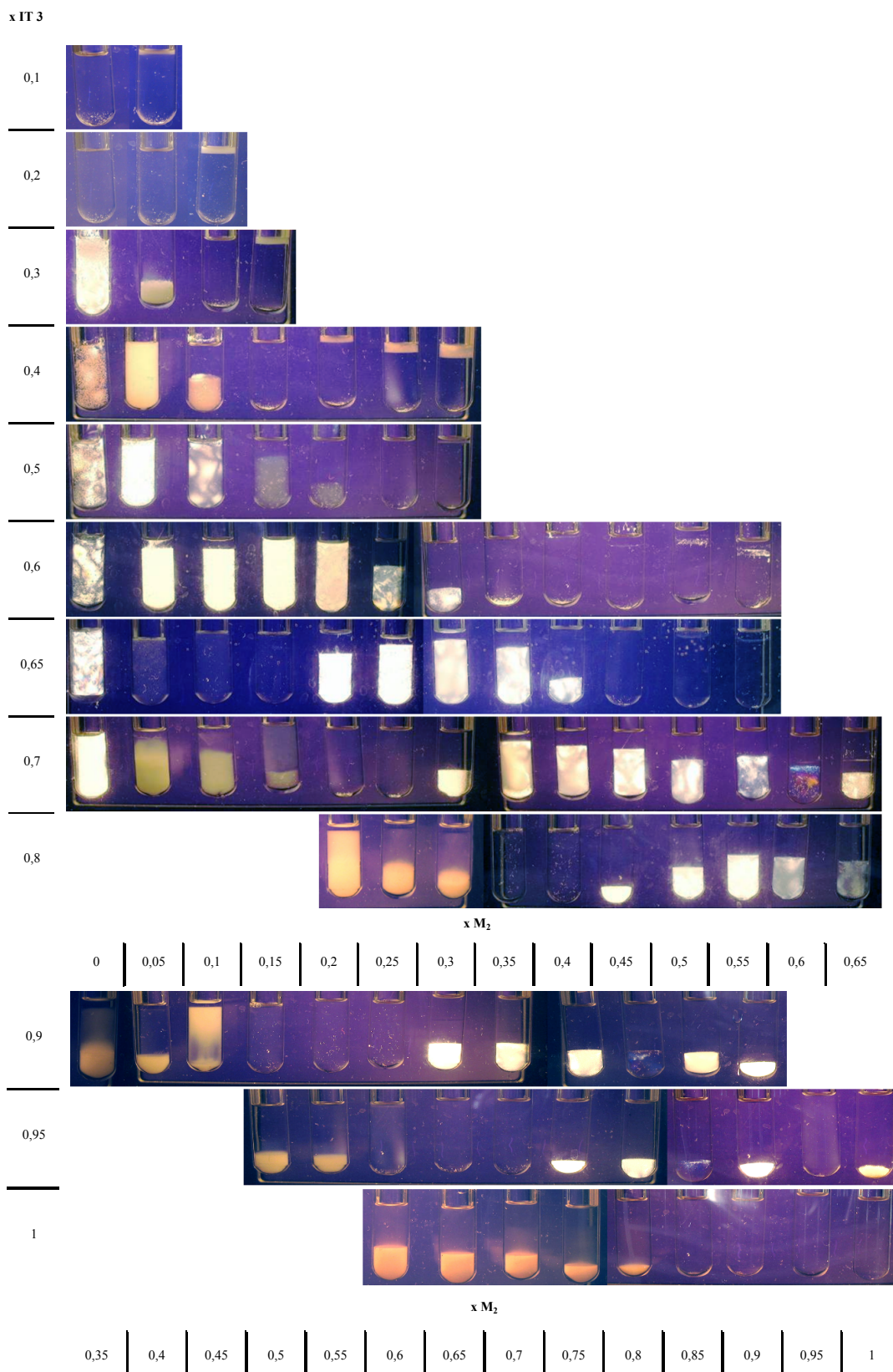
Surface/interfacial tension measurements, conductivity and rheology

The surface and interfacial tensions were measured with the help of the volume-drop tensiometer TVT1 from the Lauda Co., Königshofen. For conductivity measurements, the Microprocessor Conductivity Meter LF2000 from the WTW Co., Weilheim was used. The rheology was measured with the cone-plate rheometer RheoStress 600 from the Haake Thermo Scientific Co., Karlsruhe.

Notes and references

- 1 C. Stubenrauch, *Microemulsions: Background, New Concepts, Applications, Perspectives*, Wiley-VCH, 2009.
- 2 D. Langevin, *Annu. Rev. Phys. Chem.*, 1992, **43**, 341–369; C. A. Miller, *J. Colloid Interface Sci.*, 1983, **91**(1), 223–243.

- 3 R. Strey, *Colloid Polym. Sci.*, 1994, **272**, 1005–1019.
- 4 M. Borkovec, *Adv. Colloid Interface Sci.*, 1992, **37**, 195–217.
- 5 T. Tlustý, S. A. Safran, R. Menes and R. Strey, *Phys. Rev. Lett.*, 1997, **78**(13), 2616–2619.
- 6 B. Lindman, K. Shinoda, U. Olsson, D. Anderson, G. Karlstrom and H. Wennerström, *Colloids Surf.*, 1989, **38**, 205–224.
- 7 S. H. Chen, S. L. Chang, R. Strey, J. Samseth and K. Mortensen, *J. Phys. Chem.*, 1991, **95**, 7427–7432.
- 8 K. Fontell, A. Ceglie, B. Lindman and B. W. Ninham, *Acta Chem. Scand., Ser. A*, 1986, **40**, 247–256.
- 9 F. Lichterfeld, T. Schmeling and R. Strey, *J. Phys. Chem.*, 1986, **90**, 5762.
- 10 M. Kahlweit and R. Strey, *Angew. Chem., Int. Ed. Engl.*, 1985, **24**, 654.
- 11 R. Strey, *Colloid Polym. Sci.*, 1994, **272**, 1005–1019.
- 12 B. Schwarz, G. Mönch, G. Ilgenfritz and R. Strey, *Langmuir*, 2000, **16**, 8643–8652.
- 13 J. A. Silas, E. W. Kaler and R. M. Hill, *Langmuir*, 2001, **17**, 4534–4539.
- 14 H. Hoffmann and A. Stürmer, *Tenside Surfactants Deterg.*, 1993, **30**(5), 335–342.
- 15 V. K. Bansal, D. O. Shah and J. P. O'Connell, *J. Colloid Interface Sci.*, 1980, **75**(2), 462.
- 16 T. Sottmann and R. Strey, *J. Chem. Phys.*, 1997, **106**(20), 8606–8615.
- 17 H. Hoffmann, Plenary lecture, *Prog. Colloid Polym. Sci.*, 1990, **83**, 16–28.
- 18 C. A. Miller, M. Gradzielski, H. Hoffmann, U. Krämer and C. Thunig, *Colloid Polym. Sci.*, 1990, **268**, 1066–1072.
- 19 H. Hoffmann, D. Gräbner, U. Hornfeck and G. Platz, *J. Phys. Chem. B*, 1999, **103**(4), 611–614.
- 20 A. Zapf, R. Beck, G. Platz and H. Hoffmann, *Adv. Colloid Interface Sci.*, 2003, **100–102**, 349–380.
- 21 IT 3 is commercially available under the name Marlupal O13/30 from Sasol Germany GmbH, Auckelmannsplatz 1, 20537 Hamburg, Germany.
- 22 C. B. Douglas and E. W. Kaler, *J. Chem. Soc., Faraday Trans.*, 1994, **90**(3), 471–477.
- 23 M. Kahlweit, B. Faulhaber and G. Busse, *Langmuir*, 1994, **10**, 2528–2532; J. A. Silas, E. W. Kaler and R. M. Hill, *Langmuir*, 2001, **17**, 4534–4539.
- 24 A. Zapf, U. Hornfeck, G. Platz and H. Hoffmann, *Langmuir*, 2001, **17**, 6113–6118.
- 25 R. Strey, W. Jahn, G. Porte and P. Bassereau, *Langmuir*, 1990, **6**, 1635–1639.
- 26 R. Strey and R. J. Schomäcker, *J. Phys. Chem.*, 1994, **98**, 3908.
- 27 H. N. W. Lekkerkerker, *Physica A (Amsterdam)*, 1989, **159**, 319.
- 28 M. Bergmeier, M. Gradzielski, C. Thunig and H. Hoffmann, *IL Nuovo Cimento D*, 1998, **20**, 2251.
- 29 C. A. Miller and C. Neogi, *AIChE J.*, 1980, **26**, 212–220.
- 30 F. Mori, J. C. Lim and C. A. Miller, *Prog. Colloid Polym. Sci.*, 1990, **82**, 114–121.
- 31 U. Lenz and H. Hoffmann, *Ber. Bunsen-Ges. Phys. Chem.*, 1992, **96**.
- 32 R. Strey, W. Jahn, G. Porte and P. Bassereau, *Langmuir*, 1990, **6**, 1635.
- 33 C. Stubenrauch, C. Frank, R. Strey, D. Burgemeister and C. Schmid, *Langmuir*, 2002, **18**, 5027–5030.
- 34 M. Kahlweit, *J. Colloid Interface Sci.*, 1987, **118**, 436–453.
- 35 W. Jahn and R. Strey, *J. Phys. Chem.*, 1988, **92**, 2294.
- 36 L. Wolf, H. Hoffmann, K. Watanabe and T. Okamoto, *Soft Matter*, 2010, **6**, 5367–5374.



Supplementary data: Surfactant mixtures of the system $\text{Ca}(\text{DS})_2/\text{IT } 3$ at 40°C with constant 15% (w/w) surfactant concentration and increasing amount of silicone oil M_2 , shown between crossed polarizers. Samples with $x \text{ IT } 3$ 0.1 and 0.2 prepared with $\text{Mg}(\text{DS})_2$ instead of $\text{Ca}(\text{DS})_2$.

5.1.2. Cryo-TEM imaging of a novel microemulsion system of silicone oil with an anionic/non-ionic surfactant mixture

Lukas Wolf, Heinz Hoffmann*, Yeshayahu Talmon, Takashi Teshigawara and Kei Watanabe

*corresponding author

Published in *Soft Matter* **2010**, *6*, 5367-5374.

DOI: 10.1039/C0SM00049C.

Cryo-TEM imaging of a novel microemulsion system of silicone oil with an anionic/nonionic surfactant mixture

Lukas Wolf,^a Heinz Hoffmann,^{*a} Yeshayahu Talmon,^b Takashi Teshigawara^c and Kei Watanabe^c

Received 3rd March 2010, Accepted 1st August 2010

DOI: 10.1039/c0sm00049c

We report the nanostructures in a novel microemulsion system of silicone oil, water and a surfactant mixture of an anionic and a nonionic surfactant. The phase diagram of the investigated system exhibits two isotropic single-phase channels for constant temperature. The upper channel, that is the channel with the higher mass fraction of nonionic surfactant, starts with an L₃-phase at the water side, and passes through a minimum continuously to the oil side. The channel with the lower mass fraction of nonionic surfactant starts with an L₁-phase at the water side, and passes with increasing oil content and increasing mass fraction of nonionic surfactant to the middle of the phase diagram and ends there. No connection between the two channels was detected at a surfactant concentration of 15%. The two channels are separated by a single L_α-phase and multiphase regions. In contrast to the results from microemulsions with nonionic surfactants, cryo-TEM micrographs on this system show that the upper phase channel has a bicontinuous structure from zero to only about 35% of oil. At higher oil content the channel contains water droplets in a continuous oil phase. At a water/oil ratio of 1 : 1, the structure looks like a polyhedral foam structure or a high internal phase emulsion (HIPE) structure, and not like the usual bicontinuous structure, as generally assumed. Nevertheless, the dimensions of the imaged bicontinuous and water-in-oil-structures were consistent with the theoretical consideration for nanostructures in microemulsions. The lower channel with its o/w-structure could not well be imaged with the cryo-TEM method. Instead of small droplets, small vesicles were imaged, that obviously were formed by the loss of oil in the thin film during the specimen preparation process for cryo-TEM.

Introduction

Microemulsions are thermodynamically stable phases of oil, water and surfactants.¹ Two types of microemulsions can be distinguished on the basis of the used surfactants, ionic surfactant microemulsions and nonionic surfactant microemulsions. Only a few microemulsion systems of ionic surfactants, where the ionic charge has not been shielded by excess salt, have been studied.^{2,3} The best known system is probably the one of dodecane, water and didodecyltrimethylammoniumbromide (DDAB). In the triangular phase diagram the system contains a large single-phase area. Surfactant concentrations of more than 10% are needed to produce single-phases from equal amounts of oil and water. The single-phase region has been studied in detail by different techniques. It contains regions with different macroscopic properties, *e.g.* viscous and non-viscous, conducting and not conducting regions.^{4,5} In this system it is not possible, at constant surfactant concentration, to pass from the single aqueous phase to the oil phase without crossing phase boundaries. The situation in that respect is very different from microemulsions of nonionic surfactants.^{6,7} Those systems usually contain a single-phase channel which reaches from the water side to the oil side of the phase diagram.⁸ However, the temperature has usually to be varied to remain in the single-phase channel.

These types of systems have been well studied, and their behaviour and the microscopic structures in the single-phase channel are known and well understood.⁷ The occurrence of the single-phase channel has to do with the change of the amphiphilic properties with temperature. With increasing temperature the curvature of the amphiphilic monolayer changes from convex, to flat, to concave. As a consequence the microemulsion structures change, from the water side, from small oil droplets in water, to bicontinuous structures in the middle of the phase diagram, to w/o droplets on the oil side. The interfacial tension between the oil and the water is a sensitive parameter for the change of curvature.⁹ Optimum solubilisation of oil in an aqueous surfactant solution is obtained at the minimum of the interfacial tension of the surfactant.

A change of the interfacial tension of a surfactant can also be brought about by adding a co-surfactant to the surfactant solution.¹⁰ In the present investigation we chose therefore a binary mixture of a hydrophilic surfactant with a lipophilic surfactant. We hoped that by changing the mass fraction of two molecules it would be possible to find a single-phase channel for constant temperature. For the ionic surfactant we chose Ca²⁺ or Mg²⁺-salts of SDS, and for the lipophilic co-surfactant we used iso-tridecyl-triethyleneglycolether (IT 3). It is commercially produced and is worldwide available under the name "Marlipal O13/30" like other well-known nonionic surfactants like Triton X 100.¹¹ The compound has a polydisperse distribution of EO-groups with average 3 EO-units.

By changing the mass fraction of the two molecules in the surfactant solution, it turned out to be possible to pass from an

^aUniversity of Bayreuth, BZKG/BayKoll, Gottlieb-Keim-Str. 60, D-95448 Bayreuth, Germany. E-mail: heinz.hoffmann@uni-bayreuth.de

^bDepartment of Chemical Engineering, Technion-Israel Institute of Technology, Haifa, 32000, Israel

^cShiseido Research Center, 2-2-1 Hayabuchi, Tsuzuki-ku, 224-8558, Japan

L_1 -phase with only $\text{Ca}(\text{DS})_2$ over an L_α and an L_3 -phase with the surfactant mixtures to an L_1/L_2 two phase situation for the solution with pure IT 3.¹² Some nonionic surfactants show the same sequence of phases with increasing temperature.

Results and discussion

Phase diagram of $\text{Ca}(\text{DS})_2/\text{IT 3}-\text{H}_2\text{O}/\text{M}_2$

The plot of the surfactant mixture against the mass fraction x of oil between $x = 0$ and $x = 1$ is shown in Fig. 1. As oil, we chose the short silicone oil hexamethyldisiloxane (M_2). The total surfactant concentration was kept constant at 15% (w/w), and the temperature at 40 °C (for details see ref. 12).

The phase diagram contains two isotropic single-phase channels, a lower one and an upper one. The upper one begins on the axis with the mass fraction of IT 3 at the L_3 -phase. With increasing oil concentration, the channel first shifts to a lower IT 3 ratio and then again to a higher IT 3/ $\text{Ca}(\text{DS})_2$ ratio for higher oil ratios. It ends on the oil side with pure IT 3.

The lower channel begins at the water side on the phase boundary to a two phase L_1/L_α -region, and ends in the middle of the phase diagram at an IT 3 ratio of 0.65. We did not find a connection of the two channels.

For an IT 3 ratio of 0.7 we found two isotropic samples with increasing oil, one at 2% of oil and one at 25% of oil.

It is furthermore noteworthy that the L_α -phases of the $\text{Ca}(\text{DS})_2/\text{IT 3}$ mixtures can solubilise large amounts of oil without breaking down. With the mass fraction of IT 3 $x = 0.55$ in the surfactant mixture it is possible to solubilise the same amount of oil as surfactant. Samples with x IT 3 = 0.55 and increasing amount of oil are shown in Fig. 2.

The L_α -phase, which is stable up to 15% of oil, is transformed with 20% oil into a two-phase system, and with 30% of oil finally into the single microemulsion phase.

The microemulsions in the lower channel are transparent phases with low viscosity, which show no flow birefringence

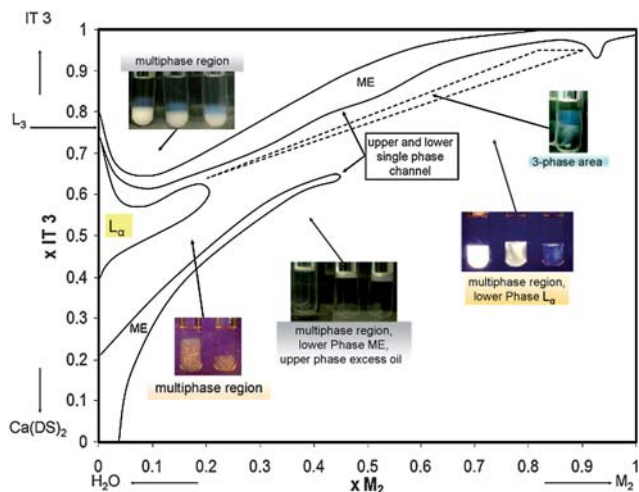


Fig. 1 Phase diagram of system $\text{Ca}(\text{DS})_2/\text{IT 3}-\text{H}_2\text{O}/\text{M}_2$ at 15% (w/w) surfactant and 40 °C. x is the mass fraction, the abbreviation “ME” stands for “microemulsion” and indicates area of isotropic single-phase channel.

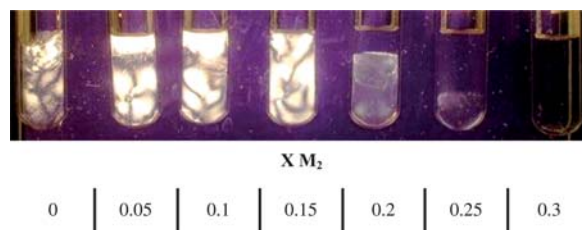


Fig. 2 Samples with constant 15% (w/w) surfactant mixture $\text{Ca}(\text{DS})_2/\text{IT 3}$, mass fraction x IT 3 = 0.55, and increasing mass fraction x of silicone oil M_2 in the solvent at 40 °C, photographed in between crossed polarisers. Single L_α -phases are seen up to 15% oil in the solvent; transparent microemulsion with low viscosity is seen with 30% oil.

under shear. The samples in the upper phase channel have somewhat different properties. The samples are not as transparent as samples from the lower channel. The samples look somewhat bluish, and their scattering intensity increases continuously from the water side to the middle of the phase diagram. For higher oil content the samples are transparent again. Pictures of samples from the lower and upper single-phase channel are shown in Fig. 3.

The different apparent macroscopic properties in the upper and lower phase channel for the same amount of oil are an indication that the structures in the two single-phase channels are different. The conductivity measurements in both single-phase channels, which are shown in Fig. 4, underline this assumption. For the lower channel (Fig. 4B), the conductivities decrease linearly with the oil content to the middle of the phase diagram, which is where the channel ends. The reason for the decrease is mainly the decreasing mass fraction of $\text{Ca}(\text{DS})_2$. The conductivities therefore indicate that the microstructure in the lower channel does not change, and that the channel consists of a continuous water phase in which oil droplets are dispersed. The situation is very different in the upper single-phase channel (Fig. 4A), where the conductivity drops for a few percent of oil (5%) to only about 18% of its value in the L_3 -phase, even though the fraction of $\text{Ca}(\text{DS})_2$ is increasing from 23% to 35%. The conductivities there indicate a dramatic change in the nanostructure of the bi-continuous channel with solubilisation of small amounts of oil into the L_3 -phase. Obviously the constraints

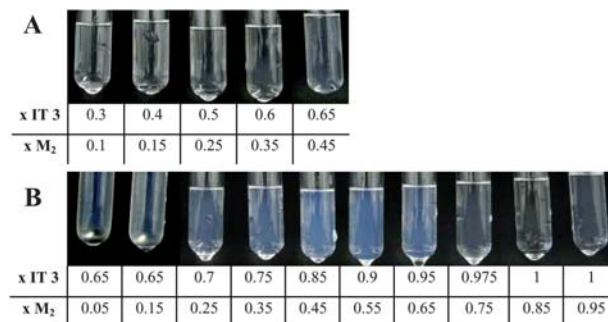


Fig. 3 Samples with 15% (w/w) surfactant mixture $\text{Ca}(\text{DS})_2/\text{IT 3}$ at 40 °C and increasing mass fraction x of IT 3 and M_2 , shown without polarisers. (A) Selected samples from lower single-phase channel. (B) Selected samples from upper single-phase channel.

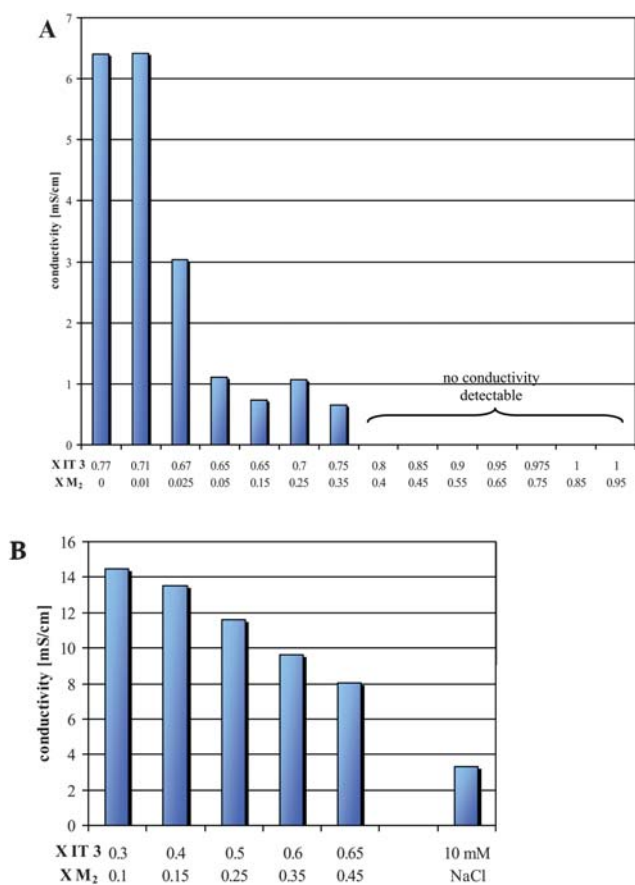


Fig. 4 Conductivity measurements in the upper (Fig. 4A) and lower (Fig. 4B) single-phase channel of the system $\text{Ca}(\text{DS})_2/\text{IT } 3\text{-H}_2\text{O}/\text{M}_2$ at 40°C .

in the microemulsion for the transport of the ions must be much larger than in the L_3 -phase.

This means that the water channels in the ME-phase must be much smaller than in the L_3 -phase where the conductivity is only about $2/3$ of the value of the normal aqueous phase without surfactant. For higher mass fraction of oil, the conductivities remain about constant and drop to zero for x M₂ > 0.35. The complete breakdown of the conductivity means that the system changes from a bi-continuous structure to a w/o-structure. The conductivity results differ a lot from conductivity measurements on microemulsions with nonionic surfactant, in which the conductivity decreases continuously with increasing oil concentration.¹³

In many previous publications of microemulsions it was assumed that the nanostructures in the single-phase channel varied from o/w droplets to bi-continuous structures, to w/o structures.¹⁴ The properties discussed above demonstrate that the situation in the present system must be different and more complicated.

In the following sections we show by cryo-TEM that this is indeed the case. It should, however, be clear that the situation in nonionic and in ionically charged systems may be somewhat different. Although the effect of ionic surfactants on the phase behaviour of microemulsions with nonionic surfactants already was investigated,¹⁵ our system is the first detailed system with an ionic/nonionic surfactant mixture, for which the ionic charge was

not shielded by excess salt, that forms an isotropic channel from the water side to the oil side at constant temperature.

Cryo-TEM micrographs in the upper channel

The phase diagram of this investigation was constructed with 15% surfactant. This is a high concentration to obtain high-resolution micrographs, because the bilayers are close together. It is likely that several structures are superposed in the thin film. Thus the structures are probably not as well resolved as they would be in more dilute samples.

The micrograph in Fig. 5 was prepared with 15% (w/w) surfactant with x IT 3 = 0.77, without oil and quenched from 40°C . The micrograph shows a bi-continuous structure in which the dark lines are the folded bilayers of the L_3 -phase, and the lighter grey areas are water. The thickness of the bilayers, as determined from the micrograph, is about 3 nm. The dimension of the water domains is about 10–20 nm.

As we know for sure, the direct imaging of a bi-continuous L_3 -phase with a high surfactant concentration by the cryo-TEM method is very rare, but similar structures were already reported.¹⁶

The micrograph of Fig. 5 looks very different compared to micrographs from L_3 -phases that are typically prepared with the FF-TEM technique. The most obvious difference is that in FF-TEM micrographs one observes that both the white and grey areas cover about 50% of the area while in the cryo-TEM micrographs the white area is much larger than the grey area. During preparation of the sample with the FF-technique the fracture follows the midplane of the bilayers because this is where the sample breaks most easily.¹⁷ The result of the fracture process is a surface that is half formed from the frozen water phase and half covered by the midplane. This situation is independent from the surfactant concentration in the samples. No fracture is produced with the cryo-TEM method and the structure in the thin films is directly imaged on the micrograph. The grey and white areas reflect therefore the surfactant water ratio of the sample. In total, the three dimensional nature of the water phase

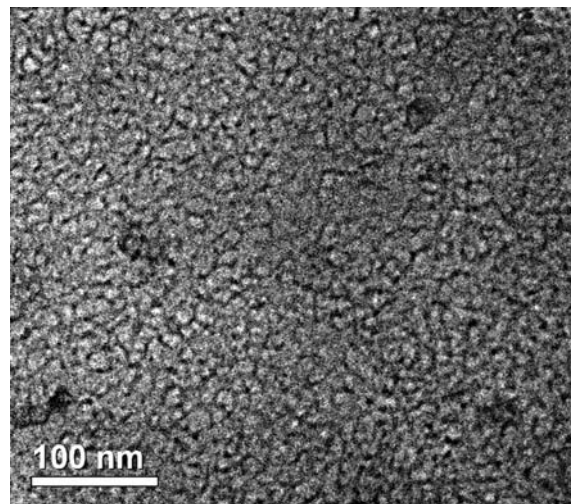


Fig. 5 Cryo-TEM micrograph of sample with 15% (w/w) surfactant $\text{Ca}(\text{DS})_2/\text{IT } 3$, x IT 3 = 0.77, prepared at 40°C . Micrograph shows bi-continuous network-structure of the L_3 -phase.

is not so clearly seen in the cryo-TEM preparation as the three dimensional nature of the bilayer network. The cryo-TEM micrograph in Fig. 5 actually looks somewhat like a two dimensional projection of a three dimensional polyhedral foam. The L_3 -phase is formed only in the very narrow composition of the samples with x IT 3 = 0.76 to 0.77. In the neighbouring L_α -phase with a composition of x IT 3 = 0.75 the structures are very different.

For comparison with the microstructure of the L_3 -phase, micrographs are shown in Fig. 6 of a sample with a slightly different composition, namely with x IT 3 = 0.75.

The micrographs show the typical pattern of a L_α -phase in which the bilayers are perpendicular to the surface of the thin film (Fig. 6A). The interlamellar spacing is of the order of 10–15 nm and the bilayer thickness is about 3 nm. The micrographs of the L_3 -phase and the L_α -phases are very consistent with each other. On close inspection of the micrographs of the L_α -phase one is able to see defects in some regions (Fig. 6B).

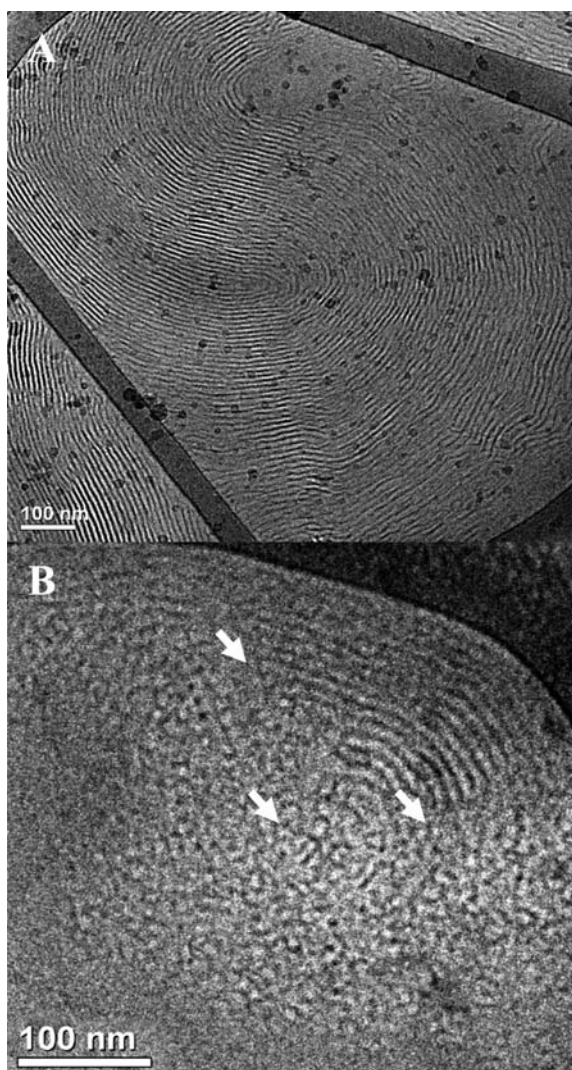


Fig. 6 Cryo-TEM of samples with 15% (w/w) surfactant $\text{Ca}(\text{DS})_2/\text{IT 3}$, x IT 3 = 0.75, prepared at 40 °C. (A) Typical pattern of L_α -phase; (B) L_α -phase with defects, shown by white arrows.

These defects are indicated on the micrographs of Fig. 6B with white arrows.

One notes situations where two adjacent bilayers seem to be connected by bridges. These could be the structures that have been theoretically predicted.¹⁸ It is noteworthy that the micrograph in Fig. 6A looks like a fingerprint with a much larger scale. It is somewhat surprising that the bilayers in the thin films are all perpendicular to the film surface. From optical microscopy, in contrast, it is known that the bilayers are very often aligned parallel to the film surface, what is known under homeotropic alignment. The reason for the different situation that is shown in Fig. 6 may be a result of the film thickness. In the holes of the polymer films the thickness of the surfactant phase varies. On parallel alignment the bilayers would have to form different numbers of bilayers at different positions in the thin film in order to keep the interlamellar distance the same. Such defects cost energy and the film might therefore prefer the perpendicular alignment.

The structures in L_α -phases with a lower IT 3 content (x IT 3 = 0.65) are somewhat different (Fig. 7).

Large multilamellar vesicles (MLVs) are now seen in which the spacing between the bilayers is much larger than in the micrograph with x = 0.75. The larger spacings are probably the result of applying high shear rates to the MLV during the blotting procedure.¹⁶

Cryo-TEM micrographs of samples with increasing amount of oil are shown in Fig. 8. The first two micrographs (Fig. 8A and B) show similar network-like structures to the micrograph of the L_3 -phase without oil (Fig. 5). It is generally assumed that the L_3 -phase is a symmetric phase, where the inside and outside volume of the three-dimensional tubular structure is the same. It is likely that this symmetry is lost by the solubilisation of oil, and the microemulsion is an asymmetric phase. This can be concluded from the abrupt conductivity change that occurs

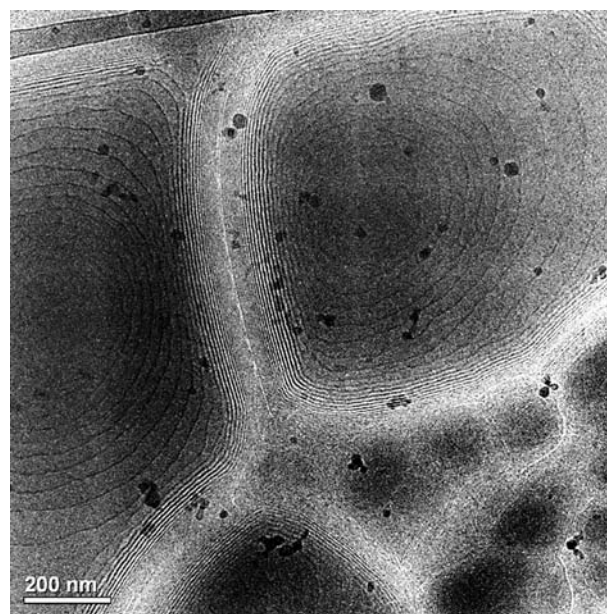


Fig. 7 Cryo-TEM image of sample with 15% (w/w) surfactant $\text{Ca}(\text{DS})_2/\text{IT 3}$, x IT 3 = 0.65, prepared at 40 °C. Large squeezed-together multilamellar vesicles are seen.

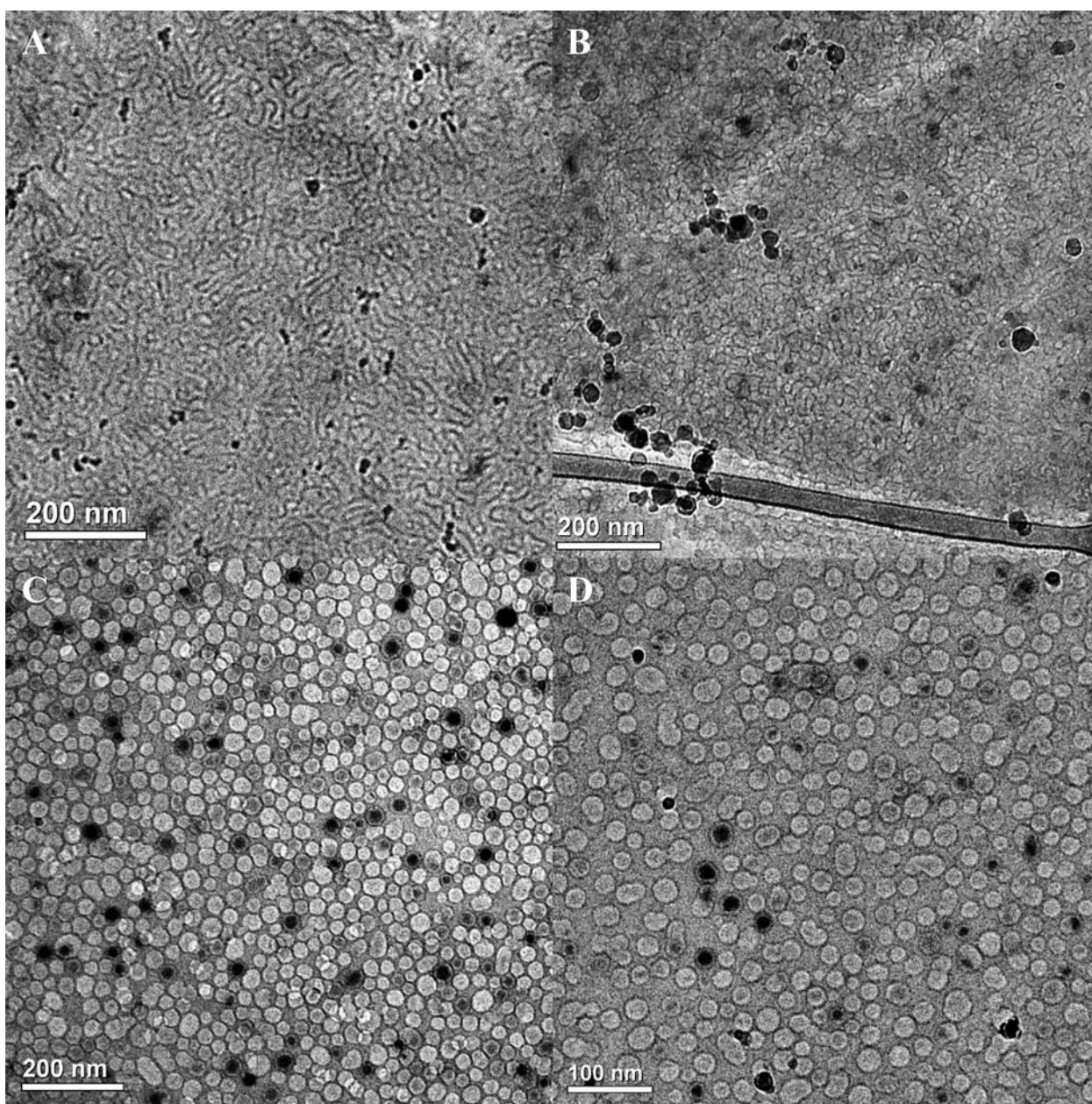


Fig. 8 Cryo-TEM micrographs of samples with 15% (w/w) surfactant Ca(DS)₂/IT 3, prepared at 40 °C: (A) composition $x_{IT\ 3} = 0.65$, $x_{M_2} = 0.05$, sponge-like structure; (B) composition $x_{IT\ 3} = 0.65$, $x_{M_2} = 0.15$, sponge-like structure; (C) composition $x_{IT\ 3} = 0.9$, $x_{M_2} = 0.5$, densely packed water droplets and (D) composition $x_{IT\ 3} = 0.975$, $x_{M_2} = 0.75$, less densely packed water droplets.

around $x_{M_2} = 0.05$. Indeed, the observed bi-continuous structures by the TEM micrographs of samples with solubilised oil look somewhat different from the micrographs of the L_3 -phase without oil. However, some micrographs also show typical structures of L_α -phases or MLV phases. It is likely that these structures result from evaporation of M_2 in the thin film. M_2 is an extremely volatile compound. In order to decrease the evaporation as much as possible, the atmosphere in the preparation chamber had to be saturated with the microemulsion solution and the preparation had to be carried out as quickly as possible. The samples with the highest oil content (Fig. 8C and D) have different structures. In both samples globular particles are observed that are in a lighter grey than the background.

Obviously, the structure has now changed from the bi-continuous structure to w/o droplets. At 50% oil the droplets are densely packed while in the sample with 75% oil the droplets are more dispersed. The droplets have about the same size in the two samples. The diameter of the droplets varies from 20 to 30 nm. Similar globular particles already have been observed in the system AOT-*n*-decane- D_2O by FF-TEM.¹⁹

The micrographs with 50% and 75% oil show some interesting details that are worth emphasizing. In Fig. 8C some of the small globular particles are very dark in comparison to the light grey for most of the other droplets. These particles make up a few percent of the total number of particles. All those particles are crystalline ice, formed during the rapid cooling process. The

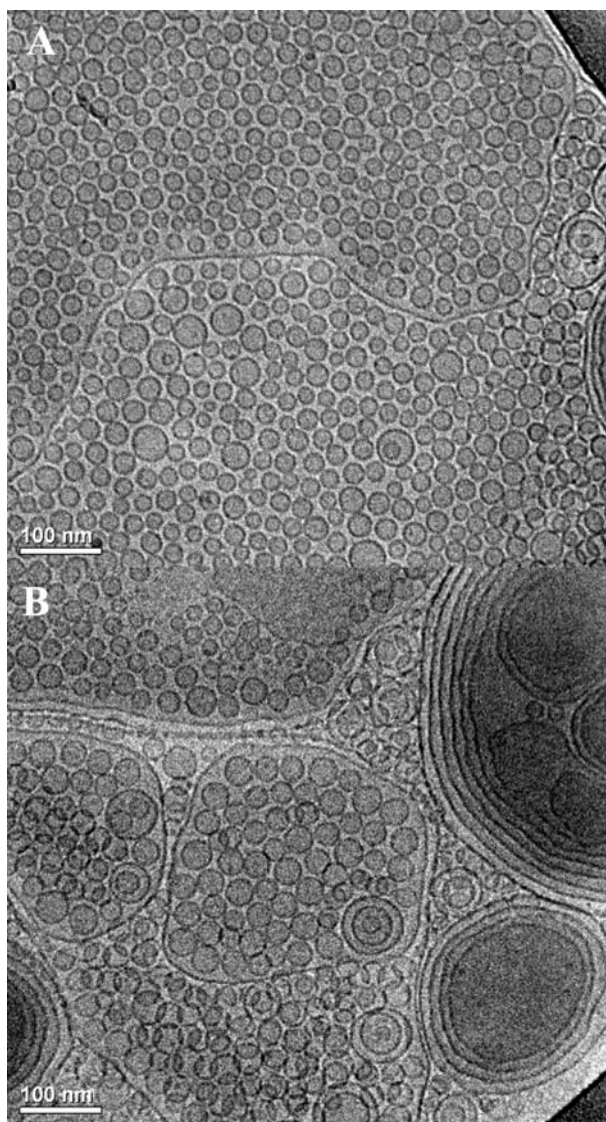


Fig. 9 Cryo-TEM micrographs of sample with 15% (w/w) surfactant $\text{Ca}(\text{DS})_2/\text{IT} 3$, $x \text{ IT} 3 = 0.4$, $x \text{ M}_2 = 0.15$, prepared at 40°C . (A) Small unilamellar vesicles with diameter from 13 to 40 nm. (B) Small unilamellar vesicles and multilamellar vesicles.

cooling rates achievable by liquid nitrogen, used here to avoid oil dissolution, are insufficient to vitrify water (but are sufficient to vitrify the oil!). Thus, the small water domains freeze into crystalline hexagonal ice. These nano-crystals are randomly oriented with respect to the electron beam, so that only a few satisfy Bragg's law for electron diffraction, and those appear dark. The ice crystals that do not diffract appear light grey. The micrographs show that the ice particles could only grow to the size of the droplets, because the droplets were not connected to surrounding droplets.

Micrographs, Fig. 8A and B, with an oil fraction of 0.05 and 0.15 seem to represent situations that are in between the L_3 -phase and the microemulsion situation with 50% of oil. For both samples the crystalline ice structures are somewhat larger than the water domains. These results are in agreement with conductivity measurements in the channel, which show a transition from the conductivity of the L_3 -phase to a lower

conductivity at an oil content of 5%, and finally to loss of conductivity at 40% oil. The development of the structures can therefore at best to be represented by a HIPE like (High Internal Phase Emulsion) structure with varying connectivity between the water domains. In some of the micrographs one can actually observe that some of the droplets are deformed to polygonal structures. Besides the apparent polyhexagon the micrograph also shows that some of the droplets have coalesced with the neighbouring structures, and have formed larger structures. All these details demonstrate that the original droplets are very dynamic species. When the equilibrium conditions are changed, they can quickly adjust to the new conditions. In contrast to the micrograph of the sample with 50% oil, the micrograph with 75% oil shows practically no irregularities. Only very few droplets seem to have formed doublets, while the large majority of the small droplets is randomly distributed in the oil matrix. All in all, clean micrographs of a w/o-microemulsion by cryo-TEM are astonishing and rare, as it had been often assumed, that oil-rich samples cannot be imaged directly,²⁰ as the oil gets dissolved in the regularly used cryogen liquid ethane, or the alternative cryogen liquid nitrogen would not provide the sufficient cooling-rate to vitrify the specimen.²¹

Cryo-TEM micrographs in the lower channel

The lower single-phase channel has a large slope with increasing oil concentration. In addition, the channel is very narrow. As a result of these two conditions it is difficult to obtain good micrographs from the structures in the channel. As it is obvious from the channel, the structures in the channel could change, and the original structures are no longer in equilibrium with their surroundings, when the samples of the channel lose a few percent of oil by evaporation. This is indeed the case, as is demonstrated in Fig. 9, where two micrographs are shown that were obtained from a sample with $x \text{ IT} 3 = 0.4$ and 15% oil. One micrograph (Fig. 9A) shows only small unilamellar vesicles with diameters ranging from 13 to 40 nm. The other micrograph (Fig. 9B) also shows uni- and multilamellar vesicles with interlamellar spacings that are consistent with the surfactant concentration of 15%.

In addition, both micrographs show long lines that separate or surround large domains of different shades. Those represent an encapsulation of small vesicles by larger ones.

Model for the calculation of the microemulsion droplet size

Dimensions for the water or oil droplets in the microemulsions can easily be calculated with the core-shell model and with the help of the oil-surfactant or water-surfactant ratio.

With the volume of the core

$$v_C = \frac{4}{3} r^3 \pi$$

and the volume of the shell which is equal to the volume of the surfactant,

$$v_S = 4\pi r^2 d$$

one obtains the simple equation

$$\frac{v_C}{v_S} = \frac{4\pi r^3}{3 \times 4\pi r^2 d} = R$$

and $r = R3d$.

In this equation d is the thickness of the surfactant monolayer, namely the thickness of the shell. The thickness d can experimentally be appreciated from the cryo-TEM micrographs of the L_α -phase or can be estimated from the number of CH_2 -groups in the surfactant molecules. In an exact calculation, the different lengths of the two surfactant molecules and their different mole ratios in the upper and lower channel have to be considered.

The assumed d value, the volume ratio of the core and shell v_C/v_S , the calculated diameters $D_{\text{cal}}=2r + 2d$ of the droplets and the experimentally determined diameters D_{exp} from the cryo-TEM images are given in Table 1.

Table 1 Overview of the calculated diameters D_{cal} and experimentally determined diameters D_{exp} of the microemulsion droplets from the lower and upper single-phase channel

Size of droplets in lower channel						
$x M_2$	d/nm	v_C/v_S	r/nm	D_{cal}/nm	D_{exp}/nm	
0.15	1.5	1.12	5	13	13–40	
Size of droplets in upper channel						
$x M_2$	$x \text{H}_2\text{O}$	d/nm	v_C/v_S	r/nm	D_{cal}/nm	D_{exp}/nm
0.5	0.5	1.5	2.83	12.8	29	36 ± 6
0.75	0.25	1.5	1.42	6.4	16	25 ± 6

For the calculation of v_C/v_S , the density of the surfactant mixture was estimated to 1 g cm^{-3} , for the volume of the oil, we used the density of 0.76 g cm^{-3} for M_2 .

The agreement between the calculated and experimental determined diameters in the lower channel are not very good. The micrograph of the microemulsion with $x M_2 = 0.15$ from the lower channel shows a large variety of small vesicles with diameters from 13–40 nm, which does not agree with the model.

In contrast to the lower channel, the measured size of the droplets from the upper channel differs only little from the calculated values. Although the droplets show a certain variety in size distribution, the experimental determined diameters are in good agreement with the core-shell model, considering the difficult conditions for sample preparation as the high volatility of the silicone oil and the high temperature.

Conclusion

The nanostructures in the two isotropic channels of a microemulsion of the silicone oil hexamethyldisiloxane (M_2) and a surfactant mixture of the anionic surfactant calcium dodecyl sulfate $\text{Ca}(\text{DS})_2$ and the nonionic surfactant iso-tridecyl-triethyleneglycolether (IT 3) have been determined by cryo-TEM. Contrary to microemulsions with a pure nonionic surfactant, the channels can be formed in this system at constant temperature by adjusting the mass fraction of the two surfactants. The channel with the higher mass fraction of nonionic surfactant begins with the L_3 -phase on the water side, and runs with a shallow slope to the oil side, when the mass fraction is plotted against the oil

content. Conductivity results and cryo-TEM micrographs indicate that bicontinuous structures exist in this channel from the water side to a microemulsion with a 65/35 water oil ratio. The micrographs show that the structure in the bi-continuous region changes from an L_3 -type structure to a HIPE-type structure. Water droplets in the oil matrix exist from the middle of the phase diagram until the oil side. This differs from the nanostructures of microemulsions with nonionic surfactants, where elements of bicontinuous microstructures, even at high oil contents, are reported.²² The sizes of the w/o-droplets in the upper channel are consistent with simple geometrical considerations. They increase, as expected, with an increasing mass fraction of water.

The lower channel begins on the water side with an L_1 -phase and reaches with increasing oil concentration to the middle of the phase diagram. The channel contains o/w droplets in a continuous water matrix. No connection was found between the two channels. Because of the high volatility of the oil, the droplets in this channel were difficult to image with the cryo-TEM method. Small vesicles were obtained in many preparations, instead of the droplets. The vesicles were obviously formed in the thin cryo-film in the time between forming and fixation by temperature quenching. Therefore, we are trying to improve the design of our CEVS to allow us work with more highly volatile solvents such as M_2 , with even smaller concentration changes. We are also looking for a microemulsion system based on a lower-volatility oil, that gives a similar phase diagram.

Experimental

Materials

The nonionic surfactant iso-tridecyl-triethyleneglycolether, abbreviated as IT 3, was obtained from Sasol, Co., Hamburg (Marlipal O13/30). Sodium dodecyl sulfate (SDS, cryst. research grade) was purchased from the Serva Co., Heidelberg. $\text{MgCl}_2 \times 6\text{H}_2\text{O}$ and $\text{CaCl}_2 \times 2\text{H}_2\text{O}$ were purchased from the Grüssing Co., Filsum. The silicone oil hexamethyldisiloxane, abbreviated M_2 , was purchased from the Wacker Co., München, *n*-decane was obtained from the Merck Co., Darmstadt.

Preparation of $\text{Ca}(\text{DS})_2$ and $\text{Mg}(\text{DS})_2$

For the preparation of $\text{Ca}(\text{DS})_2$ and $\text{Mg}(\text{DS})_2$, 400 mM SDS-solution were mixed with either 200 mM CaCl_2 or MgCl_2 solution under stirring. The bivalent counterions Ca^{2+} and Mg^{2+} bind stronger to the dodecyl sulfate than the sodium-ion, leading to a precipitation of $\text{Ca}(\text{DS})_2$ in solution below its Krafft-temperature of 50°C , and $\text{Mg}(\text{DS})_2$ below its Krafft-temperature of 25°C . The solutions were heated up to 60°C for the solution with CaCl_2 , or warmed up above 25°C for the solution with MgCl_2 to obtain a clear solution, and then cooled down to 20°C . After precipitation, $\text{Ca}(\text{DS})_2$ and $\text{Mg}(\text{DS})_2$ were washed several times with de-ionised water to remove excess salt. The purity of the filtered surfactant thus could be checked by measuring the conductivity of its flow through. The washed $\text{Ca}(\text{DS})_2$ and $\text{Mg}(\text{DS})_2$ were dried for several days in a cabinet dryer at 50°C , and later used without further purification.

Preparation of samples

All samples were prepared by weighing in directly the components in test tubes, first surfactant and co-surfactant, H₂O, and, as last component, M₂, due to its high volatility. The test tubes were sealed with Teflon tape, tempered at 40 °C in a water bath, and vortexed several times thoroughly. All samples were incubated at least 3 days at 40 °C before being investigated for their phase behaviour. For the phase diagram, the samples below x IT 3 0.3 had to be prepared with Mg(DS)₂ instead of Ca(DS)₂ to avoid problems with precipitation of Ca(DS)₂. In general, a phase diagram was scanned with a resolution of 5% in the composition of the mass fraction of IT 3 and M₂. Finer steps were investigated in the beginning of the upper single-phase channel, and in between the two single-phase channels to find a possible connection of both channels. The multiphase samples were viewed and imaged without and in between crossed polarisers, to visualise the birefringence of lamellar regions.

Cryo-Transmission Electron Microscopy (Cryo-TEM)

The specimens for cryo-TEM were prepared in a controlled environment vitrification system (CEVS) and plunged into liquid ethane at its freezing point.²³ For oil continuous samples, the specimens were plunged into liquid nitrogen in order to overcome problems with solvent dissolution.²⁴ The CEVS was kept at 40 °C and the atmosphere either saturated with H₂O for the samples without oil, or directly with the investigated microemulsion solution for samples containing oil. Due to high volatility of the silicone oil, the specimens were prepared as quickly as possible. Specimens, kept below –178 °C, were examined in an FEI TI2 G² transmission electron microscope, operated at 120 kV, using a Gatan 626 cryoholder system. Images were recorded digitally in the minimal electron dose mode by a Gatan US1000 high-resolution CCD camera, with the Digital Micrograph software package.

Acknowledgements

We want to thank the Russell Berrie Nanotechnology Institute, Technion (RBNI), for providing us the opportunity to investigate our specimen by electron microscopy. For the excellent technical assistance, we especially thank Judith Schmidt and Dr Ellina Kesselman, and all members of the Lab of the Department

of Chemical Engineering, Technion-Israel Institute of Technology, Haifa 32000, Israel.

Notes and references

- 1 R. Strey, *Curr. Opin. Colloid Interface Sci.*, 1996, **1**, 402–410.
- 2 S. J. Chen, D. Fennell Evans and B. W. Ninham, *J. Phys. Chem.*, 1984, **88**, 1631.
- 3 S. H. Chen and S. L. Chang, *J. Phys. Chem.*, 1991, **95**, 7427–7432.
- 4 C. Mathew, Z. Saidi, J. Peyrelasse and C. Boned, *Phys. Rev. A*, 1991, **43**(2), 872–882.
- 5 J. Bergenholtz, A. A. Romagnoli and N. J. Wagner, *Langmuir*, 1995, **11**(5), 1559–1570.
- 6 T. Sottmann and C. Stubenrauch, Phase Behavior, Interfacial Tension, and Microstructure of Microemulsions, in *Microemulsions: Background, New Concepts, Applications, Perspectives*, ed. C. Stubenrauch, John Wiley & Sons, Oxford, 2009, ch. 1.
- 7 T. Sottmann and R. Strey, Microemulsions, in *Soft Colloids V—Fundamentals in Interface and Colloid Science*, ed. J. Lyklema, Elsevier, Amsterdam, 2005, ch. 5.
- 8 F. Lichtenfeld, T. Schmeling and R. Strey, *J. Phys. Chem.*, 1986, **90**, 5762–5766.
- 9 T. Sottmann and R. Strey, *J. Chem. Phys.*, 1997, **106**, 8606–8615.
- 10 C. Stubenrauch and T. Sottmann, Microemulsions stabilized by Sugar Surfactants, in *Sugar-Based Surfactants: Fundamentals and Applications*, ed. C. C. Ruiz, Taylor & Francis, CRC Press, Boca Raton, 2009, ch. 12.
- 11 IT 3 is commercially available under the name “Marlipal O13/30” from Sasol Germany GmbH, Auckelmannsplatz 1, 20537 Hamburg, Germany.
- 12 L. Wolf, H. Hoffmann, K. Watanabe and T. Okamoto, PCCP, submitted.
- 13 M. Kahlweit, et al., *J. Colloid Interface Sci.*, 1987, **118**, 436–453.
- 14 R. Strey, *Colloid Polym. Sci.*, 1994, **272**, 1005–1019.
- 15 M. Kahlweit, B. Faulhaber and G. Busse, *Langmuir*, 1994, **10**, 2528–2532.
- 16 D. Danino, D. Weihs, R. Zana, G. Orädd, G. Lindblom, M. Abe and Y. Talmon, *J. Colloid Interface Sci.*, 2003, **259**, 382–390.
- 17 H. Hoffmann, C. Thunig, U. Munkert, H. W. Meyer and W. Richter, *Langmuir*, 1992, **8**, 2629–2638.
- 18 R. Strey, W. Jahn, G. Porte and P. Bassereau, *Langmuir*, 1990, **6**, 1635–1639.
- 19 W. Jahn and R. Strey, *J. Phys. Chem.*, 1988, **92**, 2294–2301.
- 20 L. Belkoura, C. Stubenrauch and R. Strey, *Langmuir*, 2004, **20**, 4391–4399.
- 21 V. Agarwal, M. Singh, G. McPherson, V. John and A. Bose, *Langmuir*, 2004, **20**, 11–15.
- 22 S. Burauer, L. Belkoura, C. Stubenrauch and R. Strey, *Colloids Surf., A*, 2003, **228**, 159–170.
- 23 D. Danino, A. Bernheim-Groswasser and Y. Talmon, *Colloids Surf., A*, 2001, **183**, 113–122.
- 24 Y. Talmon, D. Danino, J. Satayavolu and R. Gupta, *J. Colloid Interface Sci.*, 2002, **249**, 180–186.

5.1.3. Dynamic Properties of Microemulsions in the Single-Phase channels

Lukas Wolf*, Heinz Hoffmann, Walter Richter, Takashi Teshigawara and Tohru Okamoto.

*corresponding author

Published in *Journal of Physical Chemistry B*, **2011**, *115*(38), 11081-11091.

DOI: 10.1021/jp2036789.

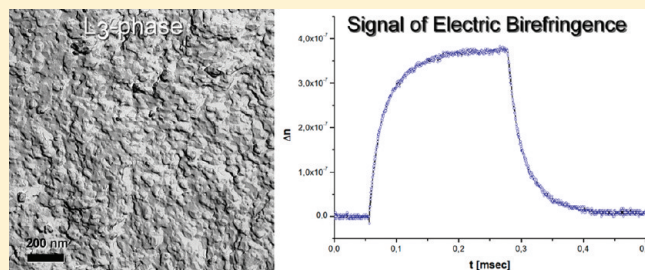
Dynamic Properties of Microemulsions in the Single-Phase Channels

Lukas Wolf,^{*,†} Heinz Hoffmann,[†] Walter Richter,[‡] Takashi Teshigawara,[§] and Tohru Okamoto[§][†]University of Bayreuth, BZKG and BayColl, Gottlieb-Keim-Str. 60, 95448 Bayreuth, Germany[‡]Friedrich-Schiller-University, Centre for Electron Microscopy, Ziegmühlengeweg 1, 07743 Jena, Germany[§]Shiseido Research Center, 2-2-1 Hayabuchi, Tsuzuki-ku, Yokohama, Japan 224-8558

Supporting Information

ABSTRACT: We have studied the dynamic and rheological properties in the single-phase channels of a microemulsion system with a mixed anionic/nonionic surfactant system and decane from the aqueous to the oil phase. One isotropic channel, called the “upper” channel, begins at the L_3 phase (sponge-like phase) of the binary surfactant mixture on the water side and passes with a shallow minimum for the surfactant composition to the oil side. The other “lower” single-phase channel begins at the micellar L_1 phase and ends in the middle of the phase diagram. Both isotropic channels are separated by a

huge anisotropic single phase L_{α} channel that reaches from the water side to 90% of oil in the solvent mixture. The structural relaxation time of the viscous fluids could be measured with electric birefringence (EB) measurements, where a signal is caused by the deformation of the internal nanostructure of the fluids by an electric field. For the L_3 phase, the EB signal can be fitted with a single time constant. With increasing oil in the upper channel, the main structural relaxation time passes over a maximum and correlates with the viscosity. Obviously, this time constant controls the viscosity of the fluid ($\eta^0 = G' \cdot \tau$). It is remarkable that the longest structural relaxation time increases three decades, and the viscosity increases two decades when 10% of oil is solubilized into the L_3 phase. Conductivity data imply that the fluid in the upper channel has a bicontinuous structure from the L_3 phase to the microemulsion with only 10% oil. In this oil range, the conductivity decreases three decades, and the electric birefringence signals are complicated because of a superposition of up to three processes. For higher oil ratios, the structure obviously changes to a HIPE (high internal phase emulsion) structure with water droplets in the oil matrix.



INTRODUCTION

Microemulsions are thermodynamically stable phases from oil, water, and surfactants.¹ The phases contain well-defined structures, such as oil droplets in a continuous water phase, water droplets in a continuous oil phase, and bicontinuous structures. The detailed structures depend on the composition of the system in the ternary phase diagram. Usually, the structures change with a change in the composition of the samples. For many years, microemulsions with ionic surfactants were in the focus of interest.² More recently, microemulsions with nonionic surfactants have become the center of interest.³ As a consequence, we now have a good understanding of microemulsions. It is known, for example, how the phases can be optimized for as little surfactant as possible and how the surfactant can be optimized for a given oil. Of fundamental importance for the understanding of the systems is the value of the interfacial tension of a micellar solution against an oil phase.⁴ For a high solubilization of an oil in a micellar solution, the interfacial tension has to be minimized.⁵ One of the most fascinating features of nonionic microemulsions is isotropic single-phase channels that pass from the aqueous micellar phase continuously to the oil phase for constant surfactant concentration.⁶ Because of SANS and SAXS, we have a good understanding of the structures in these channels. Many

systems have been investigated that have two channels from the water to the oil side, one at lower temperature and one at a higher temperature, and a single channel in the middle of the phase diagram that is connected with the two channels at both sides.⁷ Today, there is a good theoretical understanding of the structures in the isotropic channels and about the thermodynamics of microemulsions with nonionic surfactant. However, very few investigations have been carried out on the dynamic behavior of the microemulsions, and no systematic investigation has so far been made in a channel from the water side to the oil side.

In this investigation, we therefore will study the dynamic properties of microemulsions in the single-phase channels by rheology and the electric birefringence method. The measurements were carried out on a system with an anionic/nonionic surfactant mixture that was similar to one that was previously studied and from which we knew the position of the single phase channels.⁸

Received: April 20, 2011

Revised: August 15, 2011

Published: August 15, 2011

EXPERIMENTAL SECTION

Materials. The nonionic surfactant iso-tridecyl-triethylglycol ether, abbreviated as IT 3, was obtained from the Sasol Company (Hamburg, Germany) (“Marlipal O13/30”). This compound has a polydisperse distribution of EO groups with an average of three EO units. Sodium dodecyl sulfate (SDS, cryst. research grade) was purchased from the Serva Company (Heidelberg, Germany). $\text{MgCl}_2 \cdot 6 \text{H}_2\text{O}$ was purchased from the Grüssing Company (Filsun, Germany). *N*-Decane (analytical grade) was obtained from the Merck Company (Darmstadt, Germany).

Preparation of $\text{Mg}(\text{DS})_2$. For the preparation of $\text{Mg}(\text{DS})_2$, 400 mM SDS solution was mixed with 200 mM MgCl_2 solution under stirring. The bivalent counterion Mg^{2+} binds stronger to the dodecyl sulfate than the sodium ion, leading to a precipitation of $\text{Mg}(\text{DS})_2$ in solution below its Krafft temperature around 25 °C. The solution was heated above 25 °C to obtain a clear solution and then cooled to 20 °C. After precipitation overnight, $\text{Mg}(\text{DS})_2$ was filtered and washed several times with deionized water to remove excess salt. The purity of the surfactant thus could be checked by measuring the conductivity of the flow through of the filtered $\text{Mg}(\text{DS})_2$. The washed $\text{Mg}(\text{DS})_2$ was freeze-dried with the freeze-drying device Alpha 1-4, Christ Company (Osterode, Germany), and used without further purification.

Preparation of Samples. All samples were prepared by weighing the components directly in test tubes on an analytical balance. The test tubes were sealed with Teflon tape, tempered at 25 °C in a water bath, and vortexed several times thoroughly. All samples were incubated at least 3 days at 25 °C before being investigated for their phase behavior. In general, a phase diagram was scanned with a resolution of 5% in the composition of the mass fraction of IT 3 and decane. Finer steps were investigated in the beginning of the narrow upper single-phase channel. The multiphase samples were viewed and imaged without and in between crossed polarizers to visualize the birefringence of lamellar regions.

Freeze-Fracture Transmission Electron Microscopy (FF-TEM). The microemulsions, prepared in presence of 20% (w/w) glycerin in the aqueous phase were stored at room temperature (25 °C) and quick-frozen from RT using the sandwich technique. A small amount of the samples was sandwiched between two copper profiles (BAL-TEC/Balzers, Liechtenstein) as used for the double-replica technique and frozen by plunging these sandwiches immediately into a liquefied ethane–propane mixture (v/v 1/1) cooled in liquid nitrogen. Fracturing and replication were performed at –150 °C in a BAF 400T freeze-fracture device (BAL-TEC/Balzers, Liechtenstein) equipped with electron guns and a film sheet thickness monitor. For replication, at first, Pt(C) was evaporated under an angle of 35° (thickness: 2 nm), followed by C under 90° angle (thickness 20 nm). The replicas were placed on electron microscopic copper grids (Mesh 400), cleaned by chloroform–methanol mixture (v/v 2/1), and examined in an EM 900 electron microscope (Zeiss, Oberkochen, Germany).

Conductivity and Rheology Measurements. For conductivity measurements, we used the microprocessor conductivity meter LF3000 from the WTW Company (Weilheim, Germany). The rheology was measured with the cone–plate rheometer RheoStress 600 from the Haake Thermo Scientific Company (Karlsruhe, Germany). All samples were investigated at 25 °C.

Electric Birefringence Measurements. The electric birefringence device is a self-made device with a 632.8 nm He–Ne laser, crossed polarizers, aperture plates, a Kerr cell with temperature control, and a photomultiplier. For the generation of an electric pulse, there was used the Cober “high power pulse generator” model 606. The signal of the photomultiplier was recorded with the Voltcraft DSO-2090 USB-oscilloscope. Data were processed and evaluated with the computer software “Origin”.

SANS Measurements. For SANS measurements, samples were prepared with D_2O instead of H_2O . By replacing H_2O by D_2O , the phases in the single-phase channels are slightly shifted. To obtain transparent isotropic phases, we had to adjust the surfactant composition by increasing the mass fraction of IT 3 by ~2%. SANS data were obtained with the SANS device D11 at the Institut Laue-Langevin in Grenoble, France. Samples were filled in 1 mm quartz cuvette (Helma), and temperature was set to 25 °C.

Evaluation of data (background detection, subtraction of signal intensity, scaling of data) was performed with standard computer software.

RESULTS AND DISCUSSION

Phase Diagram $\text{Mg}(\text{DS})_2/\text{IT 3}-\text{H}_2\text{O}/n\text{-Decane}$. On microemulsion systems with a single nonionic surfactant, it is not possible to pass from a single aqueous phase to a single oil phase at constant temperature. The interfacial tension of nonionic surfactants changes with temperature, and thus the single-phase regions of microemulsions are temperature-dependent. The amphiphilic properties of surfactants can also be changed by adding a cosurfactant to the surfactant solution. In the present investigation, we therefore chose a binary mixture of a hydrophilic surfactant with a lipophilic surfactant. For the ionic surfactant, we chose the Mg^{2+} salt of SDS. $\text{Mg}(\text{DS})_2$ is more lipophilic than SDS, reduces the surface tension more effectively, and is known to form liquid crystalline L_α phases when mixed with suited cosurfactants.⁸ As lipophilic cosurfactant, we used iso-tridecyl-triethylglycol ether (abbreviation IT 3, = C_{13}E_3). By changing the mass fraction of the two molecules in the surfactant solution, it turned out to be possible to pass from a micellar L_1 phase with only $\text{Mg}(\text{DS})_2$ over lamellar L_α and an L_3 phases (sponge-like phase) with the surfactant mixtures to an L_1/L_2 (L_2 = inverse micellar phase) two phase situation for the solution with pure IT 3. The phase sequence of the binary surfactant mixture is shown in Figure S11 of the Supporting Information, and detailed rheological investigations can be found in Figure S12 of the Supporting Information. Some nonionic surfactants show the same sequence of phases with increasing temperature.

The plot of the surfactant mixture against the mass fraction x of the oil decane in the solvent mixture between 0 and 1 is shown in Figure 1. The total surfactant concentration was kept constant at 15% (w/w), the temperature was kept at 25 °C, and samples were prepared with 20% glycerine in H_2O for possible FF-TEM investigations to prevent freezing artifacts.

The phase diagram contains two isotropic channels, a lower one and an upper one. The upper one begins on the surfactant axis at the region of the L_3 phase. With increasing oil, the channel first shifts to a lower IT 3 ratio and then again to a higher IT 3/ $\text{Mg}(\text{DS})_2$ ratio for higher oil ratios. It ends on the oil side at 80% decane and pure IT 3 as surfactant. The lower channel begins at

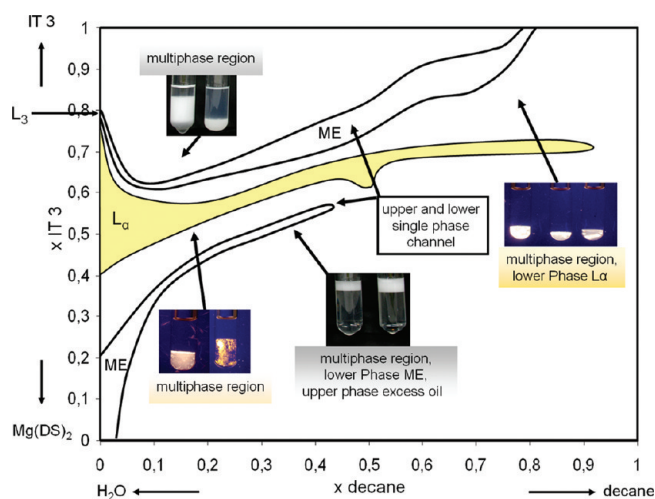


Figure 1. Phase diagram of system $\text{Mg}(\text{DS})_2/\text{IT } 3\text{-H}_2\text{O}/\text{decane}$ at 15% (w/w) surfactant and 25 °C, 20% glycerin in H_2O \times IT 3 = mass fraction of IT 3 in the surfactant mixture, x decane = mass fraction of decane in the solvent mixture. “ME” indicates isotropic microemulsion area, and L_α indicates area of anisotropic lamellar channel.

the L_1 region and ends in the middle of the phase diagram at an IT 3 ratio of 0.57.

Both channels are separated by a huge single-phase birefringent L_α region that extends from 0 to 90% decane with slightly increasing mass fraction of IT 3. All samples in the L_α channel behave like gels. However, the storage modulus G' is decreasing constantly with increasing oil content, indicating that the gels become softer. Pictures of the L_α phases between crossed polarizers at different temperatures and detailed rheology data can be found online in Figure SI3 of the Supporting Information.

A significant feature of the L_α channel is its high-temperature stability. Samples between x decane = 0 to 0.9 are stable at least between 10 and 40 °C, and samples with x decane 0 to 0.4 are even stable at least up to 60 °C. Although the L_α channel is quite narrow, its high-temperature stability is amazing. This feature is obvious due to the surfactant mixture, where the hydrophilic–lipophilic balance is determined more by the mass fraction of the cosurfactant than by the temperature. L_α phases with oil and a single nonionic surfactant of the type $C_{12}E_8$ are not so stable.³²

The microemulsions in the lower single phase channel are transparent phases that show no flow birefringence under shear. The samples in the upper phase channel have somewhat different properties. Whereas the L_3 phase without decane is completely transparent, the samples with decane look somewhat bluish and their scattering intensity is most intensive around x decane 0.03 and 0.1. For higher oil content, the scattering intensity is decreasing again. Pictures of samples from the lower and upper single phase channel are shown in Figure SI4 of the Supporting Information. The different macroscopic properties in the upper and lower phase channels for the same amount of oil are already an indication that the structures in the two single-phase channels are different. In many previous publications of microemulsions, it was shown that the micellar structures in a single-phase channel varied from o/w droplets to bicontinuous structures to w/o structures.⁹

The following chapters will show, that the situation in the present system must be different and more complicated. It

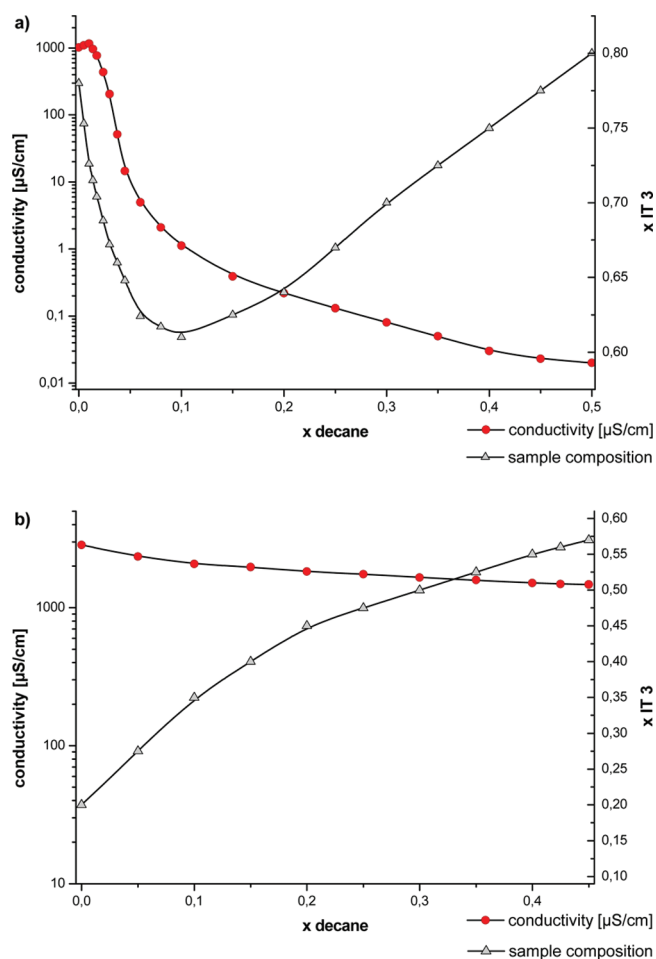


Figure 2. Plot of conductivity (red dots) and IT 3 content (gray triangles) against mass fraction of decane in solvent mixture. (a) Conductivity data for the upper single phase channel. (b) Conductivity data for the lower single phase channel.

should, however, be clear that the situation in nonionic and in somewhat ionically charged systems may be somewhat different. Our investigated system is the first system with an ionic surfactant for which the ionic charge was not shielded by excess salt that forms an isotropic channel from the water side to the oil side.

Conductivity in the Single-Phase Channels. The plot of the conductivity in the upper and lower single-phase channels against the mass fraction of decane in the solvent mixture is shown in Figure 2.

In the upper channel, the conductivity first increases slightly from $\sim 1000 \mu\text{S}/\text{cm}$ of the sample without decane to $1160 \mu\text{S}/\text{cm}$ to the sample with 1% decane. The reason for this lies in the change of the composition of the surfactant mixture. In the range from 1 to 10% decane, the conductivity decreases abruptly three orders of magnitude to $1 \mu\text{S}/\text{cm}$ even though the fraction of the anionic $\text{Mg}(\text{DS})_2$ is increasing. For higher mass fractions of decane, the conductivity values decrease continuously to low values as, for example, $0.03 \mu\text{S}/\text{cm}$ for the sample with a water/oil ratio of 1/1 (w/w). The conductivities thus indicate a dramatic change in the nanostructure of the upper channel with solubilization of small amounts of oil into the L_3 phase. The abrupt collapse of the conductivity indicates that the system

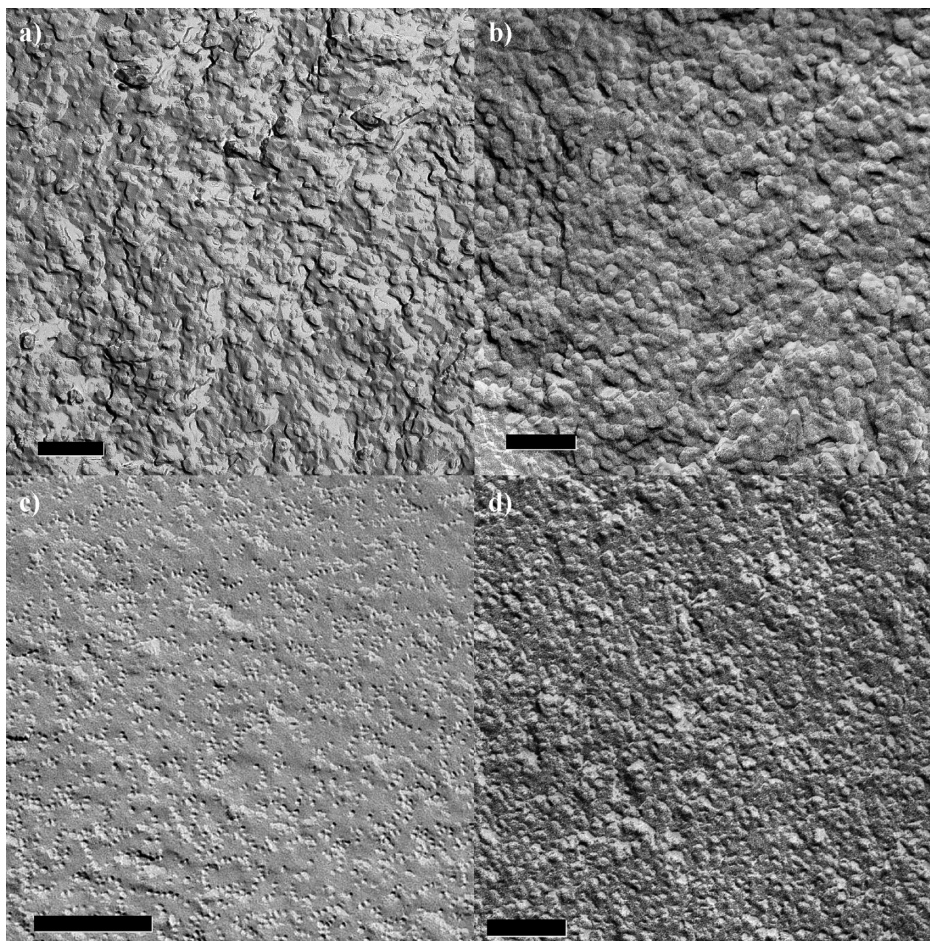


Figure 3. FF-TEM micrographs with 15% (w/w) surfactant $\text{Mg}(\text{DS})_2/\text{IT } 3$, 20% glycerine in H_2O , prepared at 25°C ; scale bar = 200 nm. (a) L_3 phase without oil at $x \text{ IT } 3 = 0.79$, (b) microemulsion of upper channel with $x \text{ IT } 3 = 0.67$, $x \text{ decane} = 0.2$, (c) microemulsion of lower channel with $x \text{ IT } 3 = 0.35$, $x \text{ decane} = 0.1$, o/w-structure, droplet size ~ 7 nm, and (d) microemulsion of lower channel with $x \text{ IT } 3 = 0.45$, $x \text{ decane} = 0.2$, droplet size ~ 14 nm.

changes from a bicontinuous structure to a w/o structure (water-in-oil). Conductivities in the isotropic channels of microemulsions from nonionic surfactants have been reported in the literature.¹⁰ In such systems, the conductivity in the upper channel decreases continuously with increasing oil content. These measurements have helped to establish the view that we have today from the structures in the upper channel. With increasing oil content, the bicontinuous L_3 phase swells with the solubilized oil between the bilayers and is finally transformed at high oil content to a w/o system. With equal amount of oil and water, SAXS data and conductivities show that this phase is still a bicontinuous phase.¹¹ Our conductivity data unambiguously show that the structures in the upper channel of the investigated system are different from the structures of known systems with nonionic surfactants. We find a rather abrupt transition from the bicontinuous L_3 structure to a w/o structure with only 10% of oil in the solvent mixture.

The conductivity data of the lower channel indicate that the nanostructure in the lower channel does not change much with increasing oil in contrast with the nanostructure in the upper channel. At the water corner, the conductivity in the lower channel with $2900 \mu\text{S}/\text{cm}$ is much higher than the conductivity of the L_3 phase of the upper channel with $1000 \mu\text{S}/\text{cm}$. The reason for this is that the $\text{Mg}(\text{DS})_2$ concentration is much higher in the lower channel. With increasing oil content, the

conductivities decrease slightly to $1500 \mu\text{S}/\text{cm}$ at the middle of the phase diagram, which is where the channel ends. The reason for the decrease is mainly the decreasing mass fraction of $\text{Mg}(\text{DS})_2$. Obviously, the lower channel consists of a continuous water phase in which oil droplets are dispersed (o/w structure).

As already mentioned, the lower and upper single-phase channels are not connected to each other in contrast with the classical microemulsion systems with single nonionic surfactant and hydrocarbons. In the present system, both channels are separated by a large single anisotropic L_{α} channel.

A plot of the conductivity in the L_{α} channel can be found in Figure SI4 of the Supporting Information. The conductivity on the water-side is $\sim 400 \mu\text{S}/\text{cm}$ and decreases with increasing oil content and increasing $x \text{ IT } 3$ constantly to a value of $40 \mu\text{S}/\text{cm}$ at the L_{α} phase with 90% decane. It is noteworthy that the sample without decane at the water side has a lower conductivity than the L_3 phase despite the fact that it contains $\sim 60\%$ more anionic $\text{Mg}(\text{DS})_2$ and also a much lower conductivity than the microemulsion from the lower single-phase channel with the same $x \text{ IT } 3$ value of 0.5. This already indicates that the structure consists of densely packed multilamellar vesicles, where the conductivity is low due to the limited movement of the ions.¹²

FF-TEM Micrographs in the Upper Channel. An FF-TEM micrograph of the L_3 phase without oil is shown in Figure 3a. In this technique, the replica of a fractured plane across the sample is

reproduced. From previous investigations with this technique, it is known that the fracture follows the midplane of the bilayers.¹³ One can see a highly structured surface in which the smallest objects that can be identified have dimensions between 10 and 20 nm. In many parts of the micrographs, it is possible to identify globular white domains that are surrounded by a gray ring. These are typical features of the L_3 phase where the fracture plane has cut through a tubular bilayer. The dimensions of these globular spots correspond to the size that is detected from the correlation peak in scattering measurements and which is close to the interlamellar distance in the neighboring L_α phase.¹⁴ The typical dimensions that are observed from the Cryo-TEM and the FF-TEM micrographs are the same and give a consistent picture. In Figure 3b, an FF-TEM micrograph from a sample is shown that contains 20% oil in the solvent mixture. The micrograph of the microemulsion with 20% decane looks different than the micrograph of the L_3 phase without oil. Now densely packed globular particles can be seen with an average diameter of 40–50 nm. The FF-TEM micrographs support the assumption of the conductivity measurements that the bicontinuous structure of the L_3 phase is transformed to a w/o droplet structure with little oil.

Such w/o structures of a similar system were already successfully imaged with help of the Cryo-TEM method.¹⁵ The droplet size is also consistent with the calculated size of 46 nm that can be obtained by the simple core–shell model.

Micrographs of samples from the lower single-phase channel with 10 and 20% decane in the solvent mixture are shown in Figure 3c,d. The micrographs show tiny droplets with a diameter of ~ 7 nm for the sample with 10% decane and ~ 14 nm for 20% decane that are randomly distributed in the surrounding matrix that is water. The droplet size for both samples also fit perfectly with the core–shell model.

Electric Birefringence Measurements in the Upper Single-Phase Channel. Electric birefringence measurements are usually carried out on colloidal systems to determine the dimension of particles and aggregates and to determine the optical anisotropy of these structures.¹⁶ The method has been used to determine the persistence length of polyelectrolytes and polymers,¹⁷ of worm-like micelles,¹⁸ of pieces of DNA,¹⁹ and so on. Good signals were also obtained on L_3 phases.²⁰ At the time of the measurement, it had not been unambiguously clear whether L_3 phases had a bicontinuous structure or were a solution of discrete disk-like micelles.²¹ It was assumed that the signals were due to the orientation of the disk-like particles in the electric field. The orientation time was therefore used to calculate the diameter of the disk-like aggregates. The results gave diameters that corresponded to the interlamellar distance of the L_α phase that is next to the L_3 phase. These results could also explain the low viscosity of the L_3 phases. Later measurements on L_3 phases, in particular, FF-TEM measurements, showed that L_3 phases have a bicontinuous structure.²² The electric birefringence signals have then to be explained by the deformation of these structures in electric fields. In both interpretations, the alignment of disk-like particles or the deformation of the L_3 structure solvent molecules has to diffuse over the length of the dimension of the structure, and it is not possible from the signal what the origin of the signal is.²³ The results lead, however, to a structural relaxation time that controls the macroscopic dynamic properties of these phases. The electric birefringence method was therefore used to determine the structural relaxation times in microemulsions and, in particular, in the single-phase channel of this system for which we had determined first the phase diagram. According to our knowledge,

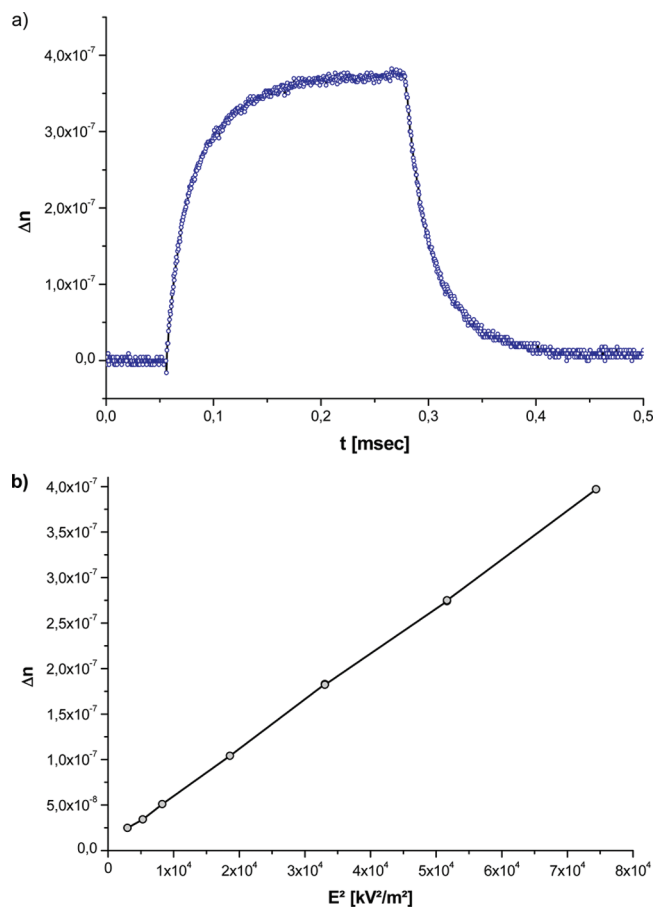


Figure 4. (a) EB signal of the L_3 phase. Sample composition: 15% (w/w) surfactant, x IT 3 0.79, 20% glycerine in H_2O . Signal recorded at an field strength E of 273 kV/m. (b) Plot of Δn against E^2 . Δn increases linearly with E^2 and therefore follows Kerr's law.

these are the first measurements of the dynamic behavior of microemulsions in the single-phase channel.

We would like to note that electric birefringence measurements have been carried out on microemulsions of the system $\text{C}_{12}\text{E}_5/\text{H}_2\text{O}/n$ -octane.²⁴ The measurements were done in the lower isotropic channel from the water side to the upper channel on the oil side. Signals with a single relaxation time were observed. The time constants showed two maxima with the oil constant at 30 and 70% of n -octane and a minimum in between the maxima at 50% of oil. The Kerr constant showed a broad maximum at $\sim 50\%$ of oil. Whereas it was not tried to interpret the results with a model in a quantitative way, the results were consistent with the generally accepted model according to which the structures along the channel developed from o/w droplets over a bicontinuous structure to w/o droplets. The results for the presently investigated system are very different, as will be shown.

In Figure 4a an electric birefringence signal of the L_3 phase is shown. The signal is a simple signal; that is, both the buildup and the decay of the birefringence can be fitted with a single relaxation time that is the same for the buildup and the decay. The birefringence amplitude follows Kerr's law, as is shown in Figure 4b.

This result is most remarkable because it could have been imagined that the amplitude saturates with increasing field strength or that the bilayers break at high fields. The structural

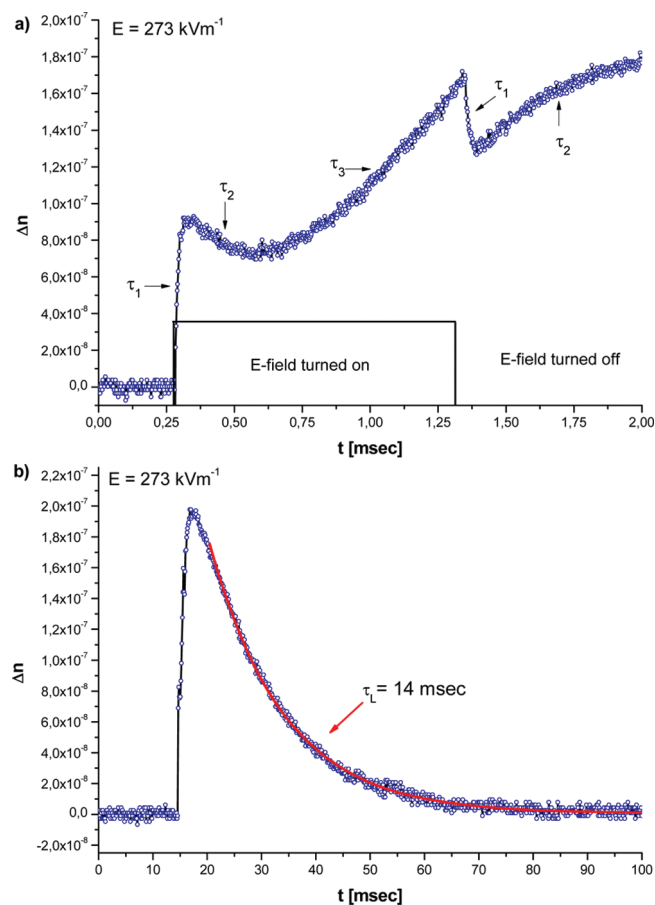


Figure 5. EB signal for a microemulsion of the upper single phase channel with 6% decane in the solvent mixture. (a) Signal shown with time sweep of 2 ms and (b) signal with time sweep of 100 ms, longest relaxation $\tau_L = 14$ ms. The signal identifies three different relaxation processes. Duration of electric pulse = 1 ms.

relaxation time depends on the concentration of the surfactant. It scales with a power exponent of the concentration of -3 ($\tau \approx (c/c^*)^{-3}$).²⁵ The result is due to the fact that the typical dimension of the L_3 phase scales as for a L_α phase with the volume fraction with the exponent -1 .

In a general sense, it is very unusual and remarkable that a structural relaxation time for a surfactant phase or for a polymer solution becomes shorter with increasing concentration as for the L_3 phase.

In most situations, the structural relaxation time becomes longer either because of the increasing interaction between the aggregates or because the aggregates become larger as for wormlike micelles in L_1 phases.²⁶

Electric birefringence signals were recorded in the same way as for the L_3 phase for the microemulsions with increasing oil content. It was assumed that the shape of the signals would not remain the same as that for the L_3 phase and the time constant and the amplitude would change because the conductivity measurement and FF-TEM images had shown that the bicontinuous structure of the L_3 phase drastically changes when only a little amount of oil is solubilized. The results revealed that this is indeed the case. The signals became very complicated with increasing solubilization of oil, as is shown in Figure 5 for a sample with 6% oil.

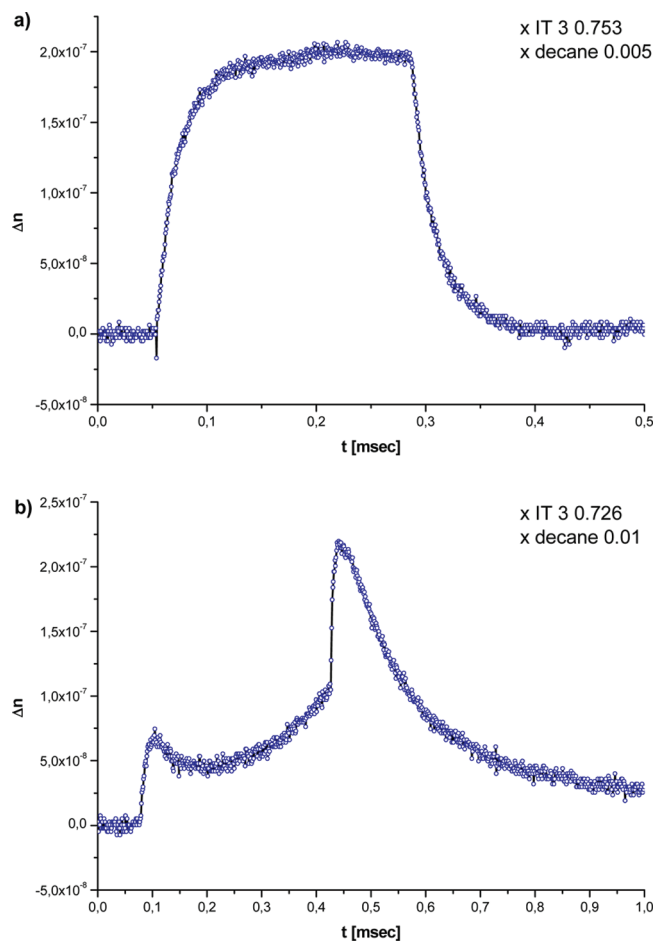


Figure 6. EB signals of microemulsion from upper single phase channel. (a) Simple signal with x decane 0.05. (b) Complicated signal with x decane 0.01.

Signals that were recorded for different field strength are shown in Figure SI6 of the Supporting Information. As is evident from the individual signals, the signals do not depend on the field strengths.

As is obvious from Figure 5a, the signal seems to indicate a superposition of three separate processes for a pulse of 1 msec duration. The first process, which is indicated as τ_1 in the Figure, has a relaxation time of $\sim 15 \mu\text{s}$. The second one, which opposes the first one, has a relaxation time around $150 \mu\text{s}$ (τ_2), and the next one (τ_3) has a relaxation time of $\sim 600 \mu\text{s}$. When the field is turned off, all three processes are visible again. The last and longest process, indicated as τ_L in Figure 5b, has the largest relaxation time of ~ 14 ms. It is remarkable and strange that the signal increases again during the second process to an even higher birefringence level as with the field left on. Similar complicated signals have been observed for electric birefringence measurements on dispersion of clay particles.²⁷ The complicated signals in these systems are due to the fact that a fraction of the particles align parallel to the electric fields, whereas another fraction aligns perpendicular to the field. The complicated signals will be discussed in a later section. We would like to emphasize here that the main signal that is also the longest process relaxes with a relaxation time that is ~ 14 ms that is much longer than the electric pulse, which is applied only for 1 ms.

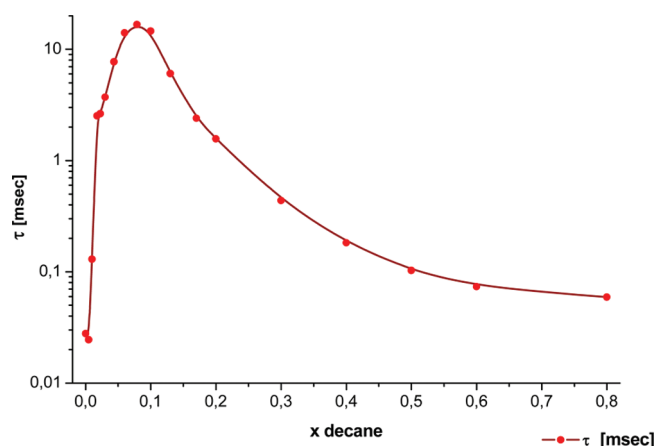


Figure 7. Plot of the longest relaxation time τ of microemulsions in the upper single-phase channel against the mass fraction of decane in the solvent mixture.

In Figure 6, EB signals of microemulsions from the upper single-phase channel with 0.5% decane and 1% decane in the solvent mixture are shown.

While the signal of the microemulsion with 0.5% decane in the solvent mixture is the same as the signal of the L_3 phase, one can see clearly that the signal with 1% decane becomes already very complicated. EB signals of microemulsions of the upper channel between 0.5 and 10% decane are shown in Figure SI7 of the Supporting Information, and signals for microemulsions from 17 to 80% decane are shown in Figure SI8 of the Supporting Information. Whereas the EB signals of microemulsions with up to 10% decane are very complicated and show a superposition of several processes, the signal becomes simpler again with further increasing oil concentration.

The longest relaxation time can easily be evaluated from all signals because the shorter relaxation processes have already relaxed to zero and need not to be considered during the evaluation of the longest process. A plot of the longest relaxation time against the oil content of the microemulsion is shown in Figure 7. Because of the larger changes of the time constant, a log scale has been used for the time constants. The plot shows a steep maximum for microemulsions around 10% of oil. The relaxation time increases four orders of magnitude.

From a general point of view on solubilization of oil in micellar phases, it is remarkable that the structural relaxation time is increasing with the oil content. For L_α phase and for entangled wormlike micelles, the structures usually become more flexible with solubilization and the time constants decrease.

As conductivity data already implied, there must be a complex transition mechanism from the bicontinuous L_3 phase to a w/o-HIPE structure with only $\sim 10\%$ oil. The complicated signals for microemulsions with low oil content are obviously related to this transition mechanism. For higher oil content above 10% oil, EB signals become less complicated. This indicates that the structural transition is complete. The structural relaxation time then is decreasing again because of the decreasing droplet size of the w/o droplets with increasing oil content.

Rheology in the Upper Single Phase Channel. It is generally assumed that microemulsions are low viscosity Newtonian fluids. Systematic investigations of the rheological behavior of microemulsions do not seem to have been carried out in the past.

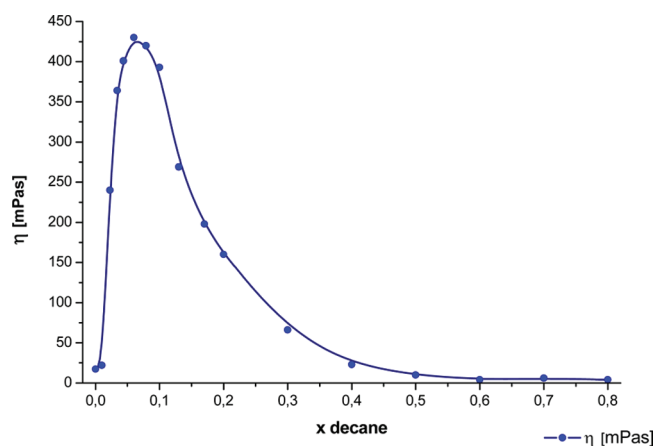


Figure 8. Zero shear viscosity η of samples of the upper single-phase channel against the mass fraction of decane.

The kinematic viscosity ν of the well-studied system H_2O/n -octane/ $C_{12}E_5$ has already been investigated along the isotropic channel.²⁸ The viscosity showed a relatively complicated behavior with two maxima and a minimum at an oil/water ratio near one. The first maximum was $\sim 20\%$ of oil. The total reported change of ν between 10 and 90% of oil was only a factor 10. There was no effort made to explain the two maxima as a function of the oil concentration. The measurements were carried out with an Ubbelohde viscometer, assuming that the fluids were Newtonian fluids. Microemulsions are structured fluids, and they should therefore show a shear thinning behavior. We therefore made rheological measurements of the microemulsions along the isotropic channel from the L_3 phase to the oil phase. The viscosities were measured with a cone/plate viscometer, and it was hoped that the structural relaxation times also could be determined.

The zero-shear viscosity η^0 , plotted against the oil content, is shown in Figure 8. The results show a strong maximum of the viscosity around 6–10% of oil. The viscosity at the maximum is almost three orders of magnitude higher than the viscosity of water or of the used oil and about two orders of magnitude higher than the viscosity of the L_3 phase. In comparison with solubilization results of oil into other micellar phases, it is surprising that small amounts of oil into the L_3 phase increase the viscosity so much. Solubilization of oil into an L_1 phase from wormlike micelles and solubilization of oil into the bilayers of a L_α phase usually leads to the decrease in the viscosity.

Whereas the rise of the viscosity could be rationalized with the increasing correlation length between the L_3 phase and the microemulsions with 10% of oil, the decrease in the viscosity with further increasing oil concentration is unclear. As seen from conductivity results, the microemulsion with 50% of oil consists of water droplets in an oil matrix. Such a phase should have a low viscosity that should be given by the Stokes–Einstein equation

$$\eta = \eta_s(1 + 2.5\phi)$$

where η_s is the viscosity of the solvent and ϕ is the volume fraction of the dispersed phase that is surfactant and water. This is really the situation. It is therefore clear that the viscosity must fall from a value of 450 mPa·s at 10% of oil to a low value at 50%. It is, however, not clear why the viscosity decreases so strongly between 10 and 50%. Perhaps the reason could be of electrostatic origin.

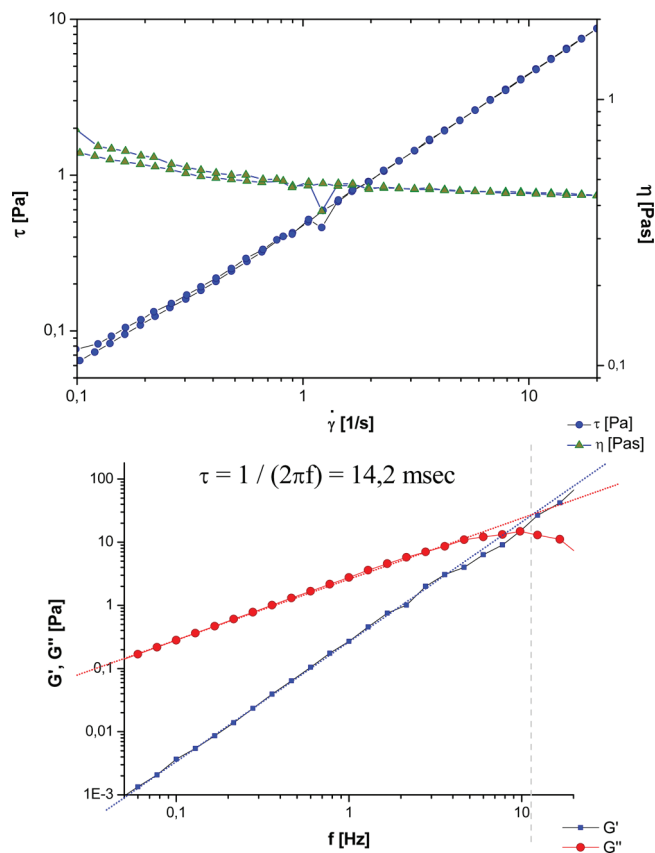


Figure 9. Rheograms of microemulsion from upper single phase channel with 6% oil in the solvent mixture. Top: shear stress τ and viscosity η against shear rate $\dot{\gamma}$; bottom: storage modulus G' and loss modulus G'' against frequency f . Evaluated structural relaxation time: 14.2 ms.

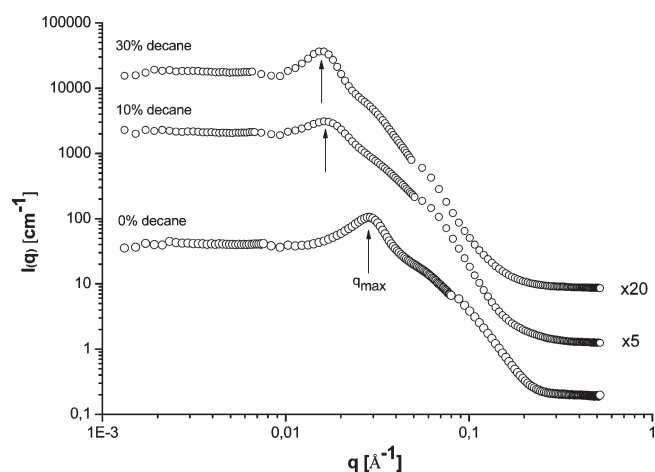


Figure 10. SANS experiment at constant surfactant concentration with increasing mass fraction of oil in the solvent. For better overview, curves for microemulsions with 10 and 30% decane are shifted by factors of 5 and 20 on the intensity scale.

In any event, the maximum of the viscosity also stands for a transition in the nanostructure around this oil content.

The viscosity of a structured fluid is in the simplest case determined by the product of a shear modulus and a relaxation

Table 1. Data Obtained from SANS Measurements: q_{max} Values and Calculated Interlamellar Distance d at Constant Surfactant Concentration in Dependency of Increasing Mass Fraction of Decane in the Solvent Mixture

surfactant (%)	x IT 3	x decane	q_{max} (Å ⁻¹)	d (Å ⁻¹)
15	0.795	0	0.02895	217
15	0.635	0.1	0.01619	388
15	0.74	0.3	0.01521	413

time ($\eta^0 = G^0 \cdot \tau$). This is the situation in L_1 phases of micellar solutions. We tried therefore to determine the structural relaxation time τ_s of the samples around the viscosity maximum.

In Figure 9, we show in a plot of the shear viscosity of the microemulsion at the viscosity maximum against the shear rate and results from oscillating measurements of the complex viscosity against the angular frequency. Both Figures show the typical results for shear thinning liquids. With help of oscillating measurements, the relaxation time can be evaluated. The value is 14 ms. This value of 14 ms is the same as the time constant that was evaluated as the longest process from the electric birefringence measurements. We therefore can conclude that the longest time constant, which is determined from electric birefringence results on the microemulsions, is the structural relaxation time of the fluid, which controls the viscosity.

SANS Measurements in the Upper Single-Phase Channel.

Intuitively, it is difficult to understand why the viscosity or the structural relaxation times are increasing so much when 10% of oil is solubilized into the L_3 phase. An answer of this puzzling question can be obtained from SANS measurements that have been made on the L_3 phase and on microemulsions from the upper channel with varying oil content (Figure 10).

The result for the sample without decane shows the typical scattering function for an L_3 phase. However, a shift is observed between the correlation peak of the L_3 phase and the correlation peak of the microemulsion with 10% of oil to a lower q value. The q value for the microemulsion with 30% decane is similar to the microemulsion with 10% decane.

Whereas the calculated interlamellar distance of the L_3 phase is ~ 22 nm, the sample with 10% decane shows an interlamellar distance of ~ 39 nm (Table 1). These results show clearly that between the L_3 phase without oil and the microemulsions with 10% of oil a massive structural reorganization must have taken place, whereas between 10 and 30% of decane the structure keeps mainly the same.

The SANS data are in good agreement with the results obtained by the FF-TEM micrographs. The interlamellar distance of the L_3 phase is in the same range, as can be seen on the FF-TEM micrograph in Figure 3. The obtained d values for the sample with 10 and 30% decane also correspond to the size of the globular particles that were seen on the micrograph for the microemulsion with 20% decane and could represent the droplet diameter. It is also noteworthy that the scattering curve for the sample with 10% decane does have a broader peak that is not as sharp as for the other two curves. This could mean that there is a larger polydispersity in the size distribution of the w/o droplets or some of them are fused together. Because the structural relaxation time is related to the deformation of the correlation peak, it is not surprising that the structural relaxation time increases strongly with the solubilization because the sample consists probably of densely packed droplets. There might be a

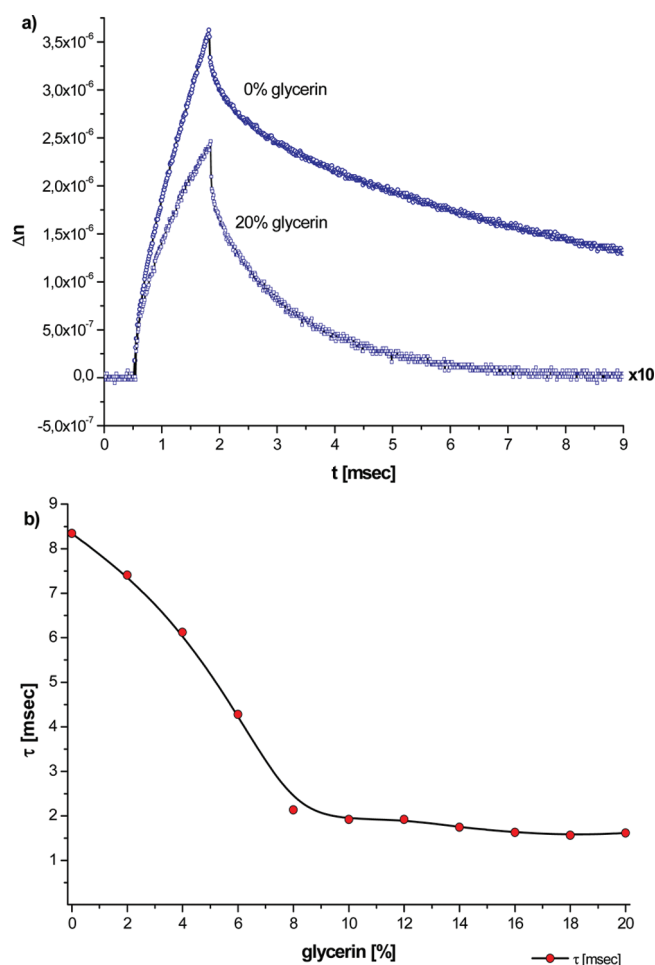


Figure 11. Dependence of structural relaxation time on solvent viscosity. (a) EB signals of microemulsions from the upper channel with 20% decane in solvent and different glycerin content recorded at a field strength of 133 kV/m. The curve for the microemulsion with 20% glycerin in water was increased by a factor of 10 for better overview. (b) Relaxation time τ in dependence of glycerin concentration of a microemulsion of the upper single-phase channel with 20% decane in the solvent mixture.

second reason for the increase in the structural times. As shown from the phase diagram of Figure 1, samples with 10% oil have a higher content of $\text{Mg}(\text{DS})_2$ than samples of the L_3 phase. The ionic charge density of the samples is considerably higher than that for the L_3 phase. This increase probably leads to a stiffening of the bilayer and also to an increase in the time constants. Qualitatively, this effect should lead to a stronger correlation peak and a stronger interbilayer interaction.

The data differ completely from SANS-measurements that were done on microemulsions with the single nonionic surfactant C_{12}E_5 and decane. In these results, the q_{max} values did not shift with constant surfactant and increasing solubilization of oil into the L_3 phase, assuming that the interlamellar distance and the structure of the L_3 phase do not change.²⁹

Dependence of the Structural Relaxation Time on the Solvent Viscosity. The signals of the birefringence results of the L_3 phase were explained by the rotation of disks in the aqueous medium. For such a mechanism, the relaxation time should be proportional to the solvent viscosity. Some measurements were carried out on a microemulsion in which up to 20% of water was

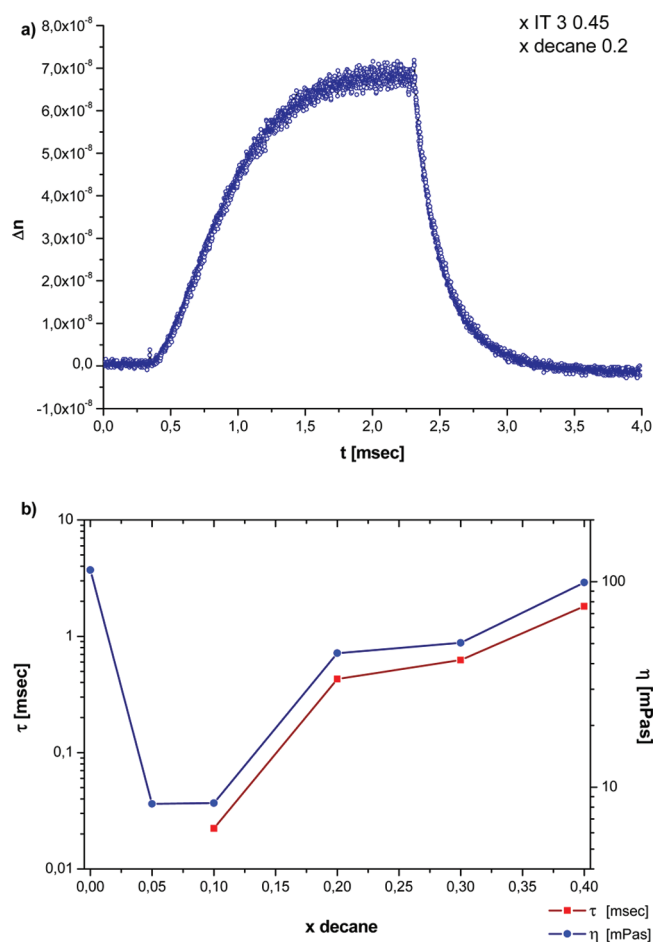


Figure 12. Results of electric birefringence in the lower single phase channel. (a) EB signal of microemulsion from the lower single phase channel with 20% decane in the solvent mixture. (b) Overview of main structural relaxation time and zero shear viscosity with increasing oil content in the lower single phase channel.

replaced by glycerin. Two signals, one with water and one with 20% of glycerin, are shown in Figure 11a. At first, it is remarkable that the intensity Δn of the sample with 20% glycerin is much lower than the intensity of the sample without glycerin. This is probably caused by matching the refractive index of the aqueous phase against the oil and also can be clearly seen by eye. Whereas the sample without glycerin scatters much and is somewhat bluish, the sample with 20% glycerin scatters less.

The signals also clearly show that the time constants indeed depend on the glycerin content. With increasing glycerin concentration, the structural time constants become shorter and not longer as expected, as can be seen in Figure 11b.

It can therefore be concluded that the relaxation times are not only determined on the viscosity of the solvent but also depend on the stiffness of the bilayers and perhaps on the interaction energy between the bilayers. Whereas the observed change of the structural relaxation time with the glycerin content is surprising, we would like to add that the change is similar to the change that has been observed on the structural relaxation time of L_1 phases with wormlike micelles.³⁰ In this case, the decrease in the structural relaxation times can be understood on the basis of the reptation mechanism for the wormlike micelles. Perhaps the relaxation

process in the investigated microemulsions is a similar process to the reptation mechanism in a L_1 phase.

Dynamic Behavior in the Lower Channel. EB signals also were recorded for the microemulsions of the lower single phase channel. A selected signal for samples with 20% decane is shown in Figure 12a. Signals from 10 to 40% decane are shown in Figure S19 of the Supporting Information. The signals for microemulsions in the lower channel are far simpler than the signals from the upper channel.

The viscosities and the structural relaxation times in the lower channel are given in Figure 12b. For no oil, the viscosity has a value of ~ 110 mPas. This value indicates that the micellar solution contains entangled wormlike micelles. With increasing solubilization, the viscosity passes through a deep minimum around 5% of oil and then increases again with increasing solubilization of oil. The decrease in the viscosity is an indication that the wormlike micelles have been transformed to small oil droplets. The transition of wormlike micelles to globular droplets by the solubilization of oil has already been studied in detail.³¹ It occurs rather sharp, and the transition concentration of oil depends on its chain length. Wormlike micelles of a given surfactant can tolerate small hydrocarbon molecules more than long ones before they are transformed to globular droplets. It is interesting to note that the minimum of the viscosity in the lower channel coincides with the maximum of the viscosity in the upper channel. It is furthermore interesting that the globular micelles give rise to an electric birefringence signal even though the particles are not anisotropic. FF-TEM measurements in Figure 3 showed that the particles are perfect spheres. The reason for the electric birefringence signal is the same as that for the signal in the L_3 phase. The droplets obviously are deformed in the electric field. The deformation seems to be small, as is evidenced by the validity of Kerr's law up to high electric fields.

The electrostatic interaction between the droplets does not seem to influence very much their rotation. If a radius for the droplets is determined from the time constant of the birefringence signals and it is assumed that this time constant is given approximately by the rotation of the droplets, then one obtains a radius that is close to the radius that is obtained from FF-TEM measurements.

With increasing solubilization of oil, the globular droplets increase in size and the viscosity and the structural relaxation time. Both parameters seem to be affected now more and more by the interaction of the particles, either hydrodynamic or electrostatic in origin.

The system is becoming denser with increasing solubilization. At maximum solubilization around 40% decane, the viscosity and the structural relaxation time of the samples are now higher than those for samples with 40% of decane in the upper channel.

CONCLUSIONS

Electric birefringence measurements give strong signals in the isotropic channel of microemulsions in the region where a bicontinuous structure exists and in the regions where w/o or o/w droplets exist. The signals are due to the deformation of the nanostructures in the electric field. It is shown in the investigation that the longest relaxation time that is evaluated from the electric birefringence signals controls the viscosity of the fluids in the channel. The structural relaxation times and the viscosities of the upper single-phase channel pass with increasing oil content over a strong maximum. The position of the viscosity maximum

occurs at $\sim 10\%$ of oil. It is concluded that the viscosity maximum is the result of switch in the nanostructure from a low viscous flexible L_3 phase to a densely packed w/o-HIPE structure. Between 1 and 10% of oil, the EB signals become very complicated because they show a superposition of up to three processes. The complicated signals are due to a complex transition mechanism from a bicontinuous L_3 phase to a w/o-HIPE structure. For higher oil content, EB signals become less complicated, which indicates a completion of the structural transition. The structural relaxation times are decreasing with increasing oil content because of the decreasing droplet size of the w/o droplets. All in all, the longest relaxation time seems to control the viscosity of the fluids. Results of the electric birefringence measurements are supported by conductivity measurements, FF-TEM micrographs, and SANS measurements.

ASSOCIATED CONTENT

S Supporting Information. More information, as detailed rheology measurements in the lamellar channel and electric birefringence signals along the microemulsion channels. This material is available free of charge via the Internet at <http://pubs.acs.org>.

AUTHOR INFORMATION

Corresponding Author

*Tel: +49-921-50736168. Fax +49-921-50736139. E-mail: lukas.wolf@freenet.de.

ACKNOWLEDGMENT

We thank Dr. Walter Richter at the Centre for Electron Microscopy, Jena, for the great FF-TEM imaging work and Dieter Gräbner for his eager assistance in operating the electric birefringence device. We also want to thank the group of Prof. Dr. Thomas Hellweg, University of Bielefeld, for the possibility to investigate samples by SANS-measurements at the Institute Laure-Langevin (ILL) in Grenoble, France.

REFERENCES

- (1) Miller, C. A.; Neogi, P. *AIChE J.* **1980**, *26*, 212–220.
- (2) Huang, J. S. *J. Chem. Phys.* **1985**, *82*, 480–484.
- (3) Strey, R. *Colloid Polym. Sci.* **1994**, *272*, 1005–1019.
- (4) Lee, L. T.; Langevin, D.; Strey, R. *Physica A* **1990**, *168*, 210–290.
- (5) Sottmann, T.; Strey, R. *J. Chem. Phys.* **1997**, *106*, 8606–8615.
- (6) Stubenrauch, C. In *Microemulsions: Background, New Concepts, Applications, Perspectives*; Wiley-Blackwell: Chichester, U.K., 2009.
- (7) Lichterfeld, F.; Schmeling, T.; Strey, R. *J. Phys. Chem.* **1986**, *90*, 5762.
- (8) Wolf, L.; Hoffmann, H.; Watanabe, K.; Okamoto, T. *Phys. Chem. Chem. Phys.* **2011**, *13*, 3248–3256.
- (9) Khan, A.; Lindström, B.; Shinoda, K.; Lindman, B. *J. Phys. Chem.* **1986**, *90*, 5799.
- (10) Kahlweit, M. *J. Colloid Interface Sci.* **1987**, *118*, 436–453.
- (11) Jahn, W.; Strey, R. *J. Phys. Chem.* **1988**, *92*, 2294.
- (12) Hoffmann, H.; Horbaschek, K.; Witte, F. *J. Colloid Interface Sci.* **2001**, *235*, 33–45.
- (13) Hoffmann, H.; Thunig, C.; Munkert, U.; Meyer, H. W.; Richter, W. *Langmuir* **1992**, *8*, 2629–2638.
- (14) Douglas, C. B.; Kaler, E. W. *J. Chem. Soc., Faraday Trans.* **1994**, *90*, 471–477.
- (15) Wolf, L.; Hoffmann, H.; Talmon, Y.; Teshigawara, T.; Watanabe, K. *Soft Matter* **2010**, *6*, 5367–5374.

- (16) Schorr, W.; Hoffmann, H. *Physics of Amphiphiles: Micelles, Vesicles and Microemulsions: Proceedings of the International School of Physics*; Degiorgio, V., Corti, M., Eds.; North-Holland: Amsterdam, 1985; pp 160–180.
- (17) Krämer, U.; Hoffmann, H. *Macromolecules* **1991**, *24*, 256–263.
- (18) Hoffmann, H.; Krämer, U.; Thurn, H. *J. Phys. Chem.* **1990**, *94*, 2027–2033.
- (19) Stellwagen, N. C. *Biopolymers* **1991**, *31*, 1651–1667.
- (20) Miller, C. A.; Gradzielski, M.; Hoffmann, H.; Krämer, U.; Thunig, C. *Prog. Colloid Polym. Sci.* **1991**, *84*, 243.
- (21) Cates, M. E.; Roux, D. *J. Phys.: Condens. Matter* **1990**, *2*, 339–346.
- (22) Strey, R.; Jahn, W.; Skouri, M.; Porte, G.; Marignan, J.; Olsson, U. In *Structure and Dynamics of Strongly Interacting Colloids and Supramolecular Aggregates in Solution*; Chen, S. H., Huang, J. S., Tartaglia, P., Eds.; Kluwer Academic: Boston, 1992; pp 351–363.
- (23) Porte, G.; Appel, J.; Bassereau, P.; Marignan, M.; Skouri, M.; Billard, J.; Delsanti, M.; Candau, S. J.; Jahn, J.; Nabre, P. *Prog. Colloid Polym. Sci.* **1991**, *84*, 264.
- (24) Kahlweit, M.; Strey, R.; Haase, D.; Kunieda, H.; Schmeling, T.; Faulhaber, B.; Borkovec, M.; Eicke, H. F.; Busse, G.; Eggers, F.; Funck, T.; Richmann, H.; Magid, L.; Soderman, O.; Stilbs, P.; Winkler, J.; Dittrich, A.; Jahn, W. *J. Colloid Interface Sci.* **1987**, *118*, 445.
- (25) Miller, C.; Gradzielski, M.; Hoffmann, H.; Krämer, U.; Thunig, C. *Colloid Polym. Sci.* **1990**, *268*, 1066–1072.
- (26) Krämer, U.; Hoffmann, H. In *The Structure, Dynamics, and Equilibrium Properties of Colloidal Systems*; Bloor, D. M., Wyn-Jones, E., Eds.; NATO ASI Series: Series C, Mathematical and Physical Sciences 324; Kluwer Academic Publishers: Boston, 1990; pp 385–396.
- (27) Yamaguchi, Y.; Hoffmann, H. *Colloids Surf., A* **1997**, *121*, 67–80.
- (28) Kahlweit, M.; Strey, R.; Haase, D.; Kunieda, H.; Schmeling, T.; Faulhaber, B.; Borkovec, M.; Eicke, H. F.; Busse, G.; Eggers, F.; Funck, T.; Richmann, H.; Magid, L.; Soderman, O.; Stilbs, P.; Winkler, J.; Dittrich, A.; Jahn, W. *J. Colloid Interface Sci.* **1987**, *118*, 443–444.
- (29) Uhrmeister, P. *Selbstorganisierende Netzwerke in Mikroemulsionen*. Ph.D. Thesis, Universität Köln, 2002.
- (30) Hoffmann, H.; Abdel-Rahem, R. *Colloid Polym. Sci.* **2010**, *288*, 603–612.
- (31) Hoffmann, H.; Ulbricht, W. *J. Colloid Interface Sci.* **1989**, *129*, 388–405.
- (32) Lichtenfeld, F.; Schmeling, T.; Strey, R. *J. Phys. Chem.* **1986**, *90*, 5762–5766.

Dynamic Properties of Microemulsions in the Single Phase Channels

Supporting Information

Lukas Wolf^{*1}, Heinz Hoffmann¹, Walter Richter², Takashi Teshigawara³, Tohru Okamoto³

¹University of Bayreuth, BZKG and BayColl, Gottlieb-Keim-Str. 60, 95448 Bayreuth, Germany

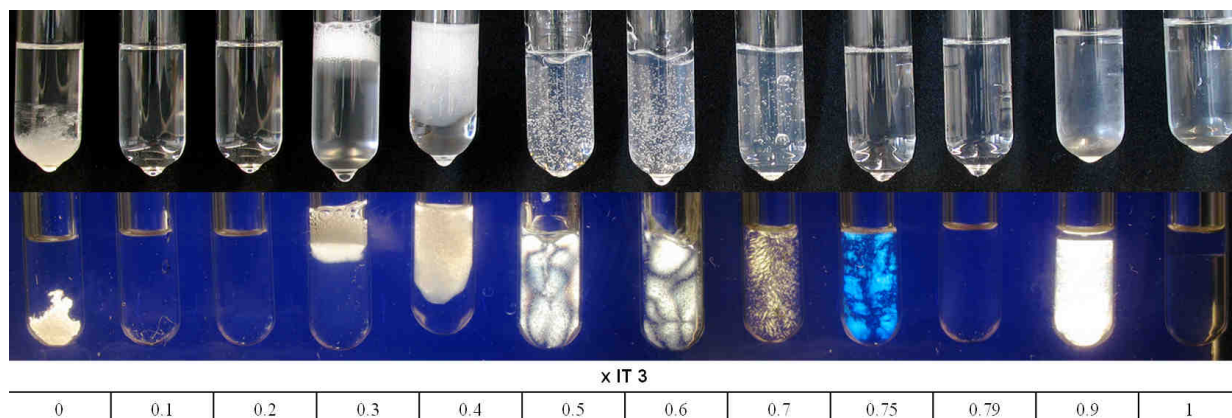
²Friedrich-Schiller-University, Centre for Electron Microscopy, Ziegelmühlenweg 1, 07743 Jena, Germany

³Shiseido Research Center, 2-2-1 Hayabuchi, Tsuzuki-ku, Yokohama, Japan 224-8558

*corresponding author, Tel.: +49-921-50736168, e-mail: lukas.wolf@freenet.de

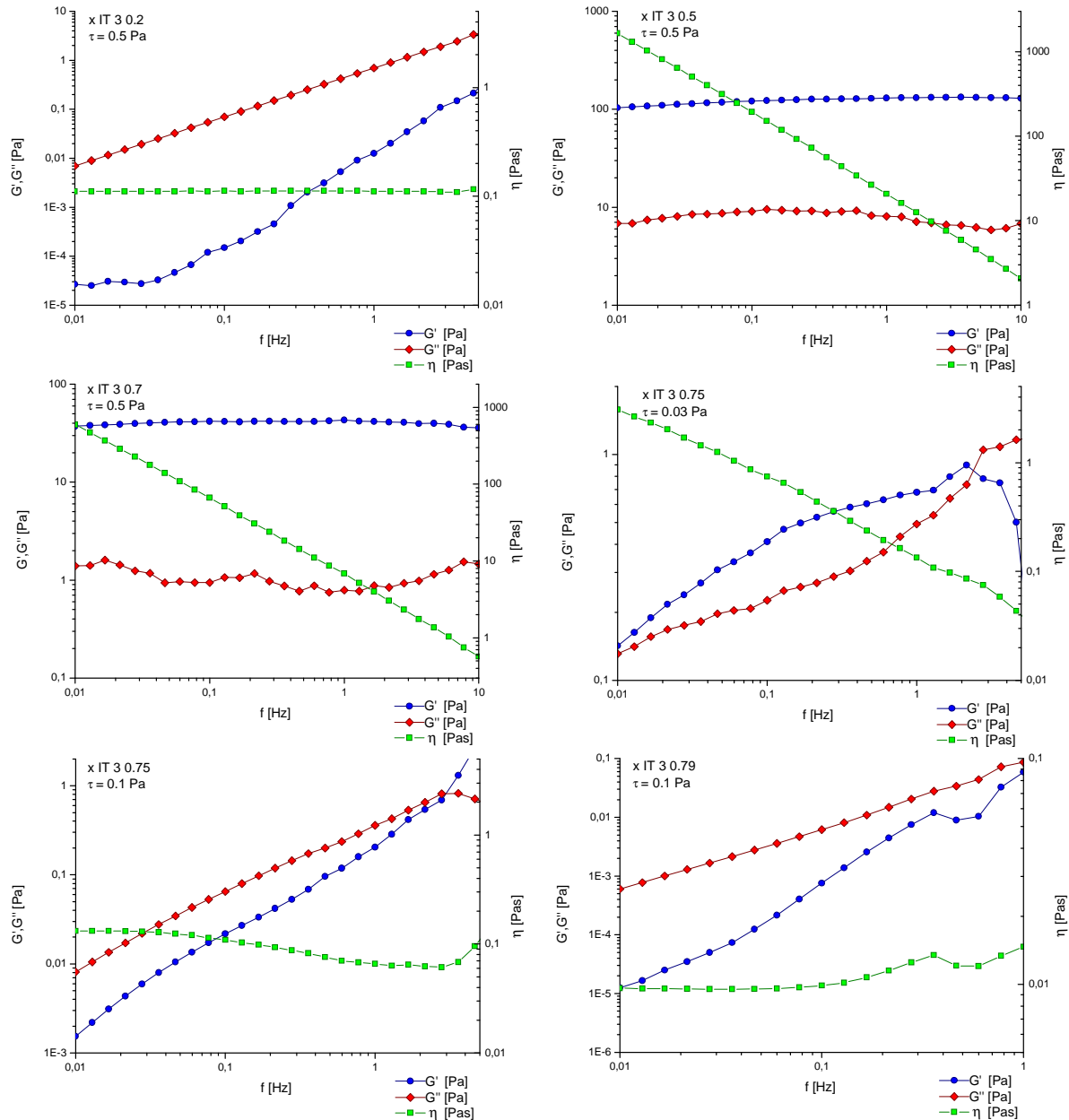
SI1: Phase sequence of binary surfactant mixture Mg(DS)₂-IT 3

Pictures are shown without and between crossed polarisers to distinguish between birefringent and non-birefringent phases. The surfactant mixture starts with the pure 15% Mg(DS)₂-solution that is a micellar L₁-Phase. The sample shows a crystalline sediment at 25 °C, whereas the samples with a mass fraction x IT 3 of 0.1 and 0.2 are isotropic. This shows, that the Krafft-Temperature of the Mg(DS)₂, that is close to 25 °C, is lowered by the co-surfactant IT 3. The isotropic micellar L₁-region is followed by a two-phase L₁/L_α-situation from x IT 3 0.3 – 0.4. From x IT 3 0.5 – 0.77, a large single birefringent L_α region is present that turns into an isotropic L₃-phase at a narrow composition range of x IT 3 ~ 0.78 – 0.79. The sample with 15% IT 3 (x IT 3 = 1) shows a two phase situation with a lower L₁ and an upper L₂-Phase (inverse micellar structure).



SI2: Rheology measurements of the surfactant mixtures without oil

Rheograms of the surfactant mixtures are shown when no oil has been solubilised but when the fraction of IT 3 is increased for constant surfactant concentration of 15%. Sample composition and measurement condition is given in each graph.

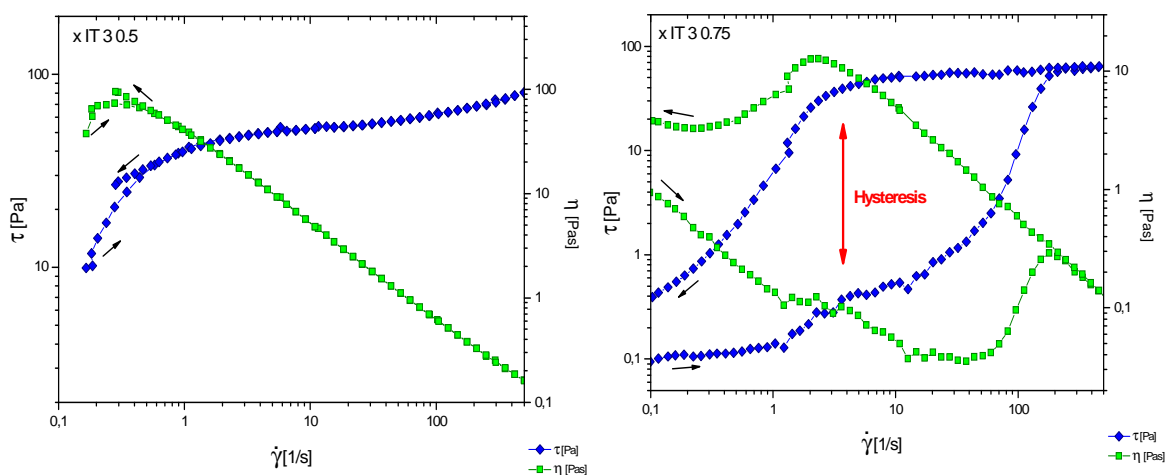


The rheogram for the sample with x IT 3 0.2 (L_1 -Phase) shows the typical characteristics of a viscous Newtonian solution, where the storage modulus G' and the loss modulus G'' are increasing with frequency f and the viscosity η stays independent of the frequency. The high viscosity of around 110 mPa·s is an indication for the presence of long entangled worm-like micelles.

Rheograms of the L_{α} -phases show different features. The stability region for the L_{α} -phases reaches from a weight fraction of IT 3 from 0.5 to 0.75. It is noteworthy that the rheological properties of the phases vary considerably. At x IT 3 0.5 – 0.7, the phases behave like soft gels. These phases have a rheological yield stress. The storage modulus is frequency independent and about an order of magnitude higher than the loss modulus. Samples of these phases can therefore be used for the preparation of stable emulsions or dispersions. The dispersed particles or oil droplets, or even air bubbles, cannot sediment or up-cream. The systems can be deformed at least 10% before they start flowing.

With increasing mass fraction of IT 3, the storage modulus of the phases decreases over a wide region of the composition. The rather high storage modulus is probably a result of the ionic charge of the bilayer phases. It is therefore the more remarkable that it decreases dramatically when the composition of the L_{α} -phase approaches the phase boundary of the L_3 -phase. With x IT 3 = 0.75, the storage modulus drops to values below 1 Pa and becomes even frequency dependent at higher shear stress and the phase no longer behaves like a weak gel, but more like a Newtonian solution. The reason for this effect lies in a change of the nanostructure from multilamellar vesicles to planar lamellas with increasing mass fraction of IT 3. At x IT 3 0.79, the rheogram for the L_3 -Phase shows the typical features of a low viscous Newtonian fluid.

Measurements with increasing and decreasing shear rates were done to investigate the stability of the L_{α} -Phases.

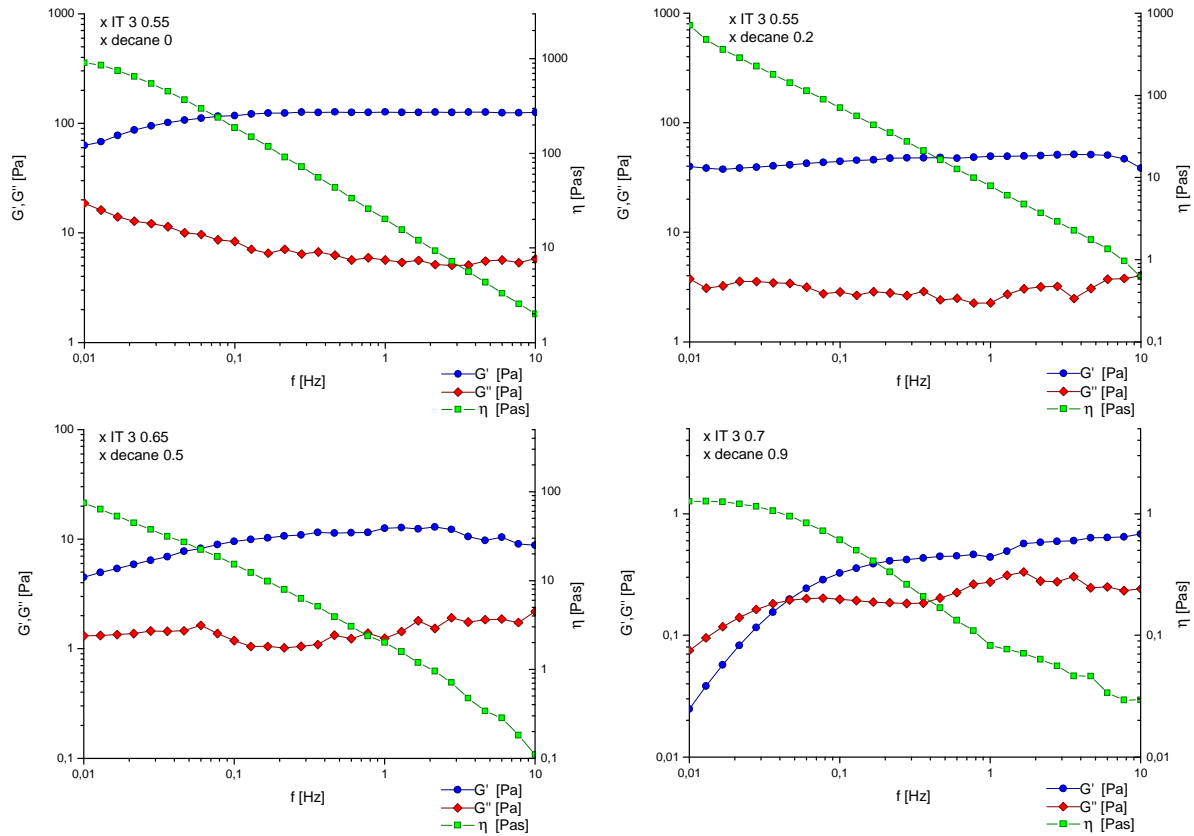


Viscosity η and shear stress τ in dependency of shear rate $\dot{\gamma}$ of samples at x IT 3 0.5 (left) and x IT 3 0.75 (right). Curves for increasing shear rate indicated with black arrows to the right, for decreasing shear rate with black arrows to the left. Hysteresis effect of sample with x IT 3 0.75 indicated with red arrow.

The data of viscosity and shear stress for in- and decreasing shear rates of the sample at x IT 3 0.5 lie perfectly together. This shows that the gel, and thus its nanostructure, doesn't get destroyed or changed when high shear rates are applied to the sample. The situation becomes very different close to the phase border of the L_3 -Phase with higher mass fraction of IT 3. In contrast to the sample with x IT 3 0.5, the curves for the sample with x IT 3 0.75 show an enormous hysteresis effect. For increasing shear rates, the viscosity first decreases, but then recovers at a higher level with decreasing shear rates. This shear thickening effect could be explained by the transformation of planar lamellas to multilamellar vesicles due to high shear. The structure relaxes to its original state within one or two hours.

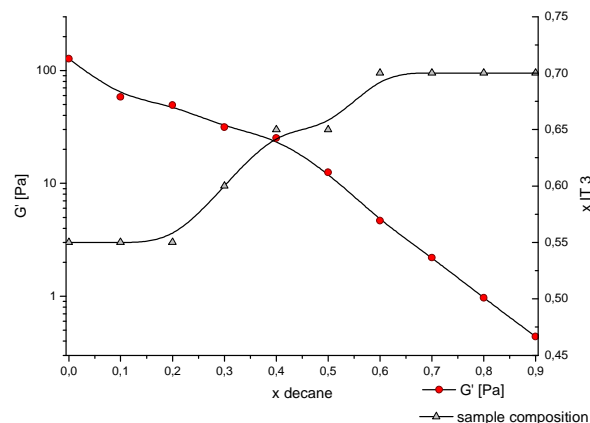
SI3: Rheology measurements in the L_{α} -channel with increasing oil content

Rheograms of samples in L_{α} -channel with increasing mass fraction of oil are shown. Sample composition is given in each graph.

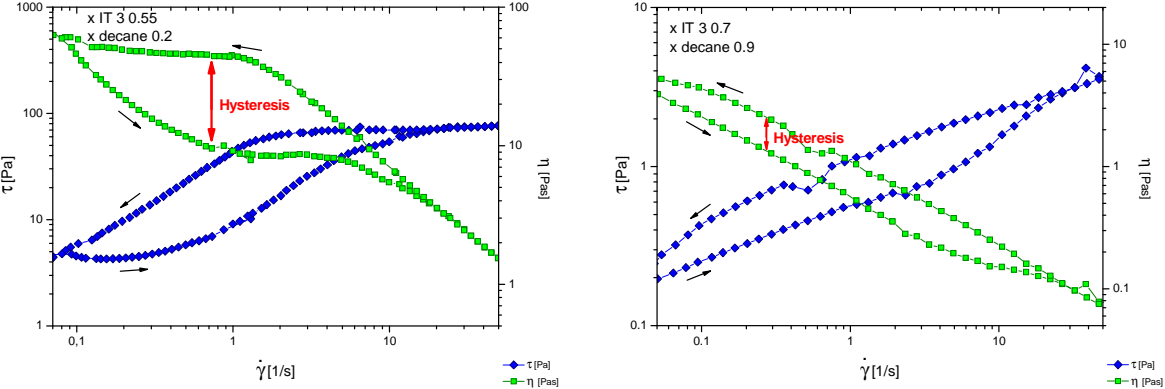


All samples along the L_{α} -channel behave like soft gels. At the sample with x decane 0.9, at very low frequencies the viscous properties are dominant while at frequencies $> 0,1$ Hz the elastic properties are dominant.

A plot of the storage moduli G' (at a frequency of 1 Hz) of the lamellar phases against the oil content is shown in the next picture. With increasing solubilisation of decane, the level of storage modulus G' decreases more than two orders of magnitude from about 130 Pa at the sample without decane to 0,4 Pa at the sample with x decane 0.9.



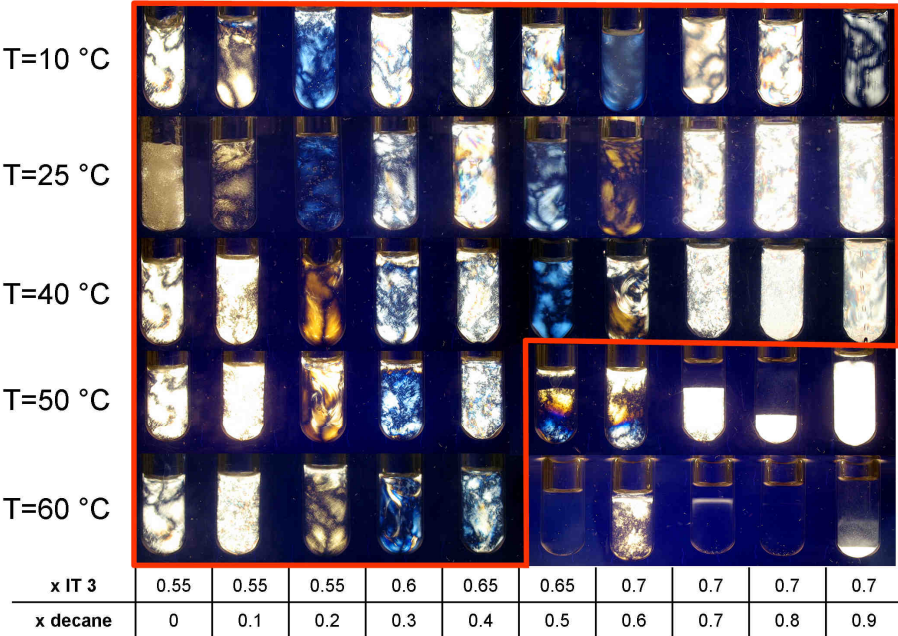
Measurements with in- and decreasing shear rates also where done within the L_{α} -channel. Two rheograms, one with low, the other with high oil content, are shown. Curves for increasing shear rate are indicated with black arrows to the right, for decreasing shear rate with black arrows to the left. Hysteresis effect indicated with a red arrow.



Compared to the rheogram of the sample without oil at low x IT 3 values, all samples with oil in the L_{α} -channel showed a hysteresis effect. However, the dimension of the hysteresis effect becomes smaller with increasing oil content.

It is conceivable that the oil swollen bilayers of the L_{α} -Phases allow fluctuations that are not possible without oil. A possible candidate for such fluctuations would be peristaltic fluctuations that are fluctuation of the thickness of the bilayers.

Another significant feature of the large L_{α} -channel is its high temperature stability. Samples between 10 °C and 60 °C between crossed polarizers are shown in the next picture.

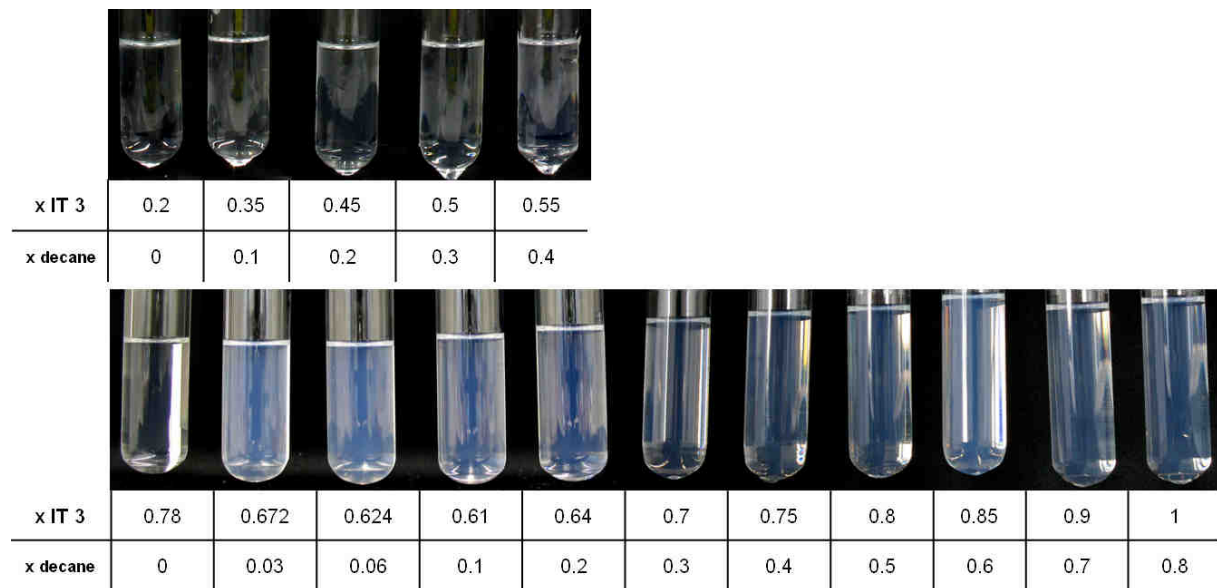


Samples between x decane = 0 – 0.9 are stable at least between 10 °C – 40 °C, samples with x decane 0 - 0.4 are even stable at least up to 60 °C. Although the L_{α} -channel is quite narrow, its high temperature stability is amazing. This feature is obvious due to the surfactant mixture, where the hydrophilic-lipophilic balance is determined more by the mass fraction of the co-surfactant than by the temperature.

SI4: Tube pictures of microemulsions of the lower and upper single phase channel

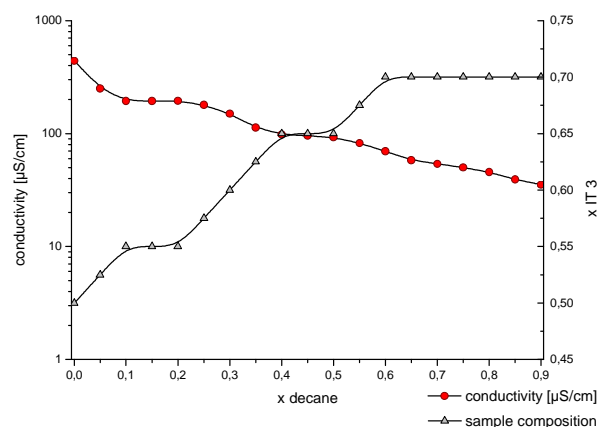
Samples with 15% (w/w) surfactant at 25 °C and increasing mass fraction x of IT 3 and decane are shown without polarizers. Upper row: selected samples from lower single phase channel, lower row: selected samples from upper single phase channel.

Note that samples from the lower single phase channel are completely transparent while samples from the upper single phase channel are slightly bluish and have a high scattering intensity around x decane 0.03 – 0.1



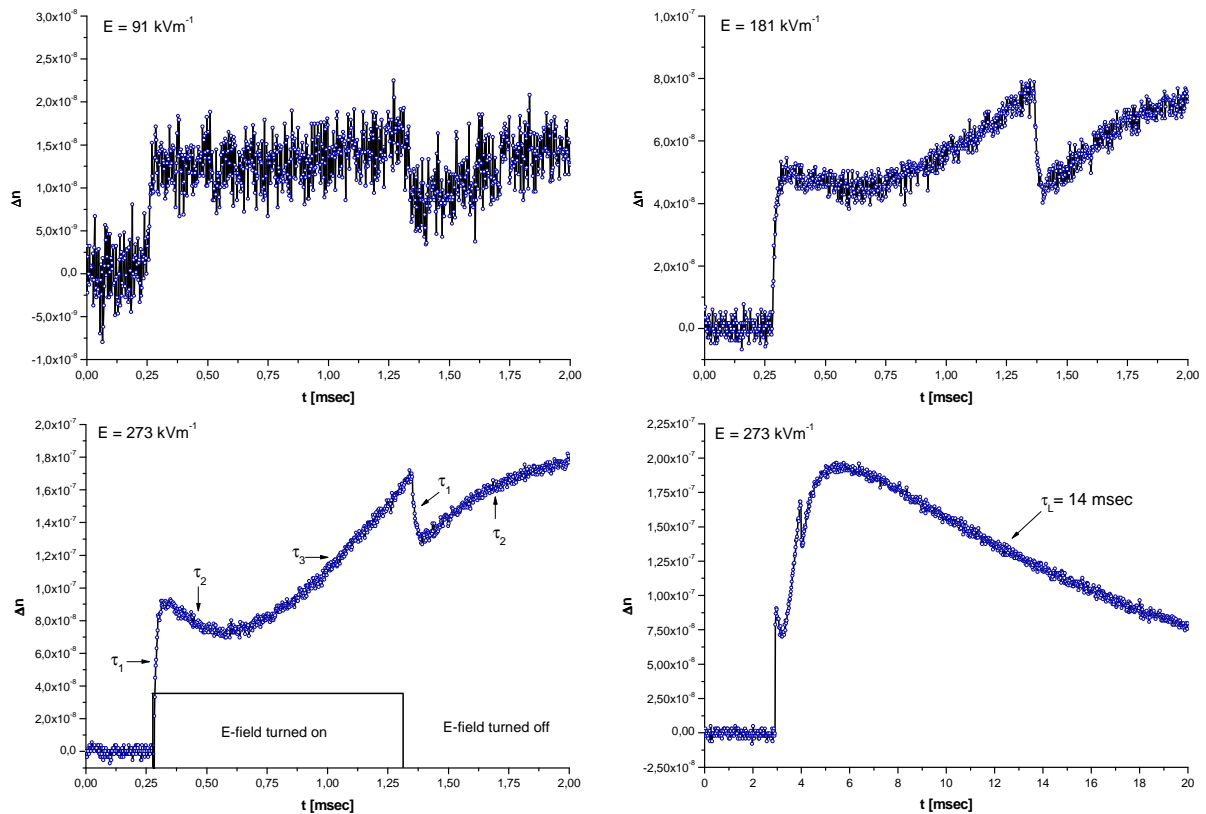
SI5: Conductivity measurements in the L_{α} -channel

The plot of the conductivities in the L_{α} -channel is shown. Conductivity values are indicated as red dots, the corresponding IT 3 ratios are indicated as grey triangles. Note that the conductivity decreases more or less constantly with increasing mass fraction of IT 3 and oil.



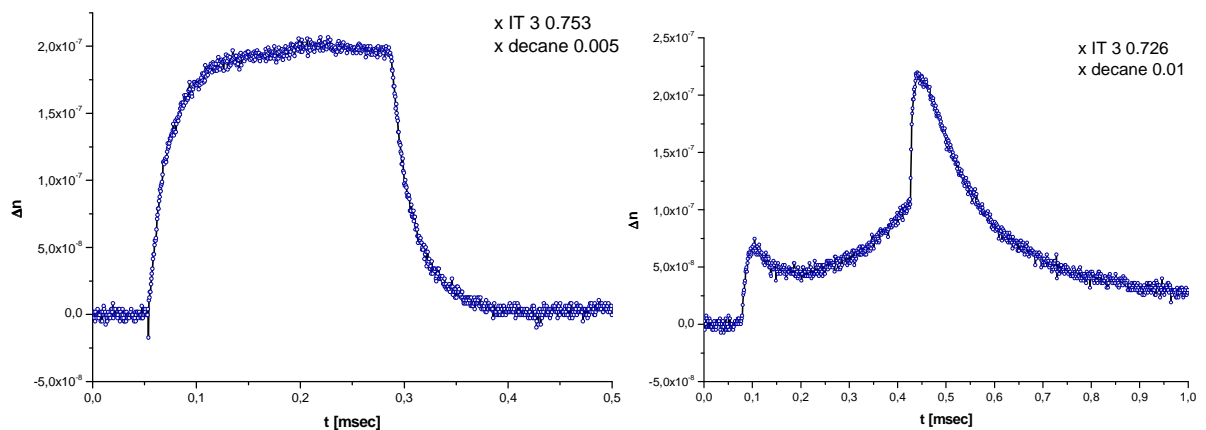
SI6: EB signals at different field strengths

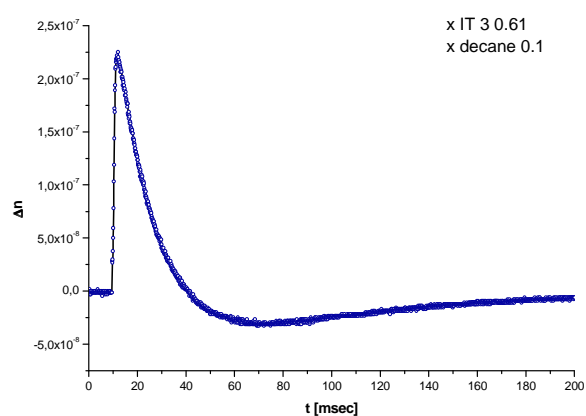
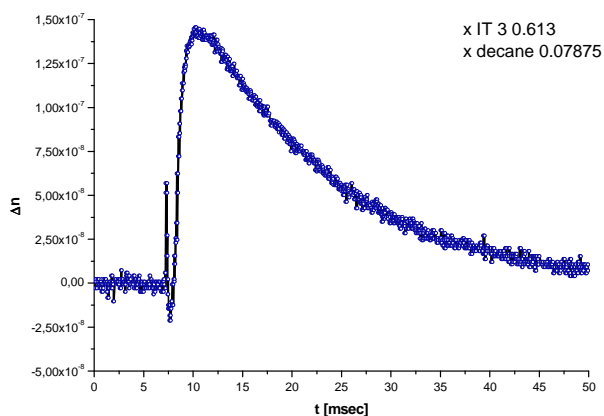
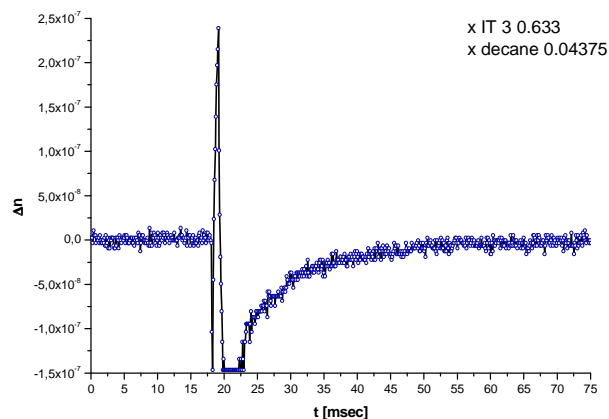
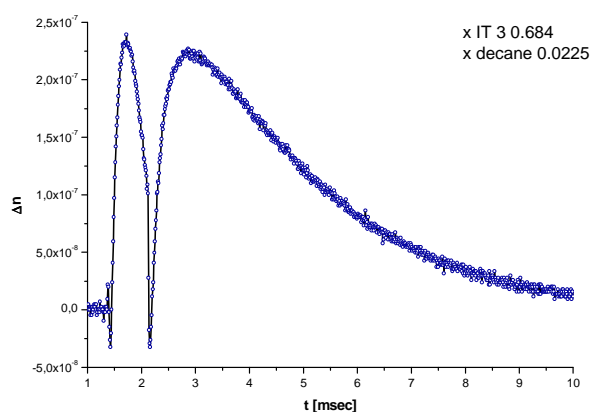
EB-signal for a microemulsion from the upper single phase channel with 6% decane in the solvent mixture, recorded at different field strengths E . Note that the signals do not depend on the field strength. The signal identifies three different relaxation processes. Duration of electric pulse = 1 msec.



SI7: EB-Signals in the upper single phase channel (x decane 0.005 – 0.1)

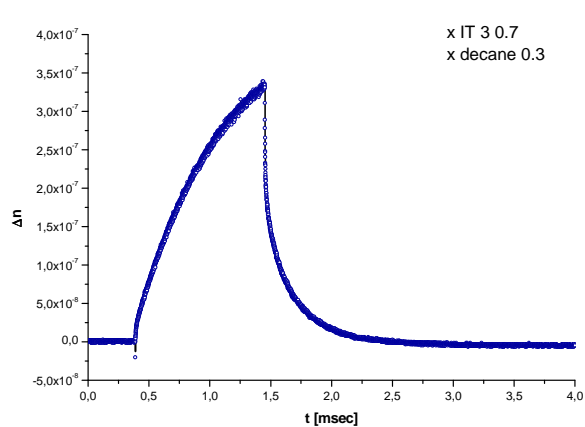
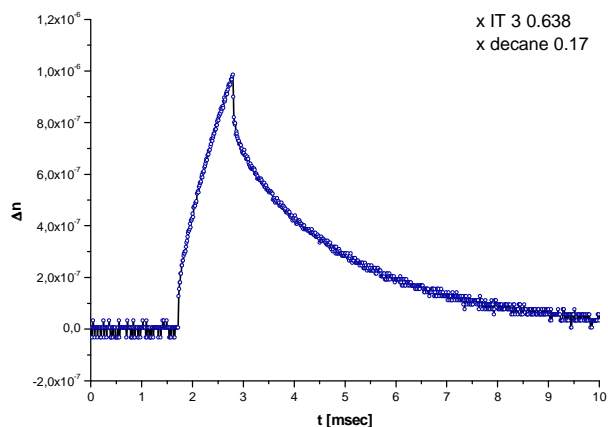
Sample composition given in each graph. Note the signals become complicated in the range between 1 and 10% decane in the solvent mixture.

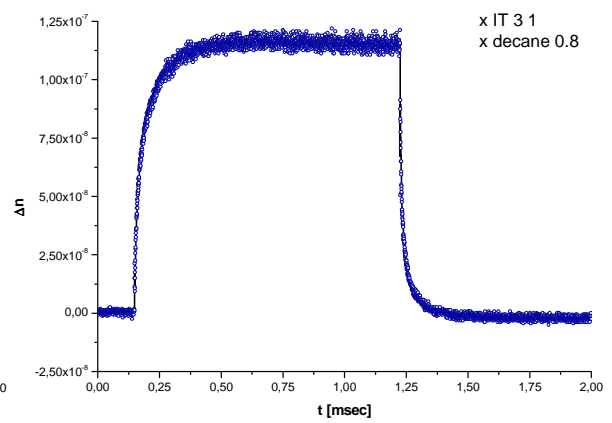
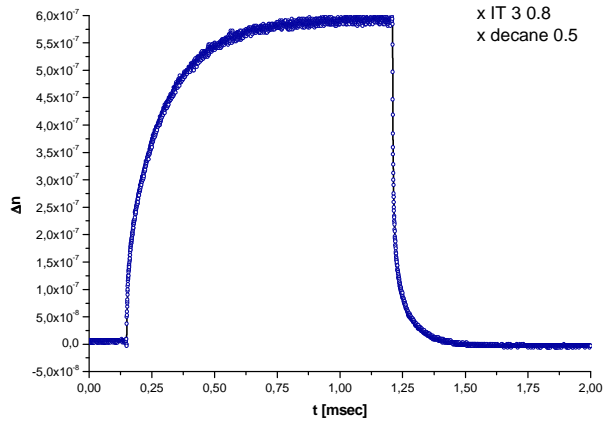




SI8: EB-Signals in the upper single phase channel (x decane 0.17 – 0.8)

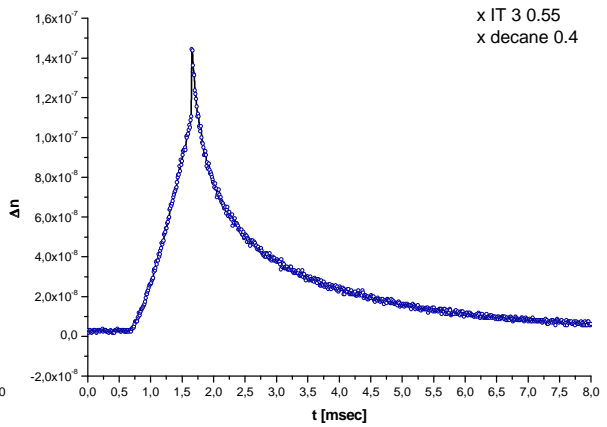
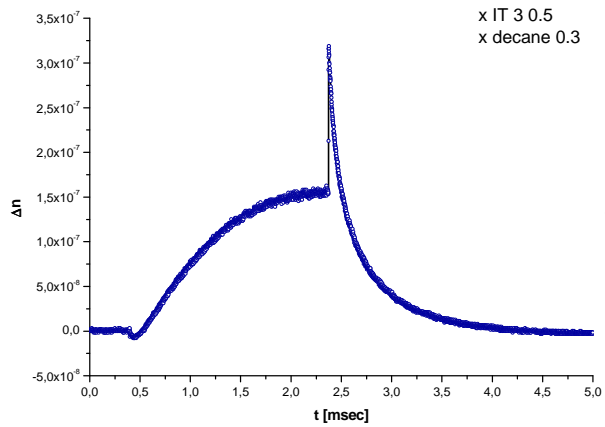
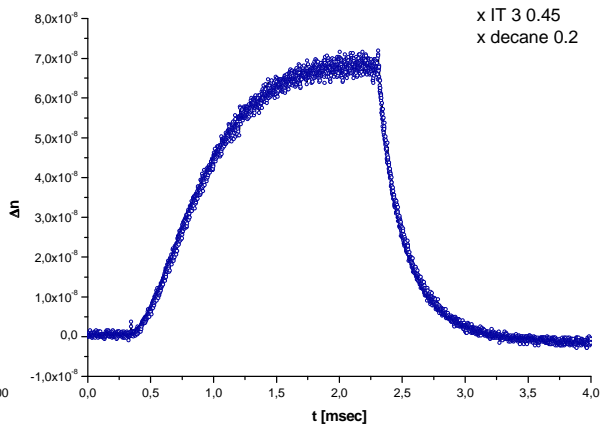
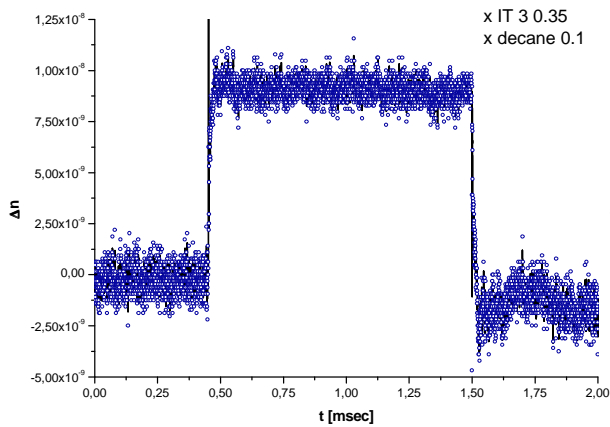
EB-Signals of microemulsion of the upper single phase channel with 17 – 80% decane in the solvent mixture. Sample composition given in each graph. Note that the signals become simple again and the main structural relaxation time decreases with increasing oil content.





SI9: EB-Signals in the lower single phase channel (x decane 0.1 – 0.4)

EB-signals for the microemulsions of the lower single phase channel. Sample composition given in each graph. Note that the signals are less complicated than signals from the upper single phase channel. Main structural relaxation time increases with increasing oil content.



5.1.4. Microemulsions with a HIPME (High Internal Phase Microemulsion) structure

Lukas Wolf*, Heinz Hoffmann, Takashi Teshigawara, Tohru Okamoto, Yeshayahu Talmon.

*corresponding author

submitted to *Journal of Physical Chemistry B*, August 15, **2011**

current status: submitted minor revised manuscript on November 13, 2011

DOI: - - -

Microemulsions with a HIPME (High Internal Phase Microemulsion) structure

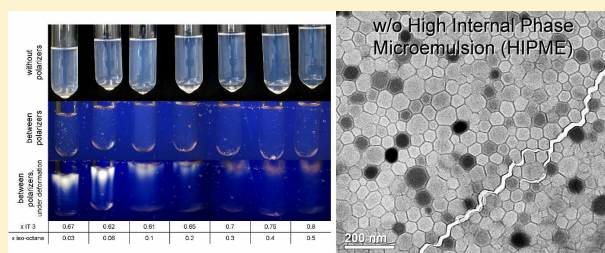
Lukas Wolf,^{*,a} Heinz Hoffmann,^a Takashi Teshigawara,^b Tohru Okamoto,^b and Yeshayahu Talmon^c

^a University of Bayreuth, BZKG and BayColl, Gottlieb-Keim-Str. 60, 95448 Bayreuth, Germany

^b Shiseido Research Center, 2-2-1 Hayabuchi, Tsuzuki-ku, 224-8558 Japan

^c Department of Chemical Engineering, Technion-Israel Institute of Technology, Haifa 32000, Israel

ABSTRACT: We report a phase diagram for a novel microemulsion that consists of oil, water and of 15% of a surfactant mixture of an anionic and a non-ionic surfactant. The phase diagram shows an optically isotropic channel that passes from the water-rich side to the oil-rich side. In contrast to the isotropic channel in microemulsions of non-ionic surfactants, the reported system undergoes an abrupt transition of the structure in the isotropic channel with increasing oil content. The structural transition is reflected in the conductivity and the viscosity of the channel. Between the L3 phase and the sample with 6 % of oil the conductivity decreases 3 orders of magnitude. Thus, the bicontinuous structure at the origin of the channel transforms already with 6% of oil to a w/o structure. The viscosity shows a strong maximum at the transition. The w/o structures with low oil content were successfully directly imaged by cryo-TEM. It can be seen that water is contained inside a polyhedral foam-like structure, where the polyhedral film is formed of the oil and the surfactant. The dimensions of the polyhedra are in the range of 20 - 100 nm. We call this structure “High Internal Phase Microemulsion” (HIPME).



INTRODUCTION

Microemulsions are thermodynamically stable, optically isotropic liquids made of water, oil, and surfactants.¹ They are structured in water rich and oil rich domains. Microemulsions produced from ionic surfactants contain a large single phase region in the phase triangle.^{2,3} The structures in this region are well known and have been studied by SAXS and SANS.⁴⁻⁷ Microemulsions of equal amounts of oil, water and a few percent of an ionic surfactant like AOT or DDAB mostly contain a water-in-oil droplet structure, in which globular oil droplets are surrounded by a palisade layer of the ionic surfactants.⁸ The dimensions of the aggregates are well understood on the basis of theoretical models.⁹ In contrast, microemulsions of non-ionic surfactants contain bicontinuous structures at equal amounts of oil and water.¹⁰ The bicontinuous structures had first been assumed on the basis of experimental results from diffusion and conductivity measurements,¹¹ and were later proven by results from scattering techniques and directly by classical freeze fracture electron microscopy (FFEM) and by the freeze fracture direct imaging technique (FFDI).^{12,13} The development of the micellar structures and properties in both systems as a function of their composition has been studied by many groups, and can be considered to be theoretically well understood.¹⁴ Nonionic microemulsions have an interesting feature in their phase behavior, namely, the single phase channels in “ χ -cut phase diagrams”. Along these channels it is possible for

systems with a constant surfactant concentration to pass from the mainly aqueous phase to the oil-rich side without crossing a phase boundary. Some measurements have already been carried out on the influence of ionic surfactants on the phase behavior of non-ionic surfactants.¹⁵ A systematic study of a microemulsion system that consists of a surfactant mixture of a hydrophilic ionic and a lipophilic non-ionic surfactant has been carried out recently.¹⁶ With such a mixture, it is possible to change the interfacial curvature of the surfactant film by adjusting the surfactant/co-surfactant ratio. The phase diagram has novel features as compared to the phase diagrams of non-ionic and ionic surfactants. It shows only one continuous isotropic single-phase channel, while microemulsions of non-ionic surfactants usually show two isotropic channels connected with each other. Furthermore, there was evidence for abrupt changes in the morphology for continuous changes in the composition of the system in that channel. No bicontinuous phase could be found for systems with equal amounts of water and oil. Surprisingly, the conductivity in the isotropic channel broke down when the system had only a few percent of oil.

Received: August 15, 2011

Revised: November 13, 2011

In the present investigation we examined by cryo-TEM the nanostructures in this isotropic channel. We therefore had to replace the n-decane of the original microemulsion system by iso-octane as a branched hydrocarbon does not crystallize upon cooling and can be vitrified in liquid nitrogen.¹⁷ The cryogen of choice, liquid ethane at its freezing point dissolves most hydrocarbons.

EXPERIMENTAL SECTION

Materials. The non-ionic surfactant iso-tridecyl-triethylglycoether, abbreviated as IT 3, was obtained from the Sasol Company, Hamburg ("Marlipal O13/30"). Sodium dodecyl sulfate (SDS, cryst. research grade) was purchased from the Serva Company, Heidelberg. $\text{MgCl}_2 \times 6 \text{H}_2\text{O}$ (99%, analytical grade) was purchased from the Grüssing Company, Filsum. N-decane and iso-octane (synthetic grade) were obtained from the Merck Company, Darmstadt.

Preparation of $\text{Mg}(\text{DS})_2$. In our surfactant system, we used $\text{Mg}(\text{DS})_2$ instead of SDS, as it leads to lower surface and interfacial tensions than SDS, and forms L_α phases in a wide composition range, when mixed with non-ionic surfactants.¹⁶ For the preparation of $\text{Mg}(\text{DS})_2$, 400 mM SDS-solution was mixed with 200 mM MgCl_2 solution under stirring. The bivalent counter ion Mg^{2+} binds more strongly to the dodecyl sulfate than the sodium-ion, leading to precipitation of $\text{Mg}(\text{DS})_2$ in solution below its Krafft-temperature around 25 °C. The solution was heated up above 25 °C to obtain a clear solution, and then cooled down to 20 °C. After precipitation $\text{Mg}(\text{DS})_2$ was washed several times with de-ionized water to remove excess salt. The salt concentration of the washing water was checked by its conductivity. The washed $\text{Mg}(\text{DS})_2$ was freeze-dried with the freeze-drying device Alpha 1-4, Christ Company, Osterode, and used without further purification.

Preparation of samples. All samples were prepared by weighing in directly the components in test tubes with an analytical balance. The test tubes were sealed with Teflon tape, equilibrated at 25 °C in a water bath, and vortexed several times thoroughly. All samples were incubated at least 3 days at 25 °C before being investigated for their phase behavior. In general, a phase diagram was scanned with a resolution of 5% in the composition of the mass fraction of IT 3 and decane. Finer steps were investigated in the beginning of the narrow upper single-phase channel. The multiphase samples were viewed and imaged without and in between crossed polarizers to visualize the birefringence of lamellar regions. Samples for cryo-TEM investigation were prepared with iso-octane instead of decane. The surfactant/co-surfactant ratio had to be adjusted slightly in order to stay in the single phase microemulsion channel when replacing decane by iso-octane.

Conductivity and rheology measurements. For conductivity measurements, we used a Microprocessor Conductivity Meter LF3000 from the WTW Company, Weilheim, Germany. The rheology was measured with the cone-plate rheometer RheoStress 600 from the Haake Thermo Scientific Company, Karlsruhe, Germany. All samples were investigated at 25 °C.

Cryo-Transmission Electron Microscopy (Cryo-TEM)

The specimens for cryo-TEM were prepared in a controlled environment vitrification system (CEVS), and plunged into liquid ethane at its freezing point.¹⁸ For oil continuous samples, the specimens were plunged into liquid nitrogen to avoid problems with solvent dissolution.¹⁹ The CEVS was kept at 25 °C and the atmosphere either saturated with water for the samples without oil, or directly with the investigated microemulsion solution for samples containing oil. Specimens, kept below -178 °C, were examined in an FEI TI2 G² transmission electron microscope, operated at 120 kV, using a Gatan 626 cryo-holder system. Images were recorded digitally in the minimal electron dose mode by a Gatan US1000 high-resolution CCD camera, with the DigitalMicrograph software package.

RESULTS AND DISCUSSION

Phase Diagram $\text{Mg}(\text{DS})_2$ -IT 3/ H_2O -oil. The system we have studied consists of decane, water and the surfactant mixture of magnesium dodecyl sulfate $\text{Mg}(\text{DS})_2$ and the non-ionic surfactant iso-tridecyl-triethylglycoether IT 3. With such a system it is possible to adjust the amphiphilic properties of the surfactant by changing the mixing ratio of the hydrophilic surfactant and the lipophilic co-surfactant. For the ionic surfactant we chose the Mg^{2+} -salt of SDS, as it reduces the surface tension more effectively and is known to form liquid crystalline L_α phases or even sponge like L_3 phases when mixed with suited co-surfactants, what is not possible for SDS.¹⁶ The phase diagram of the system with increasing oil content is shown in Figure 1.

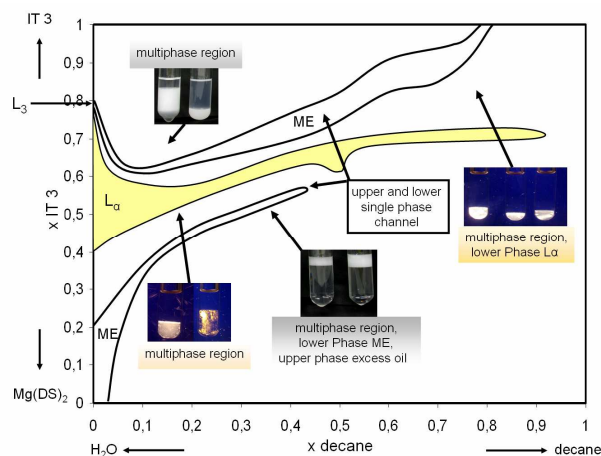


Figure 1. Phase diagram of system $\text{Mg}(\text{DS})_2/\text{IT 3} - \text{H}_2\text{O}/\text{decane}$ at 15% w/w surfactant and 25 °C, 20% glycerol in H_2O . $x \text{ IT 3}$ = mass fraction of IT 3 in the surfactant mixture, $x \text{ decane}$ = mass fraction of decane in the solvent mixture. "ME" indicates isotropic microemulsion area.

The special features of the phase diagram are two isotropic channels above and below a liquid crystalline channel that passes from the aqueous side to the oil side. It should be noted that the channels are isothermal channels. In order to stay in the channel, one has to adjust the ratio of surfactant and co-surfactant. The upper isotropic phase channel above the liquid crystalline channel begins at the water side with an L_3 phase, the lower channel begins at the L_1/L_α phase boundary at the aqueous side. The upper

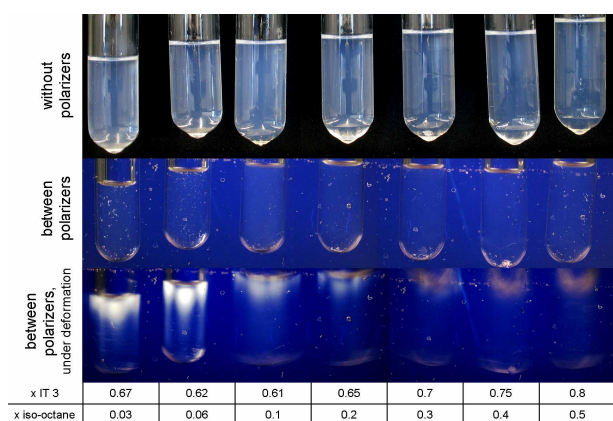


Figure 2. Samples with 15% (w/w) surfactant mixture $\text{Mg}(\text{DS})_2/\text{IT } 3$ at 25 °C and increasing mass fraction x of IT 3 and iso-octane, shown without polarizers and in between crossed polarizers. Samples containing low oil content show strong shear induced birefringence.

channel passes through a steep minimum at around 6% oil from the aqueous to the oil-rich side with increasing mass fraction of the co-surfactant. The lower channel is bent upwards, ending in the middle of the phase diagram, while the L_{α} -channel does not change much its surfactant composition with the oil content. It is noteworthy that such large liquid crystalline channels have not previously been observed in classical microemulsion systems with single nonionic surfactant. We would like to emphasize that the L_{α} phases in the liquid crystalline channel have a high tolerance to temperature variation.²⁰ While non-ionic surfactants become more lipophilic with rising temperature, ionic surfactants become more hydrophilic.²¹ Thus, these two effects are compensating each other in our system.

It is important to note that in all phase-diagrams of microemulsions of non-ionic systems the L_{α} phases are also present, but the isotropic channels are connected in the middle of the phase diagram, and are not separated by a liquid crystalline channel. The reason for this difference between the two types of microemulsions lies, probably, in the different persistence length of the bilayers. It is likely that the persistence length of charged bilayers is much longer than the persistence length of the uncharged bilayers, which is connected to the stiffness of the bilayer. As a consequence the charged bilayers can accommodate more oil than the neutral bilayers, before they fold back or form other structures.

For cryo-TEM investigation of the upper isotropic channel, samples with oil were prepared with iso-octane instead of decane, because it is known that decane, like other normal linear hydrocarbons, crystallizes when quenched in liquid nitrogen during cryo-TEM specimen preparation.¹⁹ We have to use liquid nitrogen for cryo-specimen preparation, not the better cryogen liquid ethane at its freezing point, as the latter dissolves hydrocarbons. The original microemulsion system with decane was prepared with 20% glycerol in the aqueous phase to avoid freezing artifacts in FF-TEM experiments that were performed.²⁰ Unlike the decane-system, we prepared the microemulsions containing iso-octane without glycerol in the aqueous phase, as it would have shifted the single phase channel too much towards lower x IT 3 values. Without glycerol, the sample compositions with respect to the surfactant/co-surfactant ratio, as well as the properties of the phases are similar to the decane-system.

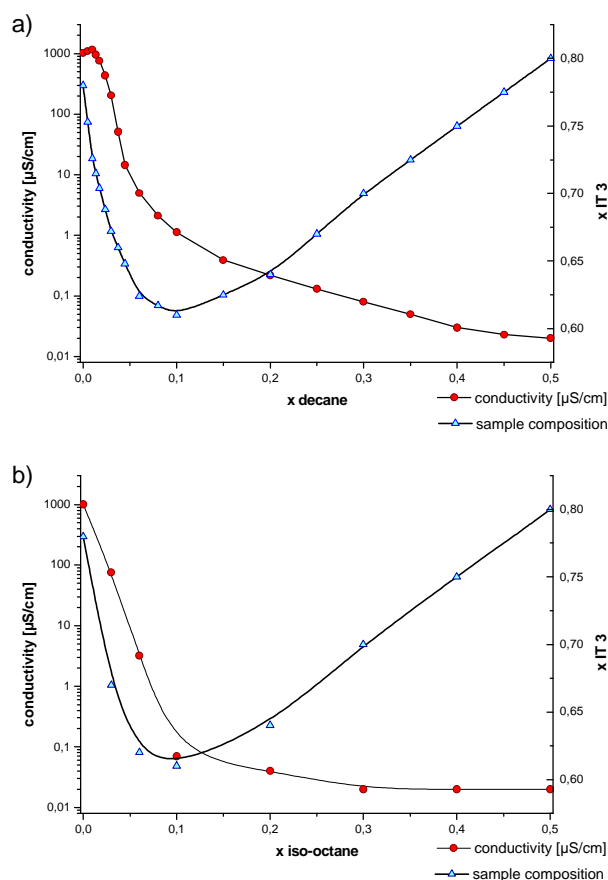


Figure 3. Plot of conductivities (red dots) and IT 3 content (blue triangles) against mass fraction of oil in the solvent mixture. 3a): values for system with decane, 3b): values for system with iso-octane.

The various domains are only slightly shifted by going from decane to iso-octane. Microemulsions with iso-octane of the upper single-phase channel are shown in Figure 2. The prepared microemulsions are slightly bluish; they do not show stationary birefringence between crossed polarizers. However, samples with low oil content around 6% iso-octane show strong flow induced birefringence.

Conductivities in the Upper Isotropic Channel. The conductivities in the upper isotropic channel were investigated with decane as the oil (Figure 3a), and compared to the conductivities when decane was replaced by iso-octane for cryo-TEM investigations (Figure 3b). The conductivity in the upper isotropic channel begins at the water side in the L_3 phase with a value of around 1000 $\mu\text{S}/\text{cm}$. The conductivity of the L_3 phase decreases, however, dramatically with the solubilization of small amounts of oil, and disappears practically for 10% of decane. The same abrupt transition in the properties is found for samples with iso-octane. No doubt, the L_3 phase changes into a different phase. the solvent mixture. 3a): values for system with decane, 3b): values for system with iso-octane.

This result is in strong contrast to conductivity measurements of microemulsions in the isotropic channel with non-ionic surfactants.²² In those systems, the conductivity from added electrolyte usually decreases slowly with increasing oil content. Such a modest decrease can be expected on the basis of the theoretical model for the structures in the channel.

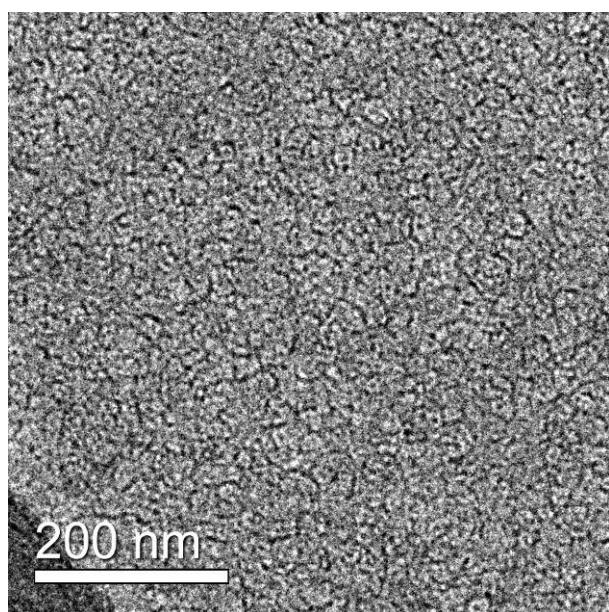


Figure 4. Cryo-TEM micrograph of the L_3 phase with the mixed anionic/nonionic surfactant mixture $Mg(DS)_2/IT\ 3$, $x\ IT\ 3\ 0.79$, 15% surfactant, at 25 °C.

The bicontinuous structure of the L_3 phase continues in the channel. The surfactant bilayers just swell with increasing oil content, as concluded from SANS measurements.²³ The conductivity results are therefore a first indication that the continuous aqueous domains disappear completely in the isotropic channel, and that the L_3 structure is replaced by another structure, in which the water is present as discrete domains, completely surrounded by oil.

Cryo-TEM of the Isotropic Channel. The nanoscopic structures in the isotropic channels of microemulsions with non-ionic surfactants have been well documented by NMR, SANS and SAXS. At the water side, the channel begins with the L_3 phase, which has a bicontinuous sponge-like structure. The bicontinuous structure of L_3 phases of ternary surfactant systems and microemulsions with non-ionic surfactant has already been directly shown by FF-TEM.^{24,25} The FF-TEM micrographs show a two dimensional micrograph of the fracture plane in which the fracture runs through both water and oil domains. The water areas and the hydrocarbon areas are well differentiated by their different graininess and grey shades. The typical dimensions between the bilayers on the micrograph are in agreement with the dimension that is evaluated by SANS.²⁶ In Figure 4, we show a direct-imaging cryo-TEM micrograph of the L_3 phase of our investigated system without oil.

In cryo-TEM micrographs, the imaged vitrified film is usually thicker than the typical correlation length in the sponge phase. Several bilayers are therefore usually on top of each other in the thin film, all projected in the detector. The structure therefore looks more like a network of thread-like micelles than a sponge structure. As part of a separate study, which we plan to publish soon, we studied the sponge structure of a bicontinuous microemulsion with a single non-ionic surfactant and oil by cryo-TEM. The sample was prepared with $C_{12}E_5$, iso-octane, H_2O and

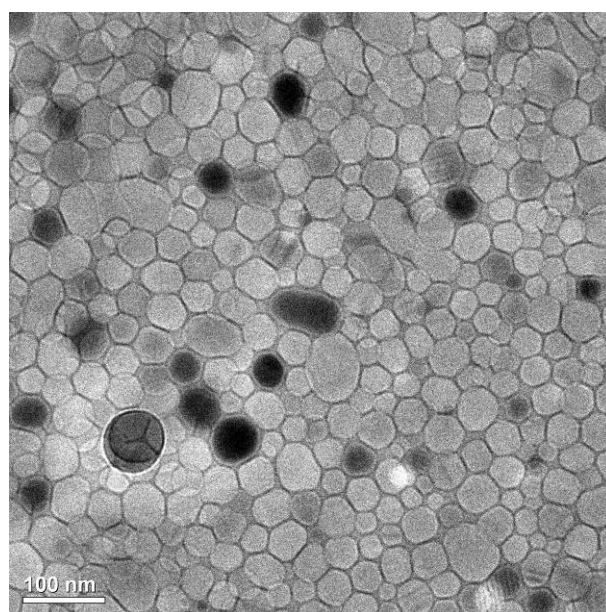


Figure 5. Cryo-TEM micrograph of a microemulsion with 15% of the anionic/nonionic surfactant mixture $Mg(Ds)_2/IT\ 3$, $x\ IT\ 3\ 0.7$, x iso-octane 0.3 (water:oil = 7:3), quenched from 25 °C.

had a water/oil ratio (w/w) of 7:3. The micrographs clearly show a sponge structure with typical dimensions of water and oil domains around 0.2 μm . In Figure 5 we show a cryo-TEM micrograph of a microemulsion of the present system, which also has a water/oil ratio of 7:3 (w/w), but was prepared with 15% of the mixed anionic/non-ionic surfactant system. In this micrograph one sees a nanostructure that is very different from what one would expect of a bicontinuous microemulsion. Now the system consists of a densely packed w/o-droplet structure, which resembles a “polyhedral foam” with thin films with a thickness of about 3 nm. The diameter of the water domains is about 50 nm. The thin film was obviously made of the surfactants with the hydrocarbon in between the two monolayers, and the water inside the polyhedra. It seems that the micrograph does not reflect exactly the 3:7 oil-to-water ratio, in the sense of the projected area of the different domains. Some of the iso-octane may have evaporated. The structures look very much like the structures found in high internal phase emulsions (HIPE). HIPEs are concentrated systems with a large volume of the dispersed phase. Those high volume fractions result in the deformation of droplets into polyhedra, which are separated by thin films of the continuous phase. In such situations the size of the structures are usually in the range of several μm and can easily be seen by light microscopy. Both o/w and w/o-systems of HIPEs are known.²⁷ Similarly to dilute emulsions, HIPEs are thermodynamically unstable.²⁸

Based on that, we call the newly found microemulsion structure HIPME (High Internal Phase Micro-Emulsion). To the best of our knowledge, such structures have so far only been observed in real emulsions. In the microemulsion sample with the HIPME structure, the water domains are not connected with each other. This can be concluded from the fact that the ice-crystals in dark have the same size as the ice crystals in grey. The crystals with the dark color are a result of a particular orientation with respect to the electron beam, which satisfies Bragg’s law. At higher oil

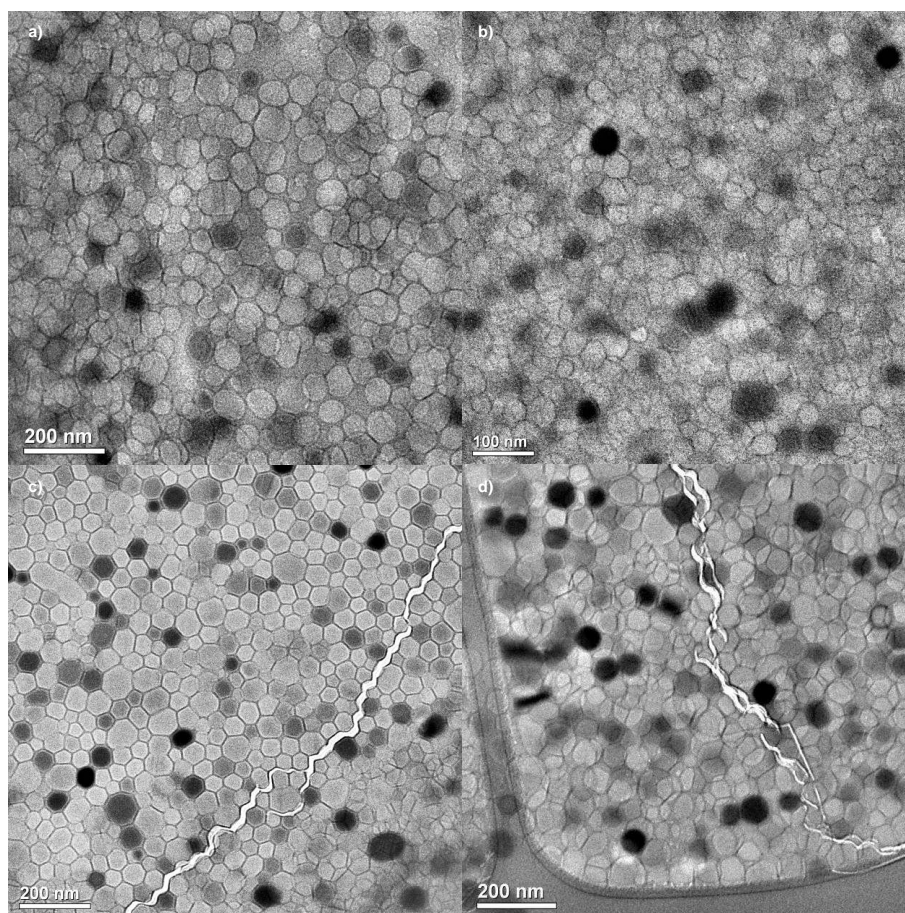


Figure 6. Cryo-TEM micrographs of microemulsions with a HIPME-structure with a) 6% iso-octane b) 20% iso-octane c) 40% iso-octane and d) 50% iso-octane in the solvent-mixture.

content, the polyhedra might have been round water domains in the liquid phase. Quenching by liquid nitrogen vitrifies the iso-octane, but freezes the water. That is manifested by the crystalline contrast causing some polyhedra to appear very dark. The polyhedral appearance may have been promoted by the crystallization, too.

In Figure 6 we show cryo-TEM micrographs of microemulsions along the upper isotropic channel from 6% to 50% iso-octane in the solvent mixture. Obviously, the HIPME structures are present all along the upper isotropic channel.

The shown HIPME structures are the first HIPE-like structures observed in microemulsions with mixed anionic/nonionic surfactant systems. The results thus show that HIPME structures can also be new dynamically stable structures. As conductivity data already indicated, HIPME-structures might also occur in systems with single ionic surfactants, like DDAB, oil and water.²⁹ The latter system is now investigated by cryo-SEM (scanning electro microscopy). We expect to report the results soon.³⁰

Rheological Results

Bicontinuous microemulsions can be visualized as L_3 phases that have oil solubilized between the surfactant monolayers. The rheological behavior of microemulsions with non-ionic surfactants is therefore similar to the rheological behavior of the L_3 phase

without oil. One of the most startling properties of the L_3 phase is its extremely low viscosity, although the phase consists of a three-dimensional network of bilayers. Most remarkable is that the rheological properties of the neighboring L_α phase are so different from the rheological properties of the L_3 phase, although both phases consist of bilayers. In the present system the differences between the two phases are even more dramatic, because the L_α phase of the system without oil, like any other ionically charged L_α phase without excess salt, has a rheological yield stress, and thus behaves like a soft gel.³¹ A rheogram of this is given in Figure 7 a. The L_3 phase, which is next to the L_α phase, differs only from the L_α phase by a small difference in the composition. It is a low-viscosity fluid with a viscosity that is only about 10 times higher than water viscosity (Figure 7 b). Rheologically speaking, the transition from the L_α to the L_3 phase can be compared to a melting transition.

Microemulsions are usually low viscosity liquids.³² The low viscosity behavior can be understood on the basis of the high deformability of the existing structures with droplets or bicontinuous shapes. This behavior is already indicated in the viscosity of the L_3 phase.³³ Viscosities in the isotropic channels have already been measured.³⁴ A modest viscosity maximum was observed with increasing oil content. The viscosities in the upper channel of the presently investigated system are shown in Fig. 8.

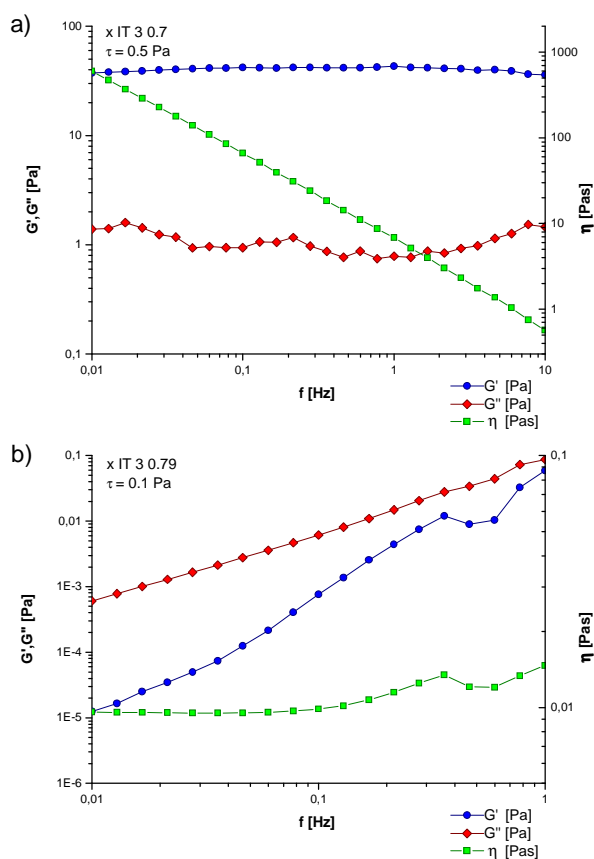


Figure 7. Rheograms of the binary surfactant mixtures at constant 15% surfactant (w/w) with increasing mass fraction x IT 3 at 25 °C. a) Rheogram of L_α phase at x IT 3 0.7, b) Rheogram of L_3 phase at x IT 3 0.79.

The results show a high maximum at around 6 % oil. At higher oil content the viscosities decrease slowly towards the oil side of the microemulsion. The abrupt maximum of the viscosity can be taken as an indication of a structural transition in the channel. The viscosity maximum is reached at about the same oil concentration where the conductivity disappeared. Obviously the transition of the structure is also expressed in the viscosity of the system.

CONCLUSIONS

We showed that w/o-HIPME structures with dimensions of about 20 - 100 nm can be thermodynamically stable structures in microemulsions. These structures occur in microemulsions formed from surfactant mixtures of anionic and non-ionic surfactants. They are observed in the isotropic channel of microemulsions, when small amounts of oil are solubilized into aqueous L_3 phases. In spite of their small oil content, the HIMPE phases have a conductivity that is about 3 - 4 orders of magnitude lower than the conductivity of the L_3 phase. These results thus demonstrate that very thin surfactant films with little oil can practically be impenetrable for the transport of ions. It can be concluded from the measurements that structural transitions can occur in micellar phases, in which bicontinuous structures of non-ionic surfactants and oil are transformed into foam-like structures, when the surfactant layers are charged by ionic surfactants. It is likely that

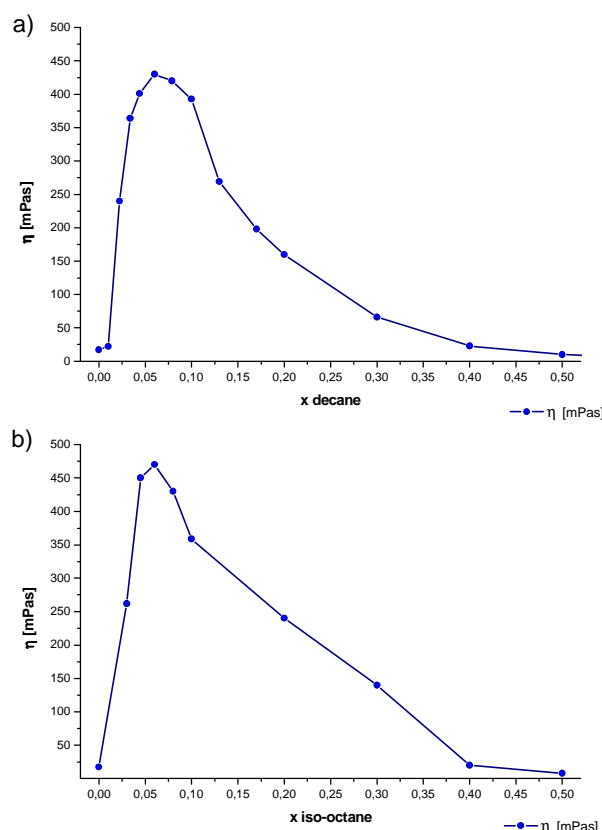


Figure 8. Zero shear viscosity, η , against the mass fraction of oil of samples from the upper single phase channel: a) Viscosity with increasing mass fraction of decane; b) Viscosity with increasing mass fraction of iso-octane.

such transitions can also be produced, when the electric double-layer in ionically charged systems is shielded by excess salt.

AUTHOR INFORMATION

Corresponding Author

*Tel:+49-921-50736168. Fax+49-921-50736139. E-mail: lukas.wolf@freenet.de.

ACKNOWLEDGMENT

We thank the Technion Russell Berrie Nanotechnology Institute (RBNI) and the Israel Science Foundation (GRANT NO. 962/07) for partial financial support. The electron microscopy was performed at the RBNI Laboratory for Electron Microscopy of Soft Matter. We thank Judith Schmidt and Dr. Ellina Kesselman for their excellent technical assistance, and all members of Prof. Talmon's group for their help.

REFERENCES

- Stubenrauch, C. In *Microemulsions: Background, New Concepts, Applications, Perspectives*; Wiley-Blackwell: Chichester, U.K., 2009.

- (1) Stubenrauch, C. In *Microemulsions: Background, New Concepts, Applications, Perspectives*; Wiley-Blackwell: Chichester, U.K., 2009.
- (2) Monduzzi, M.; Caboi, F.; Larché, F.; Olsson, U. *Langmuir* **1997**, *13*, 2184-2190.
- (3) Bergenholtz, J.; Romagnoli, A. A.; Wagner, N. J. *Langmuir* **1995**, *11*, 1559-1570.
- (4) Zemb, T. N.; Hyde, S. T.; Derian, P.-J.; Barnes, I. S.; Ninham, B. W. *J. Phys. Chem.* **1987**, *91*, 3814-3820.
- (5) Kotlarchyk, M.; Sheu, E. Y.; Capel, M. *Physical Review A* **1992**, *46*, 928.
- (6) Eastoe, J. *Langmuir* **1992**, *8*, 1503-1506.
- (7) Huang, J. S. *J. Surface Sci. Technol.* **1989**, *5*, 83-131.
- (8) Jahn, W.; Strey, R. *J. Phys. Chem.* **1988**, *92*, 2294-2301.
- (9) Strey, R. *Colloid & Polymer Sci.* **1994**, *272*, 1005-1019.
- (10) Olsson, U.; Würz, U.; Strey, R. *J. Phys. Chem.* **1993**, *97*, 4535.
- (11) Lindman, B.; Shinoda, K.; Olsson, U.; Anderson, D.; Karlström, G.; Wennerström, H. *Colloids and Surfaces* **1989**, *38*, 205-224.
- (12) Kahlweit, M. et al., *J. Colloid Interface Sci.* **1987**, *118*, 445.
- (13) Belkoura, L.; Stubenrauch, C.; Strey, R. *Langmuir* **2004**, *20*, 4391-4399.
- (14) Tlustý, T.; Safran, S. A.; Menes, R.; Strey, R. *Physical Review Letters* **1997**, *78*, 2616-2619.
- (15) Kahlweit, M.; Faulhaber, B.; Busse, G. *Langmuir* **1994**, *10*, 2528-2532.
- (16) Wolf, L.; Hoffmann, H.; Watanabe, K.; Okamoto, T. *Phys. Chem. Chem. Phys.* **2011**, *13*, 3248-3256.
- (17) Talmon, Y. "Seeing Giant Micelles by Cryogenic-Temperature Transmission Electron Microscopy (Cryo-TEM)", in "Giant Micelles", chapter 5, pp. 163-178, Zana, R. and Kaler, E.A., Eds., CRC Press, New York, 2007.
- (18) Danino, D.; Bernheim-Groswasser, A.; Talmon, Y. *Colloid Surf. A: Physicochem. Eng. Asp.* **2001**, *183*, 113-122.
- (19) Danino, D.; Gupta, R.; Satayavolu, F.; Talmon, Y. *J. Colloid Interface Sci.* **2002**, *249*, 180-168.
- (20) Wolf, L.; Hoffmann, H.; Richter, W.; Teshigawara, T.; Okamoto, T. *J. Phys. Chem. B* **2011**, *115*, 11081-11091.
- (21) Miller, C. A.; Raney, K. H. *Colloids and Surfaces A* **1993**, *74*, 169-215.
- (22) Sottmann, T.; Strey, R. Microemulsions, In: *Fundamentals of Interface and Colloid Science*, Lyklema J. Ed., Elsevier Academic Press, Heidelberg, Germany, 2005.
- (23) Wehling, A. The dynamics of L_3 phases. Ph.D. Thesis, University of Cologne, 2001.
- (24) Hoffmann, H.; Thunig, C.; Munkert, U.; Meyer, H. W.; Richter, W. *Langmuir* **1992**, *8*, 2629-2638.
- (25) Burauer, S.; Bekoura, L.; Stubenrauch, C.; Strey, R. *Colloid Surface A* **2003**, *228*, 159.
- (26) Choi, S. M.; Chen, S. H.; Sottmann, T.; Strey, R. *Physica B* **1997**, *241*, 976.
- (27) Cameron, N. R.; Sherrington, D. C. *Advances in Polymer Science*, **1996**, *126*, 163-214.
- (28) Hoffmann, H.; Ebert, G. *Angewandte Chemie* **1988**, *27*, 902-912.
- (29) Ninham, B. W.; Chen, S. J.; Evans, D. F. *J. Phys. Chem.* **1984**, *88*, 5855-5857.
- (30) Ben Barak, I.; Talmon Y., *Langmuir* (submitted).
- (31) Hoffmann, H.; Thunig, C.; Schmiedel, P.; Munkert, U. *Langmuir* **1994**, *10*, 3972-3981.
- (32) Uhrmeister, P. Selbstorganisierende Netzwerke in Mikroemulsionen, Ph.D Thesis, University of Cologne, 2009.
- (33) Miller, C. A.; Gradzielski, M.; Hoffmann, H.; Krämer U.; Thunig, C. *Progr. in Coll. & Polym. Sci.* **1991**, *84*, 243
- (34) Faulhaber, B. *J. Colloid Interf. Sci.* **1987**, *118*, 443-444.

5.1.5. PFG-NMR in the Single Phase Channels of Microemulsions with an anionic/non-ionic surfactant mixture

Lukas Wolf*, Heinz Hoffmann, Jürgen Linders and Christian Mayer

* corresponding author

Submitted to *Soft Matter* in December **2011**

current status: under revision

DOI: - - -

PFG-NMR Self Diffusion Measurements in the Single Phase Channels of a Microemulsion System with an Anionic/Nonionic Surfactant Mixture

Lukas Wolf,*^a Heinz Hoffmann,*^a Jürgen Linders*^b, Christian Mayer*^b

Received (in XXX, XXX) Xth XXXXXXXXXX 200X, Accepted Xth XXXXXXXXXX 200X

First published on the web Xth XXXXXXXXXX 200X

DOI: 10.1039/b000000x

The single phase channels of a presently reported microemulsion system were investigated by electrical conductivity and pulsed-field gradient nuclear magnetic resonance (PFG-NMR) spectroscopy. The system consists of a mixed anionic/non-ionic surfactant mixture, water and decane. At constant surfactant concentration and temperature, the phase diagram exhibits two single phase microemulsion channels, separated by an anisotropic lamellar channel. The lower microemulsion channel starts from the water side at the phase diagram with a micellar L_1 phase and reaches with increasing mass fraction of decane in the solvent mixture and increasing mass fraction of lipophilic co-surfactant in the surfactant mixture the middle of the phase diagram. The upper microemulsion channel passes from the aqueous side with an L_3 phase to the oil side of the diagram. Conductivity data and self diffusion coefficients, obtained by PFG-NMR, support the previously made conclusion, that the nanostructure in the upper channel undergoes an abrupt transition from a bicontinuous structure to a water-in-oil High Internal Phase Microemulsion (HIPME) with already less than 10% of oil in the solvent mixture, while the structures in the lower microemulsion channel are oil-in-water droplets. The HIPME structure is a feature of the surfactant mixture and probably due to a high interfacial tension between the aqueous diluted surfactant phase and the oil. By addition of salt, the HIPME structures are obviously disturbed, resulting in an increased conductivity and a faster diffusion rate for the water fraction.

Introduction

Since their discovery in 1943 by Hoar and Schulman, microemulsions were much in the focus of interest by scientists in the field of colloid and polymer science.¹ They defined microemulsions as optically isotropic transparent phases, consisting of oil, water and surfactants.² In contrast to ordinary emulsions, microemulsions are thermodynamically stable.³ Three different types of nanostructures can be distinguished in microemulsions, namely oil droplets in a continuous water phase (o/w), water droplets in a continuous oil phase (w/o) and bicontinuous structures.⁴ The type of the used surfactant plays an important role for the emerging nanostructures. The most detailed investigated microemulsion systems are those with a single non-ionic surfactant C_iE_j , water and oil. In such systems, it is possible to pass from water-rich to oil-rich single phase microemulsions, without crossing a phase boundary in the phase diagram.⁵ In order to stay in the single phase region, one has to adapt the hydrophilic lipophilic balance (HLB) by changing the temperature, as non-ionic surfactants are very temperature sensitive.⁶ The behaviour and the nanostructures in these single-phase channels are known and theoretically well understood.⁷ They have been investigated indirectly by electrical conductivity, small angle neutron scattering (SANS), NMR and directly imaged by freeze fracture transmission electron microscopy (FF-TEM).⁸⁻¹⁰ With increasing temperature and increasing oil content, the

structure undergoes a continuous transition from small oil droplets in water at the aqueous side to a bicontinuous structure at the middle of the phase diagram with equal amounts of oil and water to small water droplets in oil at the oil side.¹¹ The structural transition is caused by the change of the amphiphilic properties of the non-ionic surfactant with rising temperature. Thus, the curvature of the amphiphilic monolayer changes from convex, to flat, to concave.

The situation is somewhat different in microemulsions prepared with ionic surfactants. In such systems, it is not possible to pass from the single aqueous phase to the oil phase without crossing phase boundaries at constant surfactant concentration.¹² The best known systems with ionic surfactants are probably microemulsions with sodium bis(2-ethylhexyl) sulfosuccinate (AOT), decane or di-dodecyl-dimethylammoniumbromide (DDAB), dodecane and water.¹³⁻¹⁴ In contrast to bicontinuous microemulsions with a single nonionic surfactant, in these systems a w/o droplet structure is present at equal amounts of water and oil.¹⁵

We reported recently a new microemulsion system with a mixed anionic/nonionic surfactant mixture.¹⁶ In such systems it is possible to pass from the aqueous to the oil side in a single phase microemulsion channel at constant surfactant concentration and constant temperature. This is achieved by changing the HLB not by temperature but by adjusting the surfactant-co-surfactant ratio. Conductivity data, electric birefringence measurements and cryo-TEM pictures indicated that the nanostructure in this single phase channel has a w/o-structure at a water/oil ratio of 1/1 and not a bicontinuous

structure as achieved with a single non-ionic surfactant. We called this structure High Internal Phase Microemulsion (HIPME). Furthermore, the transition from a bicontinuous L_3 phase to a w/o high internal phase microemulsion seemed to be already completed by solubilising less than 10% oil into the system.¹⁷⁻¹⁹ In this investigation, we want to prove by pulsed-field gradient nuclear magnetic resonance (PFG-NMR) that this is in deed the case. Moreover we investigated the influence of the addition of excess salt to the microemulsion system by interfacial tension measurements, conductivity and PFG-NMR, as it was tried to transform the HIPME structures to bicontinuous structures by shielding the charge of the anionic surfactant.

Results and Discussion

Surface and Interfacial Tension Measurements

The binary surfactant mixture of our reported microemulsion system is composed of the hydrophilic anionic surfactant Magnesium Dodecyl Sulfate $Mg(DS)_2$ and the lipophilic non-ionic co-surfactant Iso-tridecyl-triethylenglycoether IT 3 ($C_{13}E_3$). We chose the Mg -salt of SDS, as it is known to cause lower surface tension values than SDS and it is possible to form sponge like L_3 phases with co-surfactants.²⁰⁻²¹ The surface tension and the interfacial tension between the aqueous surfactant and the oil phase play an important role for the formation of microemulsions with non-ionic surfactants.²² Optimal solubilisation of oil should occur when the interfacial tension of the dilute surfactant solution has its lowest interfacial tension against the oil phase.²³ Low interfacial tension values are observed for surfactant systems which form liquid crystalline L_α or L_3 phases at low surfactant concentrations.²⁴ Before we determined the interfacial tension values between our surfactant mixture and the oil decane, we first investigated the surface tension of the surfactant mixture at a mixing ratio of 1/1 (w/w) with increasing surfactant concentration.

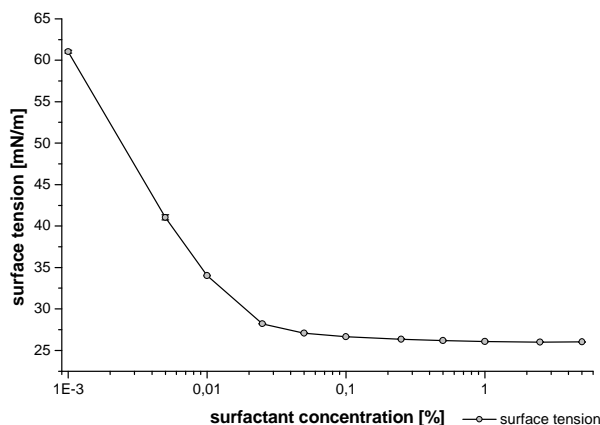


Fig. 1 Surface tension of the surfactant mixture $Mg(DS)_2$ -IT 3 at a surfactant ratio of 1/1 (w/w) with increasing total surfactant concentration at 25 °C.

As it can be seen in Fig. 1, the surfactant mixture reaches its critical micelle concentration (cmc) at a value around 0,025%

surfactant and reaches a very low surface tension of ~ 26 mN/m. This is in deed a very low value, if one considers the surface tension of SDS around 35 mN/m above its cmc.

In Fig. 2 we show the interfacial tension values of the diluted surfactant mixtures with increasing mass fraction of the co-surfactant IT 3 at constant surfactant concentration of 0,5% surfactant against the oil decane.

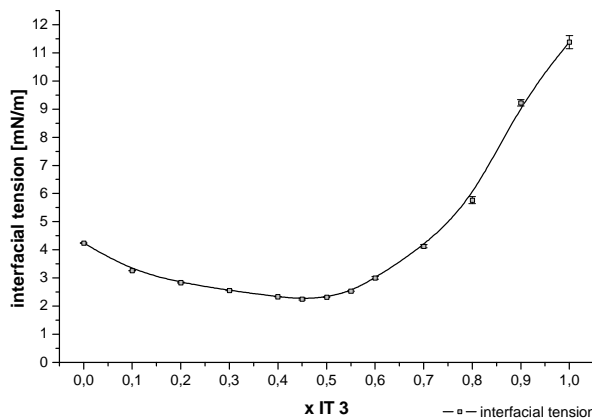


Fig. 2 Interfacial tension of $Mg(DS)_2$ -IT 3 with increasing mass fraction x IT 3 in the surfactant mixture against the oil decane. Surfactant concentration constant at 0,5%, measured at 25 °C.

A broad minimum of the interfacial tension is reached between x IT 3 = 0,4 – 0,5 with a value of $\sim 2,3$ mN/m. In this area, the binary surfactant mixture starts to form single phase liquid crystalline L_α phases at higher surfactant concentrations.¹⁸ The data are very similar compared to a previously investigated microemulsion system with a silicone oil.¹⁶ In contrast to microemulsions with a single non-ionic surfactant, where ultra-low interfacial tensions in the range of 10^{-3} mN/m are reached, the values with our surfactant system are very high. The reason for this obviously lies in the charge of the anionic surfactant. In systems with ionic surfactants, it should be possible to lower the interfacial tension by shielding the electric charge with excess salt.²⁵

Phase Diagram of $Mg(DS)_2$ /IT 3 – H_2O /n-Decane

A phase diagram of our investigated microemulsion system is shown in Fig. 3. The total surfactant concentration was kept constant at 15% (w/w) and the temperature at 25 °C. Samples were prepared with 20% glycerine in H_2O to prevent freezing artefacts in freeze fracture transmission electron microscopy (FF-TEM) investigations, that were done previously.¹⁸ The phase diagram contains two isotropic microemulsion channels, a lower one and an upper one. The upper one begins on the surfactant axis at the region of the L_3 phase. With increasing oil, the channel first shifts to a lower IT 3 ratio and then again to a higher IT 3/ $Mg(DS)_2$ ratio for higher oil ratios. It ends on the oil side at 80% decane and pure IT 3 as surfactant. The lower channel begins at the L_1 region and ends in the middle of the phase diagram at an IT 3 ratio of 0.57. Both channels are separated by a large single phase birefringent L_α region that extends from 0% to 90% decane with slightly increasing mass fraction of IT 3.

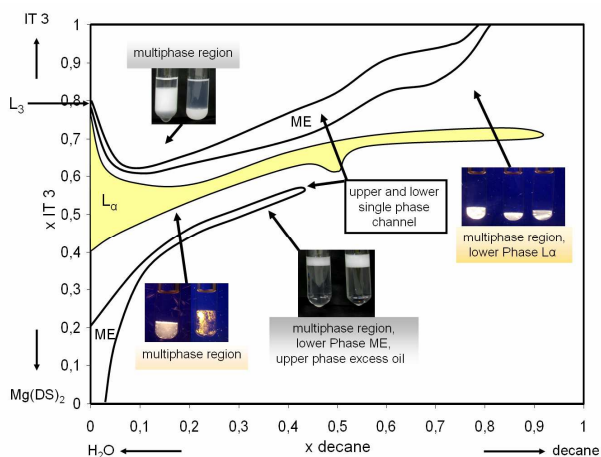


Fig. 3 Phase diagram of system $\text{Mg}(\text{DS})_2/\text{IT } 3 - \text{H}_2\text{O}/\text{decane}$ at 15% (w/w) surfactant and 25 °C, 20% glycerin in H_2O . $x \text{ IT } 3$ = mass fraction of IT 3 in the surfactant mixture, $x \text{ decane}$ = mass fraction of decane in the solvent mixture. “ME” indicates isotropic microemulsion area, L_α indicates area of anisotropic lamellar channel.

The microemulsions in the lower single phase channel are transparent phases that show no flow birefringence under shear. The samples in the upper phase channel have different properties. While the L_3 phase without decane is completely transparent, the samples with decane look somewhat bluish and their scattering intensity is most intensive around $x \text{ decane}$ 0.03 and 0.1. For higher oil content the scattering intensity is decreasing again.

A good and quick method that gives first indications for the nanostructures in microemulsions is the measuring of the electric conductivity. It helps to distinguish between conducting water continuous phases and non-conducting oil continuous phases.²⁶ Because we use a surfactant mixture with an anionic surfactant, no additional salt has to be added to follow the conductivity in the phases in contrast to microemulsions with only a single non-ionic surfactant. The plots of the conductivities in the upper and lower single phase channels are shown in Fig. 4a and 4b. In the upper channel, the conductivity first increases slightly from around 1000 $\mu\text{S}/\text{cm}$ of the sample without decane to 1160 $\mu\text{S}/\text{cm}$ to the sample with 1% decane. The reason for this lies in the change of the composition of the surfactant mixture. In the range from 1% - 10% decane, the conductivity decreases abruptly three orders of magnitude to $1 \mu\text{S}/\text{cm}$ even though the fraction of the anionic $\text{Mg}(\text{DS})_2$ is increasing. For higher mass fractions of decane, the conductivity values decrease continuously to low values as e.g. 0.03 $\mu\text{S}/\text{cm}$ for the sample with a water/oil ratio of 1/1 (w/w). The conductivities thus indicate a dramatic change in the nanostructure of the upper channel with solubilisation of small amounts of oil into the L_3 phase. The abrupt collapse of the conductivity indicates that the system changes from a bicontinuous structure to a water-in-oil (w/o) structure. Conductivities in the isotropic channels of microemulsions from non-ionic surfactants have been reported in the literature.²⁷ In such systems, the conductivity in the upper channel decreases continuously with increasing oil content. These measurements have helped to establish the

view which we have today from the structures in the upper channel. With increasing oil content, the bicontinuous L_3 phase swells with the solubilised oil between the bilayers and is finally transformed at high oil content to a w/o system.

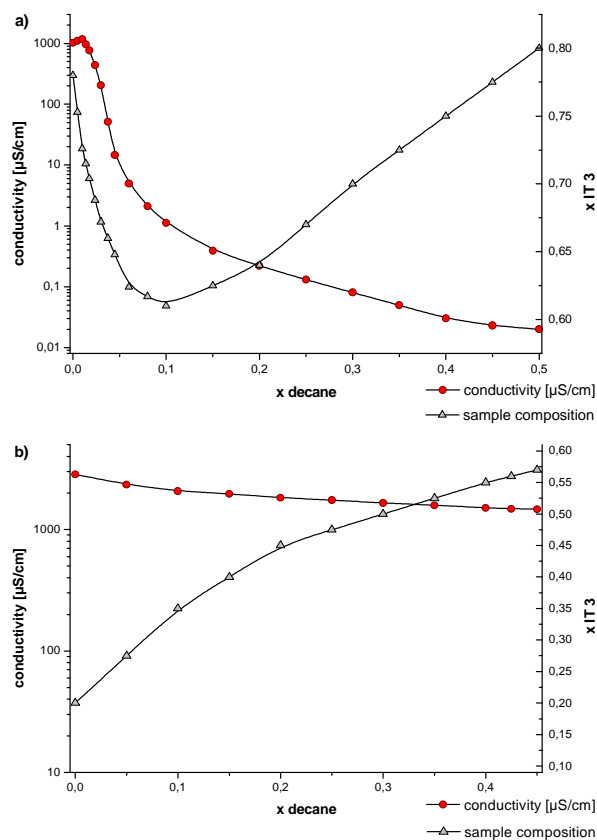


Fig. 4 Plot of conductivity (red dots) and IT 3 content (grey triangles) against mass fraction of decane in solvent mixture. a) Conductivity data for the upper single phase channel. b) Conductivity data for the lower single phase channel.

With equal amount of oil and water, SANS-data and conductivities show, that this phase is still a bicontinuous phase.²⁸ Our conductivity data unambiguously show that the structures in the upper channel of the presently investigated system are different from the structures of known systems with non-ionic surfactants. We find a rather abrupt transition from the bicontinuous L_3 structure to a w/o structure with only 10% of oil in the solvent mixture. Recently published cryo-TEM pictures show a polyhedral w/o foam structure, when 6% of oil was solubilised in the L_3 phase.¹⁹ These structures were similar to those that are found in so called High Internal Phase Emulsions (HIPE).²⁹ We therefore called the new microemulsion structures High Internal Phase Microemulsions (HIPME).

In opposition to the upper channel, the conductivity data of the lower channel indicate that the nanostructure in the lower channel does not change much with increasing oil content. At the water corner, the conductivity in the lower channel with 2900 $\mu\text{S}/\text{cm}$ is much higher than the conductivity of the L_3 phase of the upper channel with 1000 $\mu\text{S}/\text{cm}$. The reason for this is that the $\text{Mg}(\text{DS})_2$ concentration is much higher in the lower channel. With increasing oil content, the conductivities decrease slightly to 1500 $\mu\text{S}/\text{cm}$ at the middle of the phase

diagram, which is where the channel ends. The reason for the decrease is mainly the decreasing mass fraction of $\text{Mg}(\text{DS})_2$. Obviously, the lower channel consists of a continuous water phase in which oil droplets are dispersed (o/w-structure).

PFG-NMR in the Microemulsion Channels

To underline and to verify our results, we investigated the microemulsion channels by PFG-NMR, as this method delivers information about the structure, fluidity and emulsion type. Furthermore, it can give indications about the interaction between surfactant and co-surfactant at the interface. Fig. 5 shows a conventional proton NMR spectrum of the system in the upper channel at x decane 0.7, x IT3 0.85.

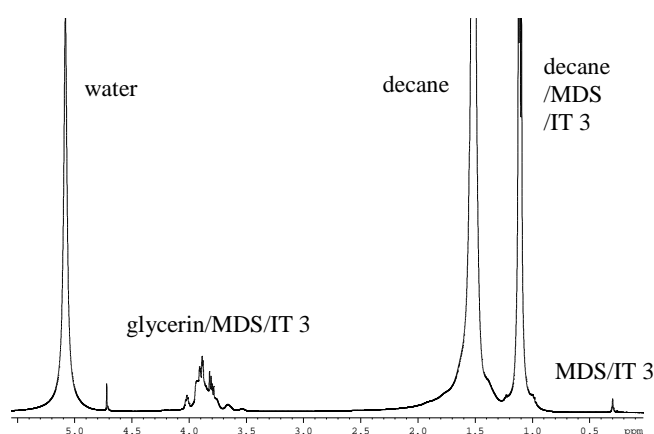


Fig. 5 Proton NMR spectrum of the system in the upper channel at x decane 0.7, x IT3 0.85.

The PFG-NMR analysis is focussed on those spectral regions which can either be clearly assigned to single system constituents (water between 4.8 and 5.3 ppm and decane between 1.3 and 2.0 ppm) or to the mixture of the surfactants ($\text{Mg}(\text{DS})_2/\text{IT}3$ between 0.2 and 0.4 ppm). The integrals of these three spectral regions strongly depend on the strength of the gradient pulse, hereby indicating the average displacement of the corresponding system constituents during the period between the pulses which was set to 50 ms. In a plot of the logarithmic relative signal intensity $\ln I/I_0$ vs. the parameter $\gamma^2 G^2 \delta^2 (\Delta - \delta/3)$ (with γ being the gyromagnetic ratio of protons, G the strength of the gradient field, δ and Δ the duration of and the spacing between the two gradient pulses), the slope is equal to the negative apparent self diffusion coefficient of the given component in the heterogeneous system (Stejskal-Tanner plot). If the component is located in two different environments leading to clearly different self diffusion properties, the plot will show two sections with clearly different slopes. If the component is encapsulated in very small droplets, the motion within the droplets becomes undetectable. In this case, the observed slope reflects the diffusive displacement connected to the Brownian motion of the droplets.

The resulting Stejskal-Tanner plots for four different states in the upper channel are shown in Fig. 6. The corresponding apparent self diffusion coefficients are listed in Table 1. The first example (Fig. 6 a) refers to the situation in absence of decane (x decane 0). Here, the water signal follows a steep

decay, corresponding to a self diffusion constant of $D_w = 6.80 \cdot 10^{-10} \text{ m}^2/\text{s}$. This is just slightly lower than the value for bulk water, indicating that water forms a continuous phase only slightly affected by dispersed phase boundaries. In contrast, the signal for $\text{Mg}(\text{DS})_2/\text{IT}3$ follows a relatively flat decay, pointing to a structure of the surfactant which only allows a restricted mobility of $\text{Mg}(\text{DS})_2$ and IT 3 molecules.

The situation changes significantly on the addition of 10% decane (x decane 0.1, Fig. 6 b). Now the mobility of water is reduced by a factor of three to $D_w = 2.22 \cdot 10^{-10} \text{ m}^2/\text{s}$. All other system constituents, decane as well as the surfactants, exhibit curved decay profiles connected to two distinctly different diffusion constants for each constituent. The largest portion of decane (and a small portion of the surfactants) show a self-diffusion constant which, with $D_d = 3.65 \cdot 10^{-10} \text{ m}^2/\text{s}$, is approximately half of the value for bulk decane. With the relatively small decane content, this indicates that we actually deal with a continuous decane phase. The slower portion of the decane (approximately 3%) seems to be associated with the majority of the surfactant ($D_d = 5.68 \cdot 10^{-11} \text{ m}^2/\text{s}$). Altogether, the diffusion profile is compatible with a high internal phase w/o-microemulsion (w/o-HIPME) of 90% water in 10% decane, stabilized by the surfactants. Obviously, a small fraction of the decane is closely associated with the surfactant layer which explains the slow fraction of decane. Correspondingly, some of the surfactant is being dissolved in the decane phase which explains the fast fraction of the $\text{Mg}(\text{DS})_2/\text{IT}3$ signal. The surprisingly high diffusion rate of the water indicates significant exchange of water molecules via the thin decane films which separate the water droplets.

With increasing decane content (x decane 0.3 and 0.7), the system gradually changes towards a conventional water in oil microemulsion (Figs. 6 c and d). The mobility of water is further reduced by an order of magnitude to $D_w = 2.14 \cdot 10^{-11} \text{ m}^2/\text{s}$ and $D_w = 2.13 \cdot 10^{-11} \text{ m}^2/\text{s}$, respectively. In addition, the mobility of the surfactant as well as the “slow” fraction of the decane is slowed down by a factor of five ($D_d = 1.02 \cdot 10^{-11} \text{ m}^2/\text{s}$ and $D_w = 8.76 \cdot 10^{-12} \text{ m}^2/\text{s}$ for x decane 0.3 and 0.7). In contrast, the “fast” fraction of the decane exhibits values which now come close to the bulk diffusion rate ($D_d = 4.32 \cdot 10^{-10} \text{ m}^2/\text{s}$ and $D_d = 7.07 \cdot 10^{-10} \text{ m}^2/\text{s}$ for x decane 0.3 and 0.7). In this situation, the observed displacement for water molecules is largely caused by the Brownian motion of small water droplets in the continuous decane phase. With the given viscosity of decane at room temperature, the diameter of the water droplets can be estimated to approximately 20 nm. As before, we assume that part of the surfactant is dissolved in the continuous decane phase, leading to the initial fast decay of the $\text{Mg}(\text{DS})_2/\text{IT}3$ signal. Also, again a small fraction of the decane is dissolved in the surfactant layer around the water droplets, leading to the shallow plateau of the decane signal ($D_d = 1.02 \cdot 10^{-11} \text{ m}^2/\text{s}$ and $D_d = 8.76 \cdot 10^{-12} \text{ m}^2/\text{s}$ for x decane 0.3 and 0.7, respectively). The fact that the self diffusion coefficient for water is still slightly larger than for the droplet wall constituents indicates the exchange of a small fraction of water molecules between the droplets via the hydrophobic phase, an effect which is linked to Oswald ripening.

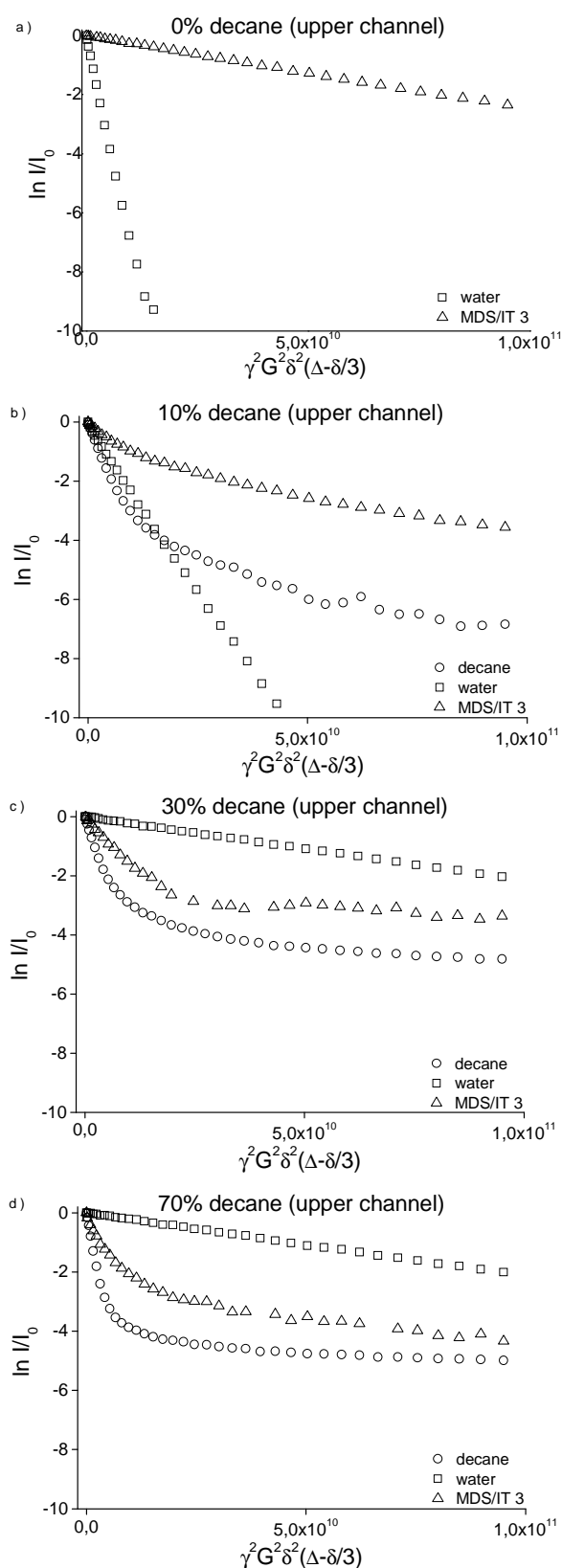


Fig. 6 a-d Stejskal-Tanner plots for decane, water and the surfactants in the upper channel.

Tab. 1 Apparent self diffusion coefficients of system constituents in the upper channel

x water	x decane	D (water)	D (decane)	D (decane) plateau
		[m ² /s]	[m ² /s]	[m ² /s]
1	0	6.80 10 ⁻¹⁰	-	-
0.9	0.1	2.22 10 ⁻¹⁰	3.65 10 ⁻¹⁰	5.68 10 ⁻¹¹
0.7	0.3	2.14 10 ⁻¹¹	4.32 10 ⁻¹⁰	1.02 10 ⁻¹¹
0.3	0.7	2.13 10 ⁻¹¹	7.07 10 ⁻¹⁰	8.76 10 ⁻¹²

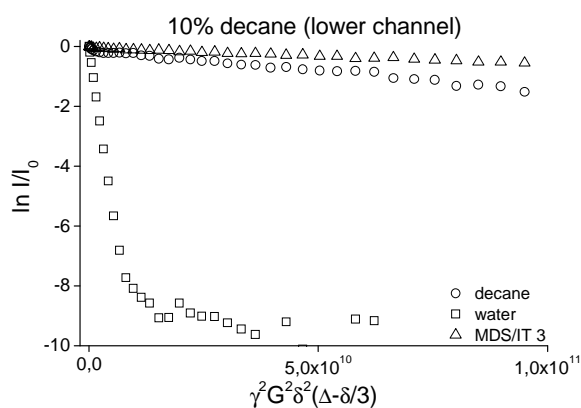


Fig. 7 Stejskal-Tanner plots for decane, water and the surfactants in the lower channel.

Tab. 2 Apparent self diffusion coefficients of system constituents in the lower channel

x water	x decane	D (water)	D (water) plateau	D (decane)
		[m ² /s]	[m ² /s]	[m ² /s]
0.9	0.1	1.04 10 ⁻⁹	1.79 10 ⁻¹¹	1.37 10 ⁻¹¹
0.7	0.3	8.36 10 ⁻¹⁰	9.04 10 ⁻¹²	2.88 10 ⁻¹³

In contrast to the results for the upper channel, the variations between the PFG-NMR results of different positions in the lower channel do not indicate dramatic structural changes, even though diffusion constants do vary significantly with x decane. An example for a corresponding Stejskal-Tanner plot for the lower channel is shown in Fig. 7. Apparent self diffusion coefficients for two points in the lower channel are listed in Table 2. The data for water and the surfactants resemble those of the upper channel in absence of decane. Again, the water signal shows very steep decays linked to self diffusion coefficients of 1.04 10⁻⁹ m²/s for x decane 0.1 and 8.36 10⁻¹⁰ m²/s for x decane 0.3, values which come close to the one in bulk water. In contrast, the decane signal indicates an increasingly slow mobility (1.37 10⁻¹¹ m²/s and 2.88 10⁻¹³ m²/s) which corresponds to Brownian motion of droplets with increasing size. The surfactant seems to be linked to the decane droplets, even though the diffusion rate is slightly larger. All in all, the data are clearly in accordance with an o/w microemulsion with a droplet size significantly growing with the decane content. Parts of the surfactant molecules may

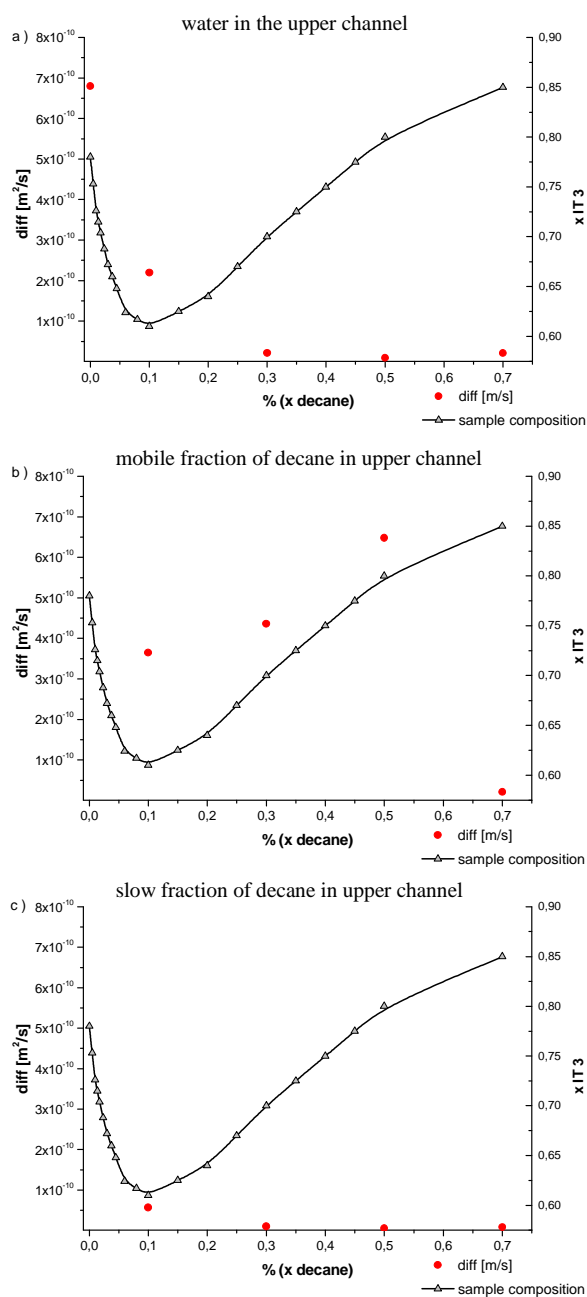


Fig. 8 Self diffusion constants of system constituents in the upper channel as a function of the decane and IT 3 content.

undergo more rapid diffusion via molecular exchange with micelles which would explain for the slight deviation between the slopes for the decane and the surfactant signals. An extremely small fraction of water molecules may be linked to the droplets and explain a possible plateau of the water signal for $\ln I/I_0 < -8$. However, with a contribution of only 0.01%, this signal fraction comes close to the noise amplitude and may be insignificant. All apparent self diffusion constants are summarized in Figs. 8 and 9 as functions of the decane content. The data for the water fraction show a clear correlation with the corresponding conductivity plots in Fig. 4. In the upper channel, the water mobility steeply declines with increasing decane concentration (Fig. 8 top).

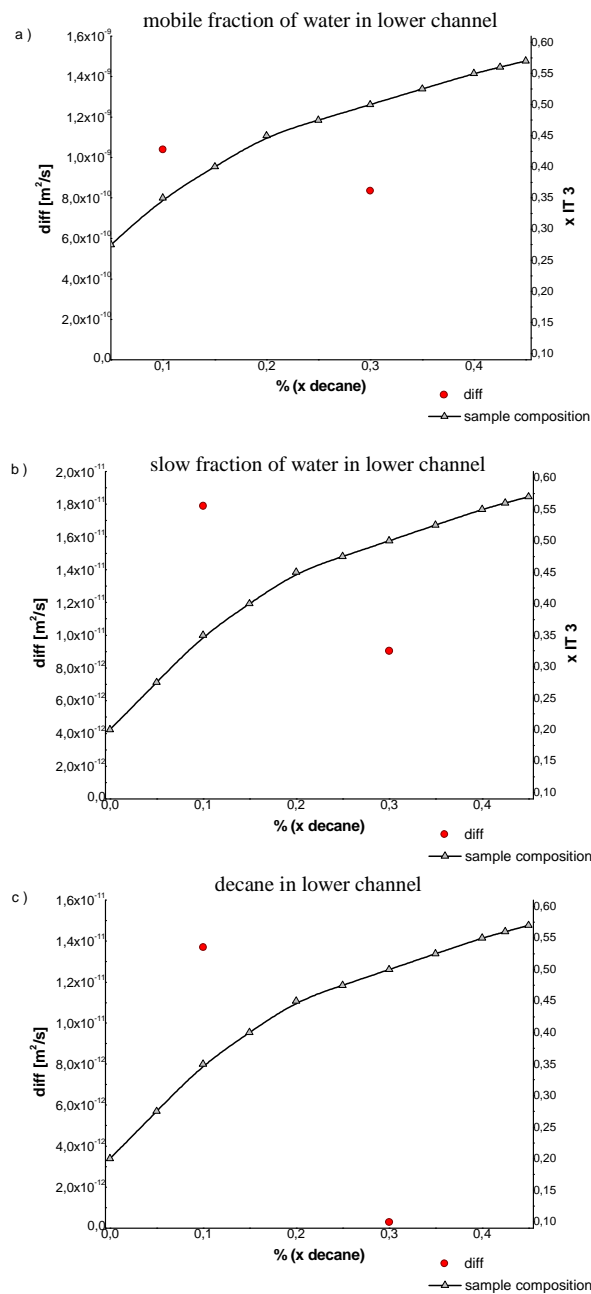


Fig. 9 Self diffusion constants of system constituents in the lower channel as a function of the decane and IT 3 content.

This behavior is reproduced by a corresponding decrease of the conductivity (Fig. 4 top) which can be regarded as a direct consequence: with less mobile water molecules, ions in the aqueous solution can be expected to be less mobile as well. However, this effect is far more dramatic on conductivity than on the mobility of individual water molecules: a reduction of the self diffusion coefficient by a factor of 30 results in a loss in conductivity by more than three orders of magnitude. This may be partially explained by a reduced overall ion concentration connected to the decreasing water content. In case of the lower channel, the loss of water mobility under increasing decane content is much smaller (Fig. 9 top). This is again reflected by the conductivity data in Fig. 4 (bottom)

which show a minor decrease on addition of decane. Here, a decrease of the water mobility by a factor of 1.2 between x decane 0.1 and 0.3 is accompanied by about the same factor of 1.25 in conductivity. The reason for this lies mainly in the decreasing mass fraction of the anionic $\text{Mg}(\text{DS})_2$ in the surfactant mixture.

Influence of Salt to the System

As already mentioned, our mixed anionic/nonionic surfactant system has a very high interfacial tension against the oil phase compared to the ultra-low interfacial tensions that can be reached with single non-ionic surfactants. We assumed that by shielding the charge of the anionic surfactant by adding excess salt would lower the interfacial tension.

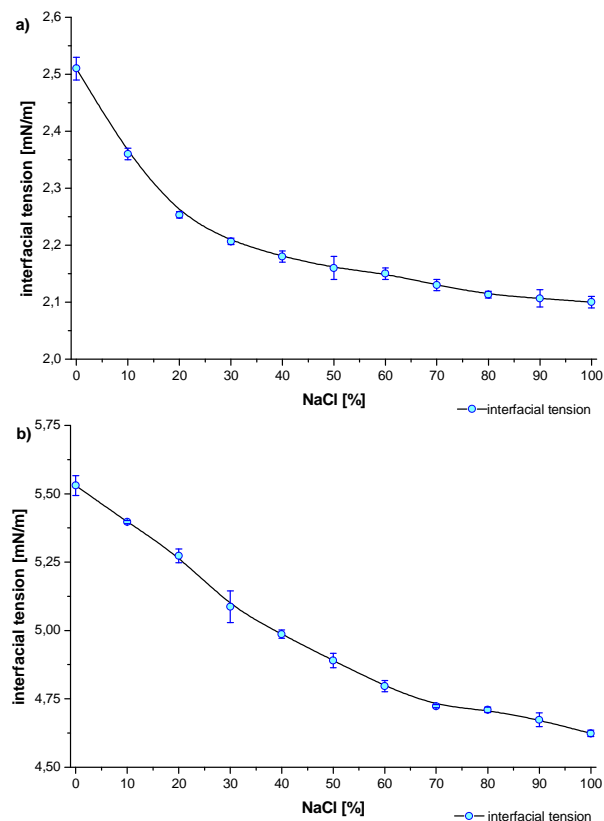


Fig. 10 interfacial tension of the surfactant mixtures against decane with increasing amount of NaCl. Surfactant concentration constant at 0.5% in the aqueous phase. 100% NaCl corresponds to a molar ratio of $\text{Mg}(\text{DS})_2:\text{NaCl} = 1:1$. a) interfacial tension at $x \text{ IT } 3 = 0.5$, b) interfacial tension at $x \text{ IT } 3 = 0.8$.

Similar effects were already reported for the anionic surfactant diethylhexyl sodium sulphosuccinate (AOT), where ultra-low interfacial tensions against oil were reached with additional NaCl.²⁵

To verify our assumption, we measured the interfacial tension at two mixing ratios of the surfactant and co-surfactant with increasing amount of NaCl, namely around the minimum of the observed interfacial tension at $x \text{ IT } 3 = 0.5$ and around the mixing ratio of the L_3 phase at $x \text{ IT } 3 = 0.8$. As it can be seen in Fig. 10, the interfacial tension is lowered only about 0.5 mN/m at the minimum of the interfacial tension at $x \text{ IT } 3 = 0.5$ and only about 0.9 mN/m around the L_3 phase at $x \text{ IT } 3 =$

0.8, when the molar ratio of $\text{Mg}(\text{DS})_2:\text{NaCl}$ in the surfactant mixtures is raised to 1:1. No ultra-low interfacial tensions were detected. As the volume-drop technique can detect low interfacial tensions down to 0.1 mN/m, there shouldn't be anything wrong with the measurements. We also checked the influence of salt on the phase behaviour of the upper microemulsion channel. Therefore, we had a closer look on the microemulsion with 30% decane in the solvent mixture and investigated how the phase boundaries would shift by adding NaCl to the system. It turned out that the upper and lower borders of the single phase region are shifted to lower $x \text{ IT } 3$ values by $x \text{ IT } 3 \sim 0.07$ when we added NaCl to the $\text{Mg}(\text{DS})_2$ in a molar ratio of 1:1. The shift to lower $x \text{ IT } 3$ values means that the system in total becomes more lipophilic, as less amount of the lipophilic co-surfactant IT 3 in the surfactant mixture is needed to solubilise 30% of decane. If the shift of the phase boundaries is accompanied also by a change in the nanostructure was first investigated by measuring the electric conductivity of the microemulsion with increasing salt concentration. A plot of the conductivity in the single phase region with increasing NaCl concentration is shown in Fig. 11.

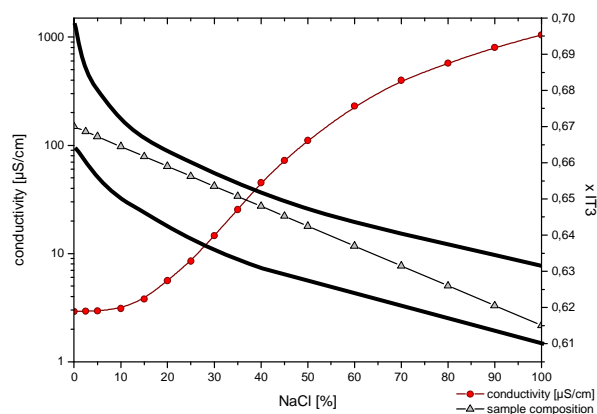


Fig. 11 Plot of conductivity in the single phase region of a microemulsion with x decane 0.3 and increasing NaCl concentration at 25 °C. 100% NaCl corresponds to a molar ratio of $\text{Mg}(\text{DS})_2:\text{NaCl} = 1:1$.

The conductivity from the NaCl-free to the microemulsion with a molar ratio of $\text{Mg}(\text{DS})_2:\text{NaCl} = 1:1$ increases about three orders of magnitude from a low value of 3 $\mu\text{S}/\text{cm}$ to $\sim 1000 \mu\text{S}/\text{cm}$. The conductivity increases in a sigmoid curve with an inflection point around 50% NaCl and not linearly with increasing NaCl concentration. At first sight, the nanostructure seems to change from a w/o-HIPME system to a bicontinuous-like nanostructure.

To verify this, we compared two microemulsions with different salt concentrations by PFG-NMR. The first sample without NaCl had the composition of $x \text{ IT } 3$ 0.7 and x decane 0.3. The second sample had the composition of $x \text{ IT } 3$ 0.615, x decane 0.3, and the molar ratio of $\text{Mg}(\text{DS})_2:\text{NaCl} = 1:1$. The resulting Stejskal-Tanner plots are shown in Fig. 12, the corresponding apparent self diffusion constants are listed in Table 3.

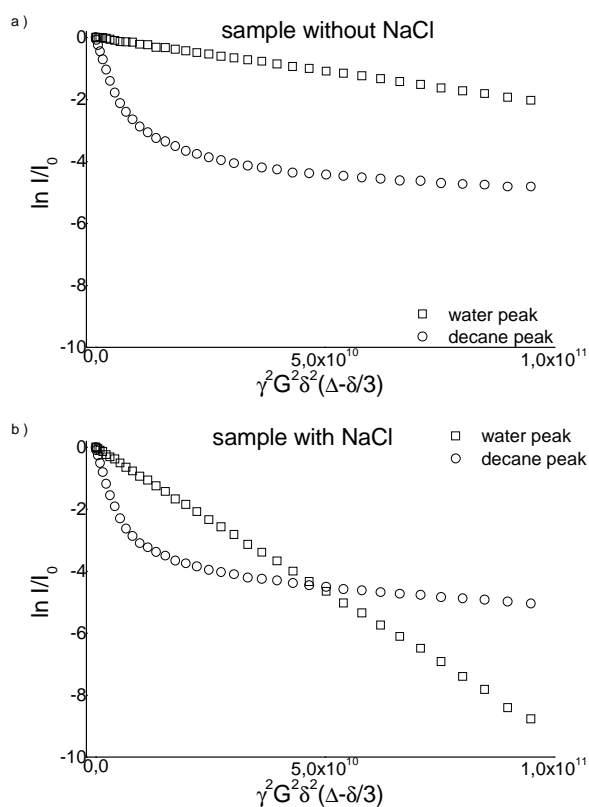


Fig. 12 Stejskal-Tanner plots for decane and water at x IT3 0.7 and x decane 0.3 in absence (top) and presence (bottom) of NaCl.

Tab. 3 The influence of electrolyte on the apparent self diffusion coefficients of system constituents in the upper channel.

sample	D (water)	D (decane)	D (decane) plateau
	[m ² /s]	[m ² /s]	[m ² /s]
without NaCl	$2,14 \cdot 10^{-11}$	$4,32 \cdot 10^{-10}$	$1,02 \cdot 10^{-11}$
with NaCl	$9,21 \cdot 10^{-11}$	$4,68 \cdot 10^{-10}$	$1,72 \cdot 10^{-11}$

Obviously, the signal decay plot of decane does not change significantly on the addition of NaCl. Hence, we believe that decane remains in a continuous phase after addition of the salt. The signal decay for H₂O, however, changes significantly. The mobility of the water signal of the sample containing NaCl is much increased to $D_w = 9.21 \cdot 10^{-11}$ m²/s. Nevertheless, it's still about a factor 2 smaller compared to the water signal of the HIPME-sample containing 10% decane without NaCl. It is likely that the water only can diffuse slowly through the organic phase. Although the conductivity-results indicate a transition from a HIPME structure to a bicontinuous structure by adding salt to the microemulsion, this is definitely not the case. First of all, one has to reconsider precisely the conductivity value of the transformed microemulsion with NaCl. This microemulsion has a fraction of $\sim 5.8\%$ Mg(DS)₂ (x IT 3 = 0.615) in the sample. This corresponds to a molar concentration of ~ 105 mM Mg(DS)₂.

The molar ratio of Mg(DS)₂:NaCl in this sample was 1:1. A 100 mM NaCl standard solution has a conductivity of about 11 mS/cm. The conductivity value of the microemulsion with NaCl is already about 10 times lower than this value. Secondly, the diffusion rates for the water fraction of the sample containing NaCl are far away from bulk-water, whereas the decane-signal doesn't change at all when salt is added to the system. Thus we assume that the morphology cannot be a bicontinuous sponge-like structure as it is the case for microemulsions with a single non-ionic surfactant. It is conceivable that the charge on the surfactant monolayer with the anionic surfactant is shielded by the addition of NaCl and thus the repulsion forces are decreased. Consequently the system becomes highly dynamic. This might allow some water-domains to fuse together and form passages, in which the ions could be transported in the aqueous phase and therefore increase the conductivity of the system. For that reason we assume the nanostructure with NaCl to be more a HIPME-structure with defects in form of bent water-domains than a classical bicontinuous sponge phase. It is, however, unclear, why there is such a discrepancy between the comparably slow diffusion constant for the water fraction and the high conductivity value.

Temperature Stability of the Microemulsions

Another interesting question emerges, namely how the microemulsion reacts to temperature changes. In order to examine this, we chose the microemulsion at the turning point of Fig. 11 for investigations, as we assumed that it might be highly sensitive for conductivity changes with temperature. For this experiment, we raised the temperature of the microemulsion by ~ 0.5 °C per minute and noted the change of the conductivity. The result is shown in Fig. 13.

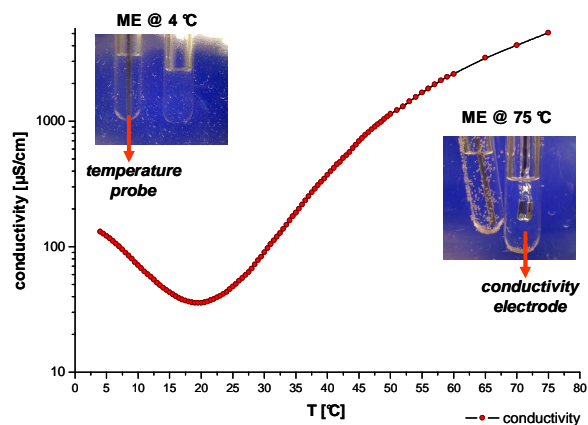


Fig. 13 Conductivity of a microemulsion from the upper single phase channel with increasing temperature. Sample composition: x IT 3 0.64, x decane 0.3, molar ratio of Mg(DS)₂:NaCl = 2:1. Phase behaviour of the microemulsion investigated by visual observation between crossed polariser foils.

First astonishing result of this experiment was, that the microemulsion didn't phase separate in an enormous temperature range from about 4 °C to 80 °C. This was

checked by visual observation of the sample between crossed polariser foils. The highly temperature stability of the sample is due to the fact, that the HLB of the surfactant mixture is more determined by the mixing ratio than by the temperature. Although the non-ionic compound IT 3 becomes more lipophilic by raising the temperature as any other surfactant of the type C_iE_j , the anionic surfactant becomes more hydrophilic, compensating the effect of the non-ionic co-surfactant. This idea was already proposed in literature.³⁰ The conductivity runs through a minimum of $\sim 30 \mu\text{S}/\text{cm}$ around 20°C and increases to $5000 \mu\text{S}/\text{cm}$ at 75°C , indicating various changes in the nanostructure of the microemulsion with increasing temperature.

Conclusion

We have shown by PFG-NMR that the nanostructure in the upper microemulsion channel of a mixed anionic/nonionic surfactant mixture transforms from a bicontinuous L_3 phase to a w/o-HIPME structure with only about 10% of oil in the solvent mixture, while the lower microemulsion channel has an o/w structure. The results are in good agreement with conductivity data and cryo-TEM pictures that were published recently. Moreover, these microemulsions are highly temperature stable. By addition of NaCl, the conductivity and the mobility of H_2O increase significantly. Nevertheless, it is unlikely that the nanostructures with NaCl have the same sponge-like morphology as bicontinuous microemulsions with single non-ionic surfactants, as the conductivity values are much lower than expected for a real bicontinuous microemulsion and the NMR signals still indicate the presence of a HIPME-structure. Based on NMR and conductivity results, we assume the structure to be a HIPME-phase with defects in relation to the isolated water-domains. The question, how the nanostructure is influenced exactly by the addition of NaCl, can surely be answered by further cryo-TEM or FF-TEM experiments.

Experimental

Materials

The non-ionic surfactant iso-tridecyl-triethylenglycoether ($C_{13}E_3$), abbreviated as IT 3, was obtained from the Sasol Company, (Hamburg, Germany) under the name "Marlipal O13/30". This compound has a polydisperse distribution of EO-groups with average 3 EO-units. Sodium dodecyl sulfate (SDS, cryst. research grade) was purchased from the Serva Company (Heidelberg, Germany). $\text{MgCl}_2 \times 6 \text{H}_2\text{O}$ was purchased from the Grüssing Company (Filsum, Germany). N-Decane (analytical grade) was obtained from the Merck Company (Darmstadt, Germany).

Preparation of $\text{Mg}(\text{DS})_2$

For the preparation of $\text{Mg}(\text{DS})_2$, 400 mM SDS-solution was mixed with 200 mM MgCl_2 solution under stirring. The bivalent counter ion Mg^{2+} binds stronger to the dodecyl sulfate than the sodium-ion, leading to a precipitation of $\text{Mg}(\text{DS})_2$ in solution below its Krafft-temperature around 25°C .

The solution was heated up above 25°C to obtain a clear solution, and then cooled down to 20°C . After precipitation over night, $\text{Mg}(\text{DS})_2$ was filtered and washed several times with de-ionised water to remove excess salt. The purity of the surfactant thus could be checked by measuring the conductivity of the flow through of the filtered $\text{Mg}(\text{DS})_2$. The washed $\text{Mg}(\text{DS})_2$ was freeze-dried with the freeze-drying device Alpha 1-4, from the Christ Company (Osterode, Germany) and used without further purification.

Preparation of Samples

All samples were prepared by weighing in directly the components in test tubes at an analytical balance. The test tubes were sealed with teflon tape, tempered at 25°C in a water bath, and vortexed several times thoroughly. All samples were incubated at least 3 days at 25°C before being investigated for their phase behaviour. In general, a phase diagram was scanned with a resolution of 5% in the composition of the mass fraction of IT 3 and decane. Finer steps were investigated in the beginning of the narrow upper single-phase channel. The multiphase samples were viewed and imaged without and in between crossed polarisers to visualise the birefringence of lamellar regions.

Conductivity Measurements

For conductivity measurements, there was used the Microprocessor Conductivity Meter LF3000 from the WTW Company (Weilheim, Germany). Before measuring, the electrode was tested by checking the conductivity of 10 mM and 100 mM KCl solutions and determining the correct cell constant. Samples were tempered with a RM6 circulating bath from the Lauda Company (Koenigshofen, Germany). The temperature of the measured samples was checked with the GMH 3750 High Precision Digital Thermometer from the Greisinger Company (Regenstauf, Germany). The temperature probe was placed directly into a water filled test tube next to the microemulsion sample. During conductivity measurements, the microemulsion samples were observed between crossed polarisers for their phase behaviour.

Surface/Interfacial Tension Measurements

The surface and interfacial tensions were measured with the volume-drop tensiometer TVT1 from the Lauda Company (Koenigshofen, Germany). The device was set to standard mode with a constant drop-volume creation speed of $3 \text{ s}/\mu\text{l}$. To assure that the drop creation speed was not set too fast, time dependent measurements were carried out.

Pulsed-Field Gradient Nuclear Magnetic Resonance Spectroscopy (PFG-NMR) Self-Diffusion measurements

For the preparation of the PFG-NMR samples, a regular 3 mm NMR sample tube was filled and embedded in an outer 5 mm sample tube filled with D_2O (lock). All PFG-NMR-measurements were performed on a Bruker DRX 500 spectrometer (Bruker AG, Karlsruhe, Germany) equipped with a BAFPA 40 gradient amplifier and a Bruker DIFF30 probe. The instrument was tuned to 500 MHz proton frequency, gradient pulses were adjusted to gradient strengths between 5 and 450 Gauss/cm with individual durations of 2 ms. For all

measurements, the stimulated echo ($90^\circ\text{-}\tau_1\text{-}90^\circ\text{-}\tau_2\text{-}90^\circ\text{-}\tau_1\text{-}$ echo) was used in combination with the gradient pulses during each τ_1 waiting period. The duration of the 90° -pulses was 8,67 μs , the waiting period between the 32 repetitions (scans) of each experiment amounts to 11 s. The spacing Δ between the two gradient pulses was 50 ms. The free induction decays resulting from the addition of each set of 32 experiments were Fourier transformed and analyzed for the echo signal decay vs. the gradient strength G and the pulse spacing Δ . Characteristic signals were chosen for the individual observation of decane, water and MDS/IT3. For the analysis of the diffusion profile, the relative signal intensities I/I_0 (I_0 referring to the signal intensity at gradient strength $G = 0$) were plotted logarithmically vs. the parameter $\gamma^2 G^2 \delta^2 (\Delta - \delta/3)$, with γ being the gyromagnetic ratio of protons, G the strength of the gradient field, δ and Δ the duration of and the spacing between the two gradient pulses.

Notes and References

^{*a} University of Bayreuth, BZKG/BayKoll, Gottlieb-Keim-Str. 60, D-95448 Bayreuth, Germany

^{*b} University of Duisburg-Essen, Institute for Physical Chemistry, CeNIDE, D-45141 Essen, Germany

- 1 T. P. Hoar, J. H. Schulman, *Nature*, 1943, **152**, 102-103.
- 2 J. H. Schulman, W. Stoeckenius, L. M. Price, *J. Phys. Chem.*, 1959, **63**, 1677-1680.
- 3 M. Gradzielski, H. Hoffmann, *J. Phys. Chem.*, 1994, **98**, 2613-2623.
- 4 F. Lichterfeld, T. Schmeling, R. Strey, *J. Phys. Chem.*, 1986, **90**, 5762-5766.
- 5 U. Olsson, K. Shinoda, B. Lindman, *J. Phys. Chem.*, 1986, **90**, 4083-4088.
- 6 K. Shinoda, H. Saito, *J. Colloid Interf. Sci.*, 1968, **23**, 70-74.
- 7 C. Stubenrauch, *Microemulsions: Background, New Concepts, Applications, Perspectives*, ed. C. Stubenrauch, John Wiley & Sons, Oxford, 2009.
- 8 L. Magid, P. Butler, K. Payne, R. Strey, *J. Appl. Cryst.*, 1988, **21**, 832-834.
- 9 B. Lindman, U. Olsson, *Ber. Bunsenges. Phys. Chem.*, 1996, **100**, 344-363.
- 10 R. Strey, *Colloid Polym. Sci.*, 1994, **272**, 1005-1019.
- 11 K. Shinoda, S. Friberg, *Adv. Colloid Interf. Sci.*, 1975, **4**, 281-300.
- 12 S.-H. Chen, S.-L. Chang, R. Strey, *J. Chem. Phys.*, **1990**, 1907-1918.
- 13 M. Kotlarchyk, S.-H. Chen, J. S. Huang, M. W. Kim, *Phys. Rev. Lett.*, 1984, **53**, 941-944.
- 14 K. Fontell, A. Ceglie, B. Lindman, B. Ninham, *Acta Chemica Scandinavica A40*, 1986, 247-256.
- 15 W. Jahn, R. Strey, *J. Phys. Chem.* **1988**, 92, 2294-2301.
- 16 L. Wolf, H. Hoffmann, K. Watanabe, T. Okamoto, *Phys. Chem. Chem. Phys.*, 2011, **13**, 3248-3256.
- 17 L. Wolf, H. Hoffmann, Y. Talmon, T. Teshigawara, K. Watanabe, *Soft Matter*, 2010, **6**, 5367-5374.
- 18 L. Wolf, H. Hoffmann, W. Richter, T. Teshigawara, T. Okamoto, *J. Phys. Chem. B*, 2011, **115**, 11081-11091.
- 19 L. Wolf, H. Hoffmann, T. Teshigawara, T. Okamoto, Y. Talmon, *J. Phys. Chem. B*, 2011, *submitted*
- 20 S. Pandey, R. P. Bagwe, D. O. Shah, *J. Colloid Interf. Sci.*, 2003, **267**, 160-166.
- 21 A. Zapf, U. Hornfeck, G. Glatz, H. Hoffmann, *Langmuir*, 2001, **17**, 6113-6118.
- 22 R. Strey, *Colloid Polym. Sci.*, 1994, **272**, 1005-1019
- 23 T. Sottmann and R. Strey, *J. Chem. Phys.*, 1997, **106**, 8606-8615.
- 24 H. Hoffmann, Plenary lecture, *Prog. Colloid Polym. Sci.*, 1990, **83**, 16-28.
- 25 R. Aveyard, B. P. Binks, S. Clark, J. Mead, *J. Chem. Soc. Faraday Trans. 1*, 1986, **82**, 125-142.
- 26 C. Boned, M. Clausse, B. Lagourette, V. E. R. McClean, R. J. Sheppard, *J. Phys. Chem.*, 1980, **84**, 1520-1525.
- 27 M. J. Kahlweit, *Colloid Interface Sci.* **1987**, **118**, 436-453.
- 28 T. Sottmann, R. Strey, S.-H. Chen, *J. Chem. Phys.*, 1997, **106**, 6483-6491.
- 29 N. R. Cameron, D. C. Sherrington, *Adv. in Polym. Sci.*, 1996, **126**, 162-214.
- 30 S. Ajith, A. K. Rakshit, *J. Phys. Chem.*, 1995, **99**, 14778-14783.

6. Abbreviations and Symbols

AOT	sodium dioctyl sulfosuccinate
Ca(DS) ₂	calciumdodecylsulfate
CEVS	controlled environment vitrification system
C _i E _j	non-ionic surfactant, alkyl polyethylene glycolether
Cryo-TEM	cryogenic transmission electron microscopy
DDAB	didodecyldimethylammoniumbromide
EB	electric birefringence
EO	ethyleneoxide
FF-TEM	freeze-fracture transmission electron microscopy
H	interfacial curvature
H ₂ O	water
HIPE	high internal phase emulsion
HIPME	high internal phase microemulsion
HLB	hydrophilic-lipophilic balance
IT 3	isotridecyltriethyleneglycolether
K _T	Krafft-Temperature
L ₁	micellar phase
L ₂	inverse micellar phase
L ₃	sponge phase
L _α	lamellar phase
M ₂	hexamethyldisiloxane
Mg(DS) ₂	magnesiumdodecylsulfate
NaCl	sodium chloride
o/w	oil-in-water
P	packing parameter
PFG-NMR	pulse-field generated nuclear magnetic resonance spectroscopy
SANS	small angle neutron scattering
SAXS	small angle x-ray scattering
SDS	sodiumdodecylsulfate
w/o	water-in-oil

7. Presentations at international meetings

- 44th Biennial Meeting of the German Colloid Society, September 28-30, 2009, University of Hamburg, Germany
Poster presentation: *Microemulsions from silicon oil with an anionic/non-ionic surfactant mixture*
- Technion – Israel Institute of Technology, February 2nd 2010, Israel (Haifa)
Oral presentation: *Microemulsions from silicon oil with an anionic/non-ionic surfactant mixture*
- 6th Zsigmondy Colloquium, March 23rd 2010, Chemnitz University of Technology, Germany
Oral presentation: *Dynamic Properties of microemulsions in the single phase channel*
- 109. Hauptversammlung der Deutschen Bunsen-Gesellschaft für Physikalische Chemie e.V (Bunsentagung), May 13-15, 2010, University of Bielefeld, Germany
Poster presentation: *Dynamic Properties of microemulsions in the single phase channel*
- Bayreuth Polymer Symposium BPS 2011, September 11-13, 2011, University of Bayreuth, Germany
Poster presentation: *Microemulsions with an anionic/non-ionic surfactant mixture and a HIPME structure*
- 58th SEPAWA Congress, October 12th 2011, Forum for Innovations, Fulda, Germany
Oral presentation: *Microemulsions with an anionic/non-ionic surfactant mixture and a HIPME structure*

8. Acknowledgement

I want to thank all those people, who contributed to this work in many different ways and made all this possible.

First of all I would like to thank my Ph.D. advisor Prof. Dr. Heinz Hoffmann. I hold him in high regard, not only because of his wisdom and extensive knowledge. He encouraged me to expand my knowledge in the field of surfactant science that was completely new for me at the beginning of this work. I learned much from him in various fruitful and interesting discussions. He stood up for me and my colleagues in many situations and supported us, be it scientifically or privately.

Moreover I want to thank all people from *Shiseido* company, Japan, who were involved in this project and supported us financially. Especially I want to thank Dr. Kei Watanabe, Tohru Okamoto and Takashi Teshigawara, who gave me the chance and freedom to research independently most of the time. Hopefully, the results of this work will help you to develop new attractive cosmetic products. I enjoyed much the years in our laboratories together with the guest-scientists from Shiseido, namely Hidefumi, Takashi, Keisuke and Yoko. They all became friends for me.

Special thanks also for Prof. Yeshayahu Talmon and his group at the Technion, Israel. I enjoyed my two stays in Haifa, not only because of the great chance to learn the basics about electron microscopy and the excellent scientific assistance. I always will remember the good times there and never forget the hospitality and friendship of all people there.

Of course, I also want thank all my colleagues in the laboratories, Martin, Dieter, Elham and Rami. Especially Dieter Gräbner, for teaching me how to operate the laboratory devices and for many regularly scientific discussions, also with Prof. Dr. Gerhard Platz, and Martin Reger, who was not only a great colleague but also a good friend for me. Without Martin, the time in laboratory, the conferences and the research would not have been as gleeful as they were.

Finally I would like to thank my family. Special thanks to my parents Anne and Bernhard Wolf, my sister Eva Wolf and my beloved Anja. They all supported me all the last years and gave me inspiration and endurance.

9. Erklärung

Ich erkläre hiermit, dass ich die vorliegende Arbeit selbständig verfasst und keine anderen als die von mir angegebenen Quellen und Hilfsmittel benutzt habe.

Ferner erkläre ich, dass ich nicht anderweitig mit oder ohne Erfolg versucht habe, diese Dissertation einzureichen. Ich habe keine gleichartige Doktorprüfung an einer anderen Hochschule endgültig nicht bestanden.

Bayreuth, den 5. Dezember 2011



Lukas Wolf